

**DEVELOPMENT OF A CONDITION MONITORING  
AND PROCESS CONTROL SYSTEM FOR WIRE  
ELECTRIC DISCHARGE MACHINING**

A THESIS

submitted by

**ABHILASH P. M.**

(131804101)

For the

AWARD OF DEGREE

Of

**DOCTOR OF PHILOSOPHY**



---

**IIT PALAKKAD**

**DEPARTMENT OF MECHANICAL ENGINEERING  
INDIAN INSTITUTE OF TECHNOLOGY PALAKKAD**

July 2021

Abhilash P. M.: *Development of a condition monitoring and process control system for wire electric discharge machining*

© Indian Institute of Technology Palakkad

July 2021

## CERTIFICATE

---

This is to certify that the thesis titled “**Development of a Condition Monitoring and Process Control System for Wire Electric Discharge Machining**”, submitted by **Abhilash P. M. (Roll No. 131804101)** for the award of the degree of **Doctor of Philosophy** of **Indian Institute of Technology Palakkad**, is a record of bonafide work carried out by him under my guidance and supervision at **Department of Mechanical Engineering, Indian Institute of Technology Palakkad**. To the best of my knowledge and belief, the work presented in this thesis is original and has not been submitted, either in part or full, for the award of any other degree, diploma, fellowship, associateship or similar title of any university or institution.

*D. Chakradhar*  
09/07/2021

Dr. D. Chakradhar

Assistant Professor

Department of Mechanical Engineering  
Indian Institute of Technology Palakkad

## **DECLARATION**

---

This is to declare that the thesis “**Development of a Condition Monitoring and Process Control System for Wire Electric Discharge Machining**” that I have submitted to the Indian Institute of Technology Palakkad, for the award of degree of Doctor of Philosophy is a bonafide record of the research work that I have carried out under the supervision of **Dr. D. Chakradhar**, Assistant Professor in the Department of Mechanical Engineering. I declare that the contents of the thesis have not been submitted and will not be submitted to any other Institute or University for the award of any degree or diploma.



Palakkad - 678557

Abhilash P. M.

131804101

Date : 09-07-2021

Forwarded



Dr. D. Chakradhar

(Research Guide)

Assistant Professor

Department of Mechanical Engineering

Indian Institute of Technology Palakkad

## ABSTRACT

Wire electric discharge machining (wire-EDM) is a non-traditional machining process whose mechanism of material removal is by controlled, repetitive electric sparks. The process is known for its capability to machine the superalloys which are difficult to machine conventionally. However, the process stability has to be controlled to ensure failure free operation and defect free parts. The current work aims to create a condition monitoring system that predicts the events of machining failure or process instability. The monitoring system consists of multiple sensors to capture the current and voltage waveform. The process condition is accessed by the proportion of short circuit discharges and misdischarges (open circuit discharges) in a pulse cycle. The extracted features from the captured waveforms can provide valuable information about upcoming process interruptions or potential surface damages to the machined parts.

Initially, an offline analysis on the effect of discharge energy on machining stability and surface integrity is conducted. The responses studied are surface topography, morphology, geometric accuracy, elemental contamination and productivity. Wire wear pattern and breakage mechanism for different wire materials are analysed. Next, an offline multi-class neural network classification model is developed to classify the machining failures. The failure conditions considered are spark absence and wire breakages. Next, the effect of spark gap variation on the wire break failures and part quality is modelled and studied using an ANFIS model. These offline models can complement the online model in preliminary screening of parameters to set the initial conditions. The next phase involves the setting up of a condition monitoring system. A pulse discrimination algorithm is developed to classify the discharge sparks into normal, open and arc/short circuit sparks. Using the developed pulse classification algorithm, proportions of different pulses are calculated. The discharge characteristics like, abnormal pulse proportion, discharge energy, and pulse frequency are experimentally found to be responsible for process failures. Considerable

variations in these characteristics are observed before events of failure. Based on these in-process data, a neural network classifier is developed to predict process failures. The classifier is found to have an accuracy of 98.1 % in classifying the machining failures. Moreover, remaining useful life (RUL) is utilized to quantify the severity of the predicted event, based on which, a process control system is designed. The process control algorithm computes and suggests the parameter revisions to restore the machining stability. Pulse on time, pulse off time, and servo voltage are incrementally adjusted in this regard. The proposed condition monitoring and process control system is successful in foreseeing and preventing the wire breakage and spark absence failures during wire EDM process. The pulse train characteristics are also compared to analyse the effects of process control. The undesirable pulse types like short circuit and open circuit discharges are replaced by ideal normal circuit pulses.

**Keywords:** *Wire EDM, machining stability, condition monitoring, wire breakage, spark absence, process control, Inconel 718, spark gap bridging, short circuit sparks, neural network classifier, remaining useful life, process failure classification.*

## PUBLICATIONS

---

### Published/Accepted

1. **Abhilash P M.**, D. Chakradhar, Failure detection and control for wire EDM process using multiple sensors, *CIRP Journal of Manufacturing Science and Technology* 2021; 33, 315–26 <https://doi.org/10.1016/j.cirpj.2021.04.009>
2. **Abhilash P M**, Chakradhar D. ANFIS modelling of mean gap voltage variation to predict wire breakages during wire EDM of Inconel 718. *CIRP Journal of Manufacturing Science and Technology* 2020; 31, 153–64 <https://doi.org/10.1016/j.cirpj.2020.10.007>
3. **Abhilash P M**, Chakradhar D. Surface integrity comparison of wire electric discharge machined Inconel 718 surfaces at different machining stabilities. *Procedia CIRP* 2020; 87, 228–33 <https://doi.org/10.1016/j.procir.2020.02.037>
4. **Abhilash P M.**, D. Chakradhar, Prediction and analysis of process failures by ANN classification during wire-EDM of Inconel 718, *Advances in Manufacturing* 2020; 8 (4), 519-536 <https://doi.org/10.1007/s40436-020-00327-w>
5. **Abhilash, P M.**, Chakradhar, D. Sustainability improvement of WEDM process by analysing and classifying wire rupture using kernel-based naive Bayes classifier. *Journal of the Brazilian Society of Mechanical Sciences and Engineering* 2021; 43, 64 <https://doi.org/10.1007/s40430-021-02805-z>
6. **Abhilash, P M.**, Chakradhar, D. Image processing algorithm for detection, quantification and classification of micro defects in wire EDM precision finish cut surfaces. *Journal of Micromanufacturing* 2021 <https://doi.org/10.1177/25165984211015410>
7. **Abhilash P M.**, D. Chakradhar, Machine vision-based electrode wear analysis for closed loop wire EDM process control, *Advances in Manufacturing* – Accepted for publication

### Under Review

1. **Abhilash P M.**, D. Chakradhar, Wire EDM failure prediction and process control based on sensor fusion and pulse train analysis, *The International Journal of Advanced Manufacturing Technology*
2. **Abhilash P M.**, D. Chakradhar, Performance monitoring and failure prediction system for wire EDM process through multiple sensor signals, *Machining Science and Technology*
3. **Abhilash P M.**, D. Chakradhar, Multi-response optimization of wire EDM of Inconel 718 using a hybrid entropy weighted GRA-TOPSIS method, *Process Integration and Optimization for Sustainability*
4. **Abhilash P. M.**, D. Chakradhar, Effect of wire material and discharge energy on productivity and surface integrity of WEDM-processed Inconel 718, *Advances in Materials and Processing Technologies*

## **ACKNOWLEDGEMENT**

---

I would like to express my sincere gratitude to my advisor Dr. D. Chakradhar for his guidance, patience, motivation, and continuous support during my PhD program. His guidance helped me throughout my research and writing of this thesis. I could not have imagined having a better advisor and mentor for my PhD study.

Besides my advisor, I would like to thank the rest of my doctoral committee: Prof. Pramod S Mehta, Dr. Ganesh Natarajan (Doctoral Committee Chairman and Dean, Administration), Dr. D. Kesavan, Dr. Lakshmi Narasimhan Theagarajan, and Dr. Sarath Sasi for their insightful comments and encouragement which widened my research from various perspectives. My sincere thanks go to Dr. Sovan Lal Das (Dean, Academics), Dr. Uma Divakaran (Associate Dean, Academics, PG), Prof. K L Sebastian (former Dean, Academic Research) and Prof. Job Kurian (former Dean, Administration) for their continuous support during my research work.

I would like to thank all the faculty members of Department of Mechanical Engineering for their whole hearted support throughout my research work. Special mention to Dr. Kanmani Subbu S and Dr. Afzaal Ahmed for their technical inputs at various stages of this research. I thank Dr. Mahesh R Panicker and Dr. Sreenath Vijayakumar of Department of Electrical Engineering for their inputs during the setting up of condition monitoring system. My sincere gratitude goes to all the technical staff members of Department of Mechanical Engineering, especially Mr. Visant P V, Mr. Bharath Krishna, Mr. Somasundaram, and Mr. Vinu V for their support. I am indebted to all my co-research scholars of Department of Mechanical Engineering, especially Mr. Rakesh P R, Mr. Pramod S, Mr. Ranju M R, Mr. Shanmuga Priyan V. G, Mr. Jibin Boban, and Mr. Simson D for their support and encouragement. I would like to thank the Central Instrumentation Facility (CIF), and associated staff who provided me access to the laboratory and research facilities. Without their precious support, it would not be possible to conduct this research.

I would like to thank my dear friend and co-research scholar Mr. Praveen K for his frequent help and support. Also, some special words of gratitude goes to my dear friends Mr. Jose George, Mr. Renjith S, and Ms. Gopika Rajagopal for their persistent support and all the fun we had during the last few years. I would also like to thank all my friends at Indian Institute of Technology Madras, especially Mr. Lalin Diwan and Mr. Vishnu Madhav Karath for their help and continuous support during my coursework and afterwards.

Last but not the least, I would like to express my gratitude to my parents Mr. N. Unnikrishnan and Mrs. P. M. Sreelatha for all their sacrifices, love and unconditional support throughout my life. I thank my sister, Mrs. Athira, for her encouragement and valuable technical inputs. Finally, I thank with love, my wife Dr. Anisha and son Adwaith Abhilash, for standing by me through all my toils, absence and impatience. The journey would not be this amazing without each of your inspiration and support.

# CONTENTS

---

<i>Certificate</i> .....	iii
<i>Declaration</i> .....	iv
<i>Abstract</i> .....	v
<i>Publications</i> .....	vii
<i>Acknowledgement</i> .....	viii
<i>Contents</i> .....	x
<i>List of Figures</i> .....	xiv
<i>List of Tables</i> .....	xx
<i>List of Symbols and Acronyms</i> .....	xxii
CHAPTER 1 – INTRODUCTION.....	1
1.1 INDUSTRY 4.0 AND SMART MANUFACTURING.....	1
1.2 CONDITION MONITORING OF MANUFACTURING PROCESSES.....	3
1.3 WIRE ELECTRIC DISCHARGE MACHINING.....	5
1.3.1 Working principle of wire EDM.....	6
1.3.2 Wire material.....	8
1.3.3 Control parameters.....	9
1.3.4 Applications of Wire EDM.....	11
1.3.5 Process stability of wire EDM.....	11
1.4 CONDITION MONITORING OF WIRE EDM.....	16
1.5 OUTLINE OF THE THESIS.....	16
CHAPTER 2 – LITERATURE REVIEW.....	19
2.1 INTRODUCTION.....	19
2.2 IMPACT OF INDUSTRY 4.0.....	19
2.3 WIRE EDM CAPABILITIES.....	22
2.4 MACHINING STABILITY OF WIRE EDM.....	26
2.5 SOFT COMPUTING TOOLS TO PREDICT WEDM PERFORMANCE.....	29
2.6 PULSE TRAIN ANALYSIS AND CONDITION MONITORING OF EDM.....	32
2.7 CONDITION MONITORING AND PROCESS CONTROL OF WEDM.....	34
2.7.1 Classification of wire EDM discharge pulses.....	35
2.7.2 Fuzzy logic models for process control.....	37
2.7.3 Wire lag and vibration control.....	38

2.7.4	Online height estimation and control.....	40
2.7.5	Wire break prevention and adaptive control systems.....	41
2.8	SUMMARY AND MOTIVATION.....	46
2.9	RESEARCH OBJECTIVES.....	48
CHAPTER 3 – EXPERIMENTAL WORK.....		49
3.1	INTRODUCTION.....	49
3.2	PILOT EXPERIMENTS .....	49
3.3	MATERIAL SELECTION.....	49
3.4	EXPERIMENTAL SETUP .....	50
3.5	EXPERIMENTAL METHODOLOGY .....	57
3.6	SOFT COMPUTING MODELS .....	60
3.6.1	ANN classification.....	60
3.6.2	ANFIS modeling .....	62
3.7	LOW PASS FILTER.....	64
3.8	MEASUREMENT OF PERFORMANCE CHARACTERISTICS.....	65
3.8.1	Cutting speed .....	65
3.8.2	Surface roughness .....	66
3.8.3	Microstructural analysis .....	66
3.8.4	Profile accuracy .....	67
3.8.5	Surface morphology .....	68
3.9	SUMMARY .....	69
CHAPTER 4 – MACHINING STABILITY ANALYSIS .....		70
4.1	INTRODUCTION.....	70
4.2	EXPERIMENTAL DETAILS .....	71
4.3	GEOMETRIC ERRORS .....	73
4.3.1	Inaccuracy due to wire deflection .....	74
4.3.2	Inaccuracy due to wire vibrations .....	74
4.4	MACHINING OUTCOMES .....	75
4.4.1	Spark absence .....	75
4.4.2	Wire breakage .....	76
4.4.3	Continuous machining .....	77
4.5	SURFACE INTEGRITY AT DIFFERENT MACHINING STABILITIES ...	77
4.5.1	Surface morphology and surface roughness .....	78

4.5.2	Microstructural analysis .....	79
4.5.3	Geometric accuracy .....	80
4.5.4	Micro-hardness .....	81
4.5.5	Subsurface damage .....	83
4.5.6	EDS analysis .....	84
4.5.7	Wire electrode comparison .....	86
4.6	SUMMARY .....	87
CHAPTER 5 – OFFLINE MODELING OF WIRE EDM FAILURES .....		88
5.1	INTRODUCTION .....	88
5.2	PREDICTION AND ANALYSIS OF PROCESS FAILURES BY ANN CLASSIFICATION .....	88
5.2.1	Wire EDM process failures .....	88
5.2.2	Experimental details .....	91
5.2.3	ANN classification .....	93
5.2.4	Performance of classifier .....	98
5.2.5	Confirmation experiments .....	99
5.2.6	Wire breakage analysis .....	102
5.2.7	Surface integrity variations during normal machining .....	107
5.3	MODELLING MEAN GAP VOLTAGE VARIATION TO PREDICT WIRE BREAKAGES .....	110
5.3.1	Introduction .....	110
5.3.2	Experimental details .....	111
5.3.3	Mean gap voltage variation ( $\Delta V_m$ ) .....	113
5.3.4	ANFIS modelling of $\Delta V_m$ and wire break prediction .....	114
5.3.5	Human computer interaction – wire break alert .....	119
5.3.6	Confirmation experiments .....	119
5.3.7	Surface integrity analysis .....	122
5.3.8	EDS analysis of worn wire surface .....	124
5.4	IN-PROCESS FAILURE PREDICTION .....	126
5.5	SUMMARY .....	128
CHAPTER 6 – DEVELOPMENT OF SENSOR BASED CONDITION MONITORING SYSTEM.....		130
6.1	INTRODUCTION .....	130

6.2	EXPERIMENTAL DETAILS .....	130
6.3	PULSE TRAIN ANALYSIS .....	132
6.4	PULSE CLASSIFICATION AND CHARACTERISATION .....	133
6.5	PULSE CLASSIFICATION ALGORITHM .....	136
6.6	EFFECT OF INPUT PARAMETERS ON PULSE CHARACTERISTICS ..	137
6.7	EFFECTS OF DISCHARGE CHARACTERISTICS ON PROCESS PERFORMANCE .....	140
6.8	PULSE CYCLE BEHAVIOUR DURING PROCESS FAILURES .....	142
6.9	PREDICTIVE MODELLING OF PERFORMANCE CHARACTERISTICS .....	145
6.10	INTELLIGENT MACHINE FAILURE CONDITION PREDICTION SYSTEM .....	146
6.11	EFFECT OF ABNORMAL PULSES ON MICROSTRUCTURE .....	148
6.12	SUMMARY .....	150
CHAPTER 7 – FAILURE DETECTION AND PROCESS CONTROL.....		151
7.1	INTRODUCTION .....	151
7.2	EXPERIMENTAL DETAILS .....	151
7.3	SIGNAL PROCESSING AND PULSE CLASSIFICATION .....	152
7.4	RULE BASED MODEL FOR FAILURE DETECTION .....	154
7.5	MACHINE LEARNING APPROACH TOWARDS FAILURE PREDICTION AND PROCESS CONTROL .....	164
7.5.1	Artificial neural network classification .....	165
7.5.2	Performance of ANN classifier .....	166
7.5.3	Assessment of failure severity .....	167
7.5.4	Process control algorithm .....	168
7.5.5	Case studies .....	170
7.6	COMPARISON WITH EXISTING MODELS.....	176
7.7	SUMMARY .....	177
CHAPTER 8 – CONCLUSIONS AND FUTURE SCOPE .....		180
8.1	CONCLUSIONS.....	180
8.2	SCOPE OF FUTURE WORK .....	182
APPENDIX.....		183
REFERENCES.....		186

## LIST OF FIGURES

FIG. NO.	DESCRIPTION	PAGE NO.
Fig. 1.1	Elements of Industry 4.0 (Menezes et al., 2019)	2
Fig. 1.2	Condition monitoring system structure (Al-Habaibeh et al., 2004)	3
Fig. 1.3	Schematic of the Wire EDM process	6
Fig. 1.4	Schematic of material removal in Wire EDM (Hsieh et al., 2009)	7
Fig. 1.5	Discharge characteristics during an EDM cycle showing pulse on and pulse off cycles (Fabrizia Caiazza et al., 2015)	10
Fig. 1.6	Wire electric discharge machined components (a) Various profiles cut by wire EDM (Sommer and Sommer, 2017) (b) Miniature gear machined by WEDM (Zhidong et al., 2014) (c) WEDM cut firtree slot (Klocke et al., 2014a) (d) WEDM of firtree root slot (Soo et al., 2013)	12
Fig. 1.7	Comparison of spark gap condition (a) during stable machining (b) during unstable machining (Pan et al., 2017)	13
Fig. 1.8	Different types of discharge pulses observed in wire EDM pulse cycle	15
Fig. 2.1	Typical subcomponents of health and usage monitoring system (HUMS) (Janak and Hadas, 2015)	20
Fig. 2.2	Smart manufacturing system based on advanced data analytics (Yan, 2007)	22
Fig. 2.3	Fig. 2.3 Surface integrity of wire electric discharge machined firtree slot (Klocke et al., 2012)	24
Fig. 2.4	Regions of wire breakage (Arunachalam et al., 2001)	28
Fig. 2.5	Comparison of ANFIS predictions with experimental readings (Caydas et al., 2009)	31
Fig. 2.6	High speed EDM pulses (Zhang et al., 2020)	33
Fig. 2.7	Different types of wire EDM discharge pulses on a pulse train (Janardhan and Samuel, 2010)	36
Fig. 2.8	Wire lag effect (wle) for a workpiece of height 60 mm (Conde et al., 2018)	39
Fig. 2.9	Regions of machining stability (Kwon and Yan, 2006)	42

Fig. 2.10	Effect of pulse in time and current on wire break frequency (Kumar and Choudhury, 2011)	43
Fig. 2.11	Pulse classification (Kwon et al., 2015)	46
Fig. 3.1	Wire electric discharge machine setup	51
Fig. 3.2	Elcam software interface	51
Fig. 3.3	Differential probe	53
Fig. 3.4	Current probe and current probe amplifier	54
Fig. 3.5	Mixed domain oscilloscope	55
Fig. 3.6	Schematic of the condition monitoring setup	56
Fig. 3.7	Condition monitoring system installed on wire electric discharge machine	57
Fig. 3.8	Flowchart of the experimental plan	59
Fig. 3.9	ANN structure	61
Fig. 3.10	ANFIS structure	63
Fig. 3.11	(a) Unfiltered signal (b) Filtered signal	65
Fig. 3.12	Integrated computer displaying the cutting speed value during machining	65
Fig. 3.13	Surface profilometer	66
Fig. 3.14	Field emission scanning electron microscope setup	67
Fig. 3.15	Coordinate measuring machine	68
Fig. 3.16	Non-contact 3D profilometer	68
Fig. 4.1	Representation of debris accumulation in spark gap at machining condition (a) C1 (b) C2 (c) C4 (d) C6 (e) C7	72
Fig. 4.2	Shape of the profile machined	72
Fig. 4.3	Wire lag effect influencing geometric accuracy (Sanchez et al., 2007)	73
Fig. 4.4	Wire vibrations influencing geometric accuracy	74
Fig. 4.5	SEM images showing stages of wire wear (a) minimal wire wear (b) severe wire wear (c) broken wire tip	77
Fig. 4.6	Non-contact surface profilometer images at machining condition (a) C2 (b) C6	78
Fig. 4.7	Surface roughness at different machining conditions	79
Fig. 4.8	Microstructural comparison at different machining conditions (a) C2 (b) C3 (c) C4 (d) C5 (e) C6	80

Fig. 4.9	(a) Flatness error, (b) Circularity error, and (c) Cylindricity error at different machining conditions	81
Fig. 4.10	Subsurface microhardness profile	82
Fig. 4.11	Recast layer defects (a) C2 (b) C3 (c) C4 (d) C5 (e) C6	84
Fig. 4.12	EDS analysis of surface machined under condition (a) C2 (b) C6	85
Fig. 4.13	Geometric accuracy comparison considering different wire electrodes	86
Fig. 4.14	Effect of wire electrode coating on cutting	86
Fig. 5.1	Straight cuts machined by wire-EDM process	93
Fig. 5.2	(a) Datapoints belonging to multiple classes in 2D space (b) non-linear 2D decision boundaries separating the classes (Ghojogh and Crowley, 2019)	94
Fig. 5.3	Structure of multi-class neural network classification model	95
Fig. 5.4	Confusion matrix for classification model	98
Fig. 5.5	Scatter plot of normal machining classification probability vs input parameters	101
Fig. 5.6	Scatter plot of wire breakage classification probability vs input parameters	101
Fig. 5.7	Scatter plot of spark absence classification probability vs input parameters	102
Fig. 5.8	Categories of wire wear (a) minimal degradation (Exp. No. 10) (b) intermediate degradation (Exp. No. 13) (c) severe degradation (Exp. No. 15) (d) failed wire tip (Exp. No. 6)	104
Fig. 5.9	EDS images of worn zinc coated brass wire surface at (a) mild wire wear (Expt. No. 10) (b) sever wire wear (Expt. No. 15)	105
Fig. 5.10	FE-SEM images showing machined surface morphology after (a) Expt. No. 11 (b) Expt. No. 15	108
Fig. 5.11	Cross sectional view of machined surfaces under SEM after (a) Expt. No. 11 (b) Expt. No. 15	108
Fig. 5.12	Surface morphology comparison of machined surfaces using non-contact 3D profilometer images after (a) Expt. No. 11 (b) Expt. No. 15	109

Fig. 5.13	(a) Real-time gap voltage reading for a set voltage of 50 V (b) Gap voltage measurement by digital multimeter	111
Fig. 5.14	(a) Machine tool (b) Integrated computer displaying mean gap voltage	111
Fig. 5.15	Method of determining mean gap voltage variation	113
Fig. 5.16	Approach for predicting wire breakage	114
Fig. 5.17	Determination of mean gap voltage variation limit ( $\Delta V_{m, \text{lim}}$ )	116
Fig. 5.18	Surface plots showing the influence of process parameters on $\Delta V_m$	118
Fig. 5.19	Comparison of predicted values with actual values for $\Delta V_m$	119
Fig. 5.20	Logic flow diagram for wire break alert	120
Fig. 5.21	Confirmation tests comparison of ANFIS responses with experimental readings	121
Fig. 5.22	SEM images of machined surfaces with (a) low $\Delta V_m$ (b) medium $\Delta V_m$ (c) high $\Delta V_m$ prediction	123
Fig. 5.23	SEM images of wire surfaces with (a) low $\Delta V_m$ (b) medium $\Delta V_m$ (c) broken wire tip at high $\Delta V_m$ (Exp. No. 3)(d) broken wire tip (Exp. No. 4) (e) broken wire tip (Exp. No. 7)	124
Fig. 5.24	EDS analysis of wire surfaces with (a) low $\Delta V_m$ (b) medium $\Delta V_m$ (c) high $\Delta V_m$ prediction	125
Fig. 5.25	Method of determining mean gap voltage variation	126
Fig. 5.26	The steps involved in developing a Naive Bayes classification model	127
Fig. 5.27	Performance evaluation of the model (a) Confusion matrix (b) ROC curve	128
Fig. 6.1	Experimental setup for the pulse-train acquisition system	131
Fig. 6.2	Methodology of pulse train analysis	133
Fig. 6.3	Typical voltage and current pulse shape for a normal discharge	134
Fig. 6.4	(a) Normal discharge (b) Open circuit discharge	134
Fig. 6.5	(a) Arc discharge (b) Short circuit discharge	135
Fig. 6.6	Pulse classification algorithm	136
Fig. 6.7	Results of pulse classification on a 2 ms wire EDM pulse data	137

Fig. 6.8	Effect of pulse on time on discharge energy and pulse proportions	138
Fig. 6.9	Effect of servo voltage on spark frequency and pulse proportions	139
Fig. 6.10	Effect of pulse off time on short circuit spark ratio and spark frequency	139
Fig. 6.11	Effect of discharge energy on (a) cutting rate (b) Surface roughness	141
Fig. 6.12	Effect of short circuit sparks on surface roughness	142
Fig. 6.13	The pulse cycle behaviour before wire breakage	143
Fig. 6.14	The pulse cycle behaviour before process interruption due to spark absence	143
Fig. 6.15	(a) Discharge energy at various machining conditions (b) Spark frequency at various machining conditions	144
Fig. 6.16	ANN structure	145
Fig. 6.17	Regression plot for the trained ANN model	146
Fig. 6.18	Flowchart for intelligent machine condition prediction system	147
Fig. 6.19	Microstructural comparison of machined surfaces when short spark ratio is reduced by 16 %	149
Fig. 6.20	Microstructural comparison of worn wire surfaces when short spark ratio is reduced by 16 %	150
Fig. 7.1	Wire EDM condition monitoring setup	153
Fig. 7.2	Process control strategy	153
Fig. 7.3	Types of discharge pulses observed from the pulse chain	155
Fig. 7.4	The pulse cycle behaviour leading to wire breakage failure	155
Fig. 7.5	The pulse cycle behaviour leading to spark absence failure	156
Fig. 7.6	Flowchart of failure detection and control method	157
Fig. 7.7	Average values of pulse characteristics at different machining conditions	158
Fig. 7.8	Discharge pulse waveform (a) leading to wire breakage (b) after parameter tuning based on the control algorithm	161
Fig. 7.9	Discharge pulse waveform (a) leading to spark absence (b) after parameter tuning based on the control algorithm	161

Fig. 7.10	(a) Worn wire surface leading to wire breakage (b) broken wire tip (c) worn wire after process control	162
Fig. 7.11	SEM image of machined surface (a) under original settings (b) after process control	163
Fig. 7.12	Non-contact 3D profilometer image of machined surface (a) under original settings (b) after process control	163
Fig. 7.13	Effect of discharge energy on the surface roughness	164
Fig. 7.14	ANN classifier structure	166
Fig. 7.15	Confusion matrix showing classifier performance	166
Fig. 7.16	Remaining useful life (RUL) based on failure condition	167
Fig. 7.17	ANN regression plot	168
Fig. 7.18	Approach for wire EDM process control	169
Fig. 7.19	Flowchart of process control	170
Fig. 7.20	(a) Original settings (Conf test: Exp. No. 1) (b) Controlled settings	172
Fig. 7.21	(a) Severely degraded wire surface under original settings (b) Broken wire tip (c) Minimal wear after process control	173
Fig. 7.22	SEM images of machined surface (a) under original settings (b) after process control	175
Fig. 7.23	Effect of process control on surface roughness of machined components	175
Fig. 7.24	(a) Original settings (Conf test: Exp. No. 5) (b) Controlled settings	176

## LIST OF TABLES

TABLE NO.	DESCRIPTION	PAGE NO.
Table 3.1	Properties of Inconel 718 (Thakur, 2009)	50
Table 3.2	Chemical composition of Inconel 718 (Reed, 2006)	50
Table 3.3	Components of condition monitoring system for wire EDM	52
Table 3.4	High voltage differential probe specification	53
Table 3.5	Specifications of the current measurement system	54
Table 3.6	Specifications of the MDO 34 oscilloscope	56
Table 3.7	Parameters of ANN based multiclass classifier	62
Table 4.1	Process parameter combinations based on machining stability	71
Table 4.2	Machining outcomes under different machining conditions considered	75
Table 5.1	Classification of machining outcomes	91
Table 5.2	Process parameters and levels	92
Table 5.3	Constant machine parameters	92
Table 5.4	Accuracies of different ANN structures	95
Table 5.5	Experimental results	96
Table 5.6	Results of confirmation experiments	99
Table 5.7	Details of machining process failure situations	106
Table 5.8	Surface roughness comparison for 'Normal machining' in confirmation tests	109
Table 5.9	RSM input parameters and levels	112
Table 5.10	Constant machining parameters	112
Table 5.11	Experimental readings and model predictions	115
Table 5.12	ANFIS training parameters	117
Table 5.13	Parameters of gaussian membership function	117
Table 5.14	Confirmation experiments	120
Table 5.15	Wire break intimation based on ANFIS model predictions	121

Table 5.16	Classification of mean gap voltage variation	122
Table 5.17	Part quality comparison at different $\Delta V_m$ predictions	123
Table 5.18	Comparison of classifier performances	127
Table 6.1	Process parameters and levels	131
Table 6.2	Extracted discharge features and recorded responses	141
Table 6.3	Results of confirmation experiments	148
Table 6.4	Performance comparison of predictive models	149
Table 7.1	Process parameters and levels	152
Table 7.2	Parameters maintained constant	152
Table 7.3	Extracted discharge characteristics leading to wire break failure	157
Table 7.4	Extracted discharge characteristics leading to spark absence failure	158
Table 7.5	Comparison of machining outcomes before and after process control	160
Table 7.6	Parameters of neural network multiclass classifier	165
Table 7.7	Machining outcome and RUL predictions during confirmation tests	171
Table 7.8	Effects of process control	174
Table 7.9	Comparison of existing wire EDM monitoring models	178

## LIST OF SYMBOLS AND ACRONYMS

ANN	: Artificial Neural Network
ANFIS	: Adaptive Neuro Fuzzy Inference System
ANOVA	: Analysis of Variance
ASR	: Arc Spark Ratio
CCD	: Central Composite Design
CM	: Continuous Machining
CMM	: Coordinate Measuring Machine
CNC	: Computer Numeric Control
CS	: Cutting Speed
DOE	: Design of Experiments
EDM	: Electric Discharge Machine
EDS	: Energy Dispersive X-Ray Spectroscopy
DE	: Discharge Energy
MRR	: Material removal Rate
NSR	: Normal Spark Ratio
OSR	: Open-circuit Spark Ratio
R <sub>a</sub>	: Surface Roughness
SA	: Spark Absence
SF	: Spark Frequency
SSR	: Short-circuit Spark Ratio
SV	: Servo Voltage
WB	: Wire Break
$\Delta V_m$	: Mean Gap Voltage Variation
T <sub>d</sub>	: Ignition delay time

# CHAPTER 1

## INTRODUCTION

In the past few decades, the manufacturing industries have become smarter and more capable in terms of automation, artificial intelligence integration and self-reliance. Fully automated manufacturing systems aimed at ‘zero defect manufacturing’ has become the need of the hour, which is made possible by advanced artificial intelligence (AI) integration combined with multi-sensory approach. Machining downtime is drastically getting reduced by developing condition monitoring and control systems for manufacturing processes. Condition monitoring systems are aimed at reducing material and energy utilization, inspection costs and equipment downtime.

### 1.1 INDUSTRY 4.0 AND SMART MANUFACTURING

Industry 4.0 refers to a new concept in manufacturing sector where the physical production is combined with digital technology. It is a data driven collaborative approach, which uses data analytics to enhance the process performance. It allows the manufacturing systems to collect, process and analyse data to monitor and optimize the production process. The vision of Industry 4.0 is to have fully automated manufacturing facilities through intelligent data driven systems. It comprises of internet of things (IoT), artificial intelligence (AI) and cloud computing (Menezes et al., 2019). The key elements of Industry 4.0 are given in Fig. 1.1. The fourth industrial revolution is also known as ‘Smart manufacturing’. Real-time decision-making capabilities are integrated to such systems through machine learning to make the processes more flexible, adaptable and failure free (Yan et al., 2017).

Internet of things is a concept where the physical objects or digital devices can share data with each other through internet without human intervention. In a smart industry, such shared data can be utilized to understand trends before

certain events and can aid in monitoring, prediction and control of events like machine breakdown or failure (Huang et al., 2018). Artificial intelligence is the science that deals with intelligence exhibited by machines, similar to natural intelligence possessed by the humans. Through AI, machines are equipped with the capacity to learn from their past experiences. Intelligent machines are capable of performing predictions and adaptive control, based on the past learnings. In artificial intelligence, soft computing or computational intelligence is referred to those computational techniques which are capable of finding approximate solutions to extremely complex problems. Machine learning (ML) is a subdiscipline of soft computing which deals with the development of algorithms that emulate human learning. Such algorithms are capable of making decisions and predictions, based on their learnings from a training data. ML is classified into supervised and unsupervised learning techniques based on whether the desired output is explicitly fed with the training data. Integration of artificial intelligence has enabled the concepts of process control, condition monitoring and machine health prognostics in modern manufacturing industries (Wang et al., 2018).

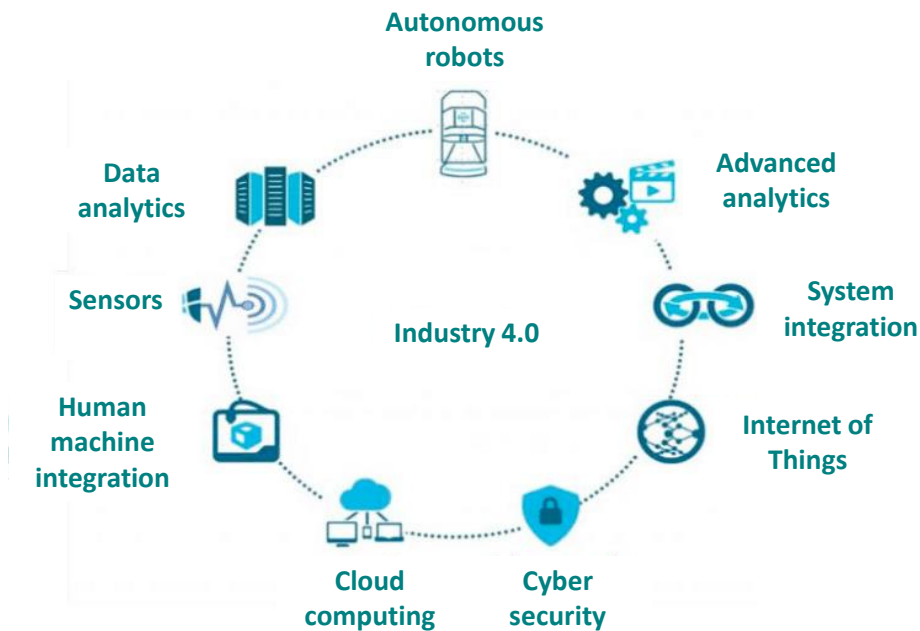


**Fig. 1.1** Elements of Industry 4.0 (Menezes et al., 2019)

## 1.2 CONDITION MONITORING OF MANUFACTURING PROCESSES

Condition monitoring (CM) of manufacturing process is one of the primary research focuses in industry for the last few decades. Process condition monitoring aims at higher productivity, lower cost of production and higher part quality (Al-Habaibeh et al., 2004). Condition monitoring involves keeping track of various features which can indicate the health status of a manufacturing process. The features are ideally extracted from raw sensor signals of a physical quantity like temperature, force, vibration, sound, voltage, current etc. The physical quantities to be sensed and the feature to be extracted are selected suitably based on the process and application. Condition monitoring system performs early detection of process failures before any serious damage is caused to the tool or machined parts. The early detection provides an option to perform some corrective measures to rectify the potential damages. The remedial actions include tool change, parameter tuning, or other process control measures. Basic structure of a condition monitoring system is given in Fig. 1.2.

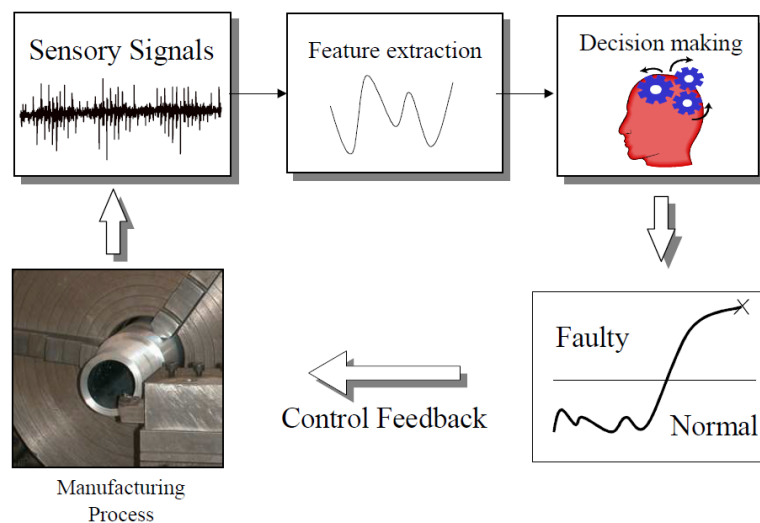


**Fig. 1.2** Condition monitoring system structure (Al-Habaibeh et al., 2004)

Typical steps in the development of a condition monitoring system are as follows:

- **Selection of sensors:** Sensor selection is based on the type of manufacturing process and condition monitoring methodology. There is a wide choice of

sensors to select from, such as acoustic sensors, current sensors, voltage sensors, accelerometers etc.

- **Signal processing:** The process involves modifying the acquired raw signals to enhance its characteristics for proper analysis. It involves techniques like filtering, amplifying etc.
- **Feature selection and extraction:** The step involves deciding and extracting the relevant features from the processed signal which can indicate the process health. The step is extremely critical since it involves identifying the features that correlates process health (tool state in the case of machining) and process conditions.
- **Developing a decision making or support system:** Based on the extracted features, various decisions are to be taken by the intelligent system to maintain the process stability. The decision model's task is to predict the machine health condition based on extracted features, so that remedial actions can be taken to prevent the undesirable outcomes.
- **Process monitoring:** Based on the features extracted in real-time, various inferences are drawn regarding the process health. The real-time process monitoring relies on the decision-making system to diagnose the process condition.
- **Adaptive control:** The step where the machine regulates the process conditions to restore the normal working conditions based on the support system recommendations.

The monitoring of conventional manufacturing process involves keeping track of a physical quantity which arises from tool and workpiece physical interaction. Usually cutting force, temperature, vibratory, and acoustic signals are monitored using sensors to assess the machine health in this case. Tool wear, tool breakage, chatter etc. are identified using the monitoring systems (Ong et al., 2019). On the contrary, monitoring of non-traditional manufacturing process involves several additional challenges since the physical interaction between the tool and workpiece is absent. Such processes involve thermal, chemical, and electro thermal material removal mechanisms. Here, extremely high sampling rate

sensors and acquisition system are required to capture the process characteristics, like in the case of electric discharge machining process, where spark discharges happen in kHz range. To monitor such a process, high bandwidth sensors, and high sampling rate data acquisition system are required. Such a setup will generate a huge amount of data in real time, which makes the signal processing and computation extremely challenging.

The presented work aims to develop a condition monitoring system for wire electric discharge machining process. More about the process is discussed in the upcoming sections.

### **1.3 WIRE ELECTRIC DISCHARGE MACHINING**

The development of high-performance materials like superalloys with improved mechanical properties even at elevated temperatures demands equally advanced manufacturing processes to machine them. Traditional machining of super alloys has proven to be extremely difficult due to the formation of build-up edge, cold working nature of the work material, and rapid tool wear. Electric discharge machining (EDM) is a non-traditional machining process that possesses several advantages over the conventional processes to machine ‘difficult-to-cut’ materials like Ti alloys and superalloys due to the non-contact nature of material removal (Ho et al., 2003). The process was developed in 1940s using resistor–capacitor (RC) circuit to machine hard materials like tungsten. Wire EDM, developed in 1960s, is a specific variant of EDM where the required profile is cut by a travelling wire electrode through controlled and repetitive sparks (Ho et al., 2004). This process is an extremely attractive option to machine superalloys into any complex and intricate shapes. The process is capable of machining any electrically conductive materials irrespective of their hardness, with excellent surface finish, minimal cutting forces, and residual stresses (Mandal and Dixit, 2014).

Wire electric discharge machining (wire EDM) is a non-traditional non-contact machining process. The process uses a thin metallic electrode to cut through any conductive materials irrespective of its hardness. This is an electro thermal

process which uses heat energy from electric sparks to melt and vaporize the workpiece material. Since the material removal happens from both the workpiece and wire electrode, fresh wire is continuously fed into the machining zone from a wire spool. A small gap, called inter electrode gap or spark gap, is maintained between the wire and workpiece which is filled with dielectric fluid. In the case of wire EDM, the preferred choice of dielectric is deionised water. The dielectric is flushed through upper and lower nozzles to the machining zone. The dielectric fluid also helps in cooling the workpiece and in removing the debris and gas bubbles from the machining zone. The wire translates with respect to workpiece in a CNC coded profile to machine the required shape. The non-contact material removal mechanism, combined with CNC coded profile, makes wire EDM capable of machining any complex and intricate profiles on even the hardest materials. The process is very precise, flexible and accurate, dimensionally and geometrically (Ho et al, 2004; Jain, 2009). Fig. 1.3 shows the wire EDM process schematic.

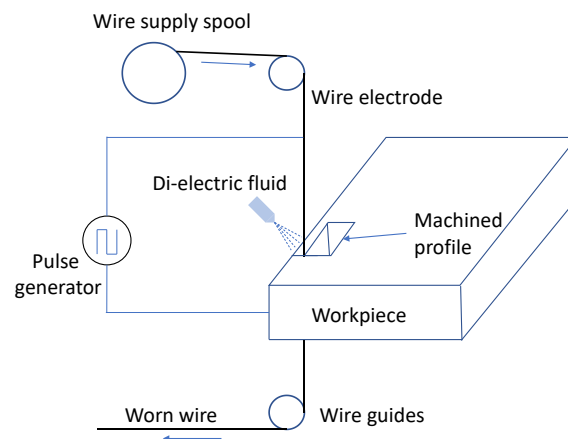


**Fig. 1.3** Schematic of the Wire EDM process

### 1.3.1 Working principle of wire EDM

The working principle of wire EDM is governed by and repetitive electric discharges. Workpiece and wire electrode are connected to the positive and negative terminal respectively. A dielectric fluid occupies the small gap between the electrodes. A transistor-controlled pulse generator supplies pulsed DC voltage with alternating on and off cycles. Discharge and material removal happens

during the pulse on time. Pulse off time is utilized to restore the dielectric properties and to clear the debris (resolidified molten material). Once the DC voltage is applied across the wire and workpiece electrodes, ionization of the dielectric fluid will be initiated in a channel of least inter electrode distance. Ionization occurs when the electrons from the wire electrode collides with dielectric molecules when they are accelerated towards the workpiece. The free electrons thus produced in the inter electrode gap moves towards the workpiece and the positive ions will move towards the wire electrode. Ionization progresses with time, and this narrow channel of free electrons and ions are called discharge channel. The resistivity of the discharge channel reduces with ionization and a point is reached where the dielectric barrier is breached and the fluid becomes conductive. Then a sudden discharge happens from the wire electrode towards workpiece through a plasma channel, vaporising the dielectric and melting the electrodes. Since the kinetic energy of fast-moving electrons are more compared to ions, higher material removal happens at the workpiece side compared to the electrode side. The temperature at the plasma channel can reach up to 10000 °C, which is high enough to melt any electrically conductive material. When the applied voltage is released, the plasma channel collapses, resulting in high pressure waves which ejects out the molten material from the spark region leaving a crater on the workpiece surface. Fig. 1.4 shows the material removal mechanism through discharge sparks.

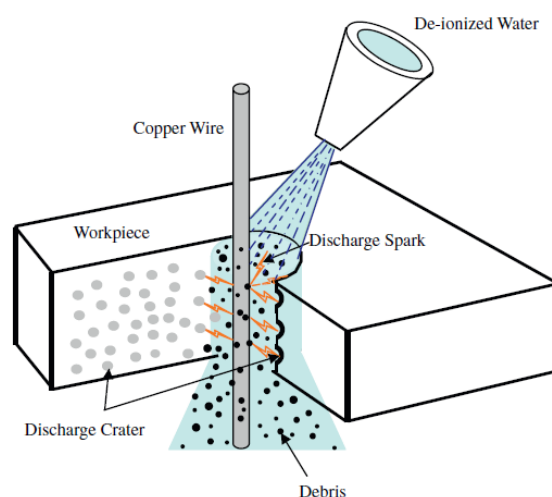


**Fig. 1.4** Schematic of material removal in Wire EDM (Hsieh et al.,2009)

The expelled molten material, resolidifies instantly and these solid particles are called debris. The debris and the vapor bubbles are flushed away from the machining zone by the dielectric fluid in the pulse off duration. Some of the molten materials are resolidified back to the machined surface forming an undesirable recast layer. The ideal process mechanism involves breaking and restoring the dielectric properties during the pulse on and off cycles repeatedly (Jain, 2009).

### **1.3.2 Wire material**

Wire material has a huge influence on the process performance. The wire electrodes vary in type, strength and size. Various types of wire electrodes generally used in wire EDM are discussed in this section.

***Uncoated brass electrode:*** The brass wire electrode, is considered as a good option for wire electrode material since brass is a very good electrical conductor. It can withstand tension better than pure copper wire, which was used earlier before brass wires were popularised. These wire electrodes give good surface finish and accuracy. These wires are also cost effective (Ramamurthy et al., 2015).

***Zinc coated brass electrode:*** Zinc coated brass electrode contains zinc coating of 20  $\mu\text{m}$  to 30  $\mu\text{m}$  thickness on a brass core. The coated electrodes are introduced to improve the cutting rate and accuracy of wire EDM process. Since the coated material is comparatively more volatile than the core, the coating gets vaporised relatively faster during the sparking operation. Due to a heat sink effect the inner core is protected from the thermal shock and the core material experiences a cooling effect. Thus, the coated wires can withstand higher discharge energy, resulting in faster cutting. Additionally, when the coating is vapourised, the instantaneous spark gap increases, thereby improving the flushability (Maher et al, 2014).

Apart from these varieties, there is diffused wire, produced by heat treating the coated wire. The wire electrodes are also available in hard (high tensile wires), half hard, or soft (low tensile) varieties, based on their tensile strengths. Hard

wires have a tensile strength of  $900 \text{ N/mm}^2$ , whereas half hard or soft wires have a tensile strength of  $400 \text{ N/mm}^2$ . Hard wires are used for straight accurate cuts, while soft wires are used for taper cutting (Prohaszka et al, 1997).

### 1.3.3 Control parameters

Right selection of process parameters is critical for any manufacturing operation since unideal process parameter settings can lead to reduced surface integrity or productivity. For wire EDM, knowledge about parameter settings is even more important since the improper selection of parameters can lead to process failures by wire breakage. The current wire EDM machine has the capability to adjust the following process parameters.

**Pulse on time:** Pulse on time is defined as the time duration during which the voltage is applied between the electrodes. During the pulse on time, a portion of the duration is consumed for ionizing the dielectric. This time period before the discharge is called ignition delay time. Remaining portion of pulse on time is the discharge duration, where the material removal takes place through melting and vaporisation of workpiece. Ideally, higher pulse on time is accounted for greater material removal and vice versa.

**Pulse off time:** Pulse on time is followed by pulse off time, defined as the time duration during which the DC voltage across the electrodes is turned off by the pulse generator. This off period is utilized by the machine to clear the debris and thus to restore the dielectric properties in the spark gap. Insufficient pulse off time can lead to partial clearing of debris leading to machining instabilities.

**Servo voltage:** Servo voltage controls the inter electrode gap using an inbuilt gap control system. The servo voltage is the average interelectrode voltage set by the operator, based on which the spark gap distance is maintained by an in-built servo feedback mechanism. Higher the servo voltage, larger is the spark gap and vice versa. During the spark erosion, as the workpiece material is getting removed, the spark gap increases momentarily increasing the average voltage between the electrodes. When this happens, the average inter electrode voltage crosses the servo voltage value to a higher value. Then the gap controller advances the wire

electrode towards the workpiece in such a way that the average gap voltage is brought back to the servo voltage parameter value.

**Wire feed rate:** During the spark erosion process, the material gets removed from both the workpiece and wire electrode. To prevent wire breakage due to this rapid wear, fresh wire is continuously supplied to the machining zone from a wire supply spool. The rate of supply of fresh wire from the spool is given by the wire feed rate. Lower than ideal wire feed rate can cause simultaneous sparks from same wire spot resulting in wire breakage. Higher than required wire feed rate causes wastage of wire electrode.

**Pulse current:** Pulse current is the average discharge current per pulse cycle. Wire EDM machines normally allows the pulse current to be varied in two modes, power mode for rough cut operation, and fine mode for trim cut operation respectively. Power pulse mode is used for regular profile cutting, whereas fine mode is employed to remove the recast layer and for a better part quality. During finishing operation, the peak pulse current is 10 A. During the rough-cut operation, the peak pulse current can reach 40 A.

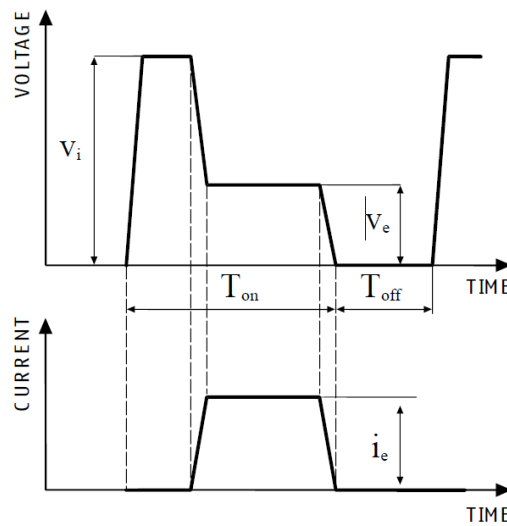


**Fig. 1.5** Discharge characteristics during an EDM cycle showing pulse on and pulse off cycles (Fabrizia Caiazzo et al., 2015)

**Flushing pressure:** The flushing pressure controls the dielectric flushing pressure from the top and bottom nozzles. The dielectric fluid flushing pressure

can be varied in a wire EDM. Higher pressure is selected during the roughing operation for effective removal of debris from the spark gap. During trim cut, lower pressure is sufficient due to lesser amount of debris. Also, then the higher pressure can cause geometric inaccuracies (Sharma et al., 2015).

Depending on the EDM machine, several other parameters like wire tension can be tuned manually. The discharge characteristics showing the discharge current, discharge voltage, pulse on and pulse off time are given in Fig. 1.5.

#### **1.3.4 Applications of Wire EDM**

Wire EDM is used to cut complex and intricate profiles in difficult to cut conductive materials. The process can machine hard, brittle and fragile parts alike, since it offers near zero cutting forces due to non-contact cutting action. Typical applications include machining of fixtures, cams, gauges, gears, punches and dies. The process is also used to produce micro electrodes for micro EDM, micro USM etc. Several advancements have been made in the past decade to enhance the surface integrity of wire EDM machined components to replace conventional machined components in aerospace applications. Wire EDM is an attractive alternate to replace the broaching operation to machine fir tree slots and fir tree roots in turbine blades and discs (Klocke et al., 2014; Anurag, 2018). Fig. 1.6 shows a few wire EDM cut components to showcase the process capabilities.

#### **1.3.5 Process stability of wire EDM**

Process stability of wire EDM depends greatly on the spark gap condition. Typically for a wire EDM process, it is expected that the debris and gas vapours produced during the discharge cycle is flushed away from the inter electrode volume during the pulse off cycle. In such a situation, the dielectric breakdown during the discharge is followed by restoration of electric properties of dielectric fluid (Kawata et al., 2017). The current discharges are preceded by an ignition delay time, which is the time taken for ionization of dielectric fluid till it becomes conductive. Such discharges repeat themselves, each spark accounting for material

removal in the form of a crater, to effectively machine the workpiece in the required profile.

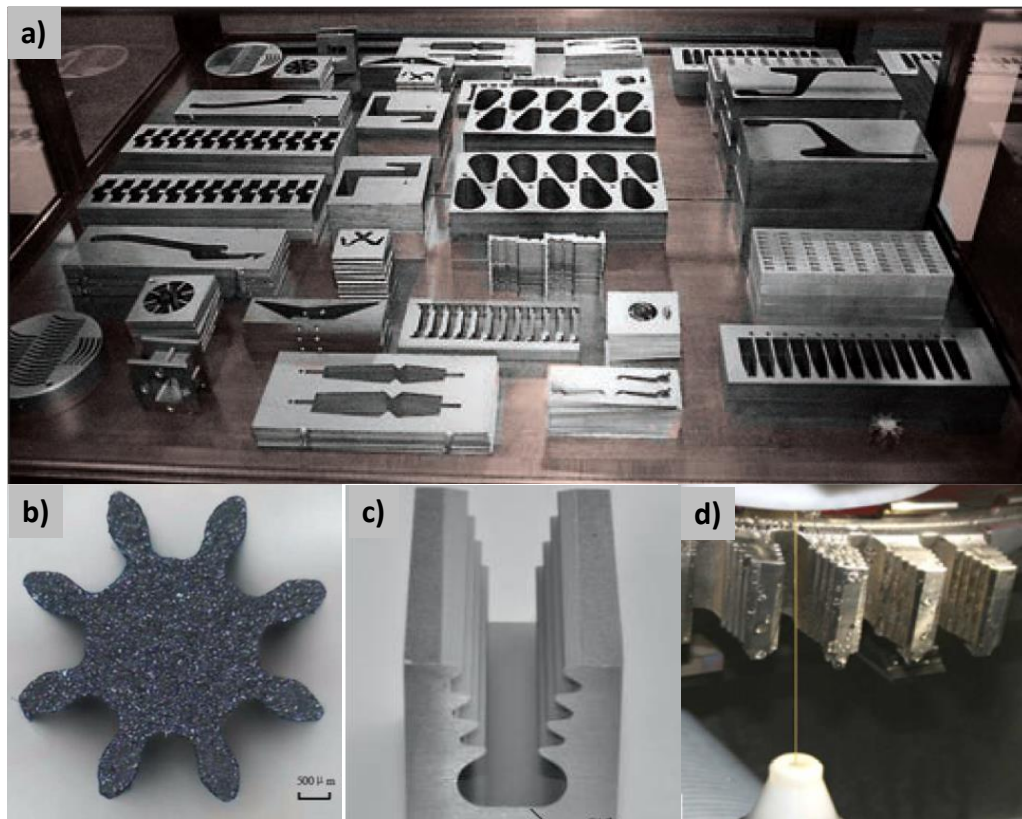


**Fig. 1.6** Wire electric discharge machined components

- (a) Various profiles cut by wire EDM (Sommer and Sommer, 2017)
- (b) Miniature gear machined by WEDM (Zhidong et al., 2014)
- (c) WEDM cut firtree slot (Klocke et al., 2014a)
- (d) WEDM of firtree root slot (Soo et al., 2013)

The above-mentioned discharge cycle behaviour is an idealized concept, typically used to explain the process mechanism of wire EDM. However, in most practical cases, the debris generated are only partially removed by the flushing action of dielectric. Under certain extreme circumstances, the debris can get accumulated in the spark gap, causing permanent stagnation and spark gap bridging. Machining conditions that promote the debris stagnation are considered as unstable conditions. The severity of the instability and its implications depends upon how fast the debris is getting accumulated. Unstable process conditions can

lead to coarser surfaces, poor surface integrity, part damages and process interruption through wire breakages (Descocudres, 2006). Fig. 1.7 demonstrates the comparison between spark gap condition for a stable and unstable machining.

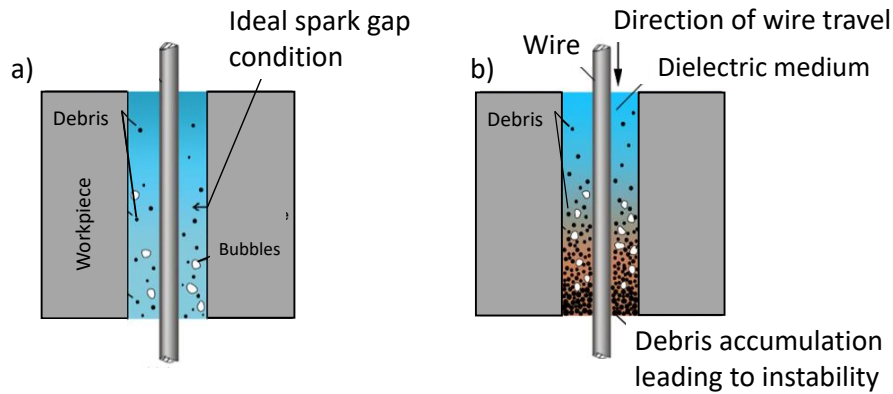


**Fig. 1.7** Comparison of spark gap condition (a) during stable machining (b) during unstable machining (Pan et al., 2017)

Duty cycle is defined as the ratio of pulse on time to total cycle duration. Selection of duty cycle plays an important role in deciding the machining stability. As the duty cycle increases, possibility of debris accumulation in spark gap is more. This is because, at higher duty cycle, amount of debris is more, but the time to flush away the debris is less. Another determining factor is the spark gap distance. The chances of stagnation are more in a narrow spark gap, compared to a wider one. Process can also be unstable if the dielectric fluid pressure is less than ideal to force the debris out from the spark gap, especially during a rough-cut operation. Apart from the above discussed control parameters, several other factors also contribute to the process instability. The higher order interactions between the parameters, can make the process unstable. Also, the uncontrollable external factors like wire vibration, ambient temperature, wire EDM vibrations, etc. causes stochastic conditions in the spark gap (Fan and Bai, 2018). In short, the mechanism of machining failures caused by process instabilities is a complex and unpredictable phenomenon. An accurate model relating the control parameters and process failures is thus difficult to develop. A better way to analyse

machining stability would be to look into the discharge characteristics which is discussed in the following subsection (Bergs et al., 2018).

#### ***1.3.5.1 Types of discharge pulses***

Four types of discharges can happen between the wire electrode and workpiece. Voltage and current pulse cycles are both required to differentiate between the discharge pulses. Fig. 1.8 shows the various discharge pulses.

***Normal discharge:*** The normal spark discharge is the one where discharge current occurs after an ignition delay period. It is the ideal discharge expected from a typical wire EDM pulse cycle. At the end of ignition delay period, voltage drops down and discharge current raises, when the conductive a plasma channel is formed. An optimal ignition delay period implies the proper restoration of dielectric properties after each discharge.

***Arc discharge:*** Arc discharge is characterised by a short ignition delay time. This implies presence of debris in the spark gap. Arc discharges are regarded as undesirable for a good surface integrity, since arcing can result in rougher surfaces and surface damages. However, often at higher cuttings rates, arc discharges are as common as the normal discharges.

***Short circuit discharge:*** The short circuit discharge happens during physical contact of wire electrode and workpiece. The phenomena of formation of plasma channel are thus absent in this case. Here, the circuit is completed physically via bridging of spark gap by the stagnant debris. Therefore, as soon as the voltage is applied, discharge happens between the electrodes without any ignition delay. Since the discharge is by physical contact, the voltage elevation is not seen for short circuit discharges. Short circuit pulses are regarded as the chief causes of wire breakages and surface damages, and shall be avoided to ensure stable and continuous machining.

***Open discharge:*** Open circuit discharges are misdischarges where the discharge current is absent for the entire duration of pulse on time. Open discharges can happen due to many reasons. If the applied voltage is not high enough for the

dielectric breakdown, or the pulse on time is too less to complete the ionization, or the spark gap is too high, the current discharge will not happen. Open discharges are not categorised under harmful discharge since it does not cause any part damage. But such discharges shall also be controlled to improve the process efficiency since the higher proportion of open circuit discharges can bring down the productivity (Liao and Woo, 1997; Osswald et al., 2015).

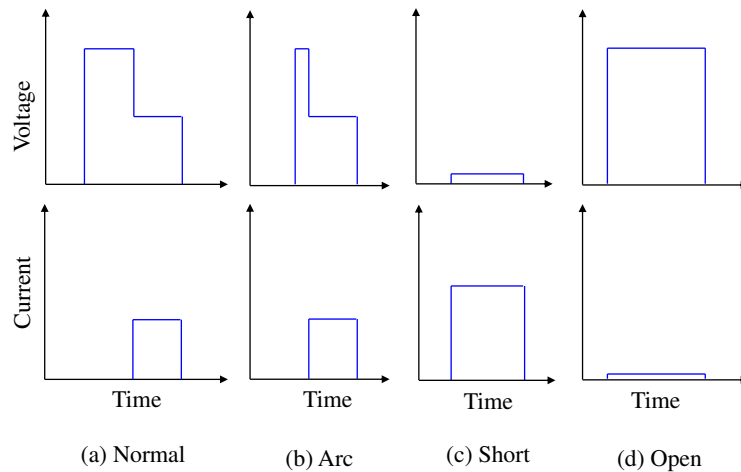


**Fig. 1.8** Different types of discharge pulses observed in wire EDM pulse cycle

### 1.3.5.2 Process failures

Process failures are those situations which cause material wastage, part damage, process interruption or energy wastage during a manufacturing process. In this regard, wire EDM process fails during wire breakages and spark absence. Predominance of arc and short circuit sparks are considered as the main reasons for wire breakage. Wire breakage causes process interruption and can cause part damages and material wastage. Often the wire breakage is associated with permanent surface damage in the workpiece too. Even if the damage is negligible, resuming the machining operation after rethreading can cause burrs and surface marks. Wire breakage also hinders the overall productivity and causes energy wastage since the time for rethreading is unproductive. Frequent wire breakages demand manual intervention and it affects the process automation. Another process interruption is spark absence situation, where the spark frequency reduces to zero soon after the commencement of machining. This situation also affects

the productivity and cause wire material wastage, and energy wastage. Open circuit discharges discussed in the previous subsection is regarded as the main cause of this failure (Cabanés et al., 2008; Gamage et al., 2016).

#### **1.4 CONDITION MONITORING OF WIRE EDM**

Wire EDM condition monitoring is aimed at preventing process failures like wire breakages and spark absence to ensure the required part quality. The monitoring system consists of suitable sensors to measure certain process data, which can indicate the machine health condition. The machine health indicators are the extracted features from the raw data, which can give information about the future process failures. Condition monitoring systems are extremely customizable due to the wide variety of sensors available to measure various physical quantities. Current sensor, voltage sensor, acoustic sensor, vision-based sensors, infrared camera, accelerometer are some of the sensors employed to develop wire EDM condition monitoring systems. Real time data from the sensors are sent to a workbench or computer system through an analog to digital converter (ADC). The signals are typically filtered to avoid noises and for easier extraction of relevant features. The extracted features will act as wire EDM process health indicators. Most of such systems predict wire breakages process interruptions. Advanced adaptive control systems can take preventive measures in case failures are predicted. The process control is performed by tuning one or more control parameters to restore the machining stability.

#### **1.5 OUTLINE OF THE THESIS**

To develop a condition monitoring system for the wire EDM process, the current study is divided into eight chapters. The brief summary of the chapters is given below.

#### **CHAPTER 1**

The chapter introduces the concept of smart manufacturing and the significance of machine condition monitoring in it. Basics of wire EDM process, including the mechanism, control parameters, capabilities, and process challenges are

discussed. Different kinds of wire EDM process failures and the reasons behind them are discussed. The idea and various steps involved in wire EDM condition monitoring are presented.

## **CHAPTER 2**

The chapter comprehensively discusses the state of the art in the field of wire EDM condition monitoring. The literature that deals with wire EDM process optimization, soft computing techniques, machine condition monitoring, wire EDM condition monitoring are discussed as various subtopics. Based on the literature review, the research gap and motivation are described. Finally, the chapter concludes by presenting the research objectives.

## **CHAPTER 3**

The details of the experimental work are discussed in this chapter. Initially, the basic experimental setup, material selection, experimental design and soft computing techniques are discussed. The chapter also details the features of sensors and acquisition system to setup the proposed condition monitoring system. The overall experimental plan of the research is presented next. Finally, different instruments and equipment used to analyse and measure wire EDM performance are described.

## **CHAPTER 4**

Analysis of machining stability of wire EDM is presented in this chapter. Process stability is varied in different stages and the process performance and failure mechanism is analysed. Two types of process failures, wire breakage and spark absence are discussed in detail. Surface integrity of machined components at different levels of process stability are also analysed.

## **CHAPTER 5**

The chapter deals with development of soft computing models to classify and predict process failures. ANN classification is employed to classify the machining outcomes into process failures and continuous uninterrupted

machining. Additionally, an ANFIS model is developed to predict mean gap voltage variation, based on which wire breakages can be predicted. These computationally fast offline techniques are used to set initial process parameter settings, before the start of condition monitoring.

## **CHAPTER 6**

The chapter discusses the setting up of process monitoring system using current and voltage sensors. Based on the extracted features, a pulse classification algorithm is developed to categorise the wire EDM pulses into normal sparks, arc sparks, short circuit sparks, and open circuit sparks. The effect of process parameters on discharge characteristics are discussed. The pulse train behaviour during normal machining and failure conditions are compared and analysed.

## **CHAPTER 7**

An algorithm for failure prediction and control is proposed in this chapter. The prediction is based on extracted features from raw signals. The severity of the predicted failures is assessed, based on which process parameters are retuned by the control algorithm. The process performance is also predicted with better accuracy using in process data and input parameters as model input.

## **CHAPTER 8**

This chapter concludes the major findings from the research study on the development of condition monitoring system for wire EDM process. Also, the future scope of research is presented.

## CHAPTER 2

### LITERATURE REVIEW

#### 2.1 INTRODUCTION

This chapter reviews the contribution of researchers in the field of condition monitoring of wire EDM. The significance of machining stability of wire EDM on process performance and wire break failure is discussed initially. Then, various soft computing predictive models for wire EDM process is reviewed. Various research works on machine condition monitoring systems are discussed briefly, after which an elaborate discussion on wire EDM condition monitoring is presented. The section covers the state-of-the-art pulse classification techniques, fuzzy control models, wire vibration control models, and wire break detection and control systems. Further, the existing adaptive control techniques for wire EDM process is reviewed. The chapter concludes by discussing the research motivation and listing the objectives of this study.

#### 2.2 IMPACT OF INDUSTRY 4.0

The synthesis of cyber and physical systems (CPS) has given rise to the fourth industrial revolution. In this ongoing trend, the physical manufacturing systems works in union with advanced communication and computational technologies like internet of things, artificial intelligence, cloud computing, big data analytics, advanced sensor technologies, automated process monitoring, control and inspection systems etc. The industry 4.0 involves smart design, smart manufacturing, smart monitoring, smart inspection, smart scheduling, and logistics. Literature covering these aspects are briefly reviewed in this section.

**Smart design:** Conventional product design has given way to advanced systems of product realization and visualization like virtual reality, augmented reality, 3D printing etc. A design developed in CAD environment can be visualized in three dimensions using a suitable AR/VR device. The prototyping, assembly,

inspection and testing can now be conducted in the advanced interactive virtual environment before the prototype is actually built. This gives the designers endless opportunities to visualize, share, test and calibrate the design before design finalization (Ong et al., 2008). 3D printing has grown in its capabilities and have become cheaper allowing the designer to directly conceive the actual product from a CAD drawing, which accelerates the prototyping and testing stages (Bogue, 2013).

**Smart machining:** The concept involves integration of several smart machines and components that communicate with each other. Smart machine tools are sensor equipped, capable of collecting and communicating data in real time. All the physical objects involved in a smart machining system are identifiable, and can communicate with one another through a uniform data code. MTCConnect is one such standard communication code for easier data collection and sharing. The machining data statistics and reports are generated and stored using standard management tools like enterprise resource management (ERP) (Zeng et al., 2018). This eases data handling and analysis. The real time manufacturing data, combined with the historical data, assists in machine health prognostics. Through the in-process data and augmented reality, the machining status can be virtually visualised, enabling smart interactions and decision making by the operator. Smart machines are also capable of real time process optimization and quality control (Park and Tran, 2014).

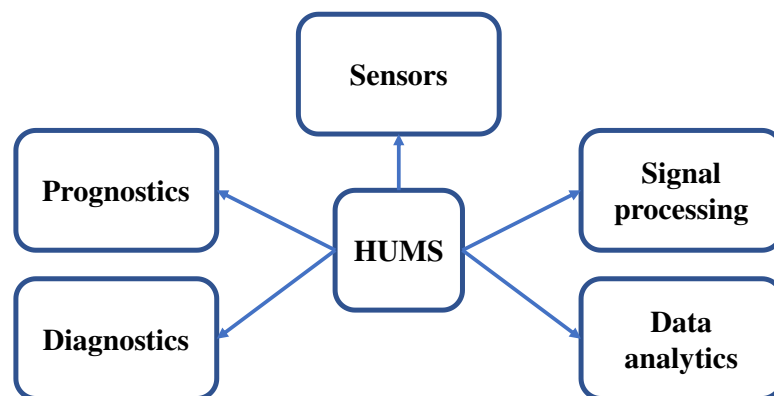


**Fig. 2.1** Typical subcomponents of health and usage monitoring system (HUMS) (Janak and Hadas, 2015)

**Smart process monitoring and control:** Smart monitoring involves real time sensing of manufacturing data containing information about machine health and performance. Sensor technology has advanced in flexibility and capability in recent times. Sensors are available in different bandwidth and measuring ranges to measure various physical quantities like temperature, force, vibration, acoustics, voltage, and current (Zeng et al., 2018). Vision based sensors have opened an entirely new research area for process monitoring through image processing. Smart monitoring systems has the following capabilities (Cheng et al., 2010):

- Alerting the user about a potent failure
- Minimizing the maintenance time and expenses
- Minimizing the downtime of manufacturing system
- Collect, process, and store data to expand the knowledge base for better decision making in future

Main components of a smart monitoring system as proposed by Hadas (2015) is given in Fig. 2.1. Lee et al. (2014) observed that advanced monitoring system senses the real time machining data and based on the machine health, feedback signals are sent to the controller for online parameter tuning. Such a system can prolong machine operation through data driven, intelligent decision making. Multi sensor fusion is utilized by advanced monitoring systems to simultaneously collect and analyse multiple sensor data to make a better-informed decision (Zhu, 2019). Xia et al. (2018) proposed a convolution neural network-based monitoring system to process multi sensor data. The proposed method was found superior in performance compared to conventional techniques for the case of bearing fault monitoring, and gearbox fault diagnosis.

**Smart data analytics:** Sensor integrated manufacturing systems are producing enormous amount of data during each second, making data handling a difficult task. Smart data analytics involves the extraction of right features, analysis of the processed data, coining the decision-making algorithms from the plethora of

available data (Yan, 2007). An overlook of smart data analytics' components is given in Fig. 2.2.

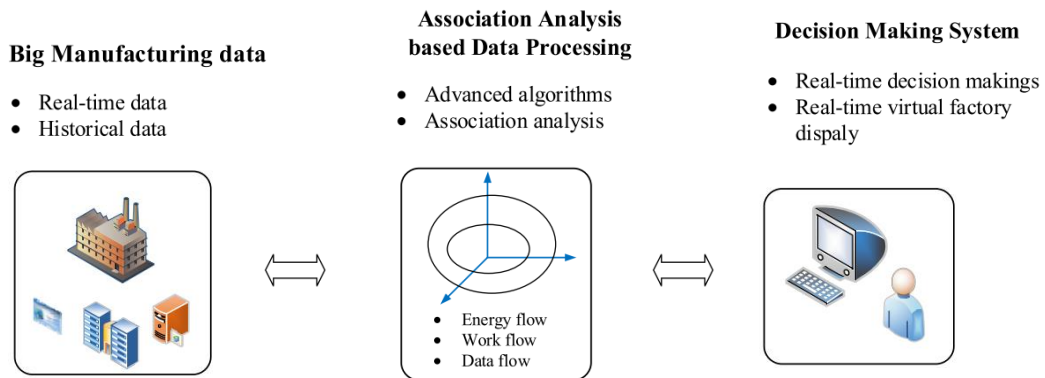


**Fig. 2.2** Smart manufacturing system based on advanced data analytics (Yan, 2007)

### 2.3 WIRE EDM CAPABILITIES

Wire EDM is one of the best cost-efficient processing techniques to machine hard materials. The non-contact material removal mechanism coupled with CNC controlled wire electrode motion, makes the process capable of cutting any intricate, complex, and precise shapes with great flexibility and control. Machining of superalloys, which is considered as difficult to cut conventionally, is one of the most sought application of wire EDM. Superalloys are high performance materials, which can retain its superior mechanical properties even at temperatures close to its melting point (Reed, 2006). The conventional machining of superalloys is considered difficult due to the tendency of superalloys to strain harden during machining, formation of built-up edge, entanglement of continuous chips, poor heat dissipation due to low thermal diffusivity causing high heat generation at tool chip interface, and higher tendency of chemical reaction with tool material (Thellaputta et al., 2017; Thakur et al., 2009). Many non-traditional techniques like laser beam machining, abrasive water jet machining, electro chemical machining, and electro discharge machining were attempted in the past to overcome these limitations. Such non-traditional processes offer near zero cutting forces and residual stresses, due to

their non-contact material removal mechanism. Even then, many of these techniques have a few limitations which restricts their wide usage in machining superalloys. Laser beam machining has a larger thermal impact and thicker recast layer (Zhong et al., 2005), die sinking electric discharge machining requires specific tooling and is less flexible, electro chemical machining requires specific tooling, has low material removal rate and can cause corrosion (El-hofy, 2005). Abrasive water jet machining cannot be used to machine ductile materials and residues of abrasive particles will be embedded into the work material (Holmberg et al., 2019).

Wire EDM process has all the advantages of the EDM process, and additionally, it is more flexible and does not require any specific tooling requirement or setting up time. The recast layer can be greatly minimized by controlling the spark energy, and the residual stresses are minimum for the process (Yan and Lai, 2007). One of the main applications of superalloys is in the aerospace industry due to the materials superior performance at elevated temperatures. In the past, wire EDM processed superalloys were not the preferred choice for aerospace applications due to the high surface integrity requirements. The thermal nature of material removal imparts undesirable tensile residual stresses on the wire electric discharge machined surfaces. Also, the recast layer formed on the wire EDM processed surface contains numerous micro cracks which can lead to fatigue failure of components (Velterop, 2003). However, since then many researchers have studied upon the capability of wire EDM for manufacturing aerospace components and have reported positive results. Klocke et al. (2012) evaluated the process performance of wire EDM during the machining of Inconel 718 and observed that the process has the potential to replace broaching to produce fir tree slots in gas turbine discs. The surface integrity requirements of gas turbine components, namely surface roughness of less than  $0.8 \mu\text{m}$ , near zero white layer thickness and geometrical accuracy in producing the fir tree profile was achieved using the wire EDM process as shown in Fig. 2.3. Antar et al. (2012) studied the fatigue life of wire EDM finish cut Udimet 720 and reported no significant difference to the milled component's fatigue life. Welling (2014) compared the

surface integrity and fatigue strength of wire electric discharge machined Inconel 718 with that of broaching and grinding. Wire EDM process was found to achieve the industrial surface integrity requirements. The fatigue strength of wire EDMed components was comparable to that of broaching process. Anurag (2017) observed that wire EDM can potentially replace broaching process to machine future aero components using gamma titanium aluminides.

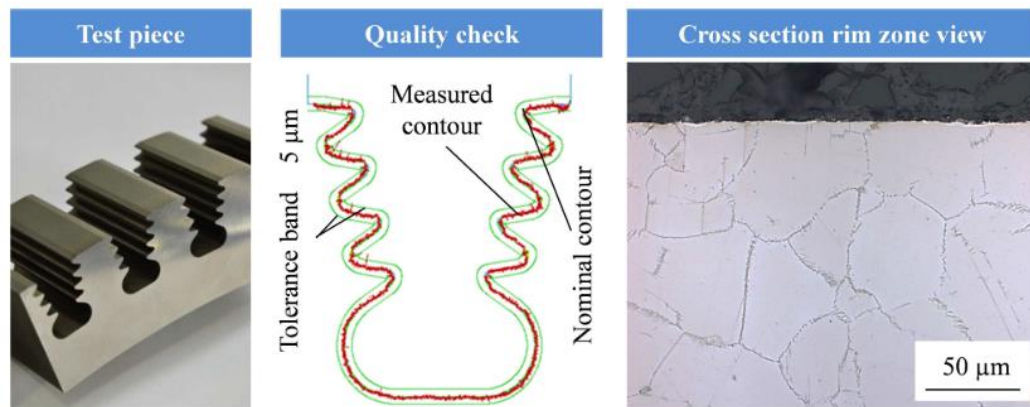


**Fig. 2.3** Surface integrity of wire electric discharge machined firtree slot  
(Klocke et al., 2012)

Wire EDM is also widely used to manufacture miniature gears, dies, fixtures and tools. The capabilities of wire EDM process to manufacture miniature components was explored by Ali and Mohammad (2008). Miniature spur gears were manufactured on copper material using the process with  $R_a$  of  $1 \mu\text{m}$  and with 1 % dimensional deviations. Gupta and Jain (2014) observed that wire EDM cut miniature gears are of superior quality than the hobbed gears. The geometrical accuracy and surface integrity aspects are considered to evaluate and compare the processes. Alhadeff et al. (2018) explored the possibility of cutting small aspect ratio miniature brass gears with wire EDM. Brass gears with good surface finish and negligible recast layer can be produced using the process. Chaudhary et al. (2020) optimized wire EDM process parameters while producing miniature gears of Nimonic superalloy. Das and Patowari (2018) manufactured micro tools for ultrasonic machining process using wire EDM on glass substrates. Micro tools of

square, circular and zig-zag geometries were manufactured with good accuracy in the study.

The process is also widely used to produce micro features like textures, channels, and fins. Miner et al. (2013) machined micro channel arrays on copper using wire EDM with  $0.6\ \mu\text{m}$  to  $0.8\ \mu\text{m}$   $R_a$ . Debnath and Patowari (2019) evaluated the machinability of wire EDM cut micro square fin arrays on copper and stainless steel. The quality of micro pins was found acceptable through SEM images and EDS analysis. The dimensional accuracy was better in stainless steel compared to copper. Ahmed et al. (2020) conducted experimental study to maximize micro channel per area in copper by minimizing inter fin distance. Wire EDM was observed to be a suitable processing method to manufacture micro channels in copper workpiece.

Wire EDM is theoretically capable of machining any conductive materials. The process is especially used to cut hard components which are difficult to cut by conventional machining. Wire EDM of Nickel based superalloys has been investigated by several researchers in the past. Extensive researches are done on wire EDM performance during the machining of Inconel 718 (Li et al., 2014; Klocke et al., 2014; Karidkar et al., 2018; Tonday and Tigga, 2019), Inconel 825 (Rajyalakshmi and Ramaiah, 2013), Inconel 706 (Sharma et al., 2015; Sharma et al., 2016), Nimonic 80A (Goswami and Kumar, 2014) and Nimonic C 263 (Mandal et al., 2016; Mandal et al., 2017). Apart from superalloys, wire EDM of Titanium alloys is also a topic of research interest. Notable works on wire EDM of Ti-6Al-4V are conducted by Prasad et al. (2014), Pramanik and Basak (2018), and Kumar et al. (2019). Wire EDM of various grades of steel have been performed by researchers in the past, which includes investigations on high speed steel (Kumar et al., 2018), AISI O1 tool steel (Camposeco-Negrete, 2019), stainless steel (Debnath and Patowari, 2019), and medium carbon steel (Alduroobi et al., 2020). Wire EDM of NiTi shape memory alloy was investigated by Chaudhari et al. (2019) and Das and Chakraborty (2020). Many researchers have studied the wire EDM machinability of metal matrix composites like

Al7075/SiCp (Rao, 2016; Phate and Toney, 2019), ZC63/SiCp (Rao and Krishna, 2013) and Al / ZrO<sub>2</sub> (Garg et al., 2013).

## **2.4 MACHINING STABILITY OF WIRE EDM**

Machining stability of wire EDM process depends on numerous factors including dielectric flushing, restoration mechanism, debris stagnation, wire vibrations, wire lag effect, discharge energy, pulse characteristics, and thermal aspects. The machining is considered as stable, if the required profile is machined without process failures and with acceptable surface integrity. On the other hand, an unstable machining process is characterised by the following situations:

- Debris accumulation which can lead to surface damages and wire breakage (Cabanés et al., 2008a).
- Wire lag effect, wire deflection, and wire vibrations leading to geometric and corner inaccuracies (Arunachalam et al., 2001).
- Excessive thermal load on the wire (Cabanés et al., 2008a).
- Spark gap fluctuations (Klocke et al., 2014b)
- Other process interruptions which cause material and energy wastage.

The process stability was studied by researchers in the past by considering the various factors described above. A few researchers have come up with numerical models to simulate the wire EDM process mechanism and wire breakage phenomena. Rajurkar and Wang (1993) observed that the thermal load on the wire is responsible for wire rupture. The rupture mechanism was studied based on a thermal model. Arunachalam et al. (2001) developed a computational model to evaluate the wire stresses aimed at understanding the wire lag, wire vibration and breakage phenomena by considering a copper bar as the work material. The primary cause of wire breakage is observed as increased wire stress. The authors have considered wire wear, electrostatic forces, spark pressure, and electromagnetic force as the four main reasons for increased wire stress. The two types of wire breakages are observed – type I and type II, depending on whether the wire breakage is late or immediate. The discharge energy was increased

sequentially to determine operating regions for the wire EDM as shown in Fig. 2.4. Saha et al. (2004) developed a finite element model to accurately predict the thermal load on the wire electrode. The study observes that the heat generated during the spark discharge is the key factor responsible for wire breakage failure. The internal heat generated, temperature, and stress distribution along the wire length for different materials are predicted by the model. Banerjee (2009) studied the effect of clustering of sparks on wire electrodes by developing a thermal model. Spark clustering is observed to increase the thermal load intensity on wire electrodes and can potentially lead to wire breakage. The spark distribution is randomized in this model with predicted peak temperature indicating risks of wire rupture. Okada et al. (2015) developed a CFD model to analyse wire deflection, debris stagnation period in the spark gap, and hydrodynamic stress distributions in wire. Based on the numerical analysis, debris stagnation and wire deflection are found as the dominant factors which affects wire breakage. Wire deflection is observed to be caused by electrostatic forces, forces due to discharge sparks, and hydrodynamic forces due to dielectric flushing. Mohapatra et al. (2016) developed a 3D finite element model to analyse the thermal and structural factors leading to wire breakage. Temperature, heat flux and stress generated are computed by the finite element model. Kawata et al. (2017) studied the debris stagnation, flow variations in spark gap, and wire electrode deflection when wire EDM operation starts from a start hole. The analysis was conducted by CFD and structural examination. The work presented an interesting observation that the wire breakage frequency is more at a certain machined length where the debris stagnation is more and wire deflection is moderately high. At start of the machining, the debris stagnation is highest due to less dielectric flow rate, but wire deflection is negligible. After a particular machining length, the deflection is high, but debris stagnation is reduced. In between these two extremes, the researchers have observed maximum wire breakage occurrences. Ebisu et al. (2018) developed a computational fluid dynamics (CFD) model to study and control wire lag and wire break during corner cutting. It was observed that debris stagnation can be regarded as chief cause of wire breakage. Also, increasing the

dielectric pressure to force the debris away from the spark gap causes wire vibration and deflection, which can cause geometric inaccuracies. From the simulation of flow field and debris motion, it was revealed that the flow field changed significantly with excess debris stagnation at a corner profile. Also, the flushing pressure affected the wire deflection equally to that of discharge force.

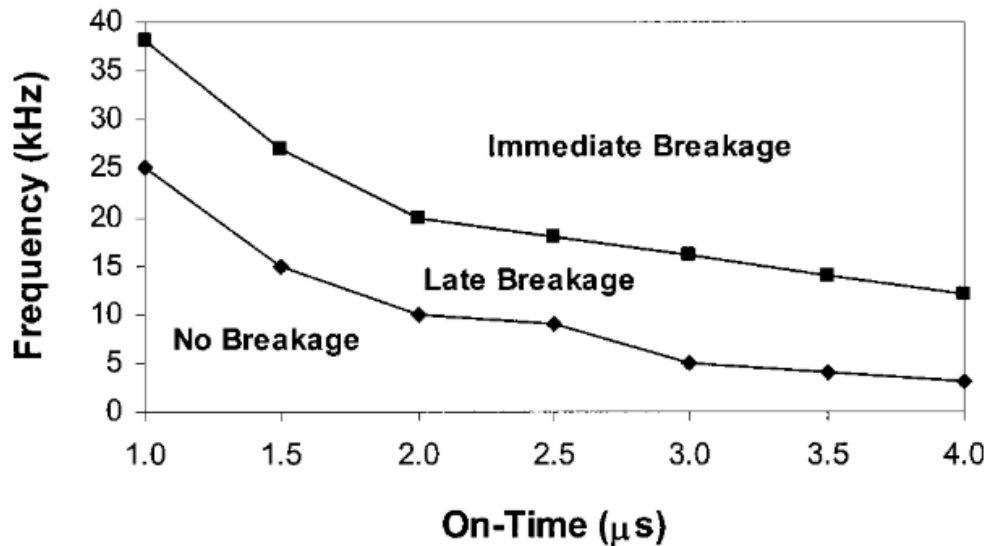


**Fig. 2.4** Regions of wire breakage (Arunachalam et al., 2001)

Another approach by the researchers was to study the crater formation in wire electrode to understand wire breakages. Luo (1999) studied the mechanism of wire rupture by investigating the mechanical failure mode and wire electrode strength. The situation is modelled as plane stress problem with Airy's function to describe the distribution of stress. Fracture toughness of wire electrode is computed based on stress intensity factor and energy release rate. The stress intensity factor is found to increase with dielectric pressure and crater size. Yield strength and fracture toughness under axial wire tension and dielectric flushing pressure are studied. Both the factors are found to be influential in wire rupture mechanism. A temperature rise was found to intensify the wire rupture mechanism by reducing the strain hardening. Tosun and Cogun (2003) investigated the effects of wire EDM process parameters on the wire wear ratio by considering AISI 4140 steel as the work material. The wire wear rate was found to increase with pulse duration and open circuit voltage, whereas the same

decreased with wire feed rate and flushing pressure. They also observed that higher wire wear ratio is associated with high material removal rate and machined surface roughness parameter,  $R_a$ . Tosun et al. (2003) has also performed an investigation on variation of wire crater dimensions with input parameters by considering AISI 4140 steel as the workpiece material. The diameter and depth of the crater is found to increase with pulse duration, wire feed rate and open circuit voltage. Pramanik and Basak (2018) studied the wire breakage failure mechanism in an attempt to improve wire EDM process sustainability during the machining of Ti-6Al-4V alloy. The wire failure is reported to occur in two modes: sudden rupture or after gradual decrease of wire cross section. Increased wire tension and reduced flushing pressure was observed as primary reasons for wire breakage failure. Also, debris accumulation causing arc discharges was found to result in instantaneous temperature rise resulting in wire breakage.

## **2.5 SOFT COMPUTING TOOLS TO PREDICT WEDM PERFORMANCE**

Modelling and prediction of wire EDM performance is challenging due to the stochastic nature of the process. This is mostly because of the complex material removal mechanism of wire EDM process. Also, the process is influenced by several random and uncontrollable external factors. Earlier attempts to model wire EDM performance was through regression analysis. However, due to the advent of artificial intelligence, soft computing tools are widely used to model complex real-world phenomena. The soft computing tools are capable of arriving at approximate, but acceptable solutions, which are difficult to compute using conventional techniques. Artificial neural networks (ANN), swarm intelligence, and fuzzy logic are some of the widely used soft computing tools. Such techniques can learn the patterns from the training data to accurately model the input output relationships even for complex, multi-dimensional, higher order problems.

Ramakrishnan and Karunamoorthy (2008) developed an ANN model to predict material removal rate (MRR) and surface roughness during wire EDM of

Inconel 718. A back propagation algorithm was chosen to tune the neural network parameters. Analysis of variance study revealed that pulse on time, ignition delay time, and pulse current are the most significant factors which influence the performance characteristics. ANN modelling of wire EDM process was also conducted by Markopoulos et al. (2008) by considering structural and high strength steels. The predictions are reported to be accurate with an R value of 0.904. Shakeri et al. (2016) compared the prediction accuracy of ANN and regression models during the wire EDM of alloy steel. The mean prediction error of the feed forward back propagation neural network model and regression model are reported to be 0.773 % and 2.547 % respectively. Alduroobi et al. (2020) have reported a prediction accuracy of 98 % for ANN model to predict MRR and surface roughness during wire EDM of AISI 1045 steel. Pulse on time is the most significant factor affecting the process performance, followed by pulse off time. Majumder and Maithy (2018) compared the accuracy of general regression neural network (GRNN) model and statistical regression analysis to predict response parameters during wire EDM of Ti- grade 6. GRNN model was found to be 5% more accurate than the regression model. Soepangkat et al. (2019) compared the optimization results using grey relational analysis (GRA) and a hybrid back propagation neural network (BPNN) – genetic algorithm (GA) method. The recast layer thickness, surface finish and crack density of machined surface are selected as the responses considering tool steel as the work material. BPNN was capable of accurately predicting the process responses and the combined BPNN-GA is proved to be better than conventional GRA in optimizing the process parameters. Manoj and Narendranath (2020) developed an ANN model to predict profile areas during the wire EDM taper cutting. The developed model was successful in accurately predicting the responses with a highest error of 9%.

Caydas et al. (2009) modelled wire EDM process using adaptive neuro fuzzy inference system (ANFIS) technique by considering AISI D5 tool steel as the work material. Recast layer thickness (RLT) and surface roughness were considered as performance criteria. The comparison of ANFIS predictions and experimental observations can be seen in Fig. 2.5. Azhiri et al. (2014) modelled

cutting speed and surface roughness of wire EDM in gaseous media using ANFIS during the machining of Al/SiC metal matrix composite. The experimental work was conducted based on Taguchi's  $L_{27}$  orthogonal array design considering pulse on time, pulse off time, discharge current, gap voltage, wire feed and wire tension as input parameters. The prediction accuracy of ANFIS model was very high with a mean absolute error of 0.1 to 0.2. Pulse on time and discharge current were the most significant factors, with wire tension being the least significant factor based on ANOVA results. Maher et al. (2016) developed an ANFIS based RLT prediction model with 2.61 % error during the machining of AISI 1050 carbon steel. RLT was observed to be least at minimum pulse on time, peak current and maximum pulse off time. Wire tension and wire speed were observed to be insignificant in RLT variation. Mandal et al. (2018) modelled kerf width and cutting speed of wire EDM using ANFIS during the machining of  $ZrB_2$  based ceramic composites. Model results were compared for different membership function shapes and the triangular membership function yielded the least root mean square error. Kumar et al. (2019) found that ANFIS model has a better prediction accuracy than the regression model during wire EDM of titanium alloy Ti-6Al-4V. Later, the parameters were optimized using grey relational analysis (GRA). Pulse on time, pulse off time and discharge current had the highest influence on MRR and surface roughness, whereas dielectric flushing pressure had the least influence.

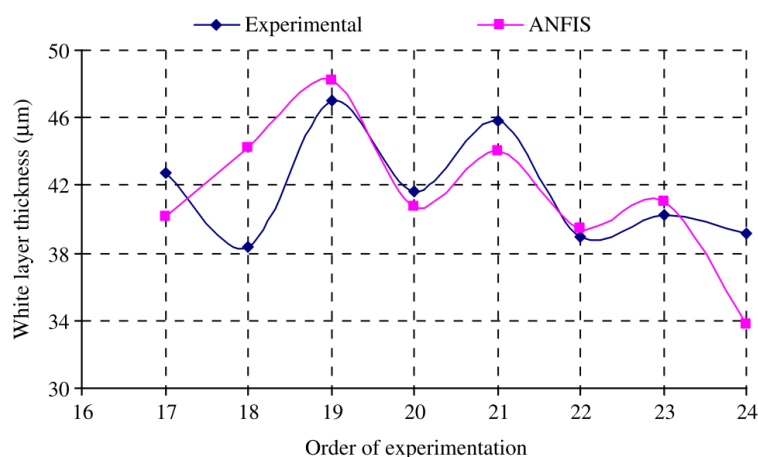


**Fig. 2.5** Comparison of ANFIS predictions with experimental readings (Caydas et al., 2009)

Shunmugam et al. (2000) developed a fuzzy logic model to predict wire EDM performance measures during the machining of Titanium alloy (Ti6Al4V). The cutting speed and surface roughness were predicted with acceptable accuracy. The authors had observed that the accuracy of the model is limited by the size of the rule base. Nain et al. (2018) modelled wire EDM responses using fuzzy logic model and compared the results with back propagation artificial neural network (BPANN) model. Udimet-L605 was considered as the workpiece material. Surface roughness and waviness were the responses considered for evaluation. BPANN model was reported to perform better compared to the fuzzy logic model. This is expected since the fuzzy model is based on an expert knowledge and is not trainable. Due to this reason, fuzzy logic is more frequently used for wire EDM process control models than for performance predictions.

## **2.6 PULSE TRAIN ANALYSIS AND CONDITION MONITORING OF EDM**

Wire EDM is a specific variant of EDM, whose process monitoring system needs to be addressed separately due to the particular nature of process failures by wire breakages. However, the process mechanism and material removal principle are very similar to other EDM techniques. The part quality deterioration by arc and short circuit sparks, debris accumulation, servo control tuning, etc. are common topics of research interest for any EDM process. Signal acquisition, processing and control techniques can also be found common for many EDM process control systems. Therefore, the current trends in pulse train analysis and process monitoring of EDM processes is to be investigated initially. In this regard, state of the art research in the area of condition monitoring of electric discharge machining, other than wire EDM, is discussed in this section.

Liao et al. (2008) developed a pulse classification system by studying the voltage pulse behaviour for a micro-EDM process by considering stainless steel as the workpiece. The pulses were classified into normal, arc, complex, short and effective arc. Pulse discrimination was conducted and compared for micro wire EDM, milling and drilling. For drilling, as the hole gets deeper, the normal pulse

ratio decreases and complex pulse ratio increases. Pandey and Brahmkar (2016) developed an ANN model to predict arching during EDM of metal matrix composites (MMC). The offline model is intended to aid the operator in avoiding the parameters which can lead to poor surface integrity and part damage.  $L_{27}$  experimental design was selected by varying input parameters, and this constitute the training dataset. The machining depth without arching was recorded as response. If no arching was observed, the entire machining depth is recorded as the response. For a new parameter set, if the ANN prediction is less than the total machining length, then arching is suspected and that settings shall be revised. Rajeswari and Shunmugam (2019) explored the effects of various EDM discharge pulses in die sinking EDM operation of hardened D3 die steel. Process is optimized for both roughing and finishing by considering novel performance indexes namely, energy spent in one second, and the ratio of spark energy over total energy spent. Pulse classification was performed and discharge characteristics were extracted by setting thresholds.

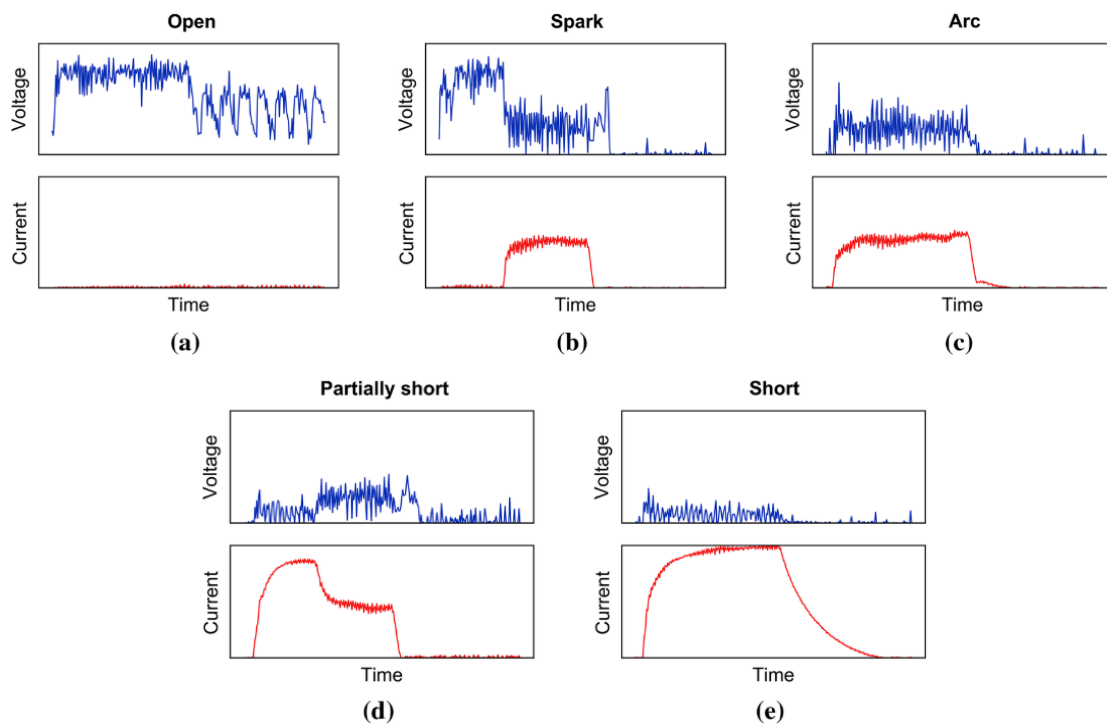


**Fig. 2.6** High speed EDM pulses (Zhang et al., 2020)

Zhang et al. (2020) proposed a novel pulse classification method for high speed EDM using recurrent neural network during the machining of AISI 1045 carbon steel. 30000 samples were considered for training and the labelled samples are fed to the model. 3 different RNN were compared for classification accuracy, namely traditional, long short-term memory (LSTM), and independently recurrent neural network. Among these, LSTM fetched the best classification accuracy of 97.85 %. The different pulse shapes identified are shown in Fig. 2.6. Mwangi et al. (2020) performed pulse train analysis and studied the effect of arcing on material properties during micro EDM of Nitinol. Experiments were conducted by sequentially increasing the discharge energies. Arcing was observed at higher discharge energies, which also accelerated the tool wear rate. Arcing was observed to degrade the mechanical properties, especially fatigue strength. The authors recommend to avoid the arc inducing discharge energy levels completely, since the extend of surface damage clearly outweighs the advantage in productivity improvement. Xia et al. (2020) proposed a breakout detection technique for EDM drilling of Cr12 steel workpieces by classifying pulse signals. Breakout happens when a though hole is almost made, but the actual machining is yet to complete. Its online detection is important, since parameters shall be adjusted at this point to stop inward feed when machining completes to avoid damages to other workpiece parts. The normal pulse ratio, short circuit pulse ratio and servo feed are chosen as the input signals to the random forest classification model. The model classifies the machining condition into 'before breakout' or 'after breakout'. The trained model was reported to have good classification accuracy and fast response time.

## **2.7 CONDITION MONITORING AND PROCESS CONTROL OF WEDM**

The stochastic nature of the wire EDM process has led to complexity in modelling the performance characteristics and wire break failure. Intervention of several random, uncontrollable factors reduces the model accuracies. Therefore, it is better to relate the discharge characteristics with the process performance using

a condition monitoring setup. Through such a system, the occurrence of failure can be predicted and controlled better. A condition monitoring system is aimed at forecasting a potent process failure before any actual harm is done, providing enough time to take preventive measures. Researchers in the past have come up with various methodologies for wire break prevention and process control of wire EDM process. Those approaches are categorized and discussed in the following subsections.

### **2.7.1 Classification of wire EDM discharge pulses**

The discharge pulses happening between the wire electrode and workpiece is the most important characteristic of wire electric discharge machining. The attempt to monitor and control the wire EDM process have to start with understanding and categorising the discharge pulses. Liao and Woo (1997) described a pulse classification algorithm to categorise the wire EDM discharge pulses while considering tool steel as the workpiece material. The proposed method involves measuring current and voltage signals by voltage divider and current probe respectively. Three types of discharges are reported, namely, arc, short and normal. Three types of machining instabilities are reported based on the increase of arc and short sparks. Janardhan and Samuel (2010) developed a pulse discrimination algorithm for wire electric discharge turning process of brass material. The algorithm is also capable of computing the ignition delay time, and discharge width. The pulses are classified by setting threshold values for voltage and current signals. Depending upon the time taken to cross the threshold and peak discharge voltage, pulses are classified to open, short, arc and normal as shown in Fig. 2.7.

Klocke et al. (2012b) observed that, to develop a process monitoring system, the specific values for discharge characteristics have to be found out. All the relevant features for process monitoring are extracted based on these values. Some of these values may be machine and generator specific and have to be experimentally found. Many deformed discharges were observed with short circuits, misdischarges, and delayed pulses. The classification algorithm sets

rules based on voltage and current values to distinguish between pulses. The unideal discharges lead to less productivity, surface damages, and wire breakages. Inconel 718 was considered as the workpiece material. Yan and Hsieh (2014) used a pulse classifier device consisting of gap monitor and signal processor card to discriminate between normal, open arc and short sparks during the wire EDM machining of SKD11 tool steel. The proportion of each pulses, along with ignition delay time are computed for monitoring the process. The authors propose that such a system can replace the monitoring systems based on average gap voltage, which were employed till then. Zhang et al. (2015) proposed a two-stage pulse classification model using support vector mechanism and random forest by considering copper, SKD 11, and tungsten steel as workpiece materials. Firstly, from the filtered voltage signals, support vector categorises pulses into open, short and other pulses. In the next stage, Random forest classifies the other pulses into arc, transition type and normal spark discharges.

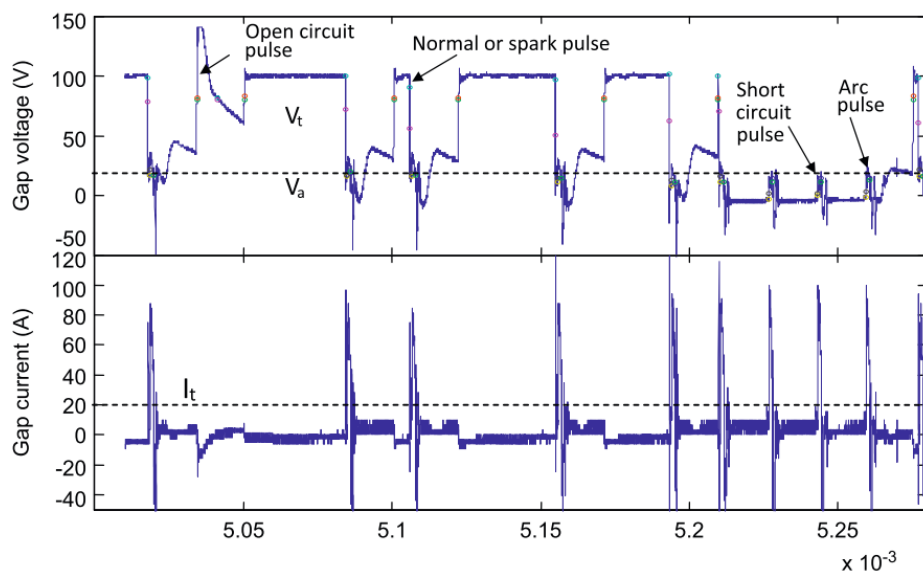


**Fig. 2.7** Different types of wire EDM discharge pulses on a pulse train  
(Janardhan and Samuel, 2010)

An advanced feature extraction technique to extract discharge characteristics for wire EDM of steel material was proposed by Caggiano et al. (2015). The study was aimed at extracting uncommon features by sensor fusion in order to predict

surface damages occurring due to process instability. The methodology for extracting various features from current pulse, voltage pulse, and the combination of both signals are described. Some of the features extracted are short circuit ratio, short circuit duration, open circuit ratio, spark frequency, ignition delay time etc. Osswald et al. (2018) categorised the high-speed wire EDM pulses into five types while machining stainless steel. The pulses are categorised as EDM discharge, thermal breakdown discharge, arc, short and open circuit discharge. The short circuit pulses are further categorised into hard and soft short circuit pulse. Spark gap bridging by severe debris stagnation causes soft type, and physical wire-workpiece contact causes hard short circuit spark. The arc and short pulses, characterised by negligible ignition delay time, are observed as undesirable, since it causes surface damage and wire breakage. Conde et al. (2018) classified the discharge pulses into four, based on the ignition delay duration during the wire EDM of AISI D2 steel. The pulses are named as D0, D1, D2 and D3 in the increasing order of delay time. D0 and D1 essentially represents the short circuit and arc sparks.

### **2.7.2 Fuzzy logic models for process control**

Fuzzy logic tool is known to process inaccurate and less precise information to give acceptable results. The model is flexible, and is based on simple if-else rules. For an experienced process expert, the fuzzy rule sets are easy to develop based on logical statements. Due to these reasons, fuzzy based control systems can be equipped in the wire EDM to give adequate process control. Thus, the earlier attempts for condition monitoring and process control were mostly fuzzy logic based. Yan and Liao (1996) modelled a fuzzy logic controller which self-adjusts pulse off time based on spark frequency to prevent wire breakages during the machining of tool steel. The researchers observed two types of wire breakage mechanism based on whether the spark frequency rise is sudden or gradual. Later they (Yan and Liao, 1998) developed a fuzzy based adaptive control system for wire EDM process based on harmful (short, arc) spark ratio and spark frequency. The effect of these features on material removal rate, surface finish and wire

breakage were also investigated. The model keeps sparking frequency below a threshold to prevent wire breakage, while adjusting pulse off time and servo feed based on abnormal spark ratio to ensure machining stability. Yan et al. (1999) proposed a fuzzy based servo feed control strategy to improve machining stability and to prevent wire breakage during the machining of SKD11 tool steel. The process control is achieved by monitoring and maintaining the spark gap voltage. Liao and Woo (2000) designed a fuzzy based process controller for wire EDM of SKD11 die steel based on short circuit spark ratio and power consumption. Fuzzy rules were formulated based on experience and discharge behaviour. Pulse off time is regulated to keep short spark ratio in check. Machine feed is adjusted to match the consumed power to a reference value. Bufardi et al. (2017) used a combined online-offline fuzzy logic approach to prevent surface damages. Recast layer thickness and surface roughness are considered as the responses. Offline model is proposed to set the initial process parameter. Online model adjusts pulse off time based on short circuit duration and pulse frequency in real time to regulate the surface integrity

### **2.7.3 Wire lag and vibration control**

Beltrami et al. (1996) proposed a wire position control algorithm based on real time wire position measurement using optical sensors. It was observed that wire lag and deflection have a significant impact in reducing the geometric accuracies of the wire cut profiles. Multiple optical sensors track the wire positions in X and Y directions, and corrective actions are taken in cases of deviations from the expected wire positions. A major improvement in cutting speeds were observed with the proposed strategy. Lin et al. (2001) developed a fuzzy logic model to improve the profile accuracy at corners during the wire EDM of SKD-11 steel. The authors aim to control the wire deflections and vibrations at the part corners to maintain the accuracy. It is reported that the profile errors at corners and small radii are caused by wire deflection, non-equilibrium state of discharges at corners and wire lag. The fuzzy model auto tunes the process parameters to ensure machining accuracy, while maintaining the machine productivity. Wang and

Ravani (2003) presented a computational method for cutting complex profiles. Tool path motion is generated considering the wire diameter and spark gap. A method is proposed which auto regulates the spark gap during the machining of tight geometries for easier flushing and wire break prevention. Yan and Huang (2004) developed a wire tension control system to reduce the wire vibrations during wire EDM of SKD11 tool steel. The system can achieve better geometrical accuracy than conventional tension control systems. Dynamic absorbers are installed to wire feed rollers and reels to control wire tension in real time.

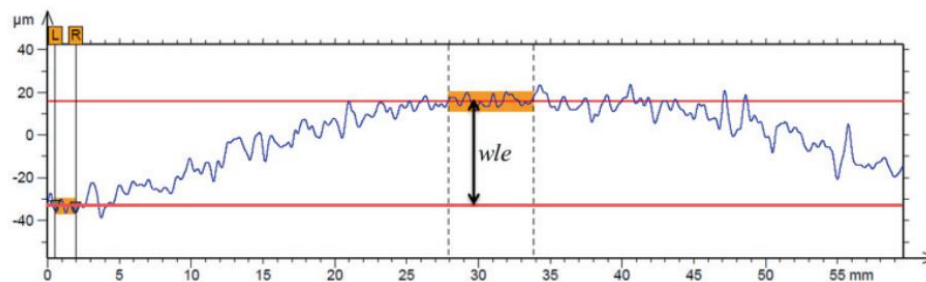


**Fig. 2.8** Wire lag effect (*wle*) for a workpiece of height 60 mm  
(Conde et al., 2018)

Sarkar et al. (2011) proposed a wire lag compensation technique based on the developed mathematical model relating wire lag and gap force. The experiments were conducted on a die steel material. Wire deflection is observed to be inversely proportional to the radius of the profile. A methodology for accurate measurement of wire lag and gap force is described in the study. Habib and Okada (2016) studied the frequency and amplitude in parallel and perpendicular directions of wire vibrations during fine wire EDM process of SKD11. High speed video camera system with up to 24000 fps capture rate was used to observe the wire motion. Wire vibration amplitude was observed to be dependent on wire tension and is greater in parallel direction. The frequency analysis revealed stronger presence of 1<sup>st</sup> and 3<sup>rd</sup> order vibrations. Conde et al. (2018) studied the effect of wire lag and vibrations on part geometry during the wire EDM of D2 steel. Corner cutting accuracy was reported to increase with wire lag. The machining process was halted in between the machining process and the wire lag

is traced using an optical instrument as shown in Fig. 2.8. Wire lag effect is influenced by workpiece height and flushing pressure. The types of discharge and unbalanced forces acting on the wire electrode combines to produce wire vibrations and lag, affecting the machined part geometry.

#### **2.7.4 Online height estimation and control**

Excessive discharge energy and debris accumulation leading to short circuits are commonly reported issues which can lead to wire breakages while machining work pieces of varying heights. In order to counter this, online height prediction and adaptive control was attempted by many researchers to avoid wire breakage.

Rajurkar et al. (1994) developed a system which monitors and regulates the discharge frequency according to workpiece thickness. Workpiece height estimation model was developed by computing the relationship between spark frequency and cutting rate. The process control technique was based on the observation that, setting a constant spark frequency can cause excessive discharge energy or ineffective flushing at different height sections of workpiece, which can lead to wire breakage. Pulse off time was regulated to adjust spark frequency according to work height. Yan et al. (2001) developed an adaptive control system that adjusts the machining condition to prevent wire breakages while cutting the workpiece SKD11 tool steel of varying thickness. The authors observed that the stair shaped workpiece causes wire breakage due to inefficient removal of debris from the spark gap. A neural network model was employed to predict the workpiece height. Based on this, a three-layer fuzzy controlled algorithm stabilizes the machining condition. Firstly, the sparking frequency is monitored and controlled to prevent wire breakages. Secondly, the harmful spark ratio is monitored and controlled. Finally, parameter settings are tuned based on the estimated workpiece thickness. Altogether, the proposed control system ensured stable and faster cutting than the gap voltage-based control algorithm while machining the workpieces of varying heights.

Liao et al. (2013) proposed a workpiece height computation methodology for wire break prevention by considering SKD11 as the workpiece. The workpiece

height was estimated based on feed rate and spark frequency. Further, a corrected variable servo voltage, as an alternate to the existing constant servo voltage is developed. The existing methodology calculates the servo voltage value based on initial work height. However, wire rupture was observed when machining variable height workpieces. The proposed system overcomes this limitation and ensures stability and performance while machining workpiece of variable height. Dou et al. (2013) has come up with an online height estimation algorithm using support vector regression (SVR). SVR predicts the workpiece height by receiving spark frequency, pulse off time, servo voltage, and servo feed as input. Based on the work height, a feedback control regulates the spark frequency to avoid wire breakages. The spark frequency is regulated by tuning pulse off time and servo voltage. Guangwei et al. (2018) developed a support vector machine (SVM) based online workpiece height computation system during wire EDM of tool steel. The SVM is trained by providing spark frequency, pulse duration, input feed, and actual feed as input. The pulse data is captured by using voltage and current sensors. Based on the predicted work height, input parameters are tuned to ensure stable machining.

### **2.7.5 Wire break prevention and adaptive control systems**

Different wire break prevention methodologies proposed by researchers in the past are discussed in this section. Rajurkar and Wang (1991) proposed a monitoring method to prevent wire breakages during wire EDM of steel. It was found from the pulse train analysis that the spark frequencies shoot up just before the wire breakages. From this observation, the approach was to monitor the spark frequency continuously during the process and to adjust it when a threshold level is crossed. Pulse off time was adjusted to control the spark frequency. Liao et al. (1997) developed a process monitoring and control algorithm for wire EDM of SKD11. From the voltage and current signals, pulse classification was performed. A number of experiments were conducted on stable and unstable process conditions to analyse the typical symptoms before wire breakage. An increase in abnormal spark ratio and spark frequency were reported before wire breakage.

Based on these indicators, control parameter values are adjusted to restore the process stability.

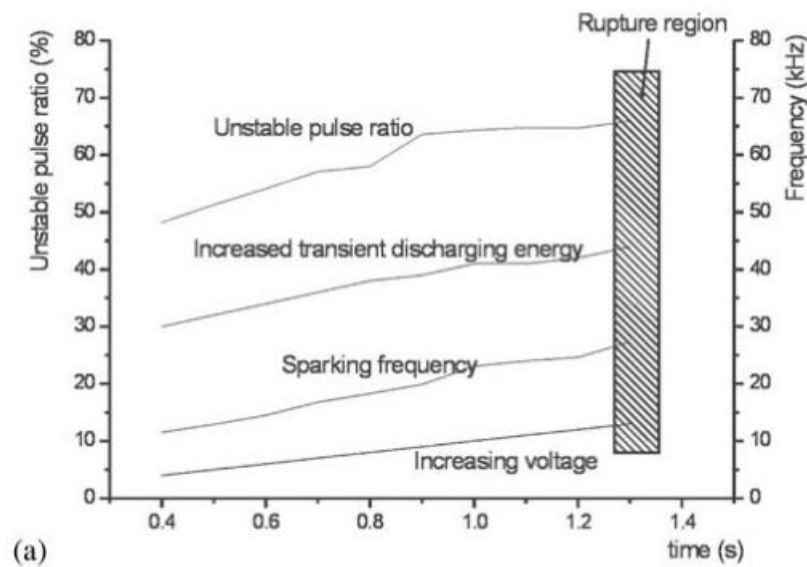


**Fig. 2.9** Regions of machining stability (Kwon and Yan, 2006)

Huang and Liao (2000) proposed an ANN expert system for failure detection. The ANN model can predict causes of wire rupture, low productivity, low surface finish or geometric accuracy. Fifteen features and 8 causes were identified for wire break situation. Training data of size 50 is used to develop the model which accepts the symptoms associated with failure as input and will suggest the reason for failure. Kwon and Yan (2006) proposed a different approach to monitor wire EDM process through instantaneous energy during wire EDM of SKD-11. The transient state of instability in the spark gap is monitored using a voltage and current sensor. A methodology to compute instantaneous energy from pulse data is described in the study. A pulse classifier distinguishes pulses into normal, stable arc, short and unstable arc by settings thresholds on voltage pulse signal. Monitoring instantaneous energy is said to improve machining stability, prevents machining failure by wire breakage and improve the process performance. Wire breakage was found to happen when the instantaneous energy crosses a threshold as seen in Fig. 2.9. Experiments were conducted to simulate the situation by increasing voltage and current.

Cabanes et al. (2008a) developed an online monitoring system that can send alarms in case of machining instability leading to wire rupture during wire EDM of tool steel. Three alarms, A1, A2 and A3, in the increasing order of criticality of instability were designed to go off according a rule set. The rules are based on discharge energy, spark frequency and ignition delay time. The most critical case will have higher discharge energy, higher spark frequency and low ignition delay time. The rules are formulated heuristically by conducting experiments under unstable machining conditions like complex profiles, ineffective flushing conditions, corner cutting etc. In a different study, Cabanes et al. (2008b) proposed another methodology to prevent wire breakages during wire EDM of tool steel. To study the behaviour of discharge characteristics during unstable conditions, such situations were purposefully created. The measured values of discharge parameters are compared with its reference values, obtained from their typical behaviour during stable cutting. The unstable conditions are characterised by rapid rise in discharge energy, decreased ignition delay along with increase in peak current, and alternating cycles of high and low-level discharge energy. During the above cases, the algorithm alarms the operator about the instability. Three levels of alarms were designed based on the severity of the instability namely low, medium and high-level alarm. Additionally, the algorithm displays the anticipated machining time left before the wire break happens.

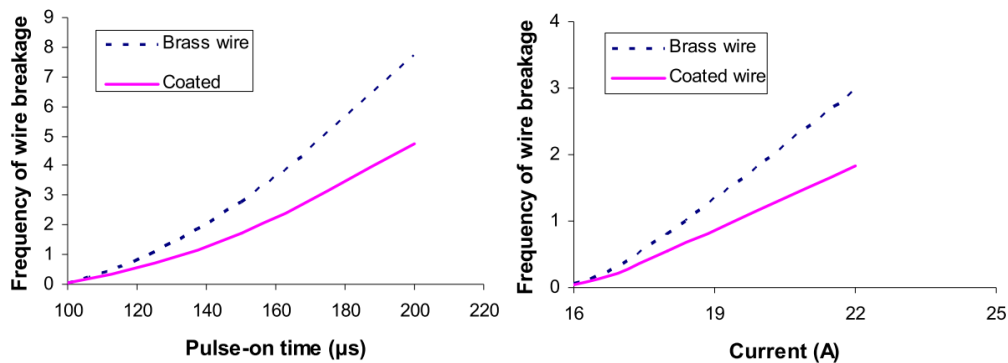


**Fig. 2.10** Effect of pulse in time and current on wire break frequency

(Kumar and Choudhury, 2011)

Kumar and Choudhury (2011) developed regression models to predict frequency of wire breakage for brass wire electrode and zinc coated brass wire electrode

during wire EDM of high speed steel. The input parameters considered are pulse on time, duty cycle, input current, and wire feed rate. The relation between wire break frequency and input parameters are given in Fig. 2.10. Kumar et al. (2013) conducted parametric study by considering wire breakage frequency as response. Based on the one factor at a time study, a safe working range was suggested for each process parameter where the wire break frequency is minimum. The study, however, has not considered any interaction effects and the suggested settings were not validated to be free from wire breakages by confirmation tests. Mendes et al. (2014) proposed a measurement system for current and voltage signal to monitor and evaluate wire EDM stability during the machining of E25 grade carbide composite material. Discharge energy and discharge duration is computed by a sealed current monitoring hardware interfaced with LABVIEW software. The specially designed sealing system enables the current probe placement close to machining zone, while resisting water pressure up to 8 bar. To compare the process performance, a performance indicator was defined as the area cut per unit energy (in KJ) per unit time (in minute). The study concludes that, using this index and the proposed in situ measurement of discharge energy, a better process optimization can be achieved. Zhidong et al. (2014) proposed a novel feedback control system for wire EDM of semiconductors. The authors observed that the existing servo control systems are incapable of distinguishing between the normal open and short pulses in case of semiconductor machining. Ratio between normal and short discharge sparks, called current pulse probability, was considered as the servo feedback parameter to maintain gap stability. A reference value of current pulse probability decides the wire advancement towards the workpiece. If the probability lags behind the reference value, wire is advanced towards the workpiece and vice versa. In this way, always the ratio of normal sparks is maintained with respect to short sparks which prevents gap short circuiting.

Klocke et al. (2014b) developed a process monitoring system to ensure part quality during wire EDM of firtree slot in Inconel 718. It was observed in the study that spark gap distance is one of the chief indicators of the process quality

during wire electric discharge machining. Too high spark gap affects process efficiency and productivity, and too less gap causes short circuits, affects surface integrity and can result in wire breakages. Since the inter electrode distance is difficult to monitor due to wire vibrations and deflections, mean gap voltage ( $U_m$ ) is considered to monitor the process, since it is proportional to spark gap. Experimentally, threshold values of  $U_m$  were found by varying wire in feeds, so as to maintain the  $R_a$  to the industrial requirements ( $< 0.8 \mu\text{m}$ ). The inspection confirmed that wherever  $U_m$  had crossed the threshold, the  $R_a$  value was above  $0.8 \mu\text{m}$ . Kwon et al. (2015) developed a real time process control system to keep process instability in check during wire EDM of SKD11. Voltage and current data sensors were used to collect discharge signals. Undesirable pulse ratio and instantaneous energy were considered to evaluate process stability. The normal and undesirable pulses are distinguished by a classifier as shown in Fig. 2.11. The instantaneous energy and undesirable spark ratio are continuously monitored and regulated against reference values from wire EDM data book. The instantaneous frequency is reduced to avoid wire breakage and harmful spark ratio is reduced to avoid wire break and enhance process performance. By this approach, unstable spark ratio was brought down from  $> 80 \%$  to  $< 6 \%$ . Also, the surface roughness was reduced by  $10 \%$  and productivity was increased by  $5 \%$ . The proposed system is reported to improve the efficiency and performance better than spark frequency monitoring systems.

Bergs et al. (2018) proposed a methodology to identify wire electric discharge machining instability by studying the discharge characteristics. Steel, TiAl6V4 and SiC were considered as the workpiece materials. The authors observed that the unstable machining is characterised by an increase in proportion of abnormal sparks, discharge energy and sparking frequency. A rapid increase in sparking frequency was reported at 20 ms to 100 ms before wire break failure. Wang et al. (2018a) developed a tolerance monitoring system based on unsupervised learning while machining firtree slots on Inconel 718 material. The machined zones were classified into various zones based on captured signal features using hierarchal and K means clustering. Ignition delay time, extracted from the voltage waveform

is chosen as the indicator of profile tolerance. Each zone corresponds to different levels of tolerance deviations. Minimum tolerance zones (cluster 1 and 2) were reported to be the ones with higher proportion of short circuit sparks. The results suggested by the model was confirmed by form measurement using a coordinate measuring machine (CMM). The same research group (Wang et al., 2018b) proposed an online geometric form error detection technique by deep learning technique during fir tree slot machining of Inconel 718. Discharges were classified into four, based on the ignition delay time. The model is trained by acquiring discharge information for various tolerance zones which are custom designed by varying the spark gap. For real world testing, the fir tree profile was divided into 10 zones, and the profile accuracy predictions were accurate on 8 occasions, resulting in a prediction accuracy of 80 %.

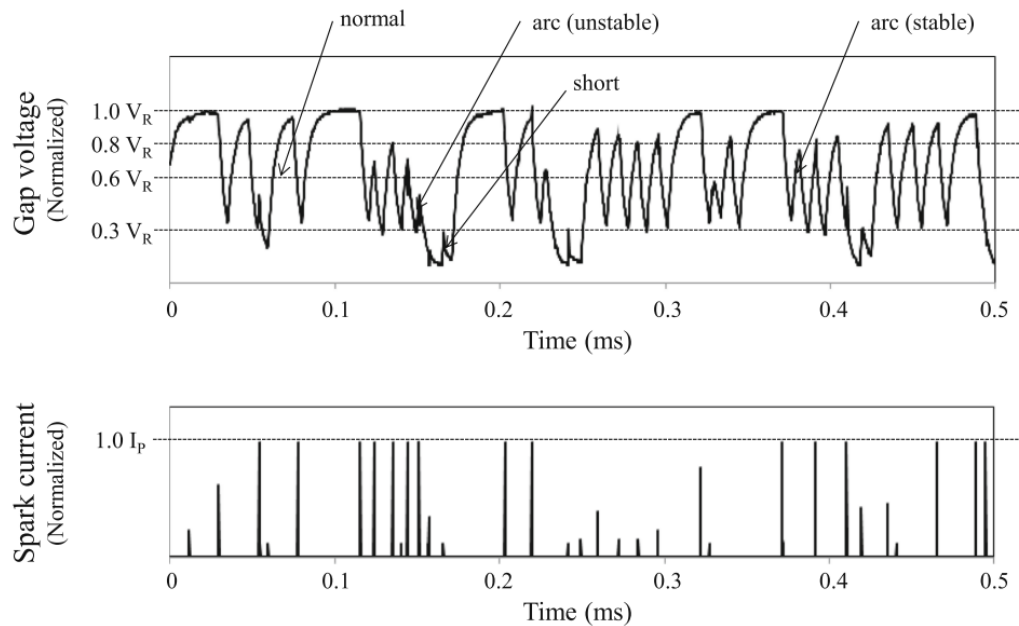


**Fig. 2.11** Pulse classification (Kwon et al., 2015)

## 2.8 SUMMARY AND MOTIVATION

Wire EDM process is having endless potential to replace conventional machining techniques to machine hard metallic components. However, the sustainability and efficiency of the process is limited by unexpected process failures. In the past,

several researchers have attempted to understand the wire wear mechanism and associated wire breakage failure. Even though the wire breakage is found to have strong relationships with phenomena of debris accumulation and spark gap bridging, an amicable solution to predict and overcome the failure situation is yet to be proposed. Several offline models are discussed which predicts wire breakage frequency based on input parameter combinations. Even though the offline models are simple, inexpensive and computationally efficient to perform quick predictions, a standalone offline model's accuracy is often limited. At best such models can be used to set the initial parameter combinations, and then an online sensor-based system should take over for real time predictions.

It is understood from the literature that pulse classification-based condition monitoring system is one of the most reliable way to predict process failures. This is based on the finding that the undesirable discharge pulses like short circuits are having a direct influence on the process stability and failures. If pulse classification is disregarded, the prediction model fails to consider the effects of abnormal sparks (open circuit, short circuit) and resulting failure prediction can be less accurate. However, most of the existing models fails to consider every discharge characteristic that lead to failure, and hence the predictions can be inaccurate. Also, many of the developed systems are capable of just alerting the operator about a potential failure, without intimating the degree of severity or they fail to propose a process control for process regulation. Another gap in the existing research work is regarding the type of failure considered. Almost the entire existing research work is addressing just one mode of wire EDM failure, i.e., wire breakages. However, there is a need to look at other modes of process interruptions which affects the process efficiency. Existing literature has not used the potential of machining learning techniques to the fullest in the area of sensor data-based failure prediction and process control. Neural network classifiers and regression models are capable of learning the patterns from acquired signals which leads to process failures.

## **2.9 RESEARCH OBJECTIVES**

The research aims to analyse the effect of machining stability on process failures, and to propose a condition monitoring and process control system for wire EDM process. The condition monitoring is performed initially through offline models and later by developing an online system. Following are the objectives of the present study:

- 1 To study the effect of wire electric discharge machining stability on the performance characteristics.
- 2 To develop a classification model to predict and analyse the failures of wire EDM process.
- 3 To predict the occurrences of wire breakages by modelling mean gap voltage.
- 4 To perform pulse train analysis and pulse classification to relate machining performance and discharge characteristics.
- 5 To develop an intelligent algorithm for performance monitoring, failure prediction and process control through multiple sensor signals.

## **CHAPTER 3**

### **EXPERIMENTAL WORK**

#### **3.1 INTRODUCTION**

This chapter details the experimental setup developed for the condition monitoring of wire EDM process. The experimental plan and procedure are discussed in detail. Details of the hardware used and methodology followed for the waveform measurement, signal processing and feature extraction are explained. Also, different test equipment used to measure the surface integrity of machined components are described.

#### **3.2 PILOT EXPERIMENTS**

Initial experiments are conducted on Inconel 718 material to understand the feasible ranges and limits of process parameters to be set for studying various responses. Since the research study involves analysing both the failure and normal machining conditions, pilot experiments are important to have an initial understanding on the process behaviours with respect to different parameters. Wire breakages are observed at high pulse on time ( $>118 \mu\text{s}$ ), low pulse off time ( $<25 \mu\text{s}$ ) and low servo voltage ( $<25 \text{ V}$ ) values. On the other hand, spark absences are observed at low pulse on time ( $<100 \mu\text{s}$ ), high pulse off time ( $>55 \mu\text{s}$ ) and high servo voltage ( $55 \text{ V}$ ) values.

#### **3.3 MATERIAL SELECTION**

Inconel 718 is chosen as the workpiece for this study due to its numerous applications in the aerospace, oil and gas and cryogenic industries. The material is known to retain its superior mechanical properties at high temperatures. The nickel-based superalloy exhibits excellent fatigue, creep performance at elevated temperatures. However, superalloys like Inconel 718 is considered as difficult to cut due to the low thermal conductivity, excessive heat generation in the

machining zone, work hardening, chemical affinity to tool material at high temperatures, and built up edge formation. These combined effects result in excessive tool wear and surface damages (Parida and Maity, 2018). Wire EDM, being a non-contact material removal process, is associated with near zero cutting forces and residual stresses. Thus, the process is an ideal alternative to machine superalloys. Also, the industrial demands for machining extremely complicated profiles in Inconel 718 like fir tree slots, fir tree blade roots etc. favours wire EDM due to its flexibility and its ability to trace any complicated contours. The process is proved to be capable of meeting the strict geometric and dimensional tolerances of gas turbine industries (Klocke et al., 2012; Klocke et al., 2014; Anurag, 2018). The chemical and mechanical properties of the material are shown in Table 3.1 and Table 3.2.

**Table 3.1.** Properties of Inconel 718 (Thakur, 2009)

<b>Property</b>	<b>Value</b>
Density	8.19 g/cm <sup>3</sup>
Melting Point	1260 – 1336 °C
Specific Heat	435 J/kg K
Average Coefficient of thermal expansion	13 µm/m K
Thermal Conductivity	11.4 W/m K
Ultimate Tensile strength	1240 MPa

**Table 3.2.** Chemical composition of Inconel 718 (Reed, 2006)

<b>Element</b>	<b>Ni</b>	<b>Fe</b>	<b>Cr</b>	<b>Nb</b>	<b>Mn</b>	<b>C</b>	<b>Co</b>	<b>Al</b>	<b>Si</b>	<b>Ti</b>	<b>Mo</b>	<b>Others</b>
<b>Weight (%)</b>	51.05	19.43	18.70	5.7	0.07	0.04	0.2	0.56	0.08	1.01	3.1	0.06

### 3.4 EXPERIMENTAL SETUP

A wire electric discharge machine (Model: Ecocut, Make: Electronica) is considered for conducting experiments in this study. The wire EDM machine is shown in Fig. 3.1. The machine is having X Y motion for translation, along with U V axis motion to provide taper. The resolution is 1 µm in each axis. The dielectric fluid used is deionized water having a conductivity of ~20 µS/cm. Maximum workpiece height and weight supported are 200 mm and 300 kg. The machine supports wire electrode of 0.25 mm diameter which is held straight

between the upper and lower wire guides. Wire spools of 3.5 kg and 5 Kg can be loaded to this machine. The machine can be operated in two different power modes. Pulse power mode and fine power mode. Power pulse mode is generally used for rough cut operation and fine pulse mode is used for trim cut operation.

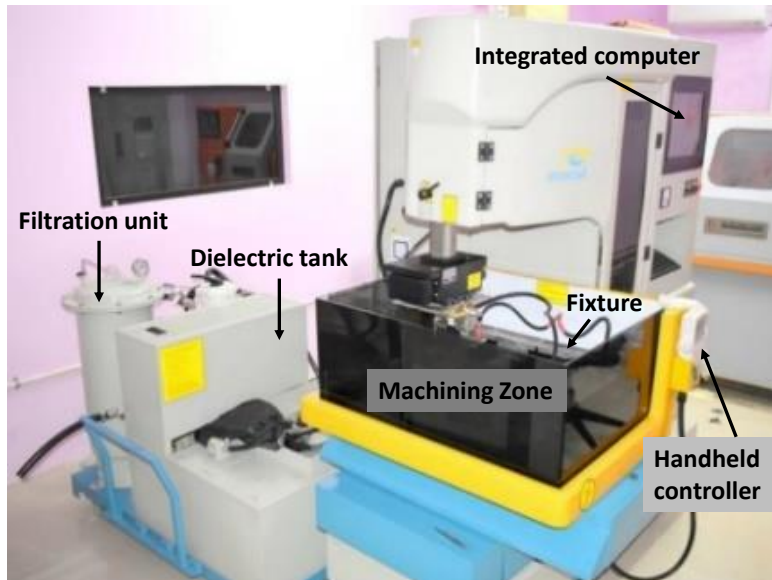


**Fig. 3.1** Wire electric discharge machine setup

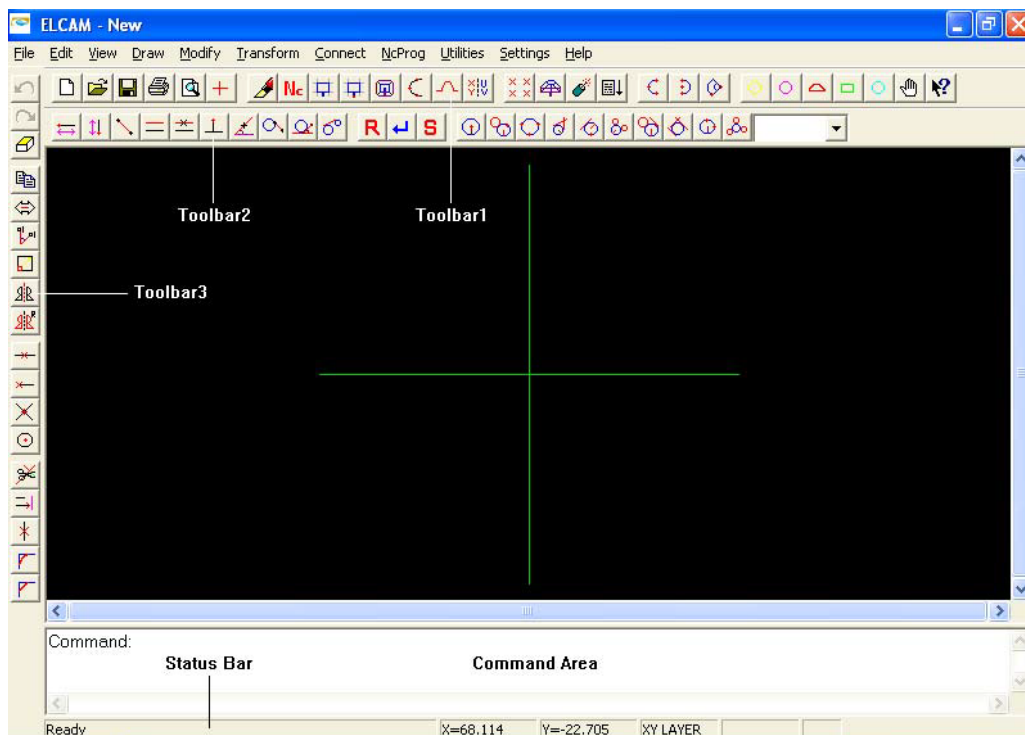


**Fig. 3.2** Elcam software interface

The profiles are CNC coded by using Elcam software. The software has all the basic draw and modify tools available in basic CAD softwares. Once the profile is drawn, the wire path start and end points are specified, followed by wire travel direction and wire compensation. Wire travel direction is simulated by the software to check for errors. Once the profile and wire travel are satisfactory, then the CNC codes to machine the profile is autogenerated by the software. The saved file can be transferred to the EDM machine using an USB drive. The software interface is given in Fig. 3.2.

### 3.4.1 Condition monitoring setup

A condition monitoring system is equipped to the wire electric discharge machine for failure prediction and process control. The system consists of high sampling rate differential probe, current probe, oscilloscope and a high-performance personal computer. The description of condition monitoring system components is given in Table 3.3.

**Table 3.3.** Components of condition monitoring system for wire EDM

S. No	Hardware	Model	Description
1	Oscilloscope	MDO 34-200	200 MHz bandwidth 2.5 GSa/s per channel 10 M points record length
2	Differential Voltage Probe	P 5200A	50 MHz bandwidth 0-1300 V measuring range
3	Current probe amplifier, Current probe	TCPA 300 TCP 303	100 MHz bandwidth, 0-150 A measuring range
4	Data acquisition system, 20 Channel Multiplexer module	DAQ 6510 + 7700 multiplexer	

**Differential probe:** A high voltage differential probe from Tektronix (model P5200A) is used for the voltage measurement between the electrodes. The voltage probes are equipped with switchable attenuation and bandwidth limits. The

measuring range of the differential probe is  $\pm 1300$  V with a bandwidth of 50 MHz. Specifications of the differential probe is given in Table 3.4. The differential probe is shown in Fig. 3.3.

**Table 3.4** High voltage differential probe specification

S. No.	Feature	Specification
1	Attenuation	50X/500X
2	Bandwidth	DC to 50MHz
3	Connector	BNC
4	Differential voltage	500X: $\pm 1300$ V, 50X: $\pm 130$ V
5	Common mode voltage	$\pm 1300$ V
6	Differential input impedance	$10\text{M}\Omega/2.0\text{pF}$
7	Input Impedance between each Input and Ground	$5\text{M}\Omega, 4\text{pF}$
8	CMRR	DC: $>80$ dB 100 kHz: $>60$ dB 3.2 MHz: $>30$ dB 50 MHz: $>26$ dB
10	Maximum input voltage to earth	1000V CAT II



**Fig. 3.3** Differential probe

**Current probe:** AC/DC current measurement system from Tektronix is used to measure the discharge current during wire EDM pulse cycle. The system includes a TCP303 current probe with TCPA300 current probe amplifier as shown in Fig. 3.4. The bandwidth of the current probe when coupled with amplifier is 15 MHz. Measuring range is from 5 mA to 150 A RMS when using the high current

range of 50 A/V. The detailed specifications of the current probe, current probe amplifier system is given in Table 3.5.

**Table 3.5** Specifications of the current measurement system

S. No.	Feature	Specification
1	Bandwidth	DC to 15 MHz
2	Rise time	$\leq 23$ ns
3	Typical Accuracy	DC: $\pm 1\%$ of reading
4	Insulation	300 V CAT III
5	Signal delay	40 nS
6	High current Range	50 A/V
7	Max DC, RMS and Peak (high current range)	150A, 150A, 500A
8	Low current Range	5 A/V
9	Max DC, RMS and Peak (low current range)	25A, 17.7A, 500A
10	Max conductor Size	21 mm x 25 mm



**Fig. 3.4** Current probe and current probe amplifier

**Oscilloscope:** A Tektronix mixed domain oscilloscope (MDO) is used to record and analyse the voltage and current signals during the machining operation. The model image is given in Fig. 3.5. The model MDO 34-200 has 4 analog channels, each with a sampling rate of 2.5 G Samples/s. The record length is 10 million and bandwidth is 200 MHz which is upgradable if required. The oscilloscope is interfaced with MATLAB using TekVISA drivers. Further specifications of the oscilloscope are shown in Table 3.6.

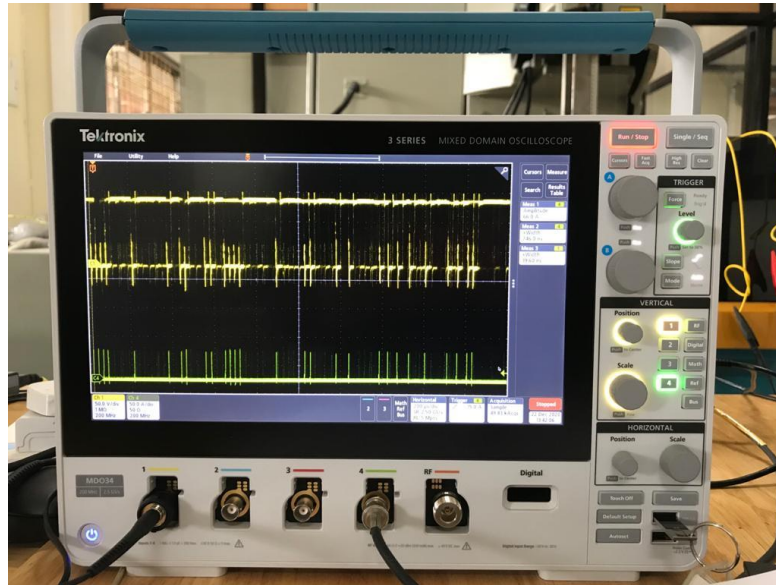


**Fig. 3.5** Mixed domain oscilloscope

The overall schematic and connections of the proposed condition monitoring system is given in Fig. 3.6. The two ends of differential probe are connected across the electrodes. Positive wire is connected to workpiece and negative to wire electrode. The current monitor is a ring type probe which is clipped around the wire electrode side (negative polarity). The current and voltage probes are connected to two separate channels of the oscilloscope. Fig. 3.7 shows the image of the condition monitoring system installed on the wire EDM.

**Table 3.6.** Specifications of the MDO 34 oscilloscope

S. No.	Feature	Specification
1	Bandwidth	200MHz
2	No of Analog channels	4
3	Record length	10 M
4	Sampling rate	2.5 Gsa/S on all channels
5	Typical rise time	2ns
6	Time base	1 ns/div to 1000 s/div
7	Time base Accuracy	±10 ppm
8	Vertical	1 mV/div to 10 V/div @ 1 MΩ
9	Waveform capture rate	>230,000 wfms/s in FastAcq acquisition mode
10	Display	11.6 in. (295 mm) TFT LCD with capacitive touch 1920 horizontal × 1080 vertical HD
11	Probe interface	TekVPI probe interface
12	Bandwidth upgradability	Available
13	Connectivity	Front and rear USB host ports, HDMI port (rear), Aux in AUX out, 10/100 Ethernet (rear)

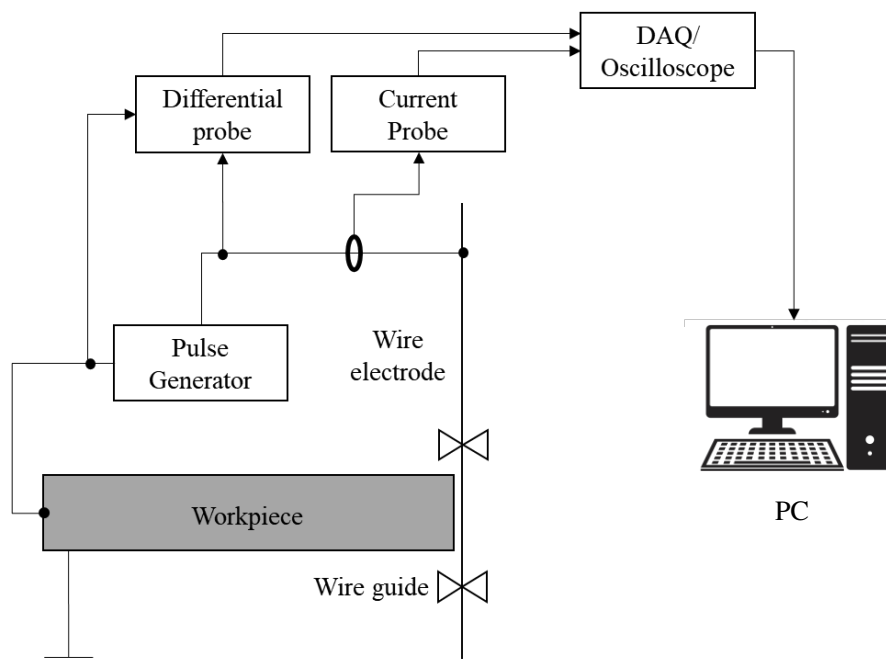


**Fig. 3.6** Schematic of the condition monitoring setup

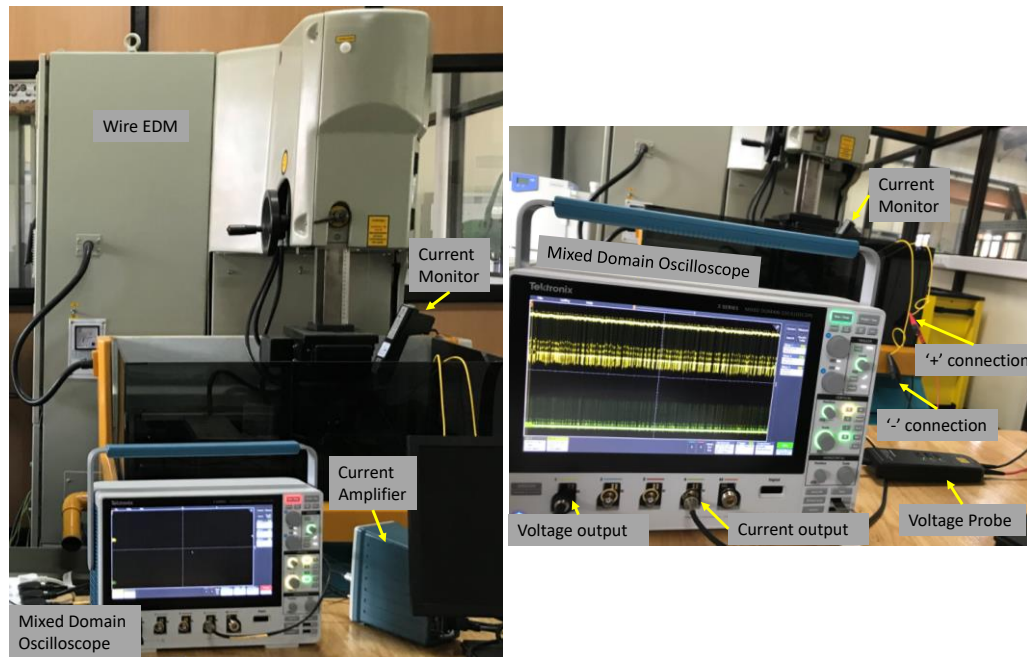


**Fig. 3.7** Condition monitoring system installed on wire electric discharge machine

### 3.5 EXPERIMENTAL METHODOLOGY

Initially pilot experiments are conducted to approximate the parameter limits and ranges for safe operation and process failures. The initial experiments are aimed to study the effect of debris accumulation on machining failure and part quality. After which, offline models are developed for failure classification and prediction. Based on the understanding of the failure mechanism from the offline models, the online condition monitoring is performed using multi sensorial data from current and voltage sensors. The experimental procedure is described as follows.

- The effect of process parameters on the machining failures is understood by conducting pilot experiments. Based on this, unideal machining situations during wire EDM of Inconel 718 is created intentionally, which will result in machining failures like wire breakage and spark absence. The approach is to increase the degree of debris accumulation in the spark gap by changing pulse on time, pulse off time and servo voltage at discrete levels.

- The effect of debris accumulation in the spark gap on the machined surface integrity is analyzed by considering the surface roughness, 3D surface morphology, microstructural analysis by SEM images, and EDS analysis. Additionally, wire wear and elemental migration is also studied.
- A multi-class classification model based on artificial neural network (ANN) is modelled to predict the machining outcomes. Eighty-one experiments are conducted based on full factorial experimental design to train the model. The class labels for this multi class classification model are normal machining, wire breakage, and spark absence.
- An in-process data parameter (mean gap voltage variation,  $\Delta V_m$ ) is introduced as an indicator of machining stability during the wire EDM process.  $\Delta V_m$  value computes the difference between the set voltage and actual gap voltage during machining. The gap voltage fluctuations are due to the debris accumulation in the inter electrode gap. Such a situation, where debris tends to accumulate without getting completely flushed away, indicates an unstable machining condition.  $\Delta V_m$  value is greater at higher instabilities, and can potentially lead to wire breakage after a limit. An ANFIS model is developed to predict  $\Delta V_m$  value, based on which a decision support model can alert the operator about a potential wire breakage. Thirty-one experiments are conducted based on central composite design (CCD) of response surface methodology (RSM) to train the ANFIS model. The effect of  $\Delta V_m$  on the machine part quality is evaluated by considering surface, morphological and topographical study. The effect of  $\Delta V_m$  on wire wear is also studied.
- A condition monitoring system is set up by installing high sampling rate voltage and current sensors to the wire EDM. A mixed domain oscilloscope and a high-performance PC is used to record, process and analyse the sensor data to make failure predictions.
- Different discharge characteristics like pulse frequency, ignition delay time, and discharge energy are extracted from voltage and current signals. One factor at a time experiments are conducted to study the effect of process parameters on the discharge characteristics.

- A pulse classification algorithm is developed to distinguish between normal, arc, short and open discharges. The effect of pulse proportions on process responses and machining failures is studied.

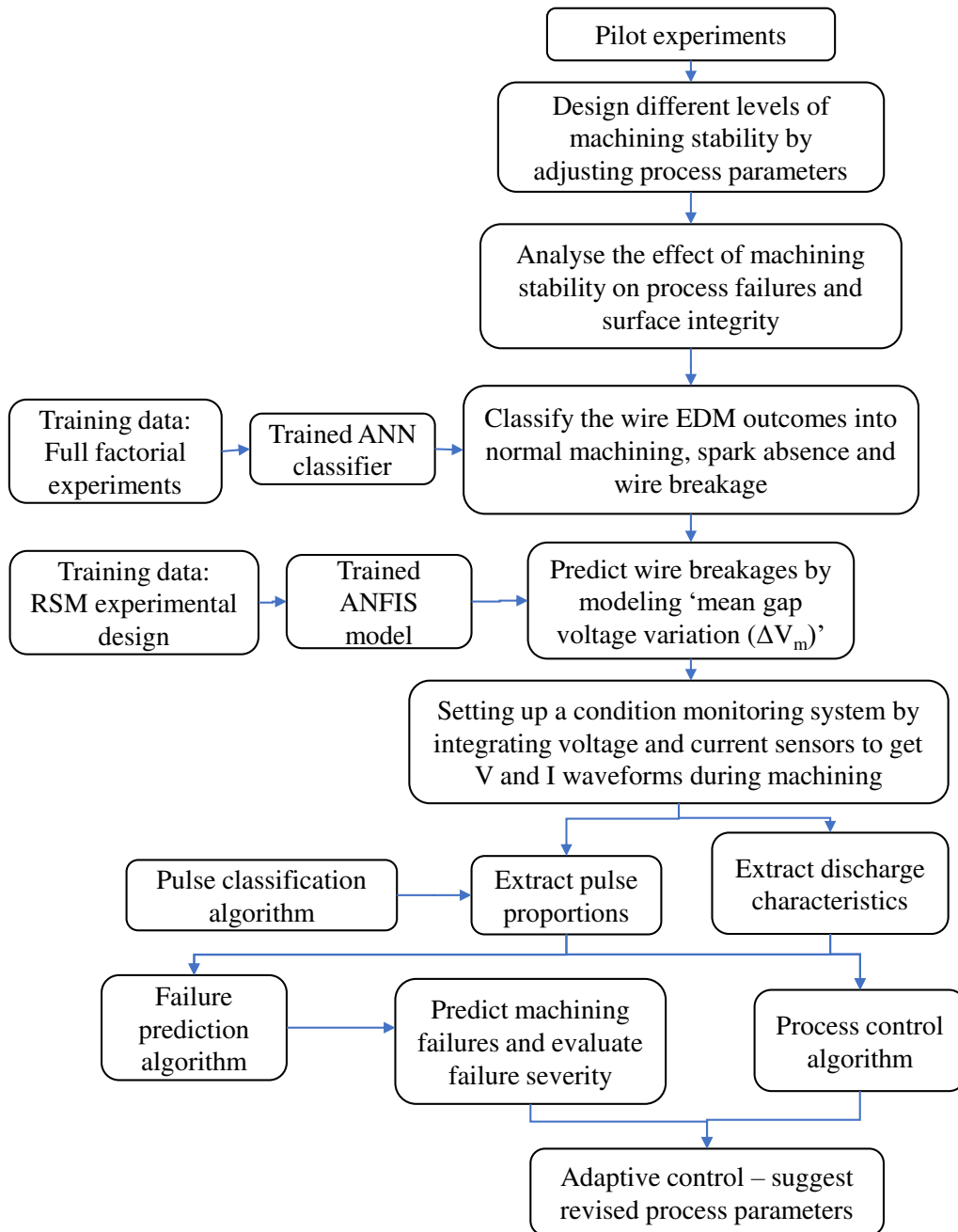


**Fig. 3.8** Flowchart of the experimental plan

- A failure detection algorithm is developed to predict the process failures like spark absence and wire breakage based on extracted discharge characteristics and pulse proportions from the sensor data.
- Finally, an intelligent process control algorithm identifies the severity of process failure and suggest alternate input parameter settings to restore the machining stability back to normal. The control system ensures continuous machining without process failures.

The experimental plan is represented as a flowchart in Fig. 3.8.

## **3.6 SOFT COMPUTING MODELS**

### **3.6.1 ANN classification**

Classification is a machine learning problem where a class label is predicted for a given sample data. If the model classifies data into two classes, then the model is a binary classifier. On the other hand, a multiclass classifier categorises the data into more than two classes. The technique involves fitting a decision boundary to separate the datapoints to separate classes. The datapoints lie in a multi-dimensional space, whose order depends on the number of inputs. For example, if the input dataset contains 4 elements, then the decision boundary is a 4 – dimensional hyper surface. As the dimension and non-linearity increases, the complexity to fit such a hyper surface also increases. Neural network classifiers are reported to perform well in such non-linear and multidimensional cases.

Artificial neural network (ANN) is a bio inspired machine learning technique which emulates the learning system of the human neurons. It is a supervised learning technique which predicts the class label of input dataset. The class label can be an event or a category to which the input dataset belongs to. To train the model, a sufficiently large training data has to be fed initially. The training dataset consists of the input data, which in the case of wire EDM modeling is a combinations of input parameters, and its corresponding class labels, which are machining outcomes. If 81 training experiments are conducted by varying 4 input parameters, then input dataset to train the model is a matrix of size [81 x 4]. Its

corresponding class labels are recorded as probability of the input dataset to fall in each category. If there are 3 class labels, then the output dataset for the training is a matrix of size [81 x 3]. Such a classification technique where a given data is classified into several classes is called multi-class classification problem.

The feed forward back propagation neural network (FFBPNN) is a common ANN architecture which is used in this study. Here, weights and biases of neurons in each layer is carried forward as neuron outputs. These weights and biases are tuned or adjusted to minimize the error between the actual class and predicted class. This model is extremely capable of understanding the patterns and is very versatile. The optimal ANN architecture is application dependent. Therefore, setting the number of hidden layers is challenging and heuristic methods are often adopted to reach the optimal ANN structure. A generic ANN structure is shown in Fig. 3.9. The output layer of the classification neural network gives the class probability of each input dataset. Using the SoftMax function,  $i^{\text{th}}$  output neuron gives the probability as shown in Eq. (3.1)

$$p_i = \frac{e^{q_i}}{\sum_{j=1}^k e^{q_j}} \quad (3.1)$$

where  $q_i$  is the input vector to the output neuron  $i$ ,  $k$  is the total number of classes in the classifier. The ANN parameters used in the classifier model is given in Table 3.7.

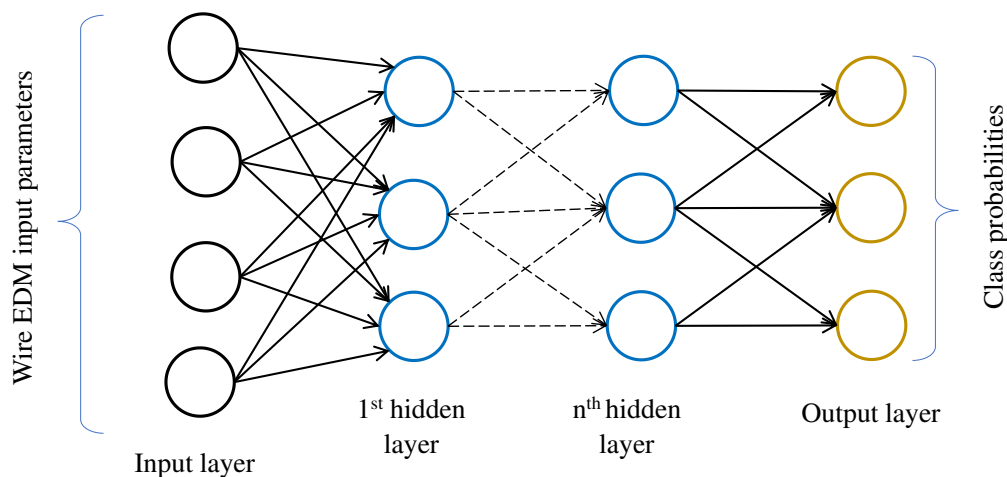


**Fig. 3.9** ANN structure

**Table 3.7** Parameters of ANN based multiclass classifier

Parameter	Properties
Number of inputs	4
Input layer neurons	Pulse on time, pulse off time, servo voltage, wire feed rate
Number of classes	3
Output layer neurons	Probability of spark absence, wire breakage and normal machining
Number of neurons in each hidden layer	10
Training algorithm	Scaled conjugate gradient backpropagation (trainscg)

### 3.6.2 ANFIS modeling

Adaptive neuro fuzzy inference system (ANFIS) combines the benefits of both fuzzy logic and artificial neural network algorithms. It is a supervised machine learning technique which uses an inference engine based on IF-THEN rule set. However, unlike fuzzy logic models, ANFIS is not entirely expert knowledge dependent and can be trained using training dataset. The membership function parameters can be tuned using gradient descent during back propagation. Also, the model uses least squares to tune output node function consequent parameters. ANFIS is regarded as computationally efficient and capable to handle non-linearities, which makes it a suitable option to model wire EDM responses. ANFIS structure has 5 layers and each layer contains several nodes as shown in Fig. 3.10. The nodes are distinguished by their node functions which are explained as follows:

**Layer 1:** This layer receives the input parameter values and identifies the corresponding membership function. This process is called fuzzification. This is a variable node, whose node function is given by

$$O_{1,i} = \mu_{A_i}(x) \text{ for } i = 1,2 \quad (3.2)$$

$$O_{1,i} = \mu_{B_{i-2}}(y) \text{ for } i = 3,4 \quad (3.3)$$

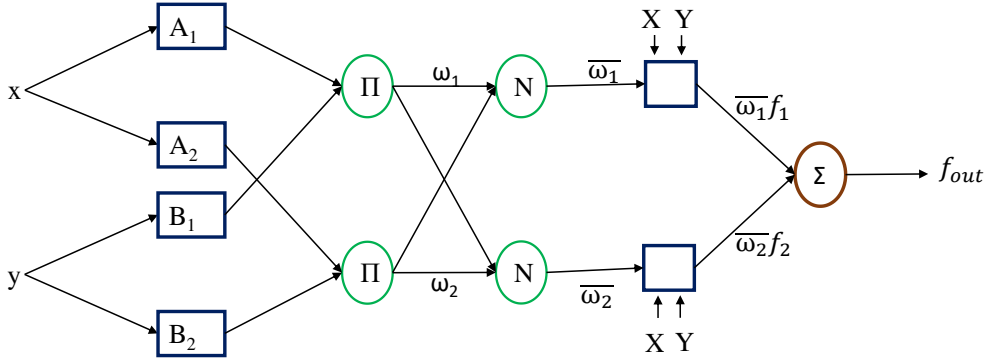


**Fig. 3.10** ANFIS structure

here  $x$  and  $y$  denote the two input parameters, and their linguistic variables are given by  $A$  and  $B$  respectively. The shapes of the membership function can be gaussian, triangular, trapezoidal etc.  $\mu(x)$  and  $\mu(y)$  represents the membership functions. A triangular membership function is defined by the equation

$$\mu(x) = \begin{cases} 0, & x \leq a \\ \frac{x-a_i}{b_i-a_i}, & a \leq x \leq b \\ \frac{c_i-x}{c_i-b_i}, & b \leq x \leq c \\ 0, & c \leq x \end{cases} \quad (3.4)$$

On the other hand, if the membership function is gaussian, then the equation changes to

$$\mu(x) = \exp\left(\frac{-(c_i-x)^2}{a_i^2}\right) \quad (3.5)$$

here, the trainable function parameters are given by  $a_i$ ,  $b_i$  and  $c_i$ , which determines the shape of the membership function.

**Layer 2:** Layer 2 is the ‘rule layer’ which consists of fixed nodes which are indicated by  $\Pi$ . Here each node computes the product of the input membership function values. The output function is thus given by the equation

$$O_{2,i} = \omega_i = \mu_{A_i}(x) \cdot \mu_{B_i}(y) \quad \text{for } i = 1,2 \quad (3.6)$$

where  $\omega_i$  is the node output which represents the firing strength of a rule.

**Layer 3:** Layer three comprises of fixed nodes represented by N. The node normalizes the rule firing strength computed by the rule layer. The node function is given by

$$O_{3,i} = \overline{(\omega_i)} = \frac{\omega_i}{\sum \omega_i} = \frac{\omega_i}{\omega_1 + \omega_2} \quad \text{for } i = 1,2 \quad (3.7)$$

**Layer 4:** This layer contains adaptive nodes. The nodes receive the normalized rule firing strength as input and multiplies it with fuzzy if then rules. The node function is thus given by

$$O_{4,i} = \overline{(\omega_i)} \cdot f_i \quad \text{for } i = 1,2 \quad (3.8)$$

here the fuzzy if then rules are given by  $f_1$  and  $f_2$  and the consequent parameters are represented by  $p_i$ ,  $q_i$  and  $r_i$

$$\text{Rule 1: if } x \text{ is } A_1 \text{ and } y \text{ is } B_1 \text{ then } f_1 = p_1 x + q_1 y + r_1$$

$$\text{Rule 2: if } x \text{ is } A_2 \text{ and } y \text{ is } B_2 \text{ then } f_2 = p_2 x + q_2 y + r_2$$

This layer is called defuzzification layer

**Layer 5:** This final layer contains fixed nodes, which gives the final output by the following equation

$$O_{5,i} = f_{out} = \sum_i \overline{(\omega_i)} \cdot f_i \quad \text{for } i = 1,2 \quad (3.9)$$

### 3.7 LOW PASS FILTER

The raw signals captured by the condition monitoring system are processed and relevant features are extracted to draw conclusions regarding the health status of the process. Filtering is a process performed to partially or completely eliminate the undesirable components of a signal. A low pass filter suppresses the high frequency noises in the raw signal allowing the lower frequencies to pass through. SignalAnalyzer toolbox in MATLAB is used to filter the raw signals. Fig. 3.11 shows a sample waveform to demonstrate the effect of lowpass filter tool.

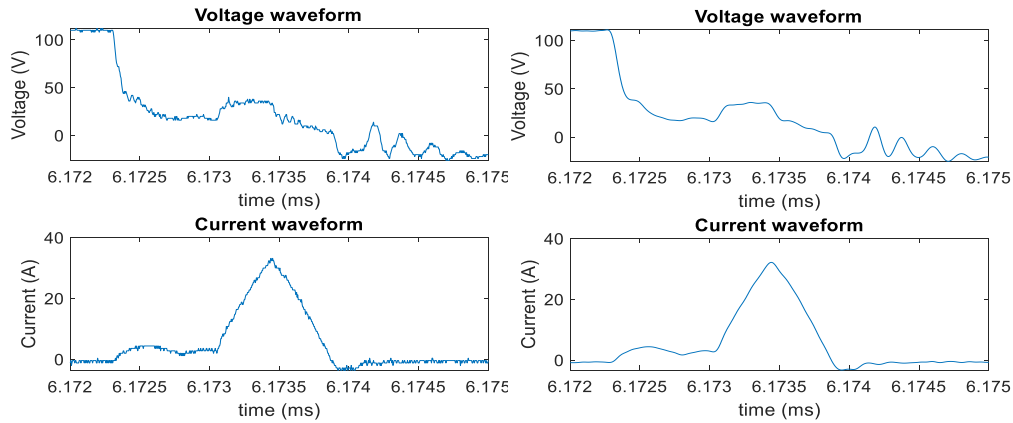


**Fig. 3.11** (a) Unfiltered signal (b) Filtered signal

### 3.8 MEASUREMENT OF PERFORMANCE CHARACTERISTICS

#### 3.8.1 Cutting speed

Cutting speed is calculated as the ratio of the length machined and time taken for machining.

$$\text{Cutting speed, } CS \text{ (mm/min)} = \frac{\text{Total profile length (mm)}}{\text{Total machining time (min)}} \quad (3.10)$$

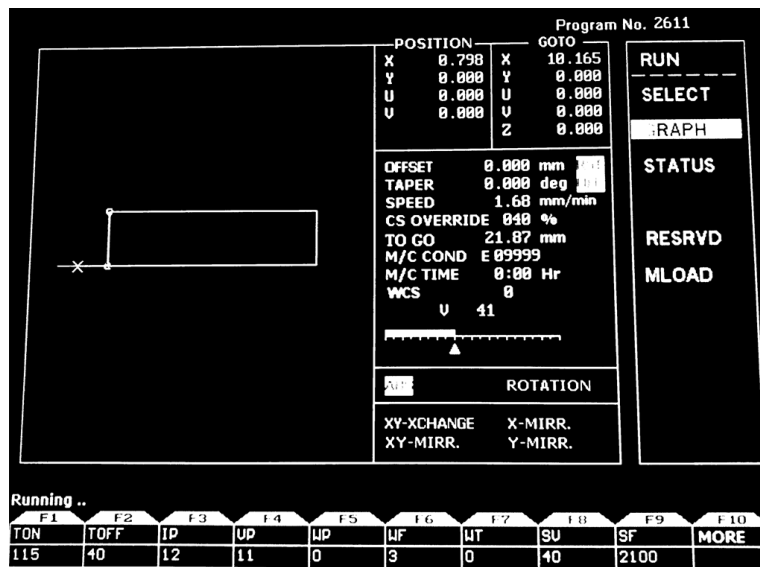


**Fig. 3.12** Integrated computer displaying the cutting speed value during machining

Once the machining starts, cutting speed is displayed in the integrated screen of wire EDM as shown in Fig. 3.12. The path length, computed from the CNC codes is also displayed in the integrated screen. To verify the displayed value, cutting speed is calculated manually by recording the machining time manually.

### 3.8.2 Surface roughness

Zeiss Surfcom Flex 35-B contact type compact surface profilometer with a diamond stylus tip and sapphire skid is used for surface roughness measurement (Fig. 3.13). Measuring range in z axis is  $\pm 160 \mu\text{m}$  with a resolution of  $0.01 \mu\text{m}$  at  $\pm 20 \mu\text{m}$ . The evaluation length was considered is 4 mm and the cut-off length ( $L_c$ ) is 0.8 mm. The probing force is 4 mN during the roughness measurement. Total traverse length is 12.5 mm with a measuring and retraction speed of 0.6 mm/s and 1 mm/s respectively.



**Fig. 3.13** Surface profilometer

### 3.8.3 Microstructural analysis

A field emission scanning electron microscope (FESEM) of Zeiss make with model number GeminiSEM 300 is used to obtain surface microstructure of machined samples and worn wire samples. The SEM is having a maximum magnification of 2,000,000X with a resolution of 0.8 nm at 15 kV. To analyse elemental compositions, the SEM is equipped with an Energy Dispersive X-Ray

Spectroscopy (EDS) attachment. The model has different detectors like back scattered electron detector (BSE), secondary electron detector (SE), and in-lens detector which are selected based on imaging requirement. The FESEM is shown in Fig. 3.14. Machined surfaces are imaged with a magnification of 1500 x for microstructural analysis and comparison. On the other hand, worn wire samples are imaged with 300 x and 500 x magnification based on the feature analysed. In both the cases, SE2 detector is selected.



**Fig. 3.14** Field emission scanning electron microscope (FESEM) setup

#### **3.8.4 Profile accuracy**

An accurate tutor spectra model, bridge type coordinate measuring machine (CMM) is used to evaluate geometric accuracies of machined parts in this study. The machine has a resolution of 0.1  $\mu\text{m}$  and a measuring range of 500 mm (x axis) x 600 mm (y axis) x 400 mm (z axis). The CMM uses a ruby probe of 5 mm diameter. An air bearing guidance is provided for accurate and smooth travel on all axes. The software Arco CAD is used to measure and analyse the profile through an integrated computer system. Dimensional and form deviations are measured, stored and analysed using this software graphics user interface. The CMM and the measuring probe is shown in Fig. 3.15.

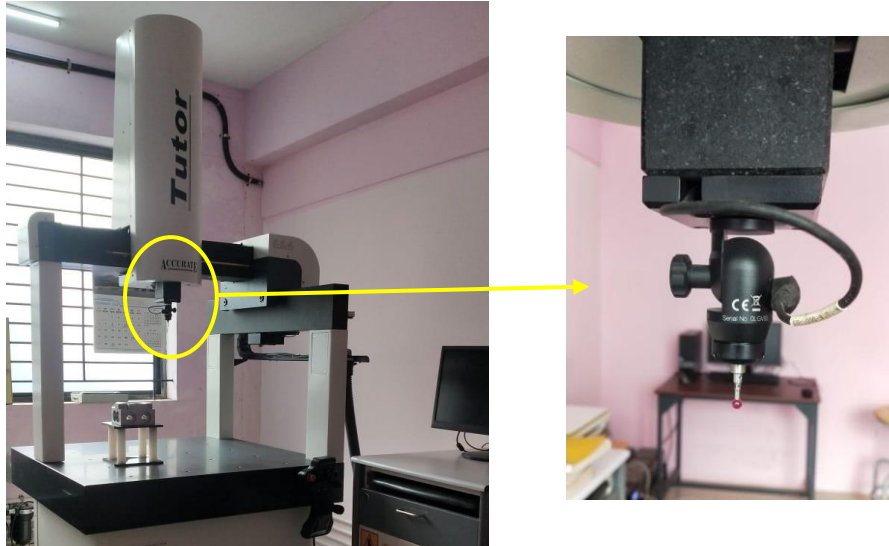


**Fig. 3.15** Coordinate measuring machine

### 3.8.5 Surface morphology

A non-contact 3D profilometer, as shown in Fig. 3.16, is used to analyse the surface morphology of machined surfaces. AEP Nanomap 1000WPI model white light interferometer is used to create high resolution 2D and 3D surface images. The XY scanning range can be up to 150 mm x 150 mm and z axis resolution is 0.001 nm. The profilometer is equipped with antivibration table to eliminate the noises. Both 2D and 3D surface roughness parameters like  $R_a$ ,  $R_z$ ,  $R_q$ , and  $S_a$ ,  $S_z$ ,  $S_q$  can be measured using this instrument.



**Fig. 3.16** Non-contact 3D profilometer

### **3.9 SUMMARY**

The chapter summarises the details of the developed condition monitoring experimental setup. The details regarding the wire electric discharge machine, consumables, workpiece and parametric settings are discussed. The overall methodology of the current research work is described emphasising on sensors and acquisition system. Different soft computing tools for classification and regression have been briefed. Also, signal processing operation like filtering, to suppress noisy data from the raw signals are described. Various responses measured, along with the details of the test equipment like FESEM, contact profilometer, non-contact profilometer, coordinate measuring machine etc. is detailed. The test accuracy and repeatability of measuring equipment was ensured in each case.

## CHAPTER 4

### MACHINING STABILITY ANALYSIS

#### 4.1 INTRODUCTION

This chapter details about the process stability of wire EDM process. Unstable machining conditions affects the productivity, part quality and process sustainability. The stability is strongly dependent on the debris generation, debris accumulation in the spark gap, and its effective removal during the pulse off time. Mechanism of wire wear leading to rupture as a result of debris stagnation in the spark gap is analysed. Experimental methodology incorporated to create unstable machining situation is also discussed. The main objective of this chapter is to understand the relevance of maintaining machining stability from a surface integrity point of view. In this regard the effect of unstable machining conditions on surface integrity and process failure are analysed.

Wire EDM machining process is said to be stable when the debris generated is flushed away entirely during the pulse off cycle. Also, the dielectric property of the spark gap is to be restored entirely during this period. A stable wire EDM pulse cycle result in breaking and restoration of dielectric barrier in the spark gap during the pulse on and off cycles respectively. This is an idealized situation to explain the material removal mechanism. Practically, the debris removal is always partial, leading to time variant dielectric properties in the spark gap. Easiness of flushing the debris from the spark gap is mainly dependent on pulse off time and the inter electrode distance. The inter electrode distance is set by a feedback voltage parameter called the servo voltage. Also, the relative amount of debris generated is directly proportional to the pulse on time.

## 4.2 EXPERIMENTAL DETAILS

To study the machining stability, several methods have been used by the researchers in the past to intentionally create unstable machining conditions. In this study, the unstable conditions are custom designed by varying the severity of debris stagnation in the spark gap. This is done by varying pulse on time, pulse off time and servo voltage together in discrete steps. Higher discharge energy implies more material removal rate and hence more debris are produced. Narrower spark gap makes it harder for the dielectric to flush away the debris. Servo voltage is the parameter which governs the spark gap. Also, lesser the pulse off time, higher are the chances of incomplete debris removal. The parameter combination chosen to generate different amounts of debris in the spark gap is shown in Table 4.1. A representation of possible debris accumulation at different machining conditions are shown in Fig. 4.1. The profile machined is shown in Fig. 4.2. This profile is chosen to evaluate form errors like flatness error, circularity and cylindricity. The parameters and ranges are selected based on pilot experiments, wire EDM manual, and literature survey.

**Table 4.1.** Process parameter combinations based on machining stability

<b>Machining condition label</b>	<b>T<sub>on</sub> (μs)</b>	<b>T<sub>off</sub> (μs)</b>	<b>Servo Voltage (V)</b>	<b>Discharge energy</b>	<b>Pulse off time</b>	<b>Spark gap distance</b>
C1	101	52	65	Lowest	Highest	Highest
C2	104	50	60	Low	High	High
C3	107	48	55	Relatively low	Relatively high	Relatively high
C4	110	46	50	Medium	Medium	Medium
C5	113	44	45	Relatively high	Relatively low	Relatively low
C6	116	42	40	High	Low	Low
C7	119	40	35	Highest	Lowest	Lowest

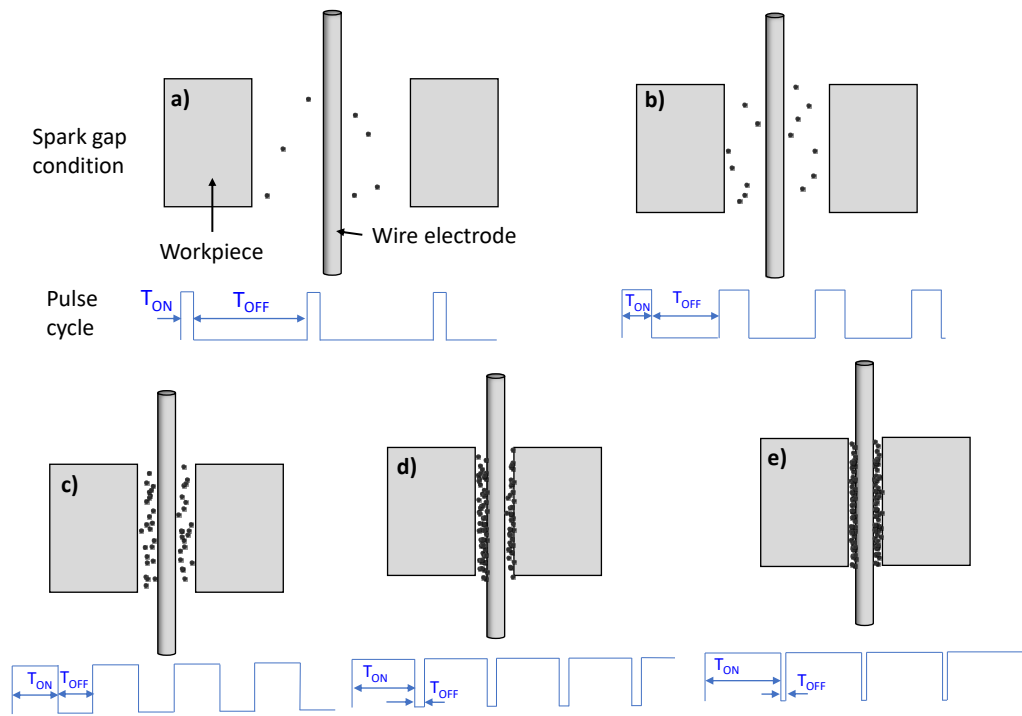


**Fig. 4.1** Representation of debris accumulation in spark gap at machining condition (a) C1 (b) C2 (c) C4 (d) C6 (e) C7



**Fig. 4.2** Shape of the profile machined

Inconel 718 material of thickness 10 mm is chosen for this study. Zinc coated brass electrode of 0.25 mm diameter is chosen for the surface integrity and process failure analysis. Coated wire is chosen because of the higher overall performance and better resistance to wire breakage which is evident from a wire electrode comparison described in this chapter. The responses measured are average surface roughness, cutting speed, flatness error, circularity, and

cylindricity. Additionally, microstructural analysis of machined surface and worn wire surface, subsurface EDS analysis of machined and wire surface, surface morphology study by 3D profilometer images, and micro hardness study are conducted to compare the surface integrity at different machining conditions.

### 4.3 GEOMETRIC ERRORS

Geometric inaccuracy during the wire EDM operation is related to the bending, fluctuation or vibration of wire electrode during the spark machining. Ideally wire electrode is expected to be in vertically straight position throughout the machining process. However, this is an idealized situation where the only force acting on the wire electrode is the axial wire tension. In reality, numerous lateral forces are acted upon on the wire electrode which deflects or vibrates the wire electrode. The forces are expected to be more for unstable machining conditions compared to stable machining conditions. The geometrical profile is traced by the top and bottom wire guides, disregarding the actual wire electrode position in the machining zone. Therefore, any deviation of wire electrode from the imaginary straight line connecting the top and bottom wire guide wire guides would result in inaccurate machining. Wire lag (deflection) and wire vibration are regarded as the two main reasons for geometrical inaccuracies.

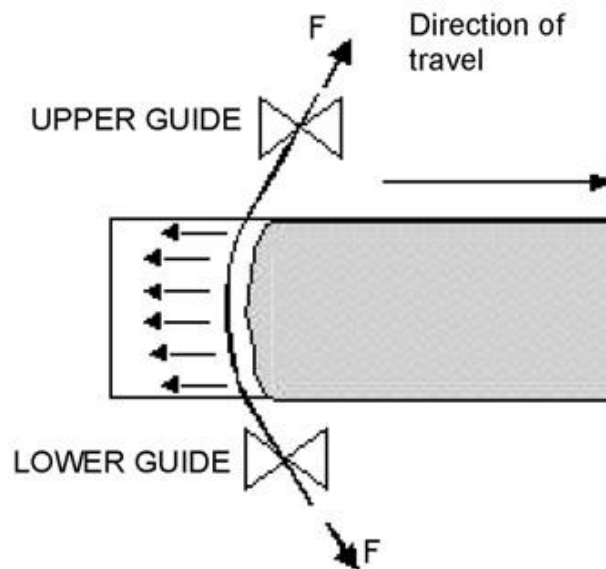


**Fig. 4.3** Wire lag effect influencing geometric accuracy (Sanchez et al., 2007)

### 4.3.1 Inaccuracy due to wire deflection

Wire lag is the prominent effect of wire deflection. Wire lag is static deflection parallel to machined path, defined as the maximum magnitude of the difference between programmed wire position and actual wire position. The reason for wire lag effect is unbalanced forces acting on the wire electrode during the spark erosion. Wire lag effect is considered as the chief cause of form error especially when the profile involves change in wire direction, as in corner cutting (Lin et al., 2001; Sanchez et al., 2007). The wire lag effect is depicted in Fig. 4.3.

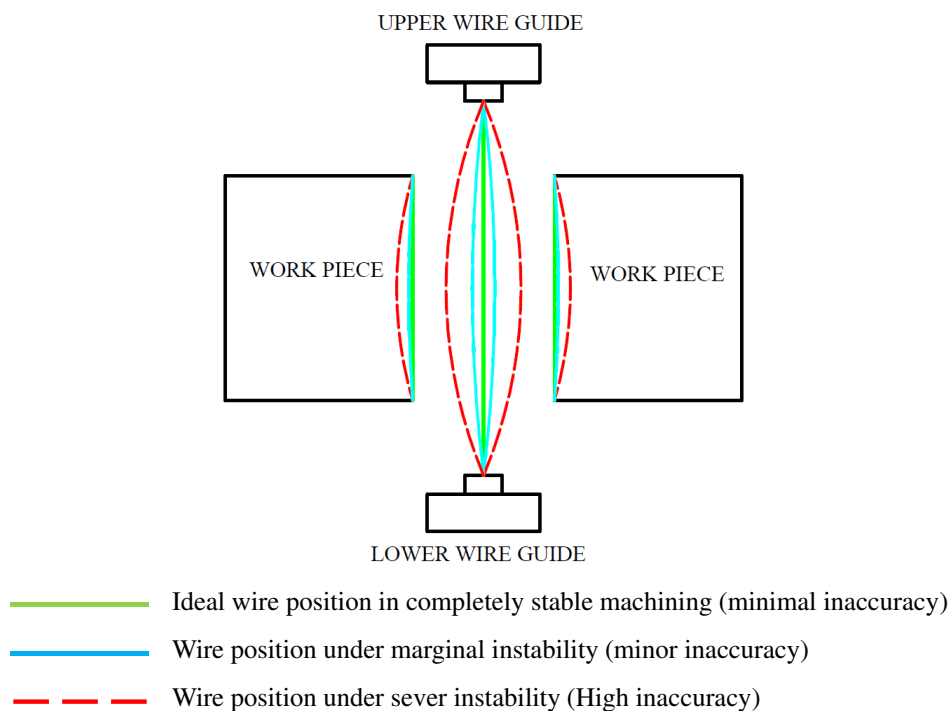


**Fig. 4.4** Wire vibrations influencing geometric accuracy

### 4.3.2 Inaccuracy due to wire vibrations

The various unbalanced forces acting on the wire electrode are electrostatic forces, electromagnetic forces, dielectric fluid flushing pressure, force due to discharge sparks, and the pressure exerted by the vapour bubbles formed during the spark erosion. These forces result in wire electrode vibrations parallel to machining direction and perpendicular to it. Fig. 4.4 shows how the wire vibrations effect the geometric accuracy of machined profile. A stable machining is expected to result in fewer wire vibrations, and vice versa. During an unstable

machining, wire electrode experiences higher lateral forces due to the combined effect of higher intensity sparks along with higher pressure exerted by vapour bubbles.

#### 4.4 MACHINING OUTCOMES

The machining outcome under each of the seven conditions are recorded as shown in Table 4.2. The machining outcome is regarded as process interruption if the machining is halted before the completion of profile. Two such cases are observed, namely spark absence and wire breakage corresponding to condition C1 and C7 respectively. Other conditions from C2 to C6 are observed to machine the profiles without any process failures. However, their surface integrity varies considerably due to differences in spark gap condition, and is discussed in detail in the upcoming section.

**Table 4.2** Machining outcomes under different machining conditions considered

<b>Machining condition label</b>	<b>Machining outcome</b>	<b>Type of failure</b>
C1	Process interruption	Spark absence
C2, C3, C4, C5, C6	Uninterrupted machining	No failure
C7	Process interruption	Wire breakage

##### 4.4.1 Spark absence

Spark absence phenomena causes similar negative effects as wire breakage and thus it shall be avoided to ensure process efficiency. Spark absence is an inefficient machining situation where the voltage applied across the electrodes is not sufficient enough to break the dielectric barrier. In such cases, the discharge spark frequency is negligible or zero causing a process interruption. The main reasons for spark absence are higher than ideal spark gap distance. Also, this can

happen if the pulse on time is not sufficiently high to complete the ionization of discharge channel. This condition is shown in Fig. 4.1 (a).

#### **4.4.2 Wire breakage**

The debris stagnation in the spark gap results in spark gap bridging and formation of secondary sparks called short circuit sparks. These high intensity sparks occur without any ignition delay time. Ignition delay time is absent since the inter electrode gap is already conductive due to excess debris and the sparks occur immediately when the voltage supply is on, as depicted in Fig. 4.1 (e). The discharge frequency will also be higher than normal in this case. The overall effect is rapid wire wear which can eventually lead to wire breakage. Stages of wire wear at different machining conditions are shown in Fig. 4.5. Images of multiple wire surfaces under each condition are examined to ensure that similar wear patterns are observed at every instance. Also multiple locations of same wire sample is imaged to confirm a similar wire wear. Zinc coated brass wire is chosen to study the wire wear due to its better endurance to higher energy sparks and wire breakage. Fig. 4.5 (a) corresponds to case C2, where the wire wear is minimal due to low discharge energy, sufficient spark gap and pulse off time. On the contrary, at condition C6, pulse on time is the higher, spark gap is narrower and pulse off time is shorter. This leads to severe wire surface degradation due to higher intensity short circuit sparks, as shown in Fig. 4.5 (b). The wire coating is seen to be removed, exposing the unprotected inner brass wire core. At this stage the wire electrode is prone to easier breakage. If the spark gap stability worsens than this level (with still higher pulse on time, narrower spark gap, and shorter pulse off time), the wire degradation will reach a stage where the wire strength is not sufficient enough to withstand the axial tension. Thus, the wire elongates, at the point of maximum wire damage, till its eventual breakage resulting in a conical tip as shown in Fig. 4.5 (c).

### 4.4.3 Continuous machining

In this study, profile completion without process interruption is regarded as continuous machining. Thus, except the extreme two cases (C1 and C7), every other condition resulted in continuous and uninterrupted machining. The surface integrity of these cases is compared in detail in the upcoming section.

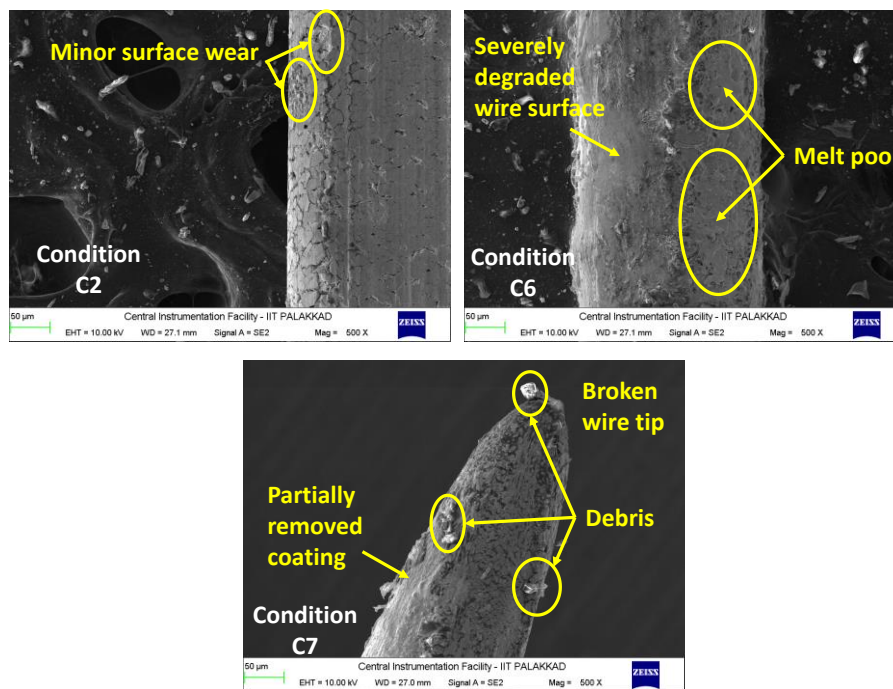


**Fig. 4.5** SEM images showing stages of wire wear (a) minimal wire wear (b) severe wire wear (c) broken wire tip

## 4.5 SURFACE INTEGRITY AT DIFFERENT MACHINING STABILITIES

Apart from process failures, unstable machining conditions can cause considerable surface integrity damages. Therefore, there is a need to investigate the effect of machining stability on surface integrity during the continuous machining conditions too. Even though machining conditions C2 to C6 resulted in failure free cutting, surface integrity analysis is performed and the differences are reported in this section. Surface integrity variations can occur due to the debris accumulation and corresponding machining stability variations. The aim is to study the importance of regulating the machining stability from the surface

integrity point of view. Henceforth, in this section, the continuous machining cases, C2 to C6 are considered for surface integrity analysis.

#### 4.5.1 Surface morphology and surface roughness

Surface morphology comparison of surfaces machined at condition C2 and C6 is given in Fig. 4.6. It is seen that condition C2 resulted in a smooth surface with shallow valleys and low peaks. But surface machined under C6 is observed to be much coarser. This is due to the surface damages and deeper craters caused by higher intensity short circuit sparks due to debris stagnation at C6 condition. Apart from the craters, the micro features of recast surface layer produced by re solidification of molten material also contributes to the coarseness. Lesser the recast layer features, smoother will be the surface. Due to the same reason average surface roughness value is seen to increase from C2 to C6 as shown in Fig. 4.7.

Since the material removal happens from both the electrodes during the spark discharges, apart from surface roughness, wire wear is also higher at unstable machining condition (C6) due to higher intensity short circuit sparks, compared to stable machining condition (C2). The relationship between surface roughness and wire wear is reported by Tosun and Cogun (2003).

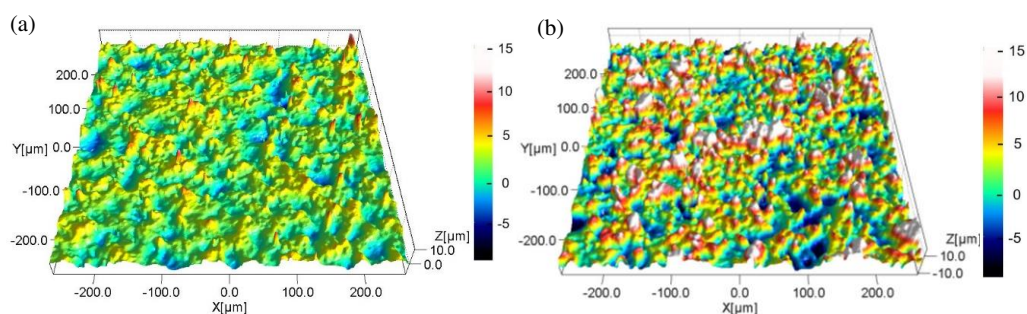


**Fig. 4.6** Non-contact surface profilometer images at machining condition

(a) C2 (b) C6

#### 4.5.2 Microstructural analysis

The microstructural study is performed by considering the SEM images of machined surfaces at different machining conditions. It can be observed that machined surface is extremely coarse at C6 which improves subsequently at better stability levels as shown in Fig. 4.8. SEM images additionally revealed the presence of micro features in the machined surface. These micro features are formed when a part of the molten material is resolidified back to the machined surface. Micro voids are caused when vapour bubbles entrapped in the recast layer are burst leaving void spaces. Micro cracks are formed by thermal impact due to quick quenching. Other micro features present are globules, pits and pores. These features are detrimental to the load bearing capacity of the machine surface, especially at higher temperatures. These surface irregularities are thus undesirable and shall be minimized.

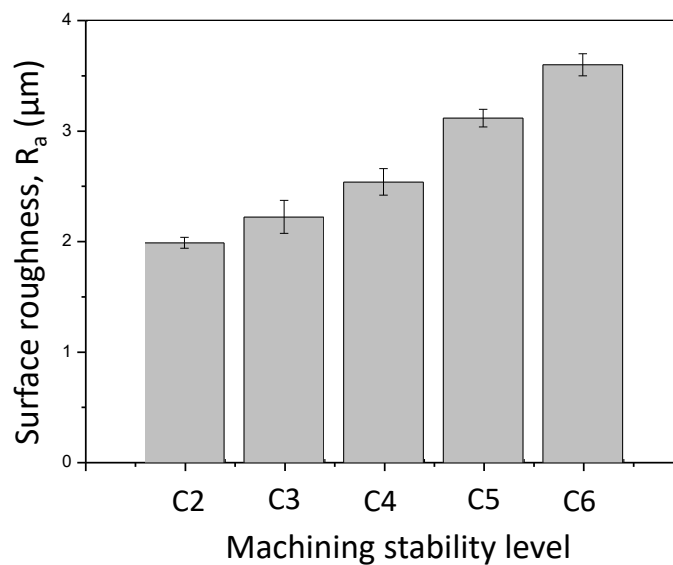


**Fig. 4.7** Surface roughness at different machining conditions

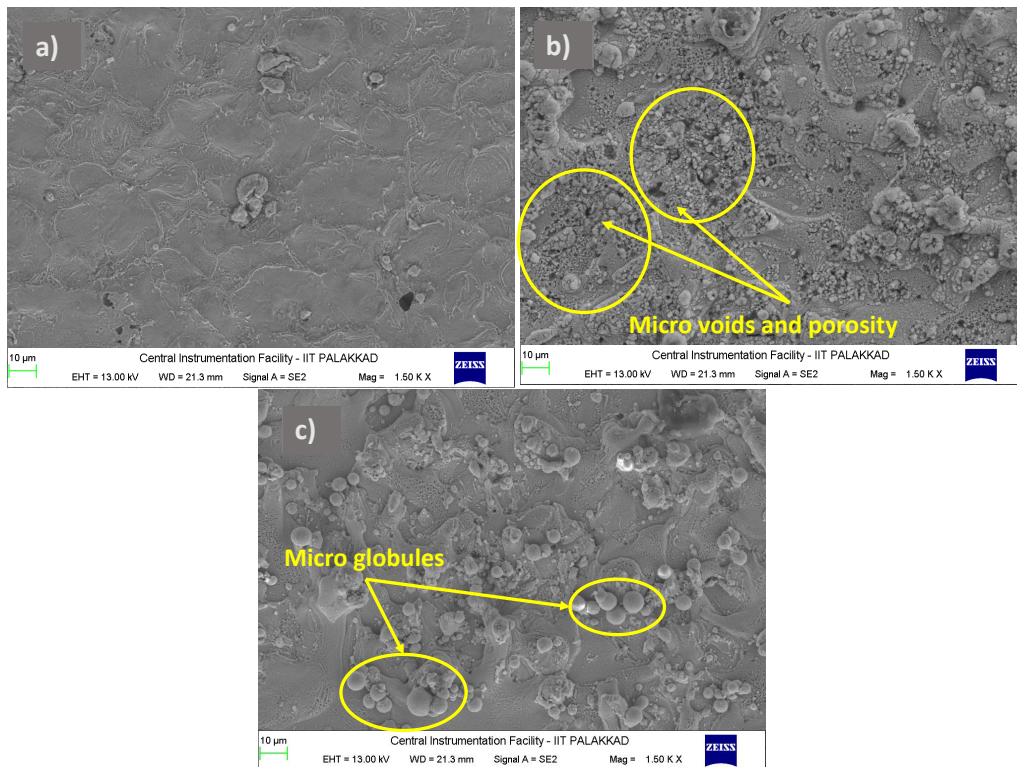


**Fig. 4.8** Microstructural comparison at different machining conditions

(a) C2 (b) C4 (c) C6

### 4.5.3 Geometric accuracy

The geometric accuracy is compared at different machining conditions considering flatness error, circularity, and cylindricity. Flatness error is the minimum distance between two imaginary parallel and perfect planes which can contain the surface under consideration. Circularity is the minimum radial distance between two perfect imaginary concentric circles within which the considered profile can be inscribed. Similarly, cylindricity is the minimum radial distance between two perfect imaginary concentric cylinders within which the considered profile can be fit.

As discussed earlier, geometric accuracy of a wire EDM machined profile is dependent on wire vibrations and deflection due to lateral forces experienced by the wire electrode. Wire electrode tends to vibrate more when there is higher amount of debris stagnation in the spark gap. This is due to multiple reasons like the interaction of debris with the wire, higher force associated with short circuit

discharges, and the higher impact of escaping vapour bubbles in the congested spark gap. This effect is shown in Fig. 4.9 where geometric errors are increased progressively from condition C2 to C6. This effect is same for all the three form errors considered: flatness error, circularity and cylindricity.

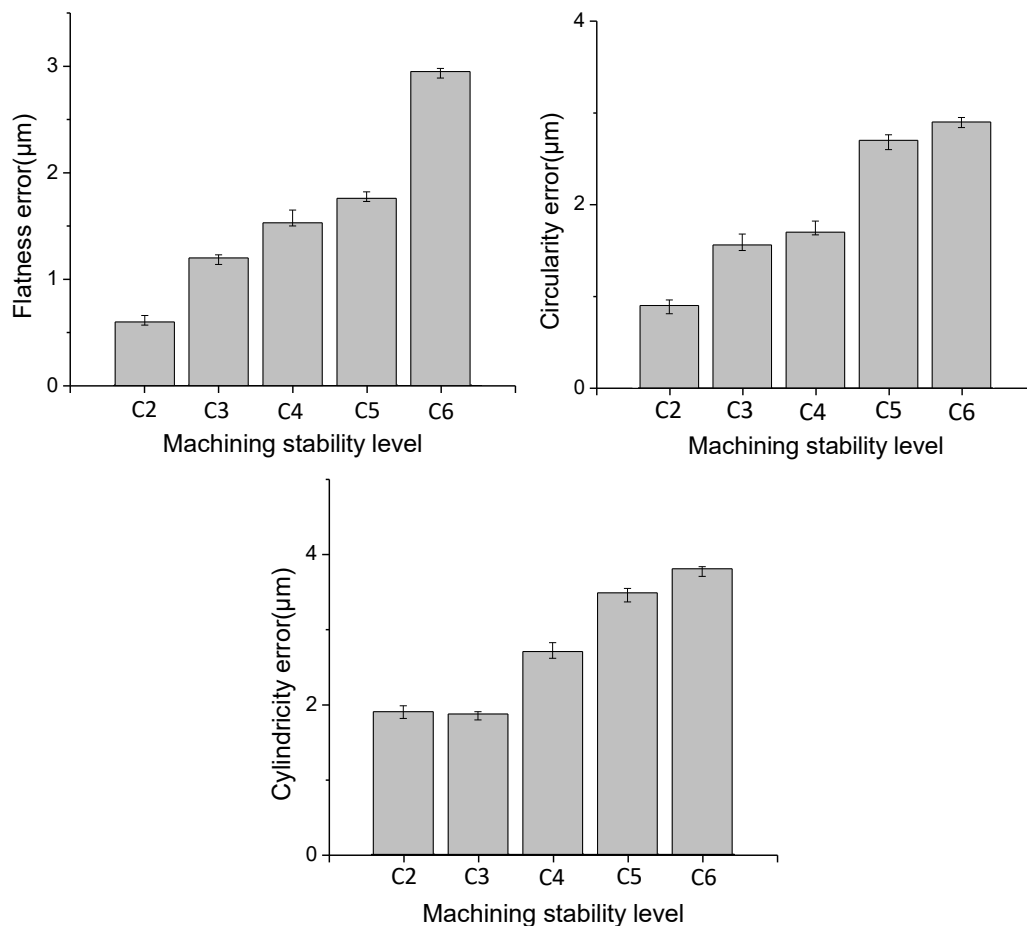


**Fig. 4.9** (a) Flatness error, (b) Circularity error, and (c) Cylindricity error at different machining conditions

#### 4.5.4 Micro-hardness

Microhardness tests are conducted to analyse the subsurface softening of machined surface under different machining conditions. Micro hardness tests are conducted on the polished cross-sectional surface at different depths away from the wire EDM processed surface. The microhardness of the material before

machining is found to be 196 HV. The test is conducted at 4 points till 80  $\mu\text{m}$  deep from the machined surface, which is the reported depth of heat affected zone during wire EDM of Inconel 718. Since the mechanism of material removal is by melting and vaporisation, the thermal impact can soften the subsurface compared to the parent matrix. It can be seen from Fig. 4. 10 that the machining condition C6 has caused maximum softening, and the effect nullifies in the subsequent conditions till C2. Also, for all machining conditions, the effect is more at layers immediately beneath the machined surface and it stabilizes as it goes away from the surface. Higher thermal impact associated with C6 condition, anneals and softens the surface more than the other machining conditions. Higher thermal impact is due to the higher discharge energy of arc and short circuit sparks during unstable machining conditions. Condition C2 is observed to have least effect on subsurface hardness, since there is only a slight dip in the microhardness near to machined surface.

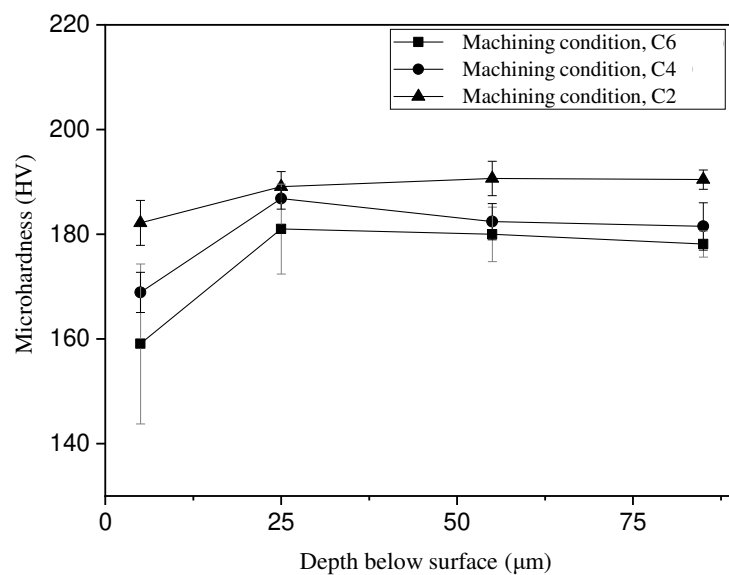


**Fig. 4.10** Subsurface microhardness profile

#### 4.5.5 Subsurface damages

Subsurface damages into the machined surface at different machining conditions are shown in Fig. 4.11. SEM images of polished cross-sectional surfaces are captured for the analysis. Sonication is performed to minimize the effect of polishing on subsurface damages. Specimens are immersed in an acetone solution which is agitated in ultrasonic frequencies to remove the debris clogged into the cracks or features. Most of the subsurface damages are recast layer (RCL) defects, which are formed by the re-solidification of molten material back to machined surface. The region of higher subsurface damage is understood to be within the recast layer by comparing the cross sectional images of wire EDM processed surfaces from literature (Sharma et al., 2015; Sharma et al., 2016). The typical defects reported in RCL like micro voids, pits, and cracks are observed here. Such cracks that run into the machined surface affects the fatigue life, and is the primary reason why wire EDM machined components needs further processing for aerospace applications. The subsurface damage is observed to deepen from machining condition C2 to C6. The deeper recast layers are due to ineffective flushing conditions (Fig. 4.11 (e), Fig. 4.11 (d)) whereas the condition which promotes easier flushing is seen with near zero recast layer defects (Fig. 4.11 (a)). The negligible recast layer is a promising result, since such machining conditions can reduce or avoid the post processing requirements.

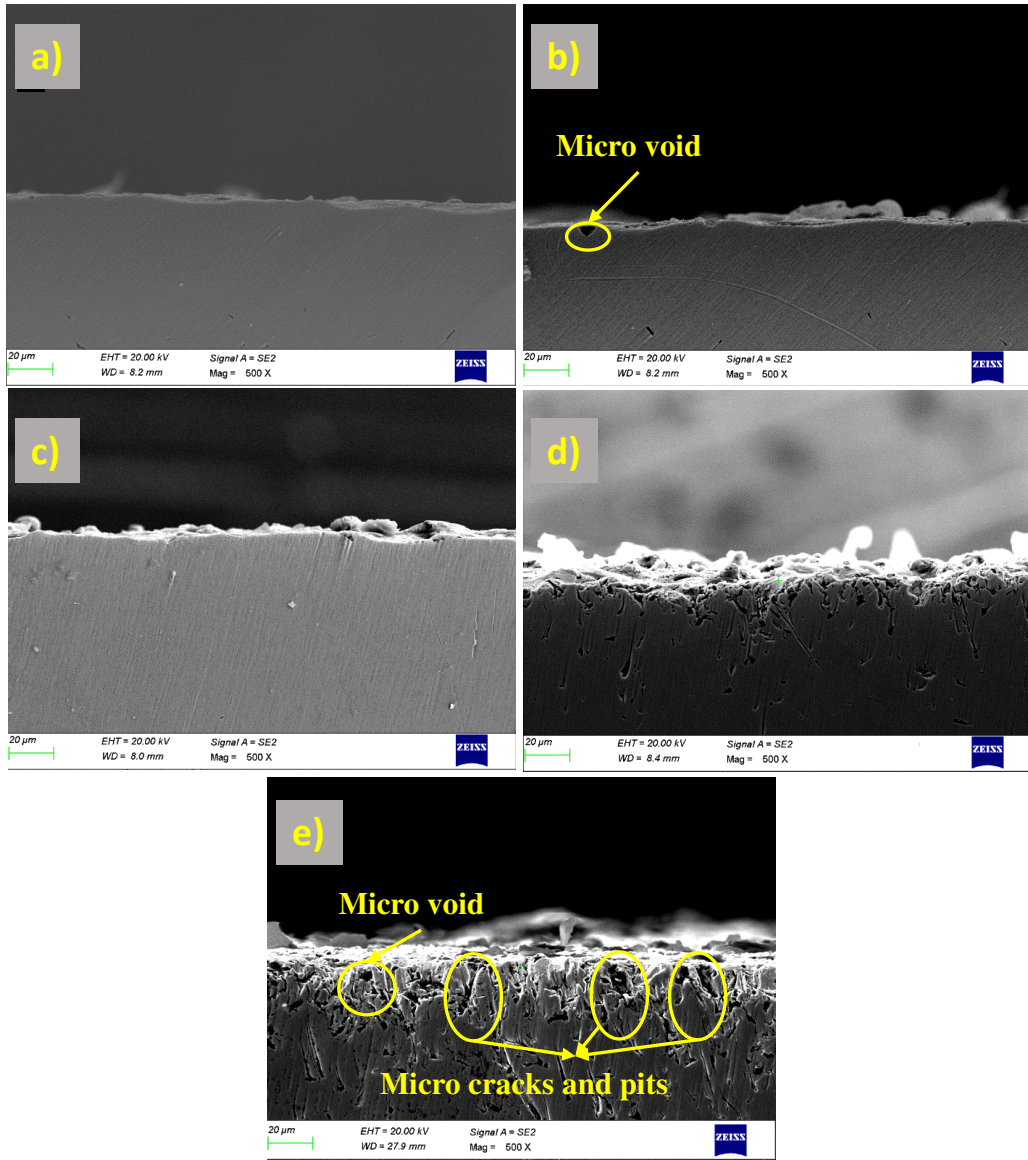


**Fig. 4.11** Recast layer defects (a) C2 (b) C3 (c) C4 (d) C5 (e) C6

#### 4.5.6 EDS analysis

Energy Dispersive X-Ray Spectroscopy (EDS) analysis is performed on the machined surfaces to understand the extent of elemental migration from the wire electrode. The traces of foreign elements on machined surface are an undesirable feature since it alters the chemical properties of parent material. Since, the wire electrode chosen for the study is zinc coated brass, zinc and copper elements are found in varying amounts in the machined surface. However, it is found that weight % of migrated elements varies with machining conditions. Weight % of

zinc reduced from 6.5 % at condition C6 to 2.4 % in C2. Similar reduction is found in the case of copper from 2.38 % to 1.81% as seen in Fig. 4.12. Compared to C2, in condition C6, wire wear is considerably high as discussed earlier. Thus, the traces of material removed from wire can be seen in the workpiece surface. This is the reason why traces of zinc and copper is more. Since zinc coating is removed almost entirely at C6, greater change is observed in zinc weight %.

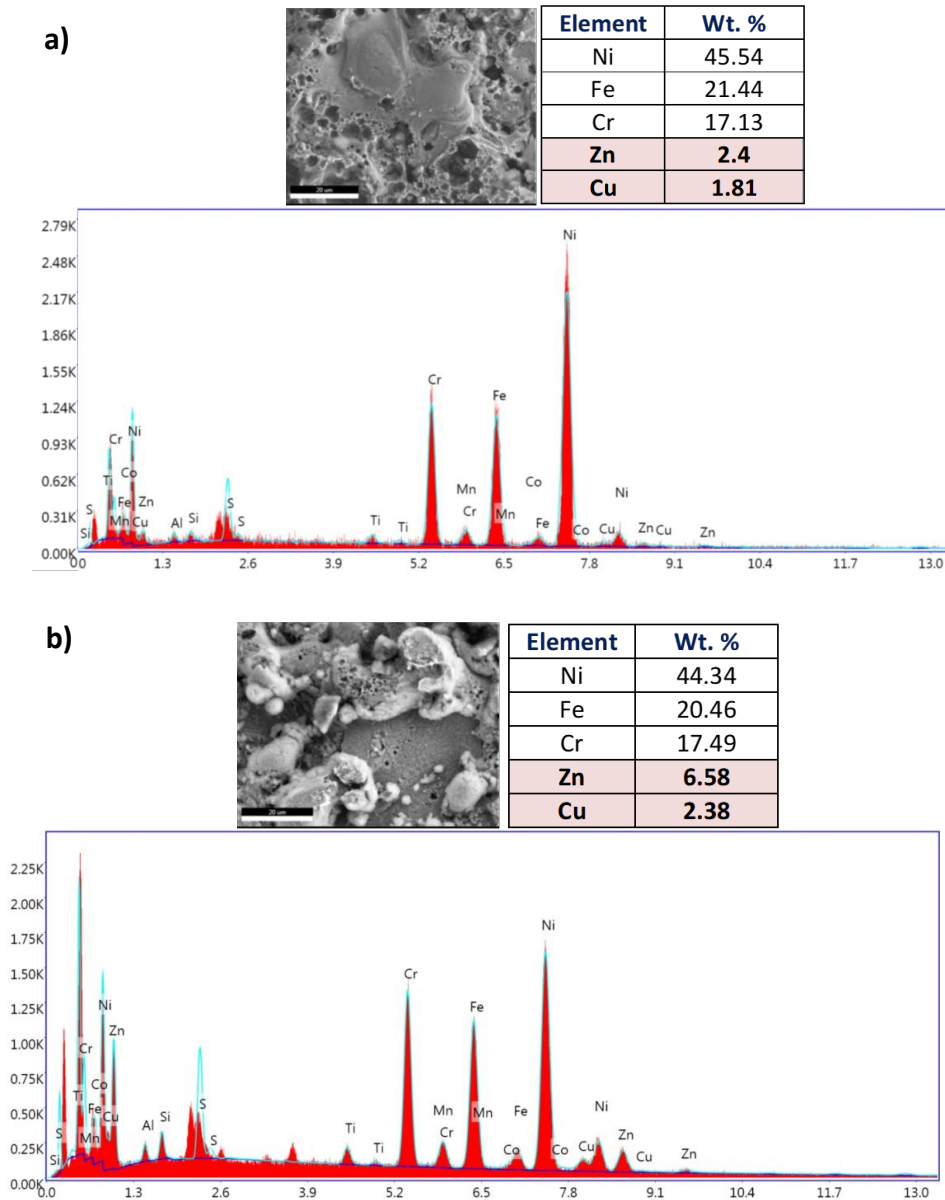


**Fig. 4.12** EDS analysis of surface machined under condition (a) C2 (b) C6

#### 4.5.7 Wire electrode comparison

Different wire electrodes are considered for performance comparison at different machining conditions. Wire electrodes considered are hard zinc coated brass, half hard zinc coated brass, hard uncoated brass and half hard uncoated brass. Following observations are made from the experiments.

- Hard wires can resist wire deflection better and thus can reduce geometric inaccuracies as seen in Fig. 4.13. The graph shows the average value at condition C3 for each wire electrode.
- Coated wires cuts faster than uncoated wire electrodes as shown in Fig. 4.14.
- Coated wires resist wire breakages better than uncoated wires. Uncoated wires are observed to rupture at an earlier stage than coated wires.

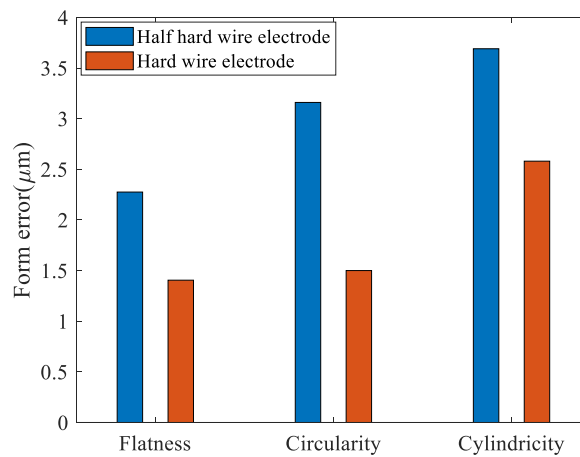


**Fig. 4.13** Geometric accuracy comparison considering different wire electrodes

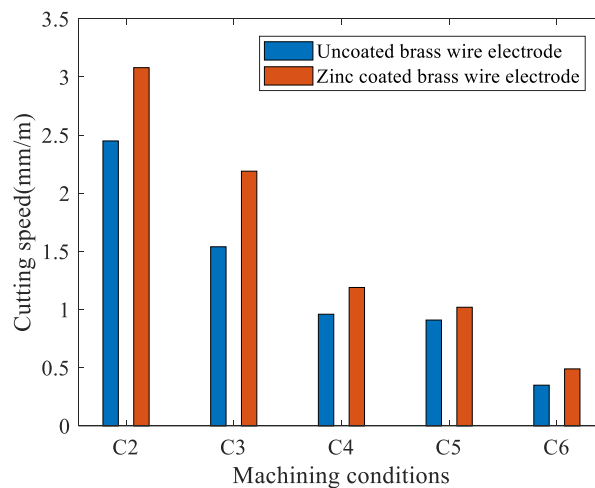


**Fig. 4.14** Effect of wire electrode coating on cutting

## 4.6 SUMMARY OF MACHINING STABILITY ANALYSIS

The chapter dealt with studying the effects of unstable machining conditions on process failures and surface integrity. The following are the notable findings from the study:

- Unstable machining conditions is experimentally created by varying the amount of debris in the spark gap. A methodology is devised to vary the debris stagnation possibility by tuning the process parameters like pulse on time, pulse off time, and servo voltage.
- By varying the process stability, two modes of process interruptions are observed in this study, wire breakage and spark absence. These two machining outcomes are defined as ‘machining failures’ throughout the research study.
- Analysis of both the failures, emphasising on causes, effects and dependency on parameters are discussed. Wire breakage happens by debris stagnation leading to short circuit predominance in the discharge cycle. Spark absence is caused by inability of the applied potential difference to breach the dielectric barrier of dielectric in the discharge channel. Wire wear analysis is performed, comparing the SEM images of worn wires that comes out of machining zone.
- Apart from causing machining failures, it is found that machining stability also affects the surface integrity of machined components. To investigate the variation of surface integrity, various aspects like surface roughness, geometric accuracies, micro hardness, elemental migration through EDS, microstructural study, subsurface defects etc. are analysed.
- Among various wire electrodes considered, hard zinc coated brass is found to perform better in terms of productivity and geometric accuracy. Thus, hard zinc coated brass wire is considered as the wire electrode throughout this research study henceforth.

## CHAPTER 5

### OFFLINE MODELING OF WIRE EDM FAILURES

#### 5.1 INTRODUCTION

The chapter deals with development of offline failure prediction models for wire EDM process. Initially a neural network multi class classifier is developed to predict machining outcomes. The mode of failure is accurately predicted by this model. Next, the machining stability is analysed by considering mean gap voltage variation ( $\Delta V_m$ ). An Adaptive neuro fuzzy inference system (ANFIS) model is trained to predict  $\Delta V_m$ . To ensure breakage free operation, a decision support system is developed based on the model predictions to set the initial parameters.

#### 5.2 PREDICTION AND ANALYSIS OF PROCESS FAILURES BY ANN CLASSIFICATION

The section presents an offline model based on artificial neural network (ANN) to classify the machining failures during wire EDM of Inconel 718. The presented offline models are inexpensive, computationally fast means of failure prediction. Offline models can work in integration with advanced sensor based online monitoring systems to a set up the initial parameters. ANN classification is a supervised learning technique in machine learning which predicts the class labels of input data. To train the model, 81 full factorial experiments are conducted. The developed multi class classifier predicts the machining outcomes – wire breakage, spark absence, or continuous machining. A detailed wire wear analysis is also presented to understand the stages of wire rupture.

##### 5.2.1 Wire EDM process failures

When an input parameter is set for a wire EDM operation, it is expected to machine the profile continuously without any interruptions. However, machining

interruptions can also happen due to unexpected machining failures. This can happen due to non-ideal process parameter combinations, or due to the inherent stochastic nature of the process, or due to external uncontrollable factors. Wire breakage or wire rupture is one of the most commonly reported failures. Another case is called spark absence when the machining halts due to very less or zero discharge frequency. These process interruptions reduce the process efficiency, productivity and sustainability by wastage of energy and consumables. The failure cases are elaborated in the following subsections.

### ***Wire breakage***

Wire breakage or wire rupture happens when the wire material deteriorates to a level, where the wire loses its strength to withstand the axial tension. Unstable machining conditions leading to debris accumulation in the spark gap causes wire breakage. The particles removed in the previous discharge cycle, called debris, are expected to be removed from the spark gap during the pulse off time. The ideal process cycle involves dielectric breakdown during the pulse on time, producing an electric discharge causing material removal, followed by the restoration of dielectric property during the off time by flushing away the debris. However, this series of breakdown and renewal of dielectric in the spark gap is a highly idealized situation. Practically, the debris generated are only partially removed from the spark gap. Thus, the dielectric properties keep varying with respect to the amount of debris suspended in the spark gap. Higher the number of debris, greater is the dielectric conductivity. This situation is difficult to control, since the amount of debris in the spark gap at any time is random and unpredictable. Also, the spark gap distance itself is difficult to be maintained by the machine feedback system. Additionally, the wire electrode, which is expected to be held straight by applying an axial tension is often subjected to lateral forces also, due to the flushing pressure, gas bubble generation and discharge phenomena. This causes the wire to deflect and vibrate during spark discharge.

The overall effect is that the sparks generated between the electrodes are not always the ideal type. Due to the instabilities in the machining zone, the sparks

often can be higher intensity short circuit discharges, which is one of the main reasons for wire breakage. The short circuit discharge happens because of spark gap bridging by debris stagnation. Debris stagnation happens when the discharge energy is higher than ideal, when the pulse off time is lesser, and the spark gap is narrower than required for an effective flushing. Predominance of short circuit sparks are undesirable in a pulse cycle, due to its higher discharge energy and spark frequency than normal sparks. Short circuit sparks accelerate the wire wear and will eventually cause rupture. At lesser wire feed rates, chances of multiple sparks to happen from the same spot is more, causing deeper craters or cracks in the wire surface.

### ***Spark absence***

The spark absence happens when the spark gap condition is not ideal for sustained repetitive sparks. This happens when the applied voltage across the electrodes is not sufficiently high to completely ionize the dielectric fluid across the electrodes. Such situations lead to gradual reduction of discharge frequency, eventually causing the machining to halt. This happens when the open circuit voltage is too less or the spark gap is too high or the pulse on time is insufficient. In such conditions, the current discharge will be absent for the entire pulse on time duration. These pulses are called open circuit pulses. In a pulse train, if the open circuit pulses predominate the other pulses, then the cutting speed will come down to zero. In spark absence case, current discharges are either absent, or its frequency is very less for any effective machining to happen. Table 5.1 gives the details of different machining outcomes.

**Table 5.1** Classification of machining outcomes

<b>Machining outcomes</b>	<b>Reason</b>	<b>Effect on machining</b>
Spark Absence	High spark gap, less discharge energy	Machining does not happen, zero cutting speed
Normal spark machining	Ideal conditions for machining	Machining happens typically
Wire breakage	Narrow spark gap, high discharge energy, less pulse off time	Process discontinuity, Machined surface defects, require manual or auto rethreading

### 5.2.2 Experimental details

Using an Electronica Ecocut wire EDM machine, straight cuts of 10 mm length are machined as shown in Fig. 5.1. The work material considered for the study is Inconel 718, due to its superior mechanical properties and industrial applications in aerospace sector. The experiments are replicated thrice to rule out experimental errors. The input parameters and levels considered to generate training dataset are shown in Table. 5.2. Four parameters are varied in three levels to have 81 experimental runs according to full factorial experimental design. Full factorial design considers every combination of considered factor levels. Input parameters considered are pulse on time, servo voltage, pulse off time, and wire feed rate. The parameters are chosen based on their higher influence on machining failures. Wire EDM machine limits, pilot experiments and literature survey helped to fix the parameter ranges and levels. The maximum permissible values of each parameter is selected as their respective range to study the failures at the limiting conditions. Once the maximum workable ranges are selected for each parameter, the levels are selected based on full factorial experimental design. Certain other parameters are kept constant due to machine constraints and its lesser influence to the failure phenomena as given in Table 5.3. The dielectric fluid chosen is deionized water of conductivity  $\sim 20 \mu\text{S/cm}$ .

**Table 5.2** Process parameters and levels

<b>Parameters</b>	<b>Pulse on time</b> T <sub>on</sub> (μs)	<b>Pulse off time</b> T <sub>off</sub> (μs)	<b>Servo voltage</b> SV (V)	<b>Wire feed rate</b> WF (m/min)
Level 1	100	20	20	3
Level 2	110	40	40	6
Level 3	120	60	60	9

**Table 5.3** Constant machine parameters

<b>Parameter</b>	<b>Value</b>
Wire electrode diameter	0.25 mm
Discharge current	11 A
Discharge voltage	12 V
Flushing pressure	1.96 bar
Wire Tension	10 N
Dielectric fluid	Deionized water

The responses considered for the study are the machining outcomes like wire breakage, spark absence, and normal (continuous) machining. Training dataset consists of the input parameters with their corresponding class labels. Class labels are the machining outcomes in this case. Response variables are considered in categorical form with either 0/1 depending on the true event. 1 denotes occurrence of an event and vice versa. For example, consider a case where a parameter combination has resulted in wire breakage. Then the ‘wire breakage’ class label is ‘1’ and both ‘normal machining’ and ‘spark absence’ class labels are ‘0’. In vectorial form, the response vector is [0 1 0] since the responses are recorded in the order ‘spark absence’, ‘wire breakage’, ‘normal machining’. The event wire breakage is recorded if the wire breaks before the 10 mm straight cut with the input parameter settings. Similarly, if the sparks die out and halts the machining before 10 mm, then spark absence is recorded.

ANN classifier is modelled using MATLAB 2019a software. Additionally, 20 experiments are conducted as confirmation experiments to test the model performance in practical situations. Zeiss GeminiSEM 300 FESEM is used for microstructural and Energy Dispersive X-Ray Spectroscopy (EDS) analysis of worn wire samples and machined surfaces. AEP Nanomap non-contact profilometer is used to capture 3D surface profile images for morphological comparison.

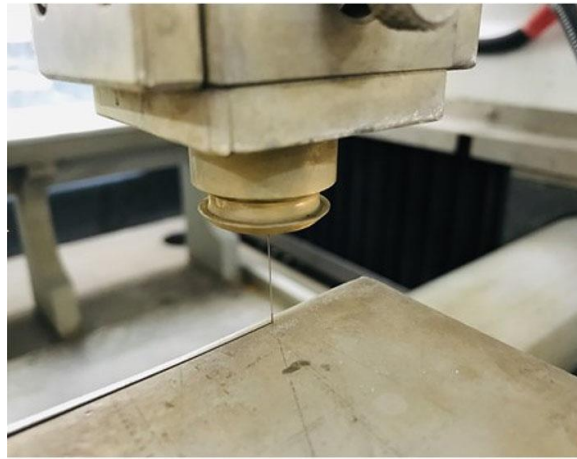


**Fig. 5.1** Straight cuts machined by wire-EDM process

### **5.2.3 ANN classification**

Classification problem recognizes the class label of a data sample, based on the learnings from a training dataset containing input datapoints and its corresponding class labels. The class label in this case is the group in which the datapoint is a part of. The datapoint is the input parameter vector and the class is the machining outcome. The classifier learns the hidden pattern or the common features of the datapoints that belong to a particular class label. The trained classifier model is capable of predicting the class label of any new dataset, outside the training data. Geometrically, the classification models construct a decision boundary in a multi-dimensional space to separate the datapoints to various groups. The decision boundary can be a curve, surface, or hyper surface depending on the dimension of datapoint. Such a decision boundary is shown in Fig. 5.2. The classification becomes complex if the class prediction involves non-

linear, higher order relationship between the samples and outcomes. Wire EDM failure prediction is one such case where a complex and stochastic relationship exists between the parameters and the machining outcomes. In this study, ANN classification is chosen based on its capability to handle higher order non-linear data efficiently.

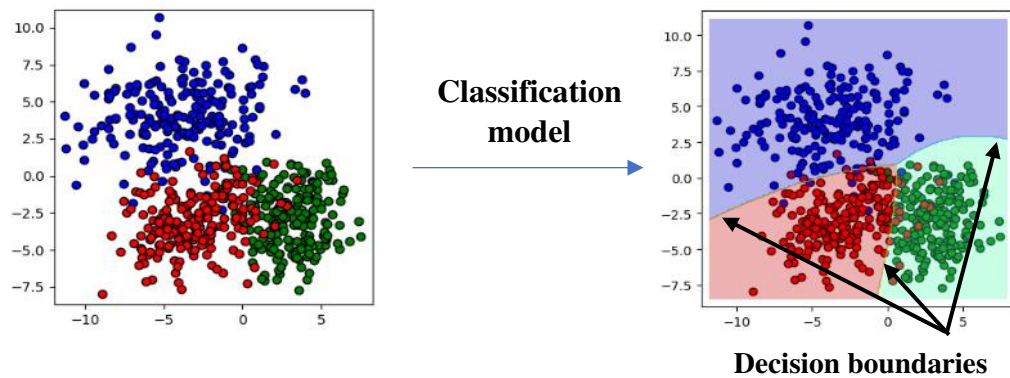


**Fig. 5.2** (a) Datapoints belonging to multiple classes in 2D space (b) non-linear 2D decision boundaries separating the classes (Ghojogh and Crowley, 2019)

The ANN model computes the probability (likelihood) of occurrence of all the three events for any given input parameter combinations. The event which is most likely to happen, is the one with maximum probability. A feed forward back propagation ANN is considered for the study. The structure of the ANN classifier is shown in Fig. 5.3. A 4-10-3 structure is chosen based on the classifier accuracy. The classifier is designed, trained and developed using neural pattern recognition tool in Matlab 2019a. A comparison of model accuracies for different ANN structures are given in Table 5.4. The optimal structure has 4 input layers (Pulse on time, pulse off time, servo voltage, and wire feed rate), 10 neurons in hidden layer and 3 output layers (Probability of spark absence, probability of wire breakage, and probability of normal machining). Out of the 81 training samples, 57 (70 %) samples are used for training, another 12 (15 %) samples for testing and remaining 12 (15 %) samples for validation. SoftMax function gives the final layer output in probabilistic terms. Since the classes are exclusive, the sum of

responses should be equal to 1. The details of the 81 experiments conducted with corresponding machining outcomes are given in Table 5.5.

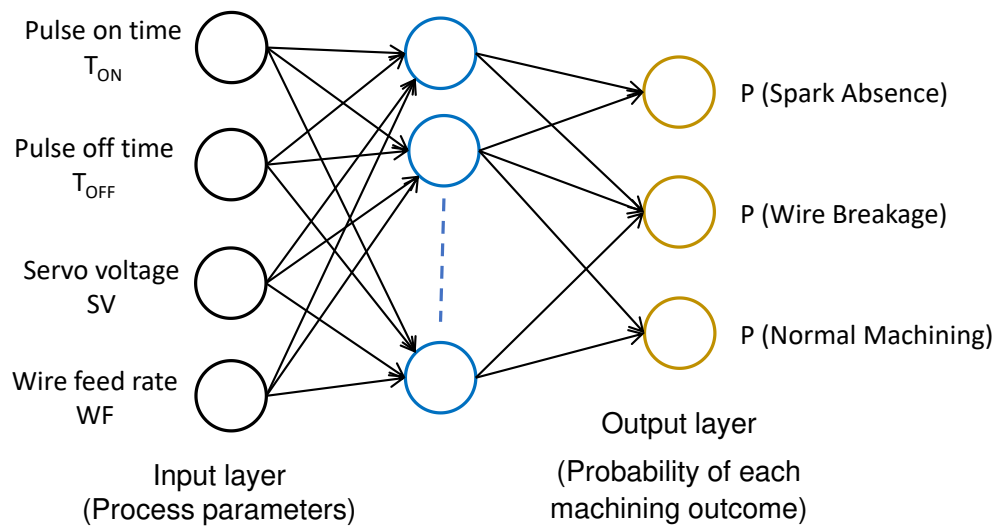


**Fig. 5.3** Structure of multi-class neural network classification model

**Table 5.4** Accuracies of different ANN structures

S. No.	Number of neurons in hidden layer	ANN structure	Model accuracy
1	1	4-1-3	74.1 %
2	2	4-2-3	85.2 %
3	3	4-3-3	71.6 %
4	4	4-4-3	24.7 %
5	5	4-5-3	82.7 %
6	6	4-6-3	86.4 %
7	7	4-7-3	81.5 %
8	8	4-8-3	86.4 %
9	9	4-9-3	88.9 %
10	10	4-10-3	90.1 %
11	11	4-11-3	79.0 %
12	12	4-12-3	84.0 %
13	13	4-13-3	80.2 %
14	14	4-14-3	75.3 %
15	15	4-15-3	85.2 %

**Table 5.5** Experimental results

S. No.	Input Parameters				Observed Outcomes		
	T <sub>on</sub> ( $\mu$ s)	T <sub>off</sub> ( $\mu$ s)	Servo voltage (V)	Wire feed (m/min)	Spark Absence	Wire Breakage	Normal Machining
					“1” – Occurrence of an event “0” – Absence of an event		
1	100	20	20	3	0	0	1
2	100	20	20	6	0	0	1
3	100	20	20	9	0	0	1
4	100	20	40	3	0	0	1
5	100	20	40	6	0	0	1
6	100	20	40	9	0	0	1
7	100	20	60	3	1	0	0
8	100	20	60	6	0	0	1
9	100	20	60	9	0	0	1
10	100	40	20	3	0	0	1
11	100	40	20	6	0	0	1
12	100	40	20	9	0	0	1
13	100	40	40	3	0	0	1
14	100	40	40	6	0	0	1
15	100	40	40	9	0	0	1
16	100	40	60	3	1	0	0
17	100	40	60	6	1	0	0
18	100	40	60	9	1	0	0
19	100	60	20	3	1	0	0
20	100	60	20	6	1	0	0
21	100	60	20	9	0	0	1
22	100	60	40	3	1	0	0
23	100	60	40	6	1	0	0
24	100	60	40	9	1	0	0
25	100	60	60	3	1	0	0
26	100	60	60	6	1	0	0
27	100	60	60	9	1	0	0
28	110	20	20	3	0	1	0
29	110	20	20	6	0	1	0
30	110	20	20	9	0	1	0
31	110	20	40	3	0	0	1
32	110	20	40	6	0	0	1
33	110	20	40	9	0	0	1
34	110	20	60	3	0	0	1
35	110	20	60	6	0	0	1
36	110	20	60	9	0	0	1
37	110	40	20	3	0	1	0
38	110	40	20	6	0	1	0

---

39	110	40	20	9	0	1	0
40	110	40	40	3	0	1	0
41	110	40	40	6	0	0	1
42	110	40	40	9	0	0	1
43	110	40	60	3	0	0	1
44	110	40	60	6	0	0	1
45	110	40	60	9	0	0	1
46	110	60	20	3	0	0	1
47	110	60	20	6	0	0	1
48	110	60	20	9	0	0	1
49	110	60	40	3	0	0	1
50	110	60	40	6	0	0	1
51	110	60	40	9	0	0	1
52	110	60	60	3	0	0	1
53	110	60	60	6	0	0	1
54	110	60	60	9	0	0	1
55	120	20	20	3	0	1	0
56	120	20	20	6	0	1	0
57	120	20	20	9	0	1	0
58	120	20	40	3	0	1	0
59	120	20	40	6	0	1	0
60	120	20	40	9	0	1	0
61	120	20	60	3	0	1	0
62	120	20	60	6	0	0	1
63	120	20	60	9	0	0	1
64	120	40	20	3	0	1	0
65	120	40	20	6	0	1	0
66	120	40	20	9	0	1	0
67	120	40	40	3	0	1	0
68	120	40	40	6	0	1	0
69	120	40	40	9	0	1	0
70	120	40	60	3	0	0	1
71	120	40	60	6	0	0	1
72	120	40	60	9	0	0	1
73	120	60	20	3	0	0	1
74	120	60	20	6	0	0	1
75	120	60	20	9	0	0	1
76	120	60	40	3	0	0	1
77	120	60	40	6	0	0	1
78	120	60	40	9	0	0	1
79	120	60	60	3	0	0	1
80	120	60	60	6	0	0	1
81	120	60	60	9	0	0	1

---

## 5.2.4 Performance of classifier

The classifier is trained using a scaled conjugate gradient algorithm. Model performance is evaluated by cross entropy loss function. The loss function compares the predicted probability with the ground truth (0 or 1), and a score is computed based the prediction error. The model performance is presented as a confusion matrix in Fig. 5.4. The matrix shows the classification accuracy based on the true class label. The classification accuracy of the model in the testing phase is 91.7 % and the overall accuracy is 90.1 %. The performance of the model is further evaluated by conducting confirmation tests in the following section.



**Fig. 5.4** Confusion matrix for classification model

### 5.2.5 Confirmation experiments

Twenty confirmation experiments are conducted to test the model performance in real world situations. To perform the confirmation tests, 20 sample datapoints are randomly considered. The model predictions are then compared with the actual machining outcome. The machining outcomes of 19 out of 20 cases are true to the predicted outcomes, which gives a model accuracy of 95 % during confirmation tests. The confirmation test results are given in Table 5.6. The prediction accuracy of the model for each class label is tabulated in Table 5.7.

**Table 5.6** Results of confirmation experiments

S. No.	Input Parameters				Outcomes	
	T <sub>on</sub> (μs)	T <sub>off</sub> (μs)	Servo voltage (V)	Wire feed (m/min)	Predicted class	Actual class
1	111	47	47	7	NM	NM
2	109	37	31	4	NM	NM
3	106	24	22	4	WB	NM
4	114	22	28	8	WB	WB
5	107	29	23	6	WB	WB
6	110	22	26	5	WB	WB
7	106	29	47	5	NM	NM
8	103	54	49	7	SA	SA
9	105	53	60	6	SA	SA
10	102	54	21	6	NM	NM
11	102	51	40	6	NM	NM
12	109	47	21	9	NM	NM
13	112	41	37	3	NM	NM
14	102	49	44	5	SA	SA
15	117	43	42	4	NM	NM
16	109	20	27	4	WB	WB
17	100	47	20	4	NM	NM
18	101	49	57	3	SA	SA
19	113	55	44	4	NM	NM
20	104	46	59	5	SA	SA

SA – Spark absence, WB – Wire breakage, NM – Normal machining

During the training phase, each data point (input parameter combination) and its corresponding ‘true class label’ is fed to the ANN classifier model. True class label is the actual machining outcome when the machining is performed with a

particular parameter combination. Here the probability of the true/actual event is 1 and other events are 0. For e.g., in case of an event of SA, WB and NM, the responses are recorded as [1 0 0], [0 1 0], and [0 0 1] respectively. During the training, the model adjusts its weights and biases in multiple iterations to minimize the error between the predicted event and true event. During the testing phase, the trained model gives the output as the probability of data points to fall into each machining outcomes (which can take the values between 1 and 0). Among the 3 probability values, the outcome with maximum probability is the predicted event.

To represent the model prediction graphically, all possible parameter combinations are considered as input datapoints. Totally, 247107 datapoints are generated and classified. The probability of all possible data points to fall into each class is represented graphically as 3D scatter plot in Fig. 5.5 to Fig. 5.7. In each figure, the datapoints are divided into three sub categories based on the probability of occurrence of an event. A probability of 0.6 and above, indicates the maximum likelihood of the event under consideration to happen. A probability of 0.4 to 0.6 indicates moderate chances of that event to happen. A probability of less than 0.4 indicates minimum possibility of occurrence of the particular event. Data points considered for the confirmation tests are shown separately in these plots. It can be observed that the events of normal machining, wire breakage and spark absence are all falling under appropriate zones in the figures.

**Table 5.7** Model performance during confirmation experiments

<b>Performance</b>	<b>Classification result</b>
Classification of normal machining	10/10
Classification of spark absence	5/5
Classification of wire breakages	4/5
Classification %	95 %

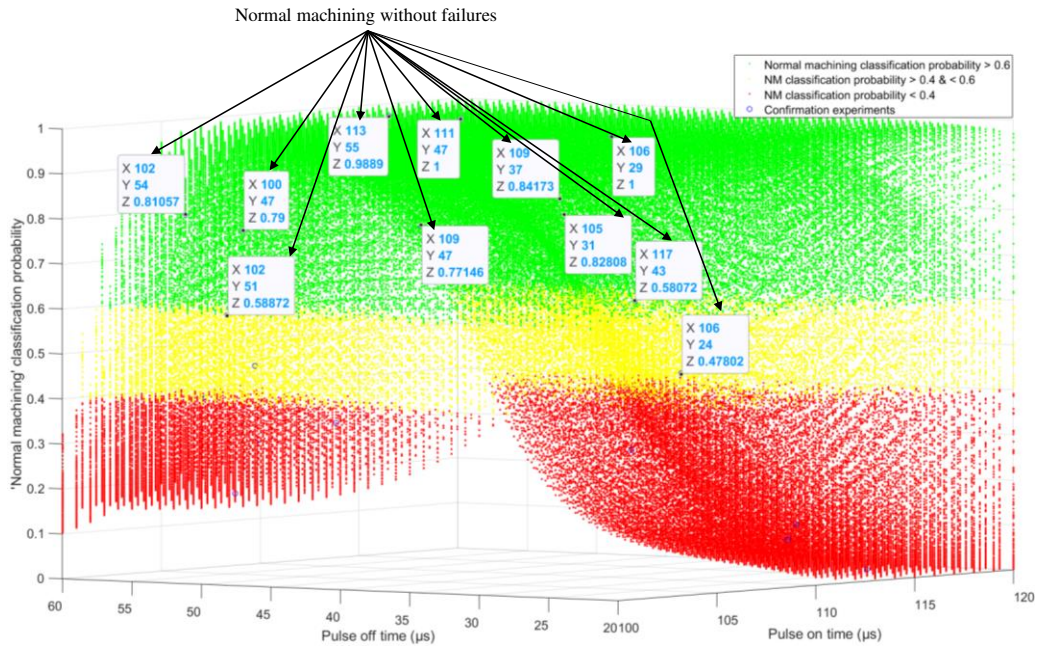


**Fig. 5.5** Scatter plot of normal machining classification probability vs input parameters

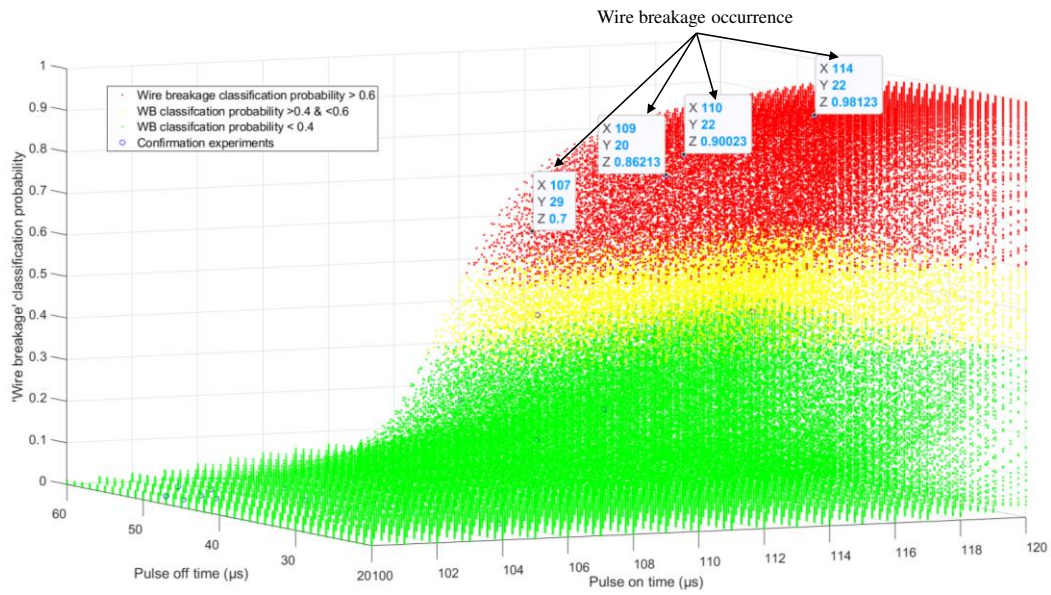


**Fig. 5.6** Scatter plot of wire breakage classification probability vs input parameters

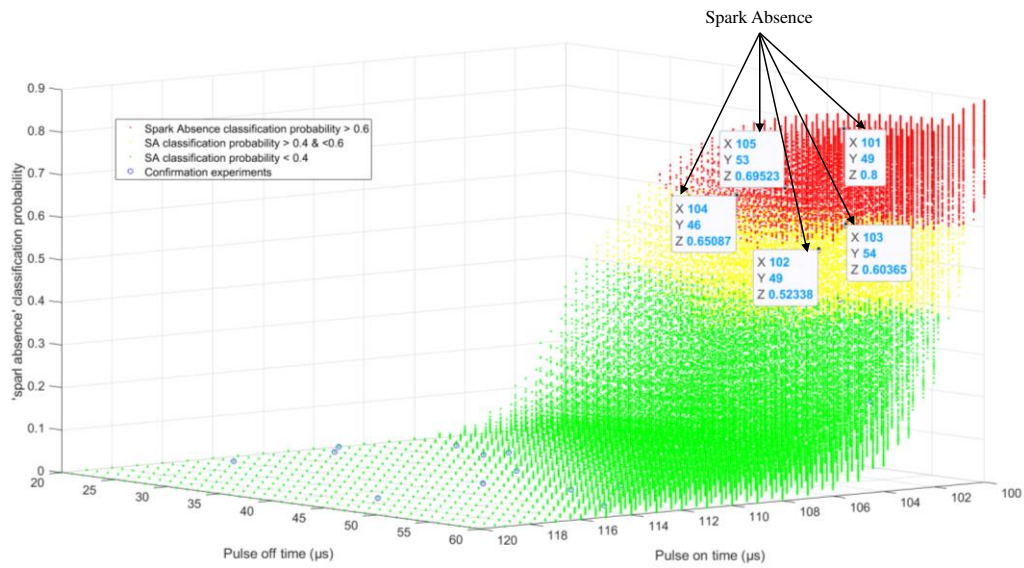


**Fig. 5.7** Scatter plot of spark absence classification probability vs input parameters

### 5.2.6 Wire breakage analysis

The zinc coated wire considered for this study possesses several advantages over the uncoated brass wires. Firstly, they cut faster since they can sustain higher discharge energy due to 'heat sink effect'. It protects the inner core from the thermal shocks during spark discharges. Also, removal of the more volatile surface coating during the machining increases the instantaneous spark gap, which enhances the flushability. Thus, the surface roughness is also comparable with that of uncoated brass wires. However, during the unstable process conditions, excessive discharge energy can cause accelerated degradation of wire coating exposing the inner core to the high process heat. Unprotected inner core, when exposed to a higher thermal load, can get softened resulting in wire breakage.

To study the mechanism of wire breakage, it is important to understand various stages of wire wear leading to wire rupture. For this, worn wire samples are examined under SEM, in the increasing order of the wire breakage probability as

predicted by the ANN classifier. The experiment numbers 10, 13, 15, and 6 having the wire breakage probabilities 0.01, 0.21, 0.42, and 0.9 respectively are chosen for this analysis. As expected, Exp. No. 6 with 90 % likelihood of wire breakage, did eventually result in wire break failure. The broken wire tip is examined in this case. Fig. 5.8 shows the SEM images of worn wire surfaces to study the stages of wire wear leading to rupture. Exp. No. 10 corresponds to minimal wire break probability (0.01) and displays negligible wear to its coated surface as evident from Fig. 5.8 (a). A melt pool showing initial phase of zinc coat removal can be seen. The wire surface belonging to Exp. No. 13, shown in Fig. 5.8 (b) displays a relatively greater damage to the zinc coating with considerable amount of coating getting removed. Exp. No. 15 corresponds to 42 % wire breakage chances, whose SEM wire image is shown in Fig. 5.8 (c). The wire coating is entirely eroded, with a visible melt pool covering the entire wire surface. There are deeper craters exposing the inner core and the surface looks coarser than the previous cases. Additionally, several debris can be seen impinged to the worn wire surface, indicating the phenomenon of debris accumulation and short circuit sparks.

Once the coating is removed, any further higher energy arc or short circuit sparks can result in accelerated wire wear and rupture. Fig. 5.8 (d) shows a case of broken wire tip (Exp. No. 6) where the tip is elongated and conical in shape with presence of debris on the wire surface. If the spark gap is stagnated with debris, the short circuit sparks will dominate the pulse cycle instead of the normal sparks. Such sparks are higher in intensity and frequency, and can cause multiple deep craters at the same or adjacent wire surface locations. As the wire damages increases, a threshold will be reached, where the wire can no longer withstand the axial tension. At this limit, the wire elongates by wire diameter reduction at the point of deepest damage. This continues till the wire ruptures at the point of minimum wire cross section. This is the reason for conical wire tip with substantial wear at the adjacent area.

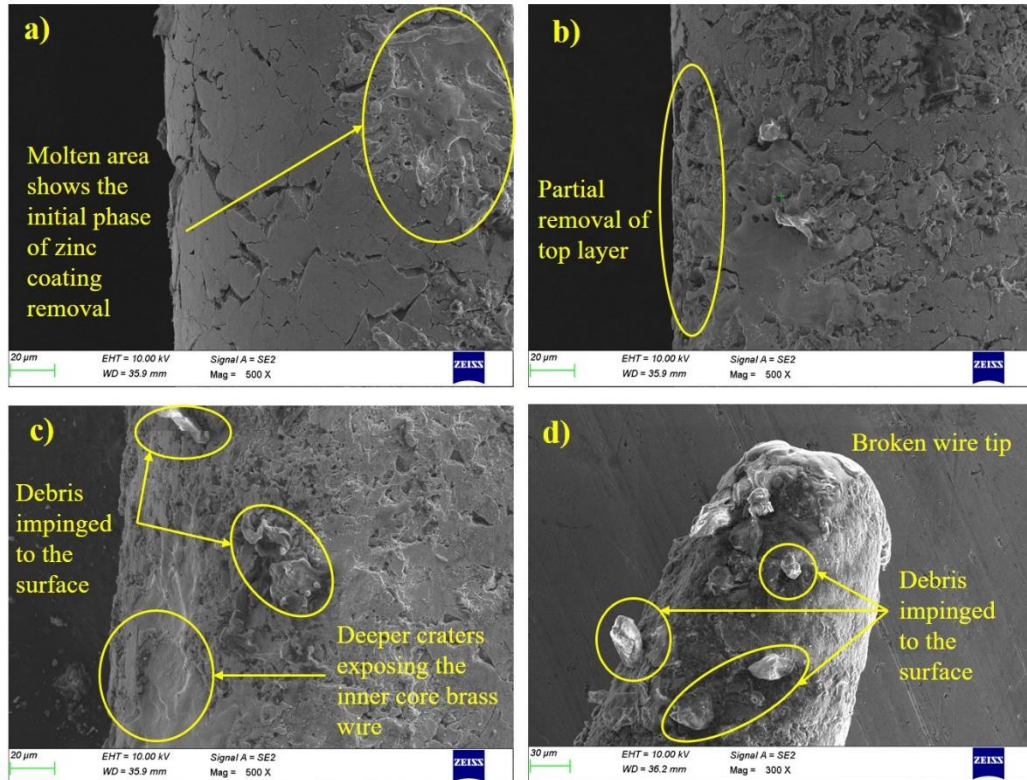


**Fig. 5.8** Categories of wire wear (a) minimal degradation (Exp. No. 10) (b) intermediate degradation (Exp. No. 13) (c) severe degradation (Exp. No. 15) (d) failed wire tip (Exp. No. 6)

To support the analysis of wire wear mechanism, EDS analysis of the worn wire surface is conducted. Fig. 5.9 shows the comparison of elemental composition of wire surfaces considering to Exp. No. 10 and Exp. No. 15. Due to higher wire wear, zinc coating is removed from the wire surface in the latter case, resulting in lesser weight % of zinc compared to the former. Higher carbon and oxygen content indicates the corrosive nature of the wire surface subjected to higher heat energy.

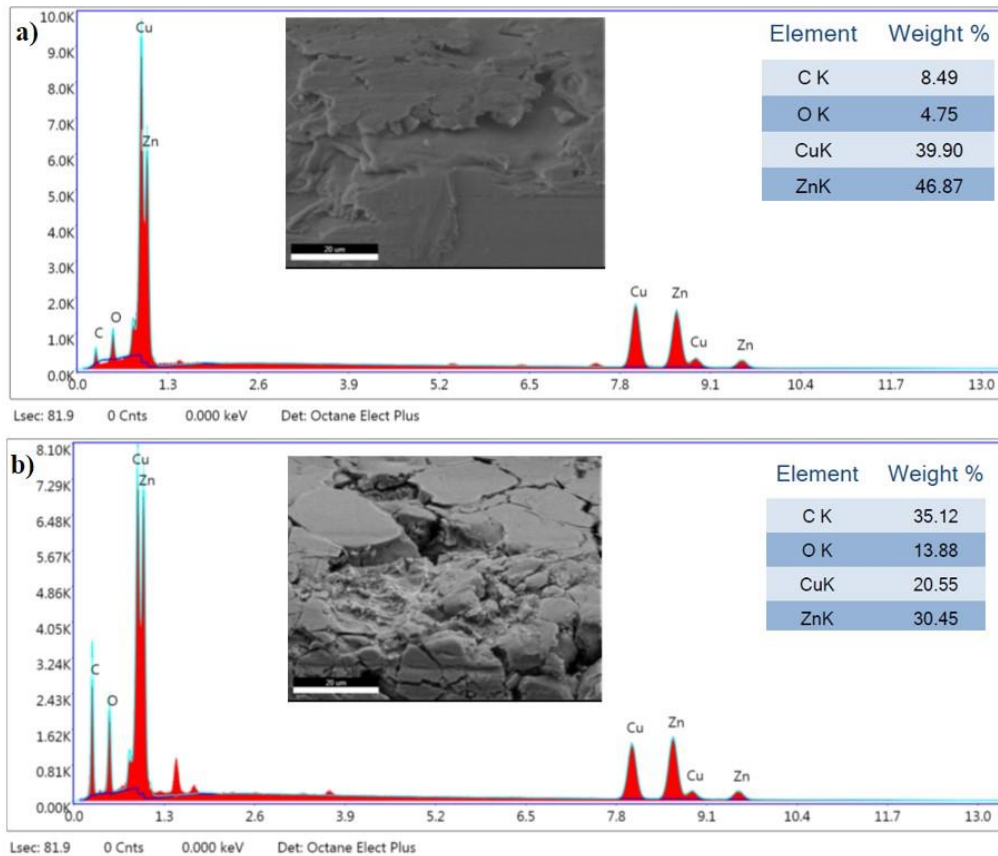


**Fig. 5.9** EDS images of worn zinc coated brass wire surface at  
 (a) mild wire wear (Expt. No. 10) (b) sever wire wear (Expt. No. 15)

The details regarding the observed failures are given in Table 5.7. Wire breakages are observed to happen in two distinct types. Type I failure is a catastrophic failure where the rupture happens almost immediately after the commencement of machining. Another case is when the instability gradually builds up and the failure happens progressively. With respect to the profile length machined, earliest occurrence of wire breakage is at 0.09 mm. The latest occurrence is reported after machining 4.81 mm length. Type I failure is observed corresponding to experiment numbers 55, 57 and 59. The reason is the highly unideal parameter combination of highest pulse on time, lowest pulse off time and servo voltage. Such a parameter setting creates high number of debris, with less time and inter electrode gap to clear them before the next pulse on cycle. This results in sudden gap bridging and thus the pulse train will be dominated by high energy short circuit discharges. The cumulative effect is a sudden machining

failure by wire breakage. Type II failure is exhibited by experiment numbers 28, 30, and 37. Here, the conditions are still unideal, but unlike in the previous case the debris accumulation takes place gradually. As the amount of debris in the spark gap increases, the proportion of undesirable sparks will increase till a critical point of sudden wire rupture. Excessive erosion of protective wire coating, coupled with high thermal loads are the reason for failure. Contrary to the wire break failures, spark absence failures happened at the start of the machining.

**Table 5.7** Details of machining process failure situations

<b>Type of failure</b>	<b>Exp No.</b>	<b>Length machined (mm)</b>	<b>Time to failure (min)</b>
Spark absence	7, 16, 17, 18, 19, 20, 22, 23, 24, 25, 26, 27	0	-
	28	4.61	3.12
	29	4.81	3.10
	30	4.64	3.09
	37	4.53	4.20
	38	3.91	3.86
	39	4.01	3.84
	40	4.57	3.16
	55	0.16	0.52
	56	0.32	0.61
Wire breakage	57	0.09	0.51
	58	0.44	0.72
	59	0.27	0.67
	60	0.33	0.68
	61	2.40	1.47
	64	2.37	1.38
	65	2.21	1.37
	66	2.36	1.37
	67	2.57	1.61
	68	2.02	1.60
	69	1.96	1.59

### 5.2.7 Surface integrity variations during normal machining

Even in failure free continuous machining cases, the machined surface integrity is dependent on the process parameter combinations. The classifier model has limited capability to perform quantitative analysis regarding the part quality. Typically, an optimization study is recommended to maximize process performance in terms of part quality. However, several useful inferences regarding the machined part quality can be made based on the classifier responses for a particular parameter setting. As a rule of thumb, higher the probability of normal machining, better will be the machined quality. This section compares the surface integrity of two cases having considerably different probability of normal machining.

Fig. 5.10 (a) and Fig. 5.10 (b) shows the SEM images of machined surface corresponding to Exp. No. 11 and Exp. No. 15 respectively. Exp. No. 11 has the following parameter settings:  $T_{on} = 102 \mu s$ ,  $T_{off} = 51 \mu s$ ,  $SV = 40 V$  and  $WF = 6 m/min$ . The smaller pulse on time indicates lesser debris generation due to low discharge energy. When combined with high pulse off time, there is enough time to flush away the debris. Spark gap is not too narrow either, preventing gap bridging. Wire feed rate of 6 m/min also ensured that consecutive sparks are not happening from the same wire spot. The effect is a smooth surface with very fewer micro defects and features as shown in Fig. 5.10 (a). Fig. 5.11 (a) shows the cross-sectional image of the same surface to understand the subsurface defects. It can be seen that the machining has caused minimal subsurface damage. There are no visible pits, cracks or craters which runs deep to the inner surface. On the contrary, SEM image of the machined surface shown in Fig. 5.10 (b), is very coarse in nature with several undesirable micro features like micro pits, voids, and globules. Also, several debris particles are impinged to the machined surface in this case. Compared to the previous case, here the pulse on time ( $T_{on} = 117 \mu s$ ) is much higher, combined with lower levels of pulse off time ( $T_{off} = 43 \mu s$ ), servo voltage ( $SV = 40 V$ ), and wire feed rate ( $WF = 4 m/min$ ). This results in larger volume of debris generation compared to the previous case, but with limited pulse off time and spark gap is available for its effective removal.

The condition can cause gap bridging and short circuit sparks, which is the reason for the coarser surface. The polished cross-sectional image of the same surface is shown in Fig. 5.11 (b). The subsurface damage is more prominent than the previous case. Numerous micro pits can be seen penetrated into the parent material.

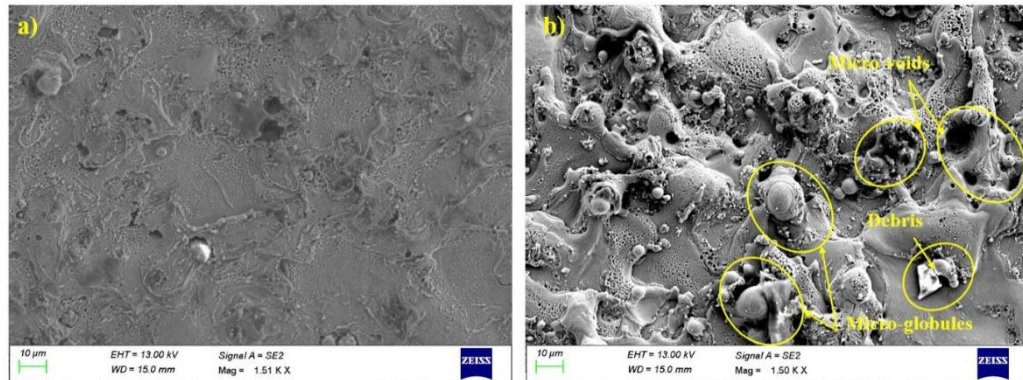


**Fig. 5.10** FE-SEM images showing machined surface morphology after  
(a) Expt. No. 11 (b) Expt. No. 15

Fig. 5.12 shows the surface morphology comparison of these two cases using non-contact 3D surface profilometer images. Fig. 5.12 (a) is much smoother with shallow peaks and valleys, whereas Fig. 5.12 (b) is coarse with high peaks and deep valleys. Table 5.8 gives the surface roughness comparison for all the ‘normal machining’ cases of confirmation tests. Exp. No. 11 and Exp. No. 15 has  $R_a$  values of  $0.97 \mu\text{m}$  and  $2.64 \mu\text{m}$  respectively. This is in agreement with the observations so far.

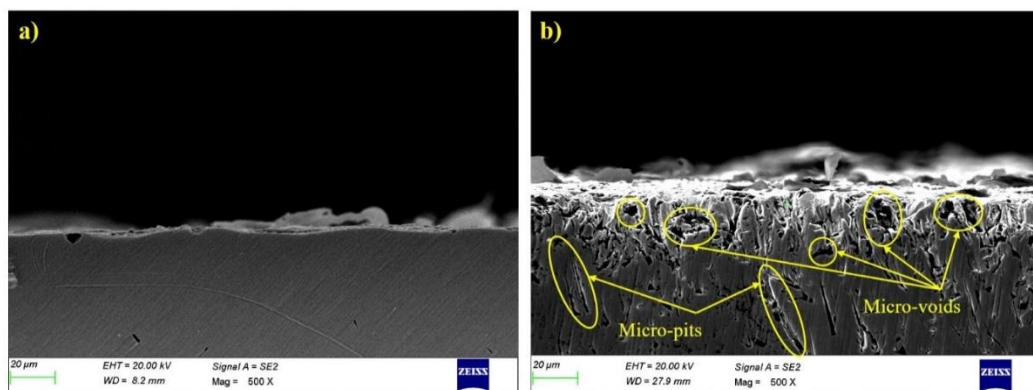


**Fig. 5.11** Cross sectional view of machined surfaces under SEM after  
(a) Expt. No. 11 (b) Expt. No. 15

**Table 5.8** Surface roughness comparison for ‘Normal machining’ in confirmation tests

S. No.	Input Parameters				R <sub>a</sub> (μm)
	T <sub>on</sub> (μs)	T <sub>off</sub> (μs)	Servo voltage (V)	Wire feed (m/min)	
1	111	47	47	7	1.36
2	109	37	31	4	1.76
7	106	29	47	5	1.24
10	102	54	21	6	1.12
11	102	51	40	6	0.97
12	109	47	21	9	1.65
13	112	41	37	3	1.97
15	117	43	42	4	2.64
17	100	47	20	4	1.60
19	113	55	44	4	1.45

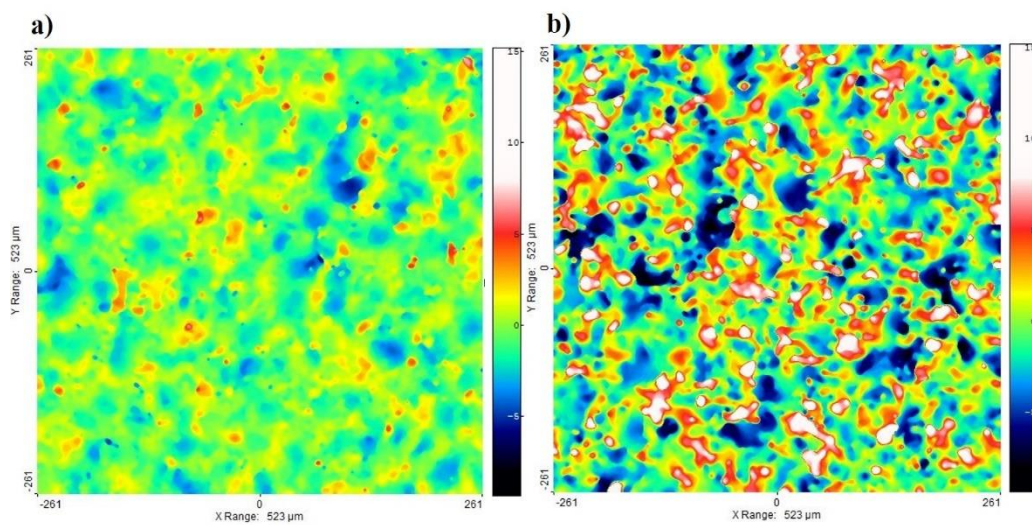


**Fig. 5.12** Surface morphology comparison of machined surfaces using non-contact 3D profilometer images after (a) Expt. No. 11 (b) Expt. No. 15

It shall be noted that only a few limited cases can be explained intuitively by considering its parameter combinations. In most of the practical cases, due to the

complex interaction effects, a separate optimization study is required to maximize the surface integrity.

### **5.3 MODELLING MEAN GAP VOLTAGE VARIATION TO PREDICT WIRE BREAKAGES**

#### **5.3.1 Introduction**

Unstable machining conditions during the Wire EDM process restricts its capability by causing machining failures and poor part quality. Wire breakage is the most commonly reported means of process failure. It hinders the productivity by consuming extra machining time for wire rethreading. Additionally, the process efficiency is affected by material and energy wastage. One main reason for unstable machining conditions are debris accumulation and stagnation due to improper flushing. A novel in-process data parameter called mean gap voltage variation ( $\Delta V_m$ ) is introduced in this section as an indicator of debris accumulation.  $\Delta V_m$  is the mean difference between set servo voltage and the actual real time voltage across the wire electrode and the workpiece. Usually, an inbuilt feedback system controls the spark gap by maintaining the set servo voltage between the electrodes.  $\Delta V_m$  represents the voltage deviations from the set voltage value over a machining period and it can be considered as an indicator of machining instability. This section deals with the modelling of this mean gap voltage variation using ANFIS soft computing technique. A decision support system is developed which utilizes model predictions to forecast events of wire breakage. Also, the parameter can give useful insights about the machined part quality. The section demonstrates the potential of extracting in-process data features to predict the overall machining stability. The knowledge gained from this section is further expanded in the forthcoming chapters to develop an online condition monitoring system using voltage and current sensors.

### 5.3.2 Experimental details

The profiles machined are straight cuts of 10 mm length. Zinc coated brass wire and deionized water is chosen as the wire electrode and dielectric fluid. The mean gap voltage variation is recorded using a Tektronix digital multimeter model DAQ 6510. The sample reading of real-time voltage fluctuation for a servo voltage of 50 V is given in Fig. 5.13. The mean voltage value is also displayed in the integrated computer of wire EDM as shown in Fig. 5.14. On cross checking, the displayed value and the measured value are found to be in good agreement.

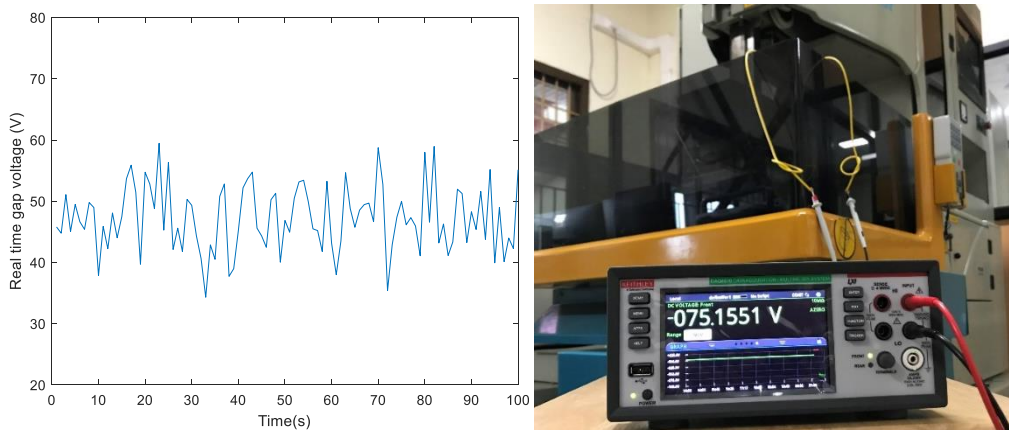


**Fig. 5.13** (a) Real-time gap voltage reading for a set voltage of 50 V  
(b) Gap voltage measurement by digital multimeter

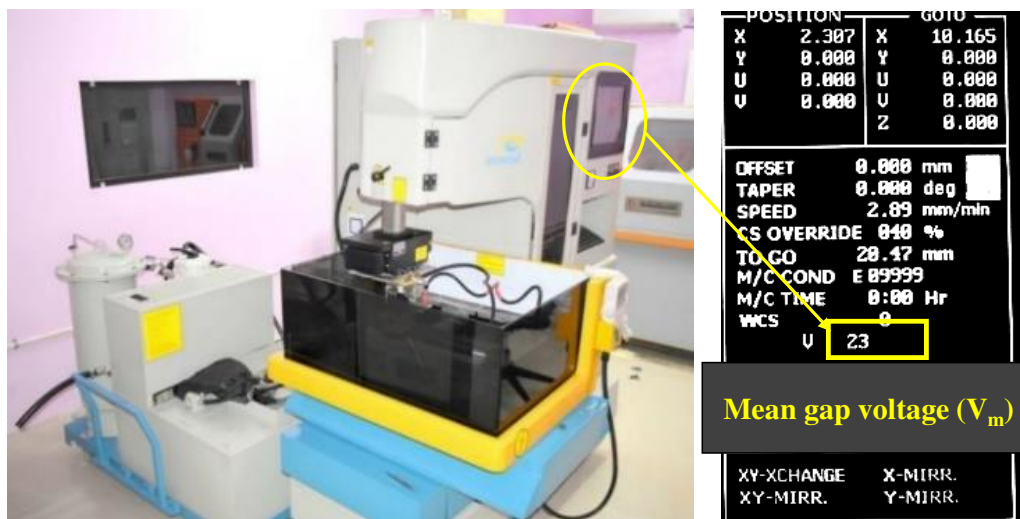


**Fig. 5.14** (a) Machine tool (b) Integrated computer displaying mean gap voltage

**Table 5.9** RSM input parameters and levels

Process parameters	Level 1	Level 2	Level 3	Level 4	Level 5
	Axial point (High)	Cube point (High)	Centre point	Cube point (Low)	Axial point (Low)
Pulse on Time ( $\mu$ s)	120	115	110	105	100
Pulse off Time ( $\mu$ s)	70	60	50	40	30
Servo voltage (V)	70	60	50	40	30
Wire feed rate (m/min)	10	8	6	4	2

Thirty-one experiments are conducted according to central composite design (CCD) of response surface methodology (RSM). The input parameters considered are pulse on time, pulse off time, servo voltage, and wire feed rate. The process parameters and levels are given in Table 5.9. The parameter ranges and levels are selected based on pilot experiments, machine manual and literature survey. Since the objective is to study the failure condition, the extreme ranges are considered for each parameter. A few other parameters are maintained constant during the experiments as given in Table 5.10 due to machine constraints. Responses recorded are events of wire breakages and mean gap voltage variation.

**Table 5.10** Constant machining parameters

Parameter	Value
Wire electrode diameter	0.25 mm
Discharge current	11 A
Discharge voltage	12 V
Flushing pressure	1.96 bar
Wire tension	10 N
Dielectric fluid	Deionized water

### 5.3.3 Mean gap voltage variation ( $\Delta V_m$ )

The mean gap voltage variation ( $\Delta V_m$ ) is an in-process data which quantifies the average deviation of inter electrode voltage from the set voltage. Ideally, under a stable EDM cycle, entire debris will be cleared after each discharge duration restoring the dielectric properties and the voltage deviation is expected to be nearly zero. However, in most practical cases the debris is not 100 % removed from the spark gap and at least a small amount is always left behind. This results in the variation of dielectric property in the spark gap leading to voltage fluctuations from the set value. Higher the amount of debris, more will be the voltage variation.  $\Delta V_m$  can thus be considered as an indicator of the machining stability, since its value can indicate the relative amount of debris accumulation in the spark gap. Higher orders of debris accumulation can lead to bridging of spark gap and cause short circuit discharges and wire breakages. The method for computing  $\Delta V_m$  value is given in Fig. 5.15. The absolute of the difference between servo voltage and mean gap voltage ( $V_m$ ) gives the  $\Delta V_m$  for a particular machining run.

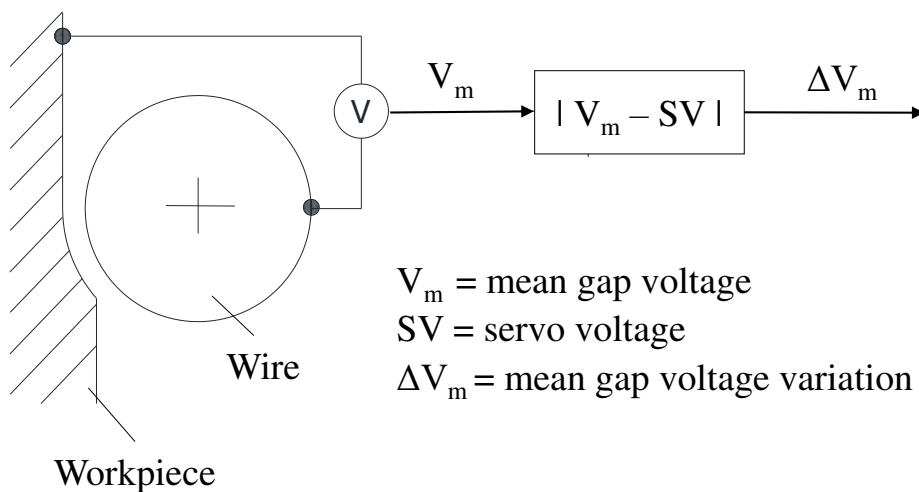


**Fig. 5.15** Method of determining mean gap voltage variation

### 5.3.4 ANFIS modelling of $\Delta V_m$ and wire break prediction

The approach for wire breakage prediction is given in Fig. 5.16. The mean gap voltage variation is recorded for all 31 experimental runs. As discussed, higher the value of  $\Delta V_m$ , greater is the process instability. The experiments are arranged in the increasing order of  $\Delta V_m$  to find a limiting value of  $\Delta V_m$  (defined as  $\Delta V_{m, \text{lim}}$ ), above which the machining failures are reported. Using the conducted experiments as training data, an adaptive neuro fuzzy inference system (ANFIS) model is developed to predict  $\Delta V_m$  value. The proposed decision support model utilizes ANFIS model predictions and experimentally found  $\Delta V_{m, \text{lim}}$  value to predict the occurrences of wire breakage for any given input parameter combinations. The system compares the predicted value of  $\Delta V_m$  with threshold value,  $\Delta V_{m, \text{lim}}$  to warn the operator regarding potential wire break possibilities.

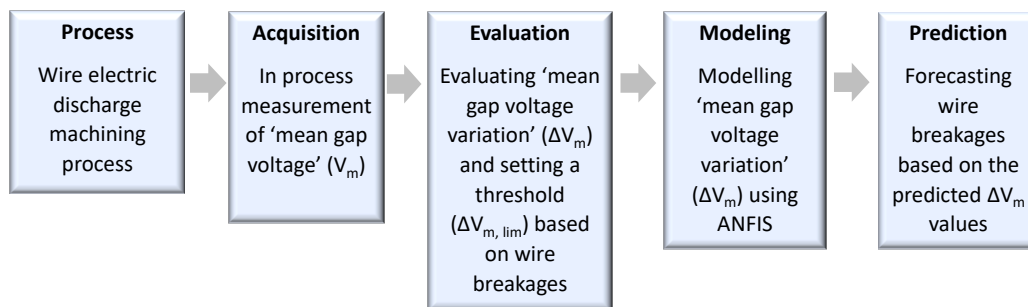


**Fig. 5.16** Approach for predicting wire breakage

The experimental runs and responses are tabulated in Table 5.11. The response  $\Delta V_m$  is plotted against the experiment numbers in Fig. 5.17. Wire breakage instances are also represented in this figure. Failure free continuous machining is observed in 25 out of 31 experiments (with  $\Delta V_m < 10.41\text{V}$ ). Remaining 6 experiments ( $\Delta V_m > 10.41\text{V}$ ) resulted in process interruption through wire breakages. Therefore, experimentally, 10.41 V (corresponding to Exp. No. 31) is found as the threshold value,  $\Delta V_{m, \text{lim}}$ .

**Table 5.11** Experimental readings and model predictions

S. No.	Ton ( $\mu$ s)	Toff ( $\mu$ s)	SV (V)	WF (m/min)	Experimental readings			Model predictions	Error
					Wire breakage	Mean $\Delta V_m$ (V)	Std. Dev.	$\Delta V_m$ (V)	(V)
1	115	40	60	4	0	9.56	0.2	9.56	0
2	110	50	50	6	0	4.9	0.4	4.67	0.23
3	105	60	60	4	0	1.63	0.6	1.63	0
4	110	50	50	6	0	4.6	0.4	4.67	-0.07
5	110	50	50	2	0	4.62	0.7	4.62	0
6	105	40	40	8	0	3.7	0.4	3.7	0
7	120	50	50	6	1	14.96	0.5	15	-0.04
8	110	50	50	10	0	5.4	0.4	5.4	0
9	100	50	50	6	0	1.63	0.5	1.63	0
10	110	50	50	6	0	5.2	0.5	4.67	0.53
11	105	60	60	8	0	1.63	0.1	1.63	0
12	105	60	40	8	0	1.63	0.1	1.63	0
13	115	40	40	4	1	11.74	0.4	11.7	0.04
14	115	40	60	8	0	8.54	0.2	8.54	0
15	110	50	50	6	0	3.5	0.3	4.67	-1.17
16	110	50	50	6	0	3.9	0.5	4.67	-0.77
17	105	40	60	8	0	1.63	0.1	1.63	0
18	110	50	70	6	0	2.08	0.5	2.08	0
19	110	70	50	6	0	2.08	0.1	2.08	0
20	105	60	40	4	0	1.63	0.1	1.63	0
21	115	40	40	8	1	11.74	0.2	11.7	0.04
22	115	60	60	4	0	9.88	0.2	9.88	0
23	105	40	60	4	0	1.63	0.1	1.63	0
24	115	60	40	4	1	11.4	0.6	11.4	0
25	110	50	50	6	0	4.55	0.6	4.67	-0.12
26	110	30	50	6	1	12.3	0.3	12.3	0
27	105	40	40	4	0	3.7	0.2	3.7	0
28	110	50	30	6	0	7.5	0.6	7.5	0
29	115	60	40	8	0	8.48	0.6	8.48	0
30	110	50	50	6	0	6.01	0.2	4.67	1.34
31	115	60	60	8	1	10.41	0.3	10.4	0.01

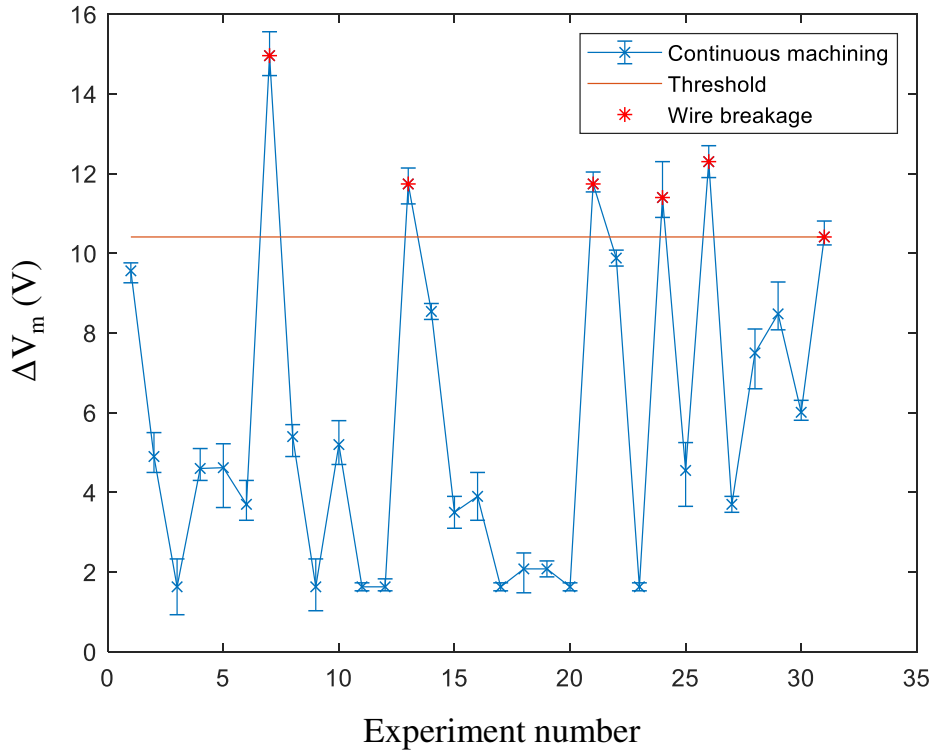


**Fig. 5.17** Determination of mean gap voltage variation limit ( $\Delta V_{m, \text{lim}}$ )

The experimental data presented in Table 5.11 is used to train the ANFIS model. The ANFIS model combines the advantages of both fuzzy and neural network tools. The model is suited to model complex non-linear systems. The model takes crisp input parameter values and perform fuzzification based on membership function. For the current application, gaussian membership functions are selected for input parameters with a constant output membership function. The model incorporates a hybrid learning algorithm combining gradient descent and least square techniques. ANFIS training parameters are given in Table 5.12. The gaussian membership function parameters according to Equation. No. 5.1 is given in Table 5.13.

$$\mu(x) = \exp\left(\frac{-(c_i-x)^2}{a_i^2}\right) \quad (5.1)$$

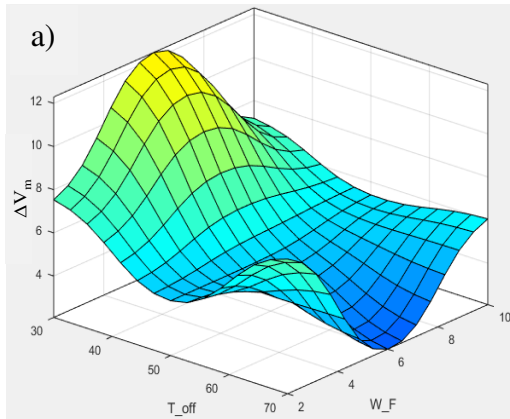
**Table 5.12** ANFIS training parameters

Layers	5
Data set	31 x 4
Responses	1
Membership function	Gaussian
Learning algorithm	Least squares, gradient descent
Number of epochs	300
Output function	Constant

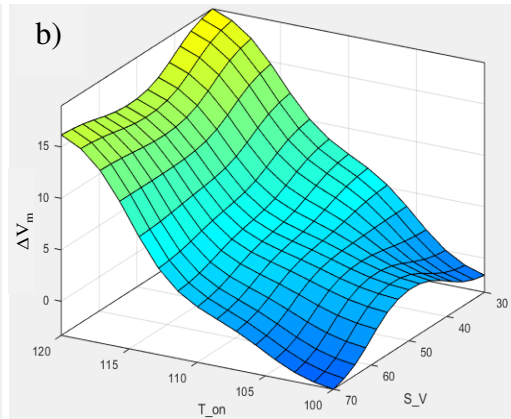
**Table 5.13** Parameters of gaussian membership function

Factors	Low		Medium		High	
	a	c	a	c	a	c
T <sub>on</sub>	4.25	100	4.25	110	4.25	120
T <sub>off</sub>	8.5	30	8.5	50	8.5	70
SV	8.5	30	8.5	50	8.5	70
WF	1.7	2	1.7	6	1.7	10

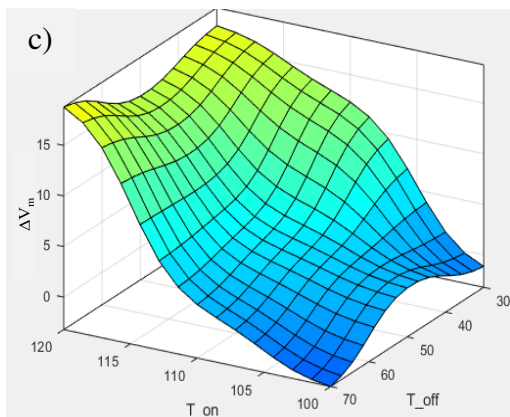
The surface plot of mean gap voltage variation with respect to input parameters is given in Fig. 5.18. The performance comparison of ANFIS model comparing the experimental and predicted values is given in Fig. 5.19. The model is found very accurate in the prediction of mean gap voltage variation value.



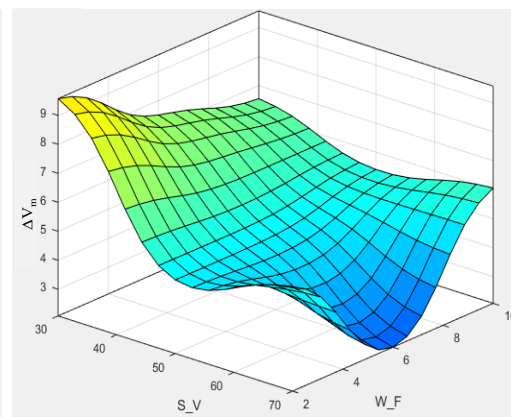
$\Delta V_m$  vs. Pulse off time and wire



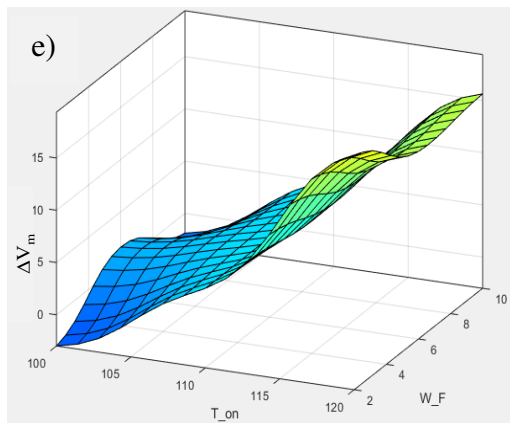
$\Delta V_m$  vs. Pulse on time and servo



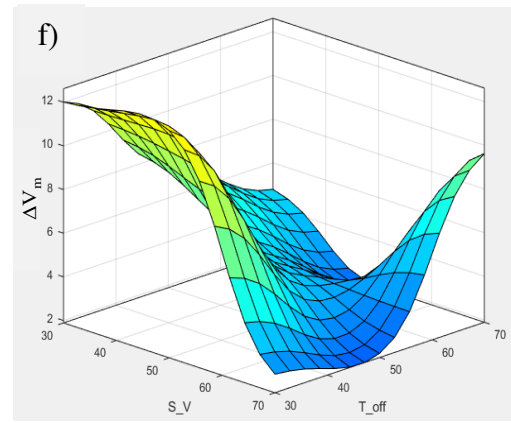
$\Delta V_m$  vs. Pulse on time and Pulse



$\Delta V_m$  vs. Servo voltage and wire



$\Delta V_m$  vs. Pulse on time and wire



$\Delta V_m$  vs. Servo voltage and Pulse

**Fig. 5.18** Surface plots showing the influence of process parameters on  $\Delta V_m$

### 5.3.5 Human computer interaction – wire break alert

A wire break alert system is developed to alert the operator regarding a potential wire break occurrence for any given parameter settings based on the predicted mean gap voltage variation value from the ANFIS model. The proposed rule-based system checks whether the ANFIS output value ( $\Delta V_m$ ) crosses the threshold ( $\Delta V_{m, \text{lim}}$ ). In case  $\Delta V_m > \Delta V_{m, \text{lim}}$ , a wire break alert is sent, requesting the operator to retune the parameter settings. Otherwise, the operator is permitted to continue with the given settings. The logic flow diagram for this interaction system is given in Fig. 5.20.

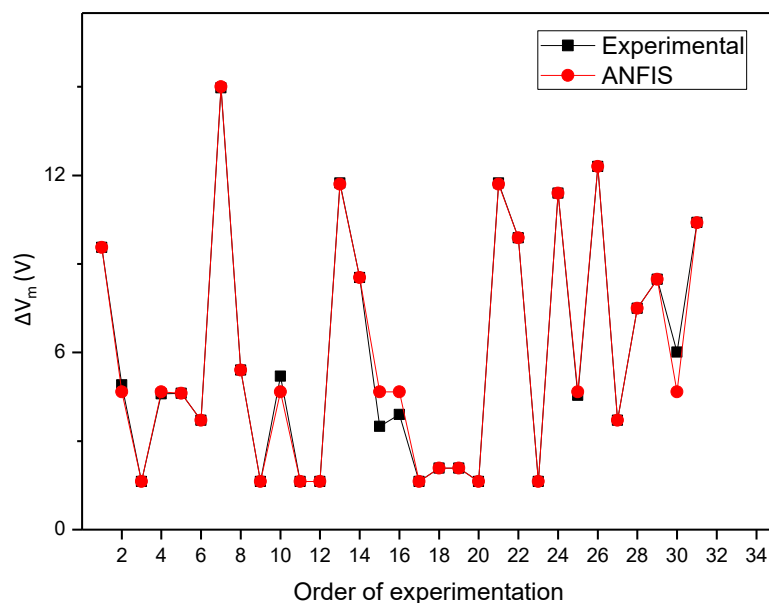
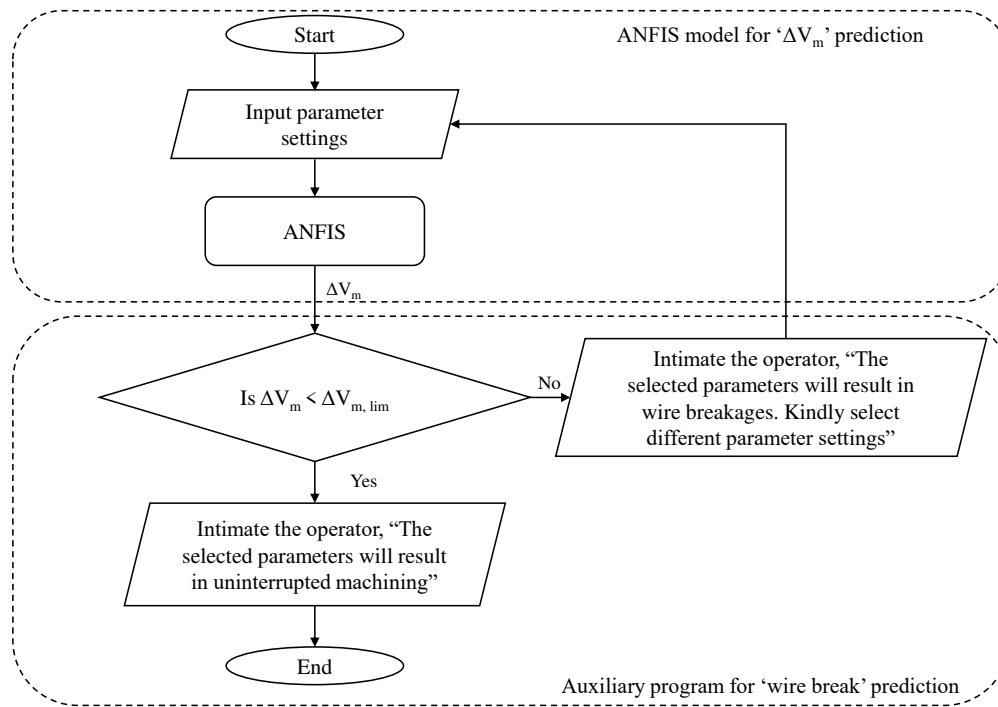


Fig. 5.19 Comparison of predicted values with actual values for  $\Delta V_m$

### 5.3.6 Confirmation experiments

Nine additional experiments are conducted to test the model performance in actual machining situations. The ANFIS model succeeded in predicting the  $\Delta V_m$  values very accurately. Also, based on ANFIS predictions, the alert system is successfully able to anticipate the wire breakages in every failure instance. The details of the confirmation test results are given in Table 5.14. The alert messages given to the operator in the case of wire breakage and normal continuous machining are shown in Table 5.15.



**Fig. 5.20** Logic flow diagram for wire break alert

**Table 5.14** Confirmation experiments

S. No.	Ton (μs)	Toff (μs)	SV (V)	WF (m/min)	ANFIS ΔV <sub>m</sub>	Exp. ΔV <sub>m</sub>	Model prediction	Experimental observation
1	115	40	30	3	9.79	8.8	CM	CM
2	115	30	40	3	8.57	8.4	CM	CM
3	120	30	30	7	14.5	15.2	WB	WB
4	120	30	40	4	12	10.8	WB	WB
5	105	45	40	5	3.28	3.5	CM	CM
6	110	35	40	10	7.91	8.05	CM	CM
7	118	33	39	4	11.8	12	WB	WB
8	112	43	49	9	7.33	7.25	CM	CM
9	103	33	31	5	2.77	2.5	CM	CM

CM – Continuous machining, WB – wire breakage

Expt. No. 3 and Exp. No. 5 from confirmation experiments are chosen to demonstrate the working of alert system. Exp. No. 3 resulted in wire breakage due to a high pulse on time (120  $\mu$ s), low pulse of time (30  $\mu$ s), and low servo voltage (30 V). In comparison, Exp. No. 5 resulted in continuous machining due to a comparatively lower pulse on time (105  $\mu$ s), high pulse off time (45  $\mu$ s) and high servo voltage (40 V). The wire break alert system suggested the operator to select different parameter settings in former case. Fig. 5.21 compares the model predictions and experimental readings of  $\Delta V_m$  during confirmation tests.

**Table 5.15** Wire break intimation based on ANFIS model predictions

Exp. No.	Model input	Model output - wire breakage prediction
3	Pulse on time = 120 $\mu$ s Pulse off time = 30 $\mu$ s Servo voltage = 30 V Wire feed rate = 7 m/min	Mean gap voltage variation = 14.5 V 'Gap voltage variation will lead to wire breakages. Kindly select different input parameter settings'
5	Pulse on time = 105 $\mu$ s Pulse off time = 45 $\mu$ s Servo voltage = 40 V Wire feed rate = 5 m/min	Mean gap voltage variation = 3.28 V 'Selected input parameter settings will result in uninterrupted machining'

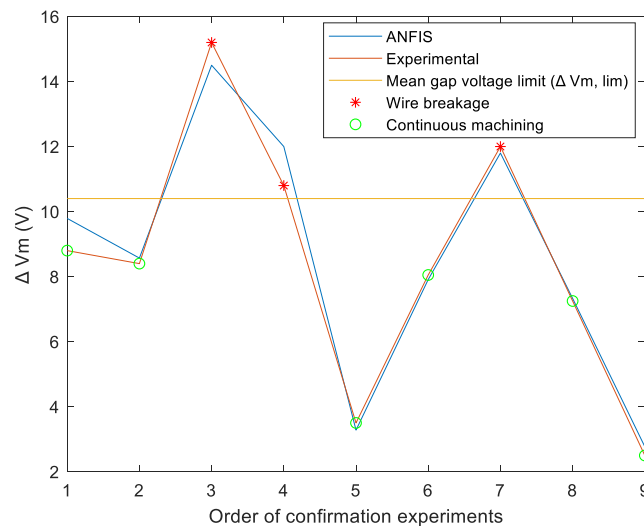


**Fig. 5.21** Confirmation tests comparison of ANFIS responses with experimental readings

### 5.3.7 Surface integrity analysis

Apart from predicting wire break failures,  $\Delta V_m$  can also indicate the part quality of the machined part. This is because, machining stability not only effects the process failures, but also the surface quality, as discussed in Chapter 4. Since  $\Delta V_m$  is an indicator of machining stability, the parameter is also capable of representing relative machined part quality. In order to compare the surface integrity of the machined surface, the predicted value of  $\Delta V_m$  is categorised into three, as shown in Table 5.16. From the SEM images of the machined surfaces shown in Fig. 5.22, it can be observed that the surface quality decreases with increase in mean gap voltage variation. Fig. 5.22 (a) shows a smooth surface with no visible micro defects or features in the machined area. Fig. 5.22 (b) is comparatively uneven with several micro voids and globules in the machined surface. Fig. 5.22 (c) on the other hand is visibly much coarser than the previous two cases with a lot of undesirable features like micro globules, pits, cracks, voids and debris. Higher value of  $\Delta V_m$  is associated with higher amount of debris accumulation, which causes more harmful short circuit discharges in the pulse cycle. Such discharges are known to produce coarser surfaces due to its high discharge energy and spark frequency. Quantitative comparison of machined surface quality is given in Table 5.17 for the confirmation tests.

Due to the reasons discussed already, wire wear also differs with respect to the mean gap voltage variation, as seen in Fig. 5.23. Wire surface damage can be seen to increase with  $\Delta V_m$  ultimately leading to wire breakage. The limit at which the wire is unable to withstand the spark gap instability is represented by the in-process data  $\Delta V_{m, \text{lim}}$ .

**Table 5.16** Classification of mean gap voltage variation

Predicted $\Delta V_m$	Category
< 5	Low
5 to 10	Medium
>10	High

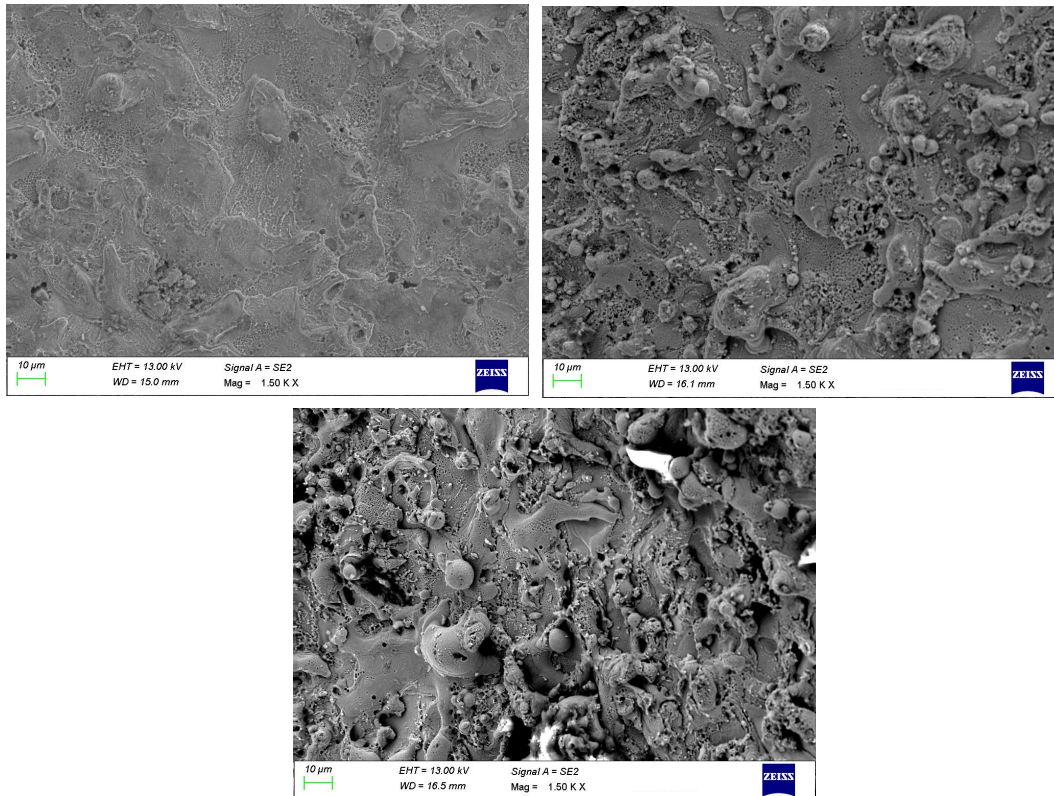


**Fig. 5.22** SEM images of machined surfaces with (a) low  $\Delta V_m$  (b) medium  $\Delta V_m$  (c) high  $\Delta V_m$  prediction

**Table 5.17** Part quality comparison at different  $\Delta V_m$  predictions

S. No.	$\Delta V_m$ (V) ANFIS	$\Delta V_m$ (V) Experimental	Surface Roughness $R_a$ ( $\mu\text{m}$ )	Flatness Error FE ( $\mu\text{m}$ )	Wire breakage
1	9.79	8.8	3.54	4.75	No
2	8.57	8.4	3.22	4.01	No
3	14.5	15.2	-	-	Yes
4	12	10.8	-	-	Yes
5	3.28	3.5	1.9	1.21	No
6	7.91	8.05	3.1	3.23	No
7	11.8	12	-	-	Yes
8	7.33	7.25	2.83	2.61	No
9	2.77	2.5	1.4	0.9	No

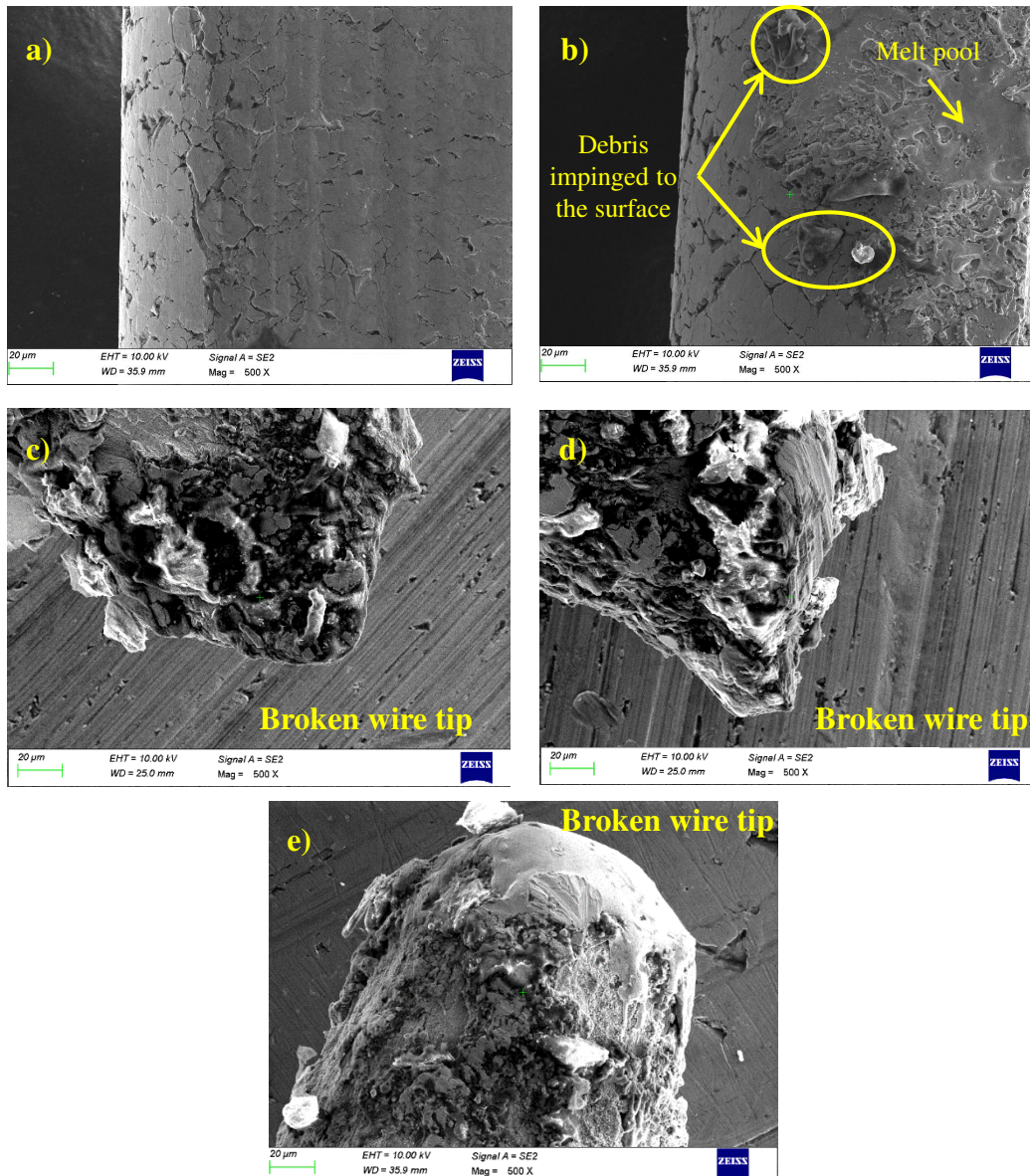


**Fig. 5.23** SEM images of wire surfaces with (a) low  $\Delta V_m$  (b) medium  $\Delta V_m$  (c) broken wire tip at high  $\Delta V_m$  (Exp. No. 3) (d) broken wire tip (Exp. No. 4) (e) broken wire tip (Exp. No. 7)

### 5.3.8 EDS analysis of worn wire surface

Energy dispersive spectroscopy (EDS) analysis is conducted on the worn wire surfaces under the three  $\Delta V_m$  categories considered in earlier section. The analysis is performed to understand the weight % of zinc element on the wire surface to compare the zinc coating removal leading to wire rupture. Wire rupture

of coated wires is strongly related to the removal of zinc coating exposing the inner core to the process heat. Higher the zinc coating removal, greater are the chances of wire breakage. The EDS analysis shows a decrease in weight % of zinc from low  $\Delta V_m$  to high  $\Delta V_m$  as shown in Fig. 5.24. This is due to the higher instability, causing short circuit sparks in the latter case resulting in greater removal of surface coating. Once the coating is removed, the wire electrode is easily prone to sudden rupture since the unprotected brass core is exposed. Therefore, the EDS analysis supports the claim that  $\Delta V_m$  can be an indicator of the gap instability and wire break failure.

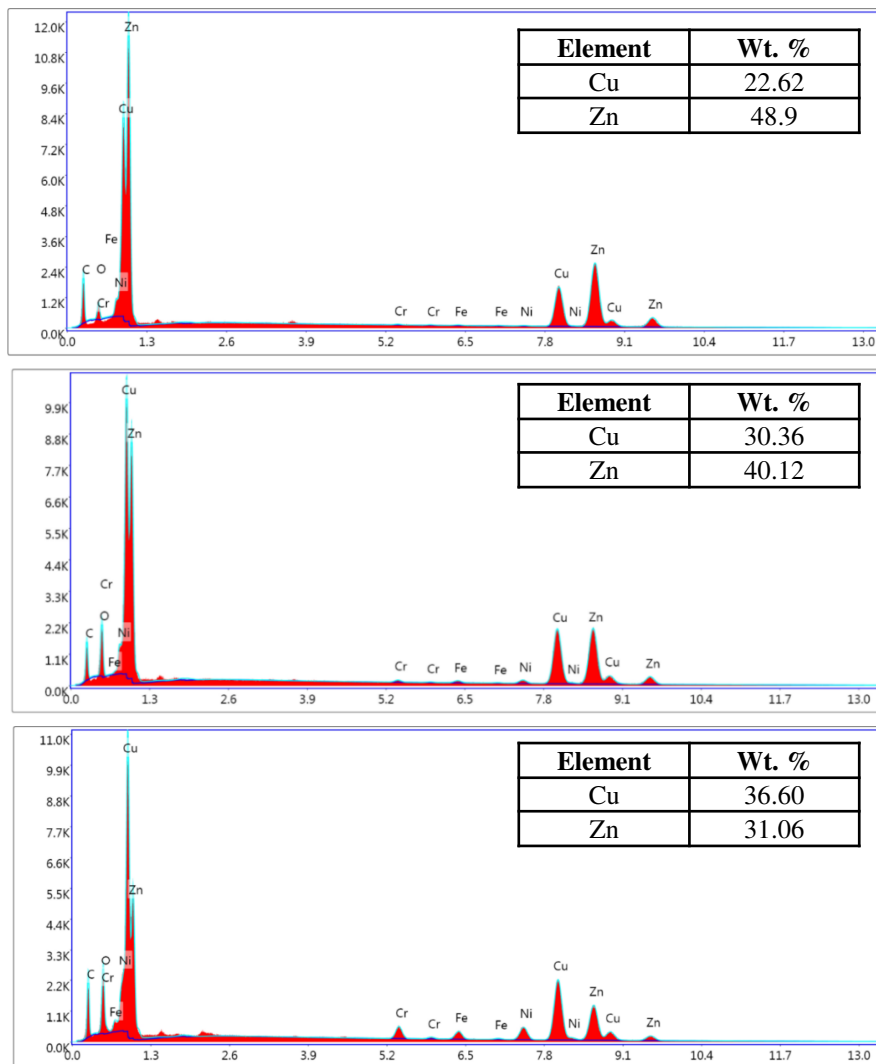


**Fig. 5.24** EDS analysis of wire surfaces with (a) low  $\Delta V_m$  (b) medium  $\Delta V_m$  (c) high  $\Delta V_m$  prediction

## 5.4 IN-PROCESS FAILURE PREDICTION

The earlier section explored the possibilities of using mean gap voltage variation as an indicator of machining instabilities to predict wire breakages. This section explores the capability to use  $\Delta V_m$  as a process data for in-process failure prediction. Here, failure prediction is performed after the process starts unlike the earlier ANN and ANFIS models. For such an analysis, certain parameters which represents the process stability, have to be extracted during the machining process, which can be utilized to draw useful conclusions regarding machining health.  $\Delta V_m$  is already reported to be a machining stability indicator for similar analysis (Klocke et al., 2014; Abhilash and Chakradhar, 2020). Therefore, in this work, the extracted  $\Delta V_m$  value is fed as an input feature along with process parameters to a machine learning (ML) classifier model to categorise machining outcomes into failure (wire breakage) and non-failure (continuous machining) cases. Failure prediction models based on the in-process data can account the effects of uncontrollable random factors on the machining process and is expected to be more accurate than conventional classifier predictions.

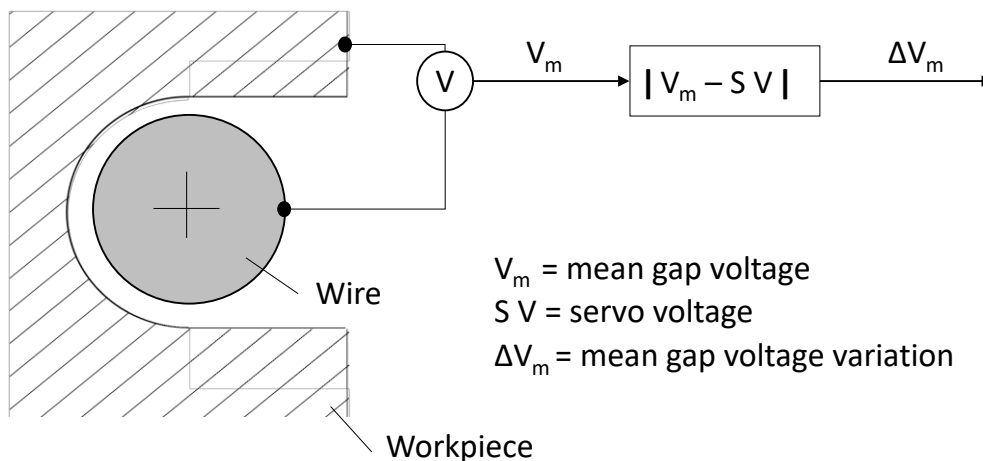


**Fig. 5.25** Method of determining mean gap voltage variation

### *Classifier performance*

The methodology of extracting mean gap voltage variation is given in Fig. 5.25. The extracted data is fed to an ML classifier along with process parameter values

for appropriate failure prediction. Several ML classifiers are considered and among them, Kernel based Naive Bayes (KNB) classifier is selected based on classification accuracy. The performance comparison of various classifiers is given in Table 5.18. KNB classifier is known to outperform other models under smaller training dataset conditions. A block diagram representing the steps involved in training and prediction of machining failures using KNB model is given in Fig. 5.26.

**Table 5.18** Comparison of classifier performances

S. No.	Machine learning classifier technique	Accuracy
1	Logistic regression	87.10%
2	Linear Support Vector Machine	83.90%
3	Gaussian Support Vector Machine	80.60%
4	K-Nearest Neighbour	80.60%
<b>5</b>	<b>Kernel Naive Bayes</b>	<b>96.70%</b>

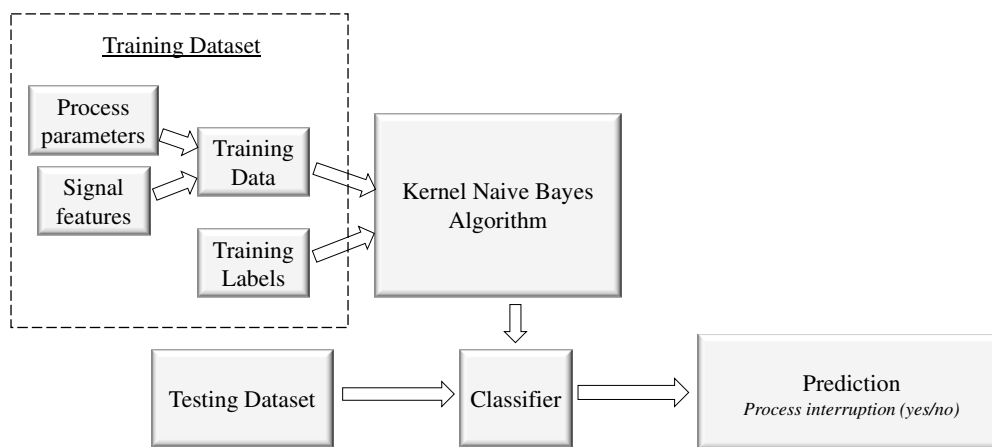


**Fig. 5.26** The steps involved in developing a Naive Bayes classification model

KNB classifier is a probabilistic classifier based on Bayes theorem. Bayes theorem computes the probability of occurrence of an incident, based on the former knowledge of a condition linked to that incident. KNB is a binomial classifier with class labels ‘wire breakage’ and ‘continuous machining’. The

training dataset consists of experimental details (input parameters), in process data ( $\Delta V_m$ ) and corresponding class label. The trained model is observed to have a classification accuracy of 96.7 % as evident from the confusion matrix and ROC curve shown in Fig. 5.28.

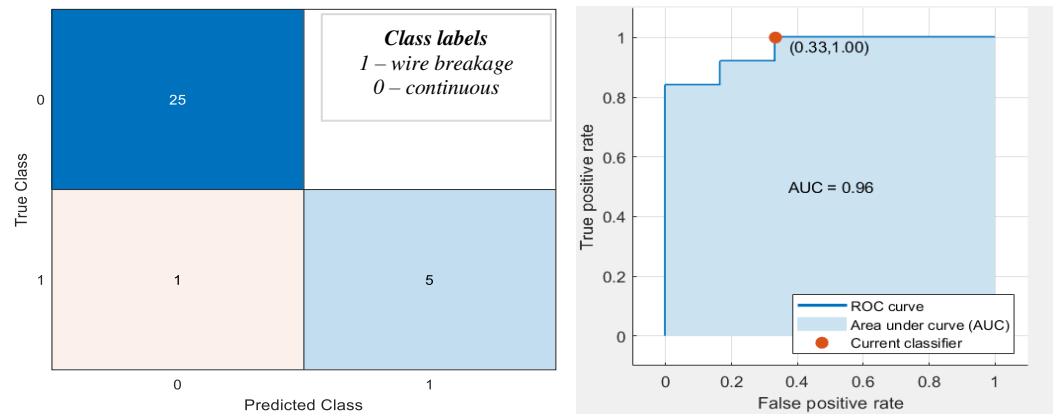


**Fig. 5.27** Performance evaluation of the model (a) Confusion matrix (b) ROC curve

## 5.5 SUMMARY

Predicting the process failures during the machining of wire EDM is difficult due to the stochastic process mechanism leading to failure. Additionally, the interference of external uncontrollable factors and complex parametric interactions can also influence the process failure. ANN classifier is a capable soft computing tool to handle such higher order multi dimension relations between the parameters and events. A multi-class classifier is developed with the class labels being the machining outcomes – ‘spark absence’, ‘normal machining’, and ‘wire breakage’. Among these, wire breakage and spark absence are considered as machining failures and the normal machining indicates the ideal uninterrupted failure free operation. The trained model is successful in predicting the machining failures during the wire EDM of Inconel 718 material with 91 % accuracy. Confirmation tests reassured the model’s ability to predict the events in real world situations. 95 % accuracy is reported during the confirmation tests. A detailed analysis on the mechanism of wire rupture is performed by considering

SEM images of wire samples corresponding to different wire break prediction probabilities.

A parameter called ‘mean gap voltage variation’ is introduced as a machining stability indicator. The parameter is utilized to forecast wire breakage failures. In this regard an ANFIS model to predict  $\Delta V_m$  is developed. Limiting value of  $\Delta V_m$  is found experimentally, above which the wire breakages occur. This value,  $\Delta V_{m,lim}$  indicates the maximum gap instability the wire electrode can sustain. Through 31 experiments based on central composite design of RSM, an ANFIS model is trained to predict  $\Delta V_m$ . Additional confirmation tests are conducted to test the model accuracy in predicting  $\Delta V_m$  values in real machining situations. Based on the predicted  $\Delta V_m$  values, a decision support model is developed which intimates the operator regarding the potential wire break situation with good accuracy. The capability of the parameter  $\Delta V_m$  to indicate machining stability is further proven by conducting wire wear analysis. Low  $\Delta V_m$  showed minor wire degradation whereas  $\Delta V_m$  values close to threshold displayed extensive wire wear. Additionally, EDS analysis of wire surface is conducted to support the claim. Machined surface quality also showed deteriorating trends with increased  $\Delta V_m$ . The surface quality is evaluated considering average surface roughness, flatness error and SEM images of machined surface under different  $\Delta V_m$  ranges. Finally, a binomial classifier (kernel based Naive Bayes classifier) is successfully modelled to predict wire break failure.

## CHAPTER 6

### DEVELOPMENT OF SENSOR BASED CONDITION MONITORING SYSTEM

#### 6.1 INTRODUCTION

The chapter describes the development of a condition monitoring system for wire EDM process. Firstly, signal acquisition, signal processing and feature extraction procedure is described. A pulse classification model is developed to discriminate between normal and abnormal discharge pulses. Next, the effect of process parameters on discharge characteristics and pulse proportions are analysed. The changes in pulse train behaviour and discharge characteristic values at different failure situations are studied. The chapter also discusses the effect of extracted features on process performance. The effects of unstable machining conditions on wire wear and surface morphology of machined components are studied. Finally, a heuristic rule-based failure detection model is proposed.

#### 6.2 EXPERIMENTAL DETAILS

Experiments are conducted based on Taguchi's  $L_{18}$  orthogonal array experimental design. Input parameters varied are pulse on time, pulse off time, servo voltage, wire feed rate, and input current. The input parameters and levels are shown in Table 6.1. The process parameters are selected based on their higher impact on machining failures. A few parameters are fixed constant due to wire EDM limitations and due to lesser impact on performance. The range of parameters are selected based on pilot experiments, information from wire EDM manual, and literature survey. Input current is selected at only two levels based on machine specification constraint. Since the aim of the study is to study the process failures, parameter ranges are purposefully selected to induce a few failure outcomes. Inconel 718 plate of thickness 10 mm is chosen as workpiece. Wire electrode considered is zinc coated brass electrode of 0.25 mm diameter.



Tektronix TCP 303 coupled with a current probe amplifier Tektronix TCPA 300 having 15 MHz bandwidth and 0 to 150 A measuring range. The voltage probe is Tektronix P 5200A with 200 MHz bandwidth and measuring range 0 to  $\pm 1300$  V. The pulse acquisition and transfer are performed by a mixed domain oscilloscope, Tektronix MDO 34-200 with 200 MHz bandwidth and 2.5 GSa/s sampling rate per channel. The experimental setup is shown in Fig. 6.1. Signal processing, feature extraction, pulse classification and other computations are performed by a dedicated windows PC workstation with advanced graphics and computational capabilities.

### **6.3 PULSE TRAIN ANALYSIS**

The voltage and current signals captured by the sensors are filtered using signal analyser toolbox in Matlab. A single capture record length is 20 ms with 250 million sample per second. The experiments are replicated thrice and each extracted feature is the average value of the three measurements. Low pass filter is applied to suppress higher frequency noises. Further, the relevant features are extracted from the filtered signal. A pulse classification algorithm, classifies each pulse into normal, arc, short or open pulse. From the pulse classification data, proportion of each pulse types in the recorded data can be computed. The extracted discharge characteristic features like discharge energy, ignition delay time, pulse frequency, and pulse proportions are used to draw useful conclusions regarding the machine health state. A future occurrence of wire breakage or spark absence can be predicted from the discharge characteristic values. Also, the performance characteristics like cutting speed and surface roughness can also be predicted from this extracted data. The methodology of pulse train analysis is given Fig. 6.2.

Ignition delay time is regarded as an important pulse characteristic to determine machining stability for EDM processes. The parameter indicates whether the breaking and restoration of dielectric is taking place ideally in the spark gap. In a stable machining condition, the current discharges will be preceded by ignition delay duration in the voltage pulse, which is essentially the time taken for

ionization of dielectric in the spark gap. A sufficient ignition delay time implies proper restoration of dielectric properties after each discharge spark. However, in case of debris stagnation or spark gap bridging, the ignition delay time is negligible or absent, resulting in arc or short circuit sparks respectively. This is due to increased conductivity of dielectric medium in the spark gap due to the presence of conductive debris particles. If not addressed, the situation can cause repeated short circuit pulse cycles. A pulse train with higher arc or short proportion have very high average discharge energy, and pulse frequency. Such a situation is regarded as the primary cause of wire breakage. Apart from debris stagnation, ignition delay time variation can also occur due to wire lag, deflection or vibrations due to the lateral forces acting on the wire due to dielectric flushing pressure, electrostatic forces, discharge spark force, etc.

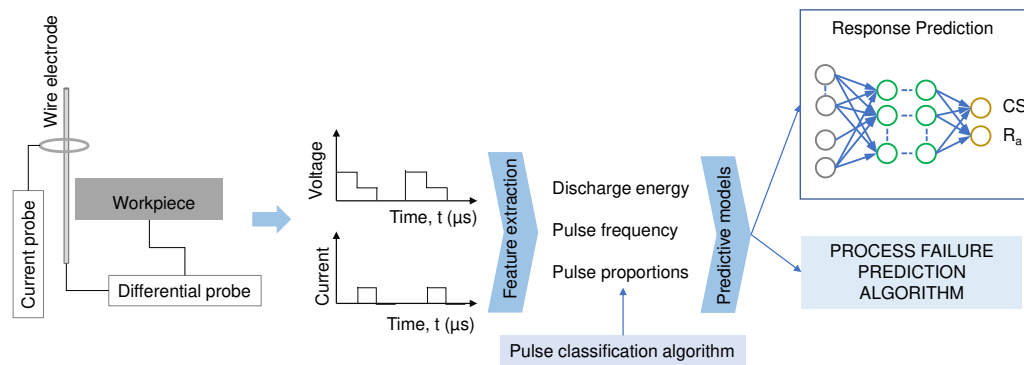


**Fig. 6.2** Methodology of pulse train analysis

## 6.4 PULSE CLASSIFICATION AND CHARACTERISATION

The ideal machining condition in wire EDM involves breaking and restoration of dielectric properties in the spark gap. As discussed in the previous section, under stable machining condition, current discharge occurs after an ignition delay period. Such ideal discharge pulses, along with typical discharge characteristics are shown in Fig. 6.3. Material removal occurs during the pulse on time. Pulse off time, follows the pulse on time to clear the debris from spark gap and to cool the workpiece. Open circuit voltage is the initial voltage applied across the

electrodes. Once the dielectric barrier is breached, the voltage drops during the spark discharge, which called discharge voltage.

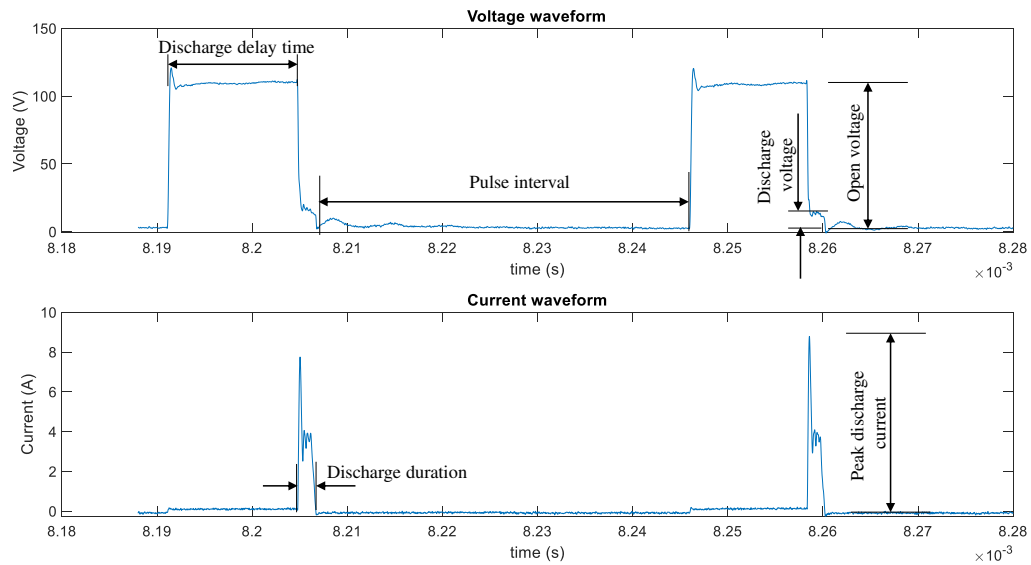


**Fig. 6.3** Typical voltage and current pulse shape for a normal discharge

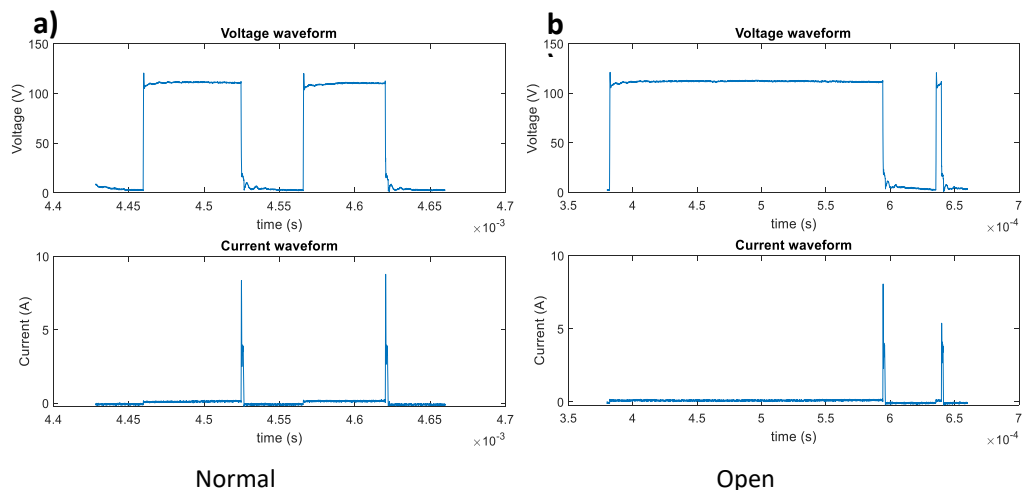


**Fig. 6.4** (a) Normal discharge (b) Open circuit discharge

During the pulse train analysis, different types of discharge pulses are identified apart from the normal spark discharges. They are open circuit pulses, arc discharges and short circuit discharges. Each pulse types are distinguishable from one another by the ignition delay duration. Open circuit sparks are characterized by longer than ideal ignition delay time. If the pulse cycle is predominated by

open circuit sparks, then the overall productivity of the machining process comes down. After a limit, excessive open sparks can lead to spark absence failure, where the machining halts due to zero or negligible spark frequency. Open circuit sparks happens when the voltage applied across the electrodes is not sufficient enough to break the dielectric barrier. This happens due to excessive spark gap distance or lesser than ideal open circuit voltage. Fig 6.4 compares the open circuit sparks with normal spark discharges.

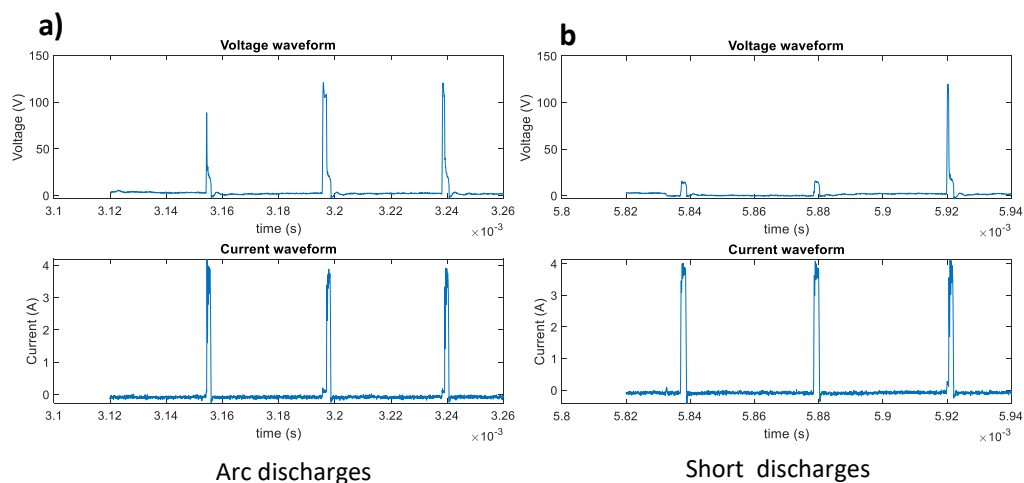


**Fig. 6.5** (a) Arc discharge (b) Short circuit discharge

Arcing happens when a fraction of debris is left behind in the spark gap at the end of pulse off time. Suspended debris in the dielectric increases the conductivity of spark gap region resulting in lower than usual ignition delay time. Arc sparks are characterised by negligible ignition delay time. In this case, as soon as the voltage pulse reaches the open circuit voltage, the channel becomes conductive and a discharge spark is initiated. Fig. 6.5 (a) shows pulse cycle having a series of arc sparks. Arcing can improve the productivity of the process but can affect machined surface integrity adversely. Often higher proportion of arc sparks cause surface damages. Increasing the spark gap, pulse off time, and dielectric pressure can restore the machining stability in case arcing is detected early.

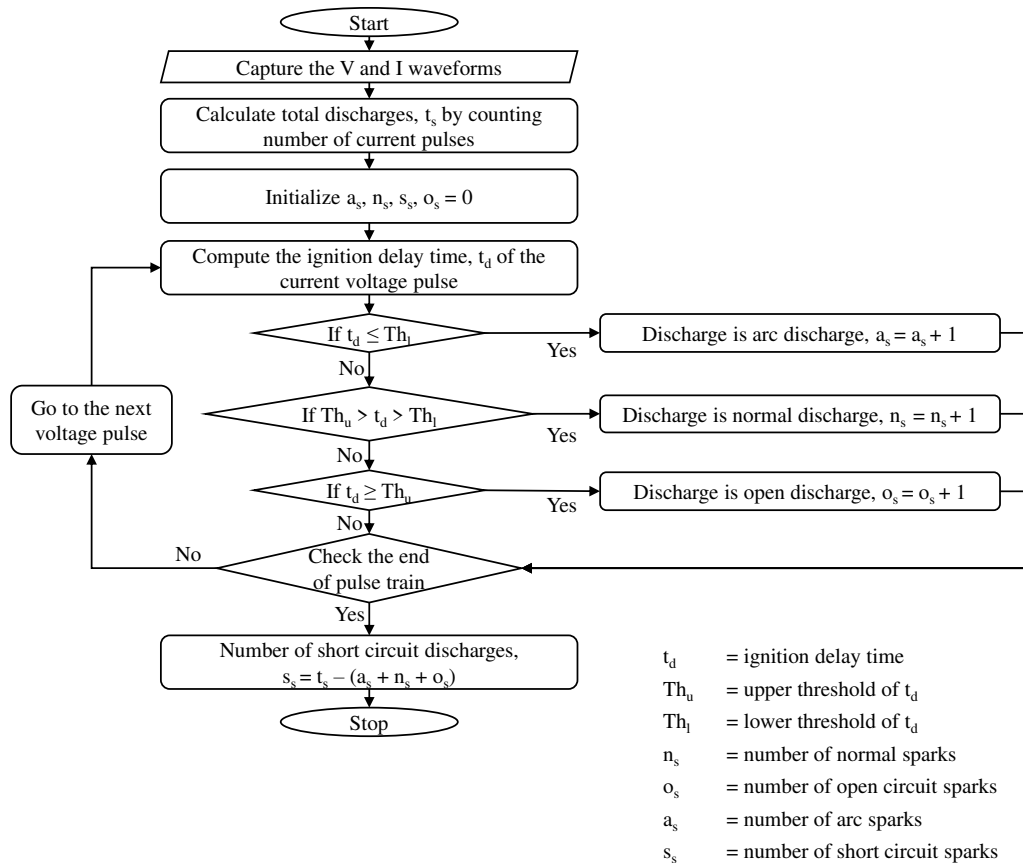


**Fig. 6.6** Pulse classification algorithm

Short circuit sparks are extreme cases of arc sparks. If the debris stagnation due to ineffective flushing builds up, a stage will be reached, when the entire inter electrode distance is bridged by debris. This causes series of short circuit sparks, when the voltage is applied across the electrodes. In such cases, as soon as the voltage is applied, a discharge spark occurs due to physical contact between the electrodes. Here the voltage pulse does not reach the peak value, contrary to the previous cases. A short circuit spark is shown in Fig. 6.5 (b).

## 6.5 PULSE CLASSIFICATION ALGORITHM

The current study proposes a pulse classification algorithm based on ignition delay time. The threshold values of the algorithm are found heuristically based on experimental study and pulse train analysis. The algorithm is shown in Fig. 6.6. A pulse counter counts the total number of discharge pulses. In the absence of an ignition delay time, the pulse is categorised as short circuit pulse.

In case of ideal ignition delay duration (from 8  $\mu$ s to 160  $\mu$ s), the pulse is categorised as normal spark discharge. If the ignition delay time is less than 8  $\mu$ s, then the pulse is arc spark. Finally, if the discharge spark is absent even after 160  $\mu$ s, then the pulse is categorised as open circuit spark.

The classifier performance is evaluated by considering pulse cycles of different record lengths, and the developed pulse classifier is observed to perform accurately in each case. Fig. 6.7 demonstrates the pulse classification results for a pulse sample size of 5 ms.

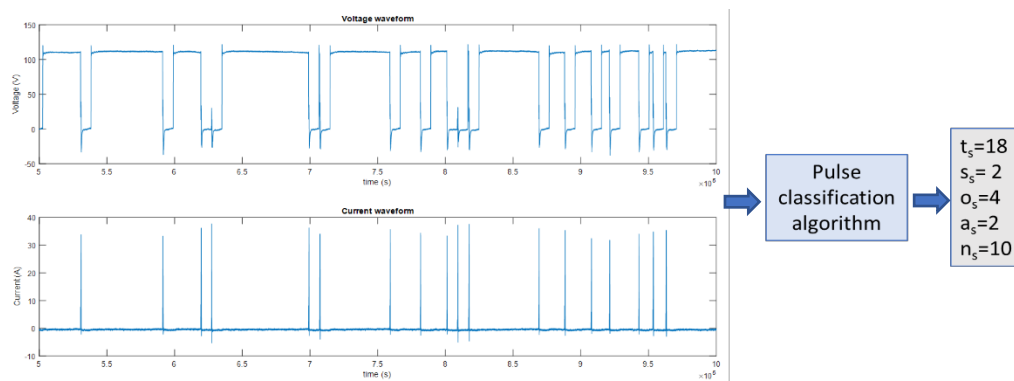


**Fig. 6.7** Results of pulse classification on a 2 ms wire EDM pulse data

## 6.6 EFFECT OF INPUT PARAMETERS ON PULSE CHARACTERISTICS

To analyse the effect of input parameters on the discharge characteristics and pulse proportions, one factor at a time experiments are conducted. Pulse on time, pulse off time and servo voltage are varied at five levels in this regard. Effect of each parameter is discussed in this section.

Since the discharge energy is proportional to pulse on time, number of debris produced can reach unideal levels at higher pulse on time values. For a fixed spark gap and pulse off time, there is a limit up to which the debris produced can be flushed away effectively. If the debris are increased progressively, by increasing pulse on time, after a limit, debris will start to accumulate creating short circuit sparks. This is why, the pulse cycle changes from normal spark dominant at lower discharge energies, to short circuit dominant at higher

energies. This effect is shown in Fig. 6.8. Spark ratios are computed as the ratio of the number of a particular pulse to total number of discharge pulse.

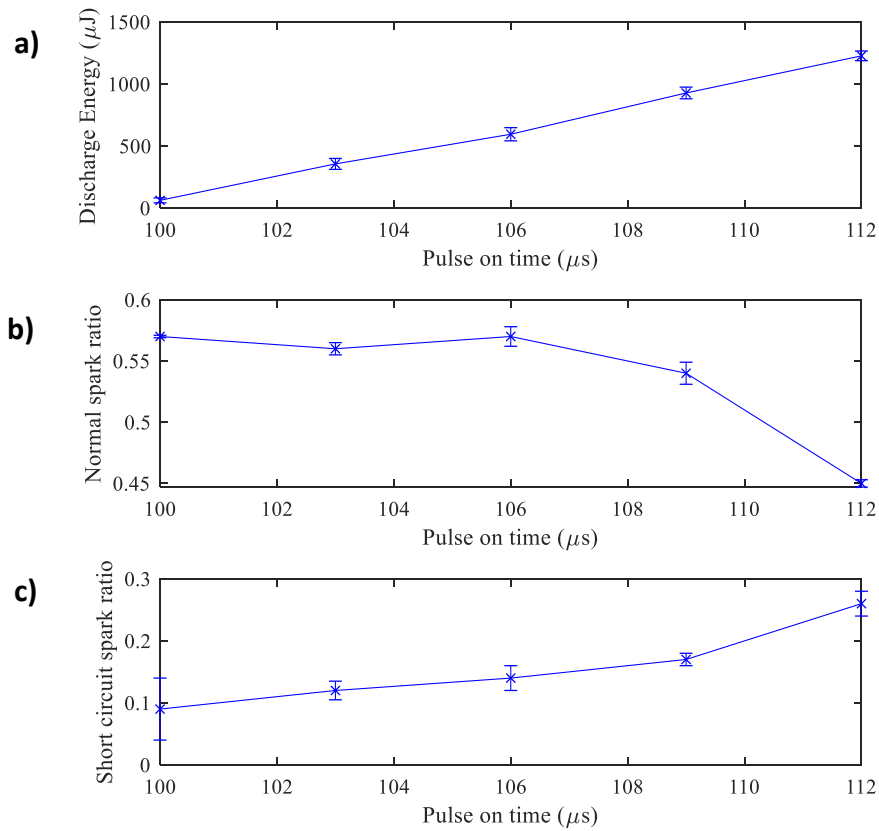


**Fig. 6.8** Effect of pulse on time on discharge energy and pulse proportions

Fig. 6.9 shows the effect of servo voltage on the discharge characteristics. Servo voltage is the reference voltage based on which the inter electrode gap is maintained. Larger the servo voltage, greater is the spark gap distance. Increasing the spark gap prolongs the ionization of discharge channel and subsequent dielectric breakdown. If the spark gap is increased beyond a limit, dielectric breakdown is not achieved during pulse on time resulting in open circuit sparks. Open circuit pulses are called misdischarges since current discharge is absent and thus higher open circuit pulse proportion implies a reduced spark frequency. This is shown in Fig. 6.9 (a) and Fig. 6.9 (b). When all other parameters are fixed, decreasing the servo voltage narrows the spark gap, which after a limit results in debris stagnation due to incomplete flushing. This is the reason why the short circuit ratio is observed to increase at lower servo voltages as shown in Fig. 6.9 (c).

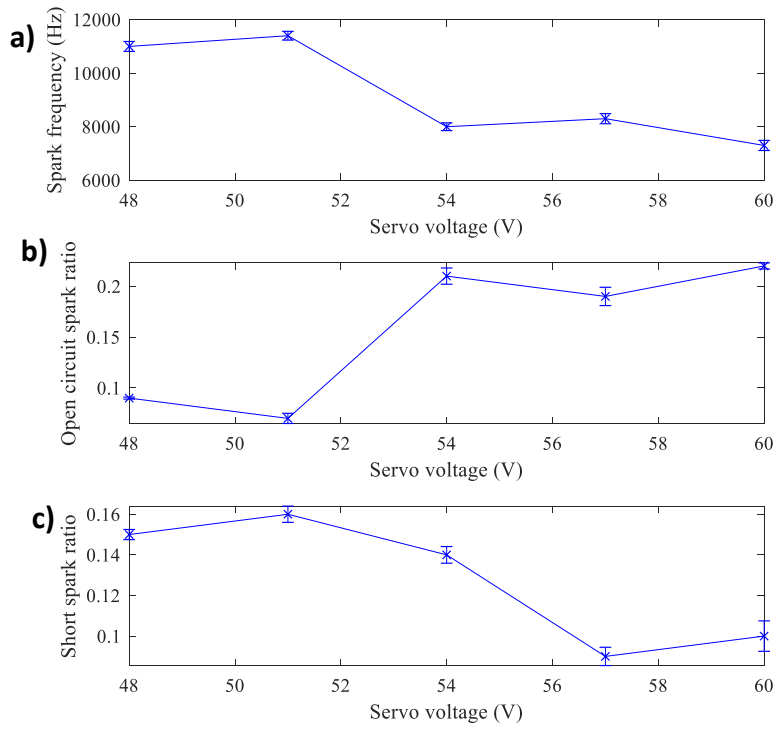


**Fig. 6.9** Effect of servo voltage on spark frequency and pulse proportions

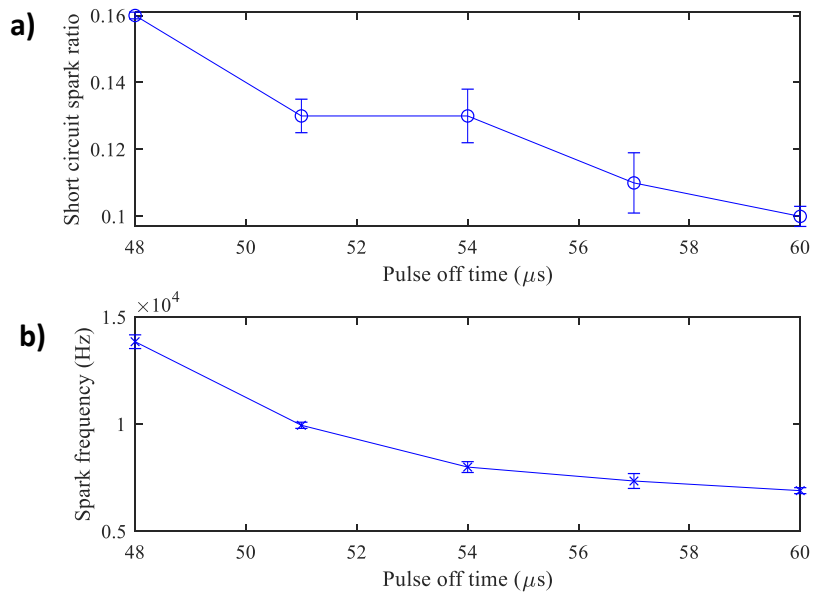


**Fig. 6.10** Effect of pulse off time on short circuit spark ratio and spark frequency

Pulse off time has a similar effect to that of servo voltage on discharge characteristics. Lower pulse off time implies lesser time for dielectric flushing.

Thus, at lower pulse off times, chances of debris stagnation are greater, resulting in higher proportion of short circuit sparks. Short circuit sparks happen at higher frequency due to direct pulse discharge by physical contact. Both these effects are shown in Fig. 6.10.

The effects discussed so far are in controlled environment where only the parameter under consideration is varied keeping all others constant. However, in actual situations the parameter interactions can result in unexpected outcomes which can be different from what has been discussed so far. This is the reason why statistical models relating input parameters and process responses are regarded as less accurate. A condition monitoring system which relates discharge features to the process outcome and response is extremely significant in this regard. Such a system can address the complex process interactions and stochastic material removal mechanism more accurately.

## **6.7 EFFECTS OF DISCHARGE CHARACTERISTICS ON PROCESS PERFORMANCE**

To study the effects of extracted features on the process responses, 18 experiments are conducted, the details of which are given in Table 6.2. Discharge energy has a significant effect on the productivity and surface quality of wire electric discharge machined parts. It is understood from the mechanism of material removal that discharge energy of individual sparks is proportional to the individual crater size formed on the workpiece. Cumulative effect of many such craters contribute to the material removal during the spark discharges. Larger the crater dimension, higher will be the material removal rate. This effect of discharge energy on cutting speed is shown in Fig. 6.11 (a). Additionally, crater sizes also dictate the roughness of the resulting machined surface. Average surface roughness is computed with regard to the deviations of the machined surface from a mean line. Deeper craters cause greater deviations and hence rougher would be the surface which is evident from Fig. 6.11 (b).

**Table 6.2** Extracted discharge features and recorded responses

S. No.	DE ( $\mu\text{J}$ )	SF $\times 100$ (Hz)	NSR	OSR	ASR	SSR	CS (mm/min)	R <sub>a</sub> ( $\mu\text{m}$ )	MO
1	538	552	0.36	0	0.35	0.29	1.09	2.12	WB
2	507	298	0.47	0	0.26	0.27	1.04	2.05	NM
3	540	124	0.58	0.05	0.15	0.22	0.38	1.82	NM
4	951	204	0.47	0	0.19	0.34	1.35	2.28	WB
5	1014	116	0.58	0.04	0.13	0.25	0.91	2.37	NM
6	1003	66	0.4	0.26	0.09	0.25	0.93	2.16	NM
7	1496	174	0.5	0.01	0.13	0.36	1.8	3.01	WB
8	1540	82	0.51	0.16	0.09	0.24	0.82	2.92	NM
9	1520	131	0.49	0.01	0.2	0.3	1.24	2.95	WB
10	47	269	0.43	0.02	0.34	0.21	0.2	0.71	NM
11	29	414	0.35	0	0.43	0.22	0.24	0.67	NM
12	48	174	0.61	0.01	0.19	0.19	0.11	0.57	NM
13	29	183	0.53	0	0.27	0.2	0.13	0.59	NM
14	26	74	0.53	0.21	0.16	0.1	0.03	0.52	SA
15	27	8.5	0.17	0.41	0.24	0.18	0.1	0.66	SA
16	31	8	0.29	0.38	0.19	0.14	0.06	0.61	SA
17	32	9.5	0.22	0.39	0.21	0.18	0.09	0.79	NM
18	33	4.5	0.17	0.64	0.11	0.08	0.01	0.72	SA

DE= Discharge energy, SF= Spark frequency NSR= Normal spark ratio, OSR= Open spark ratio, ASR= Arc spark ratio, SSR= Short spark ratio, CS= Cutting speed, R<sub>a</sub>= Average surface roughness, MO = Machining outcome, WB = Wire breakage, NM= Normal machining, SA= Spark absence

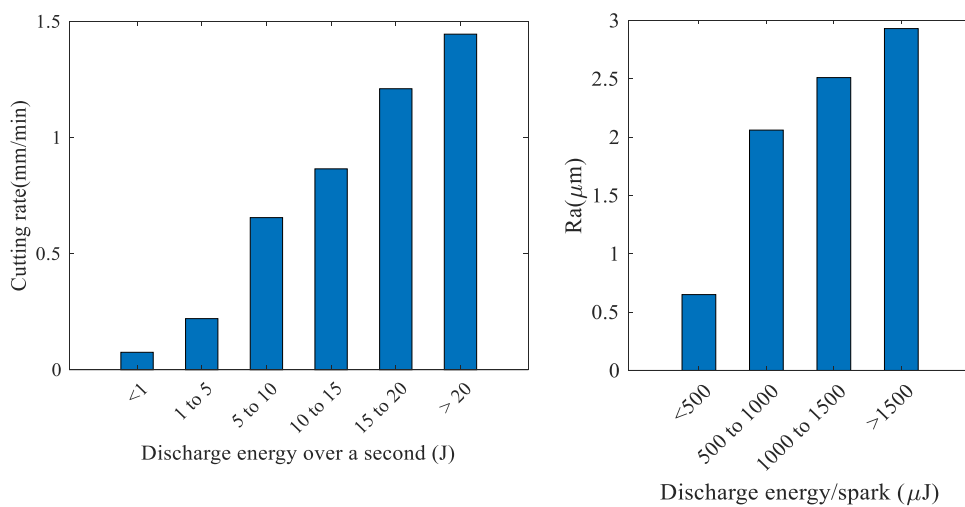


**Fig. 6.11** Effect of discharge energy on (a) cutting rate (b) Surface roughness

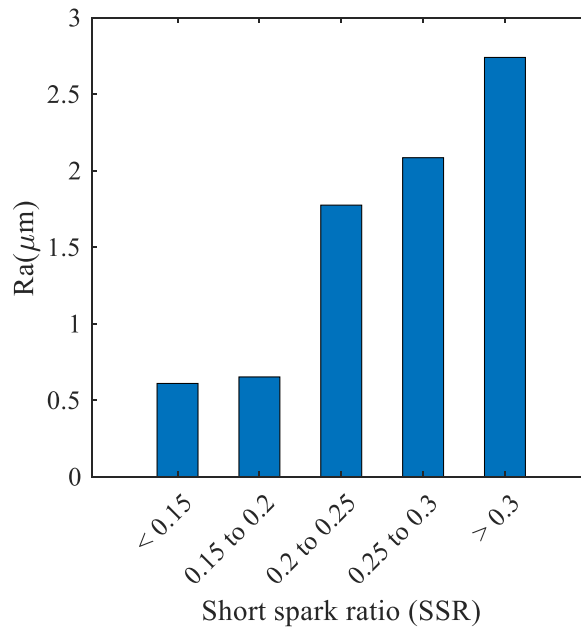


**Fig. 6.12** Effect of short circuit sparks on surface roughness

In addition to the typical material removal mechanism, at higher discharge energies, the effect of short circuit pulses also contributes to the higher material removal and average surface roughness. The short circuit pulses are regarded as undesirable because of its higher intensity and can lead to severe surface damages. The effect of short spark ratio on surface roughness is shown in Fig. 6.12.

## 6.8 PULSE CYCLE BEHAVIOUR DURING PROCESS FAILURES

Pulse train patterns during machining failures are compared with its typical behaviour in this section. Several distinct pulse characteristics are observed in voltage and current signals, leading to process failures. Based on such observations, the features to be extracted (machine health indicators) are selected. Unstable pulse cycle before wire breakage failure, is observed to have several series of short circuit discharges as seen in Fig. 6.13. Secondly, the discharge intensities are relatively higher than the normal spark discharges. Also, the spark frequencies are observed to be several times greater than the ideal cycle. The short circuit sparks happen spontaneously at the application of voltage across the electrodes by physical contact through gap bridging phenomena. Wire electrodes

erode faster due to these short discharges, rapidly melting and vaporising the zinc coating. The unprotected inner brass core is more prone to damages due to its direct exposure to thermal shocks. Higher spark frequency increases possibilities of multiple sparks from the same wire spot, which further intensifies the degradation. As the wire wear continues, at a limiting point, the wire electrode will be no longer able to withstand the axial tension. Wire elongates at the point of maximum wire wear, which will eventually lead to wire rupture.

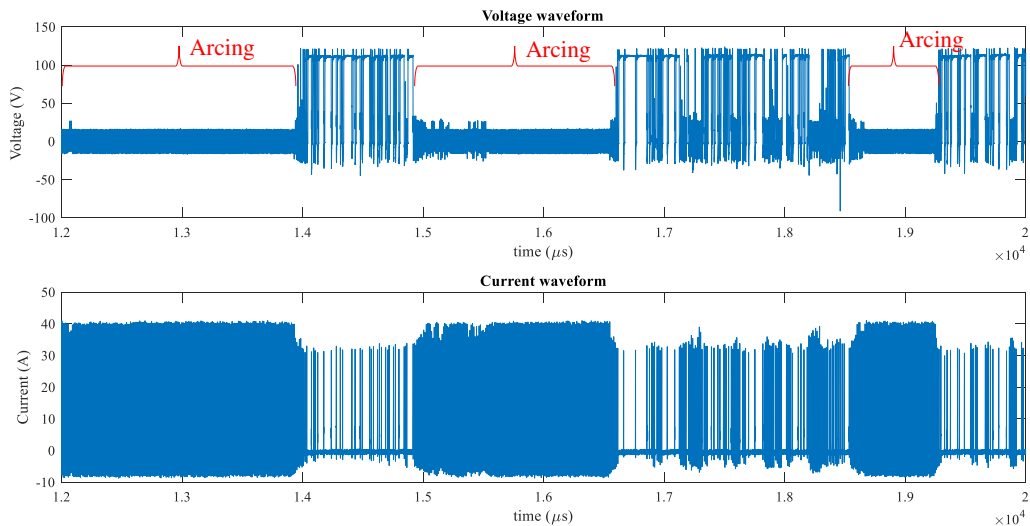


**Fig. 6.13** The pulse cycle behaviour before wire breakage

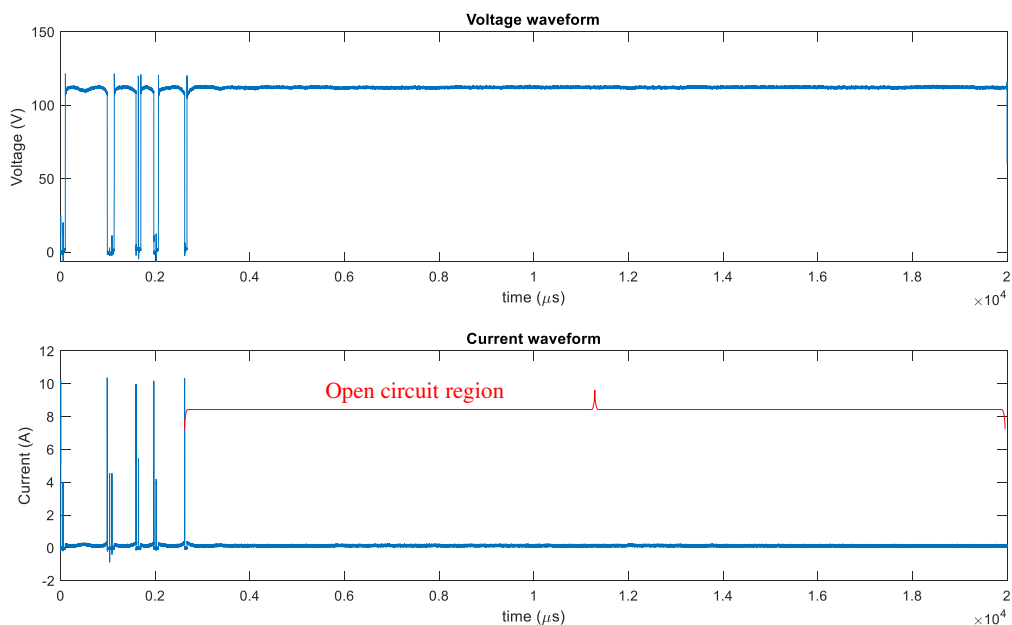


**Fig. 6.14** The pulse cycle behaviour before process interruption due to spark absence

The pulse cycle leading to spark absence, in contrary to earlier case, has very little number of discharge pulses. The pulse cycle is dominated by open circuit pulses with long ignition delay time, which affects the productivity and process efficiency. Sparks dies out with negligible discharge frequency as shown in Fig. 6.14.

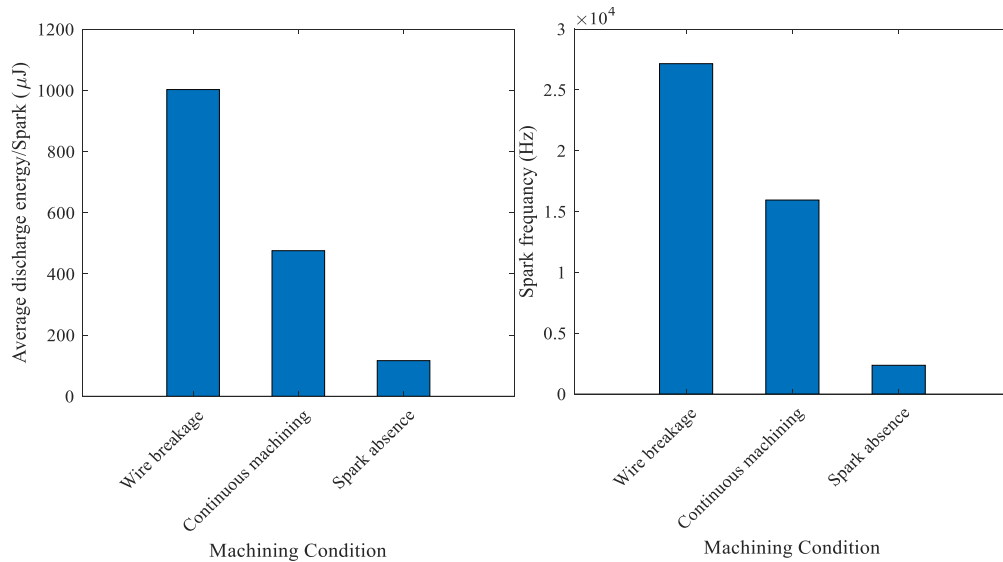


**Fig. 6.15** (a) Discharge energy at various machining conditions  
(b) Spark frequency at various machining conditions

From the analysis of pulse cycles, the discharge features – spark frequency, discharge energy, and abnormal pulse proportions, are observed to exhibit distinguishable characteristics ahead of process failures. The average discharge energy and spark frequency comparison during failure and ideal cases are shown in Fig. 6.15. Discharge energy per spark and spark frequency is maximum for wire breakage case, intermediate for normal machining, and least for spark absence. Based on these conclusions, a failure prediction algorithm is developed, the details of which are discussed in Section 6.10.

## 6.9 PREDICTIVE MODELLING OF PERFORMANCE CHARACTERISTICS

A neural network model is trained to predict cutting speed and surface roughness during wire EDM of Inconel 718. A feed forward back propagation algorithm is selected for the current predictive model. The input dataset consists of five input parameters (pulse on time, pulse off time, servo voltage, wire feed and input current), and two extracted discharge features (discharge energy, and spark frequency). The optimal ANN structure is found to be 7-10-2, based on maximum model accuracy. The ANN structure is showed in Fig. 6.16. During the training phase, the weights and biases of ANN structure are tuned to minimize the loss function. The trained model is having high accuracy with a correlation coefficient (R value) of 0.98. The regression plot of the trained model is given in Fig. 6.17. In order to test the model performance in actual machining conditions, 14 confirmation experiments are conducted. The model predictions are observed to be in close agreement to experimental values. Additional details on the confirmation tests are given in the next section.

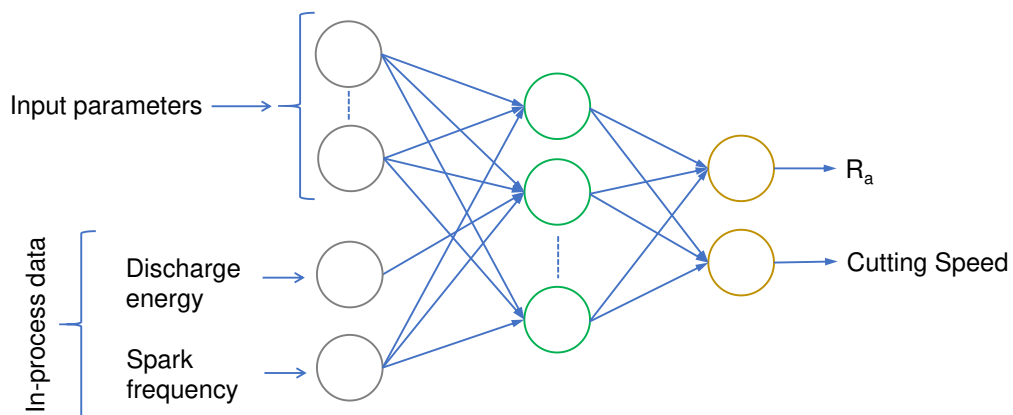


**Fig. 6.16** ANN structure

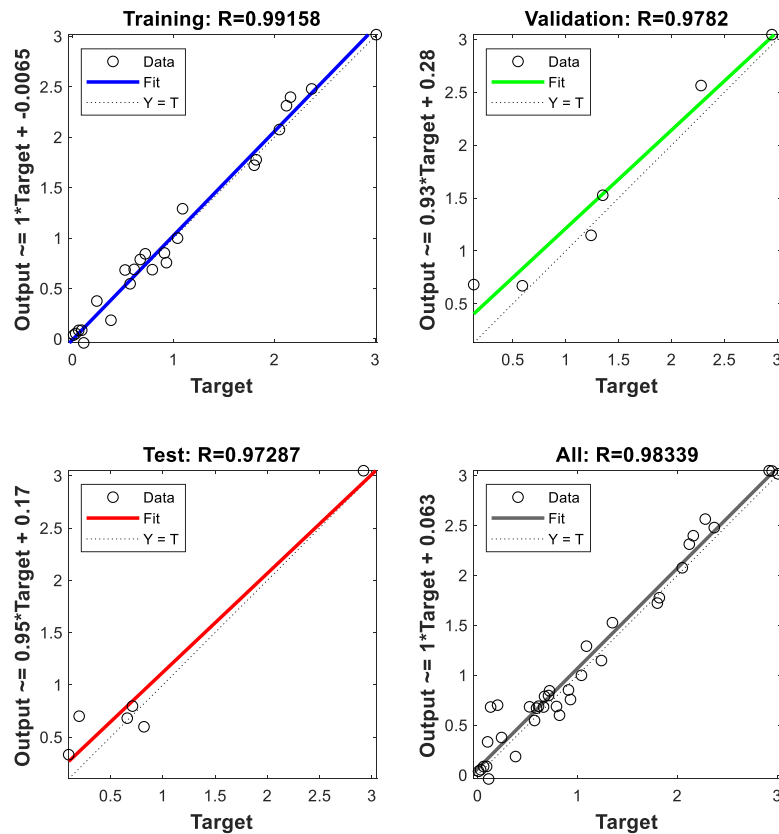


**Fig. 6.17** Regression plot for the trained ANN model

## 6.10 INTELLIGENT MACHINE FAILURE CONDITION PREDICTION SYSTEM

A heuristic rule-based failure detection algorithm is presented in this section. Based on the pulse train analysis, it is revealed that abnormal pulse proportions, discharge energy, and pulse frequency are the relevant health indicators for wire EDM process. The algorithm is based on multiple rules to categorise the machining condition into wire breakage, spark absence, or normal continuous machining. A high proportion of spark and arc pulses is an indicator of machining instability leading to wire breakage.

The threshold values are decided heuristically after performing a number of experiments that resulted in machining failures. Among all cases of wire breakages, the minimum values of undesirable spark ratios, discharge energy and spark frequency are denoted as  $(ASR+SSR)_{wb,min}$ ,  $(DE)_{wb,min}$ , and  $(SF)_{wb,min}$ . The

threshold limits for discharge characteristics are based on these minimum values above which a wire breakage failure is expected. Several failure case experiments are conducted and the discharge characteristics leading to wire break failures are extracted in order to fine tune these threshold values. Also since crossing the threshold of either one or two parameters does not necessarily result in wire breakage, AND condition is set for the rule based prediction. Thus the event is predicted as wire breakage only when all the three cases are satisfied. Therefore, higher proportion of abnormal pulses, coupled with high spark frequency and discharge energy is considered in this algorithm as a necessary condition to accurately predict wire breakage. Similarly, high proportion of open circuit discharges, coupled with low discharge energy and low sparking frequency is observed to result in spark absence. In such situations, the open circuit voltage applied across the electrodes are not sufficient enough to break the dielectric barrier. In case neither of these conditions are predicted, the machining is categorised as normal continuous machining. Flowchart of the proposed failure detection algorithm is given in Fig. 6.18.

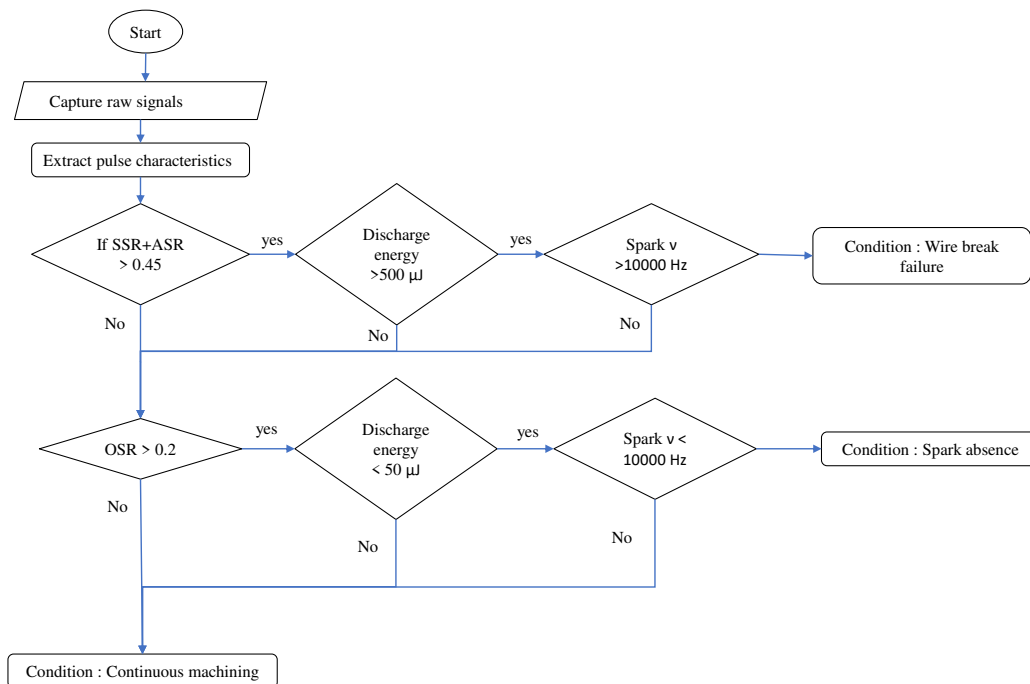


**Fig. 6.18** Flowchart for intelligent machine condition prediction system

Additional confirmation tests are conducted to test the models' performance in actual machining situations. The parameter combinations and extracted features are given in Table 6.3. Based on these features, process responses and failure mode are predicted by ANN prediction model and failure prediction algorithm respectively. The details of model predictions and comparison with experimental readings are given in Table 6.4. Both the ANN model and proposed algorithm is observed to be accurate in their predictions.

**Table 6.3** Results of confirmation experiments

S. No.	I <sub>p</sub> (A)	T <sub>on</sub> (μs)	T <sub>off</sub> (μs)	SV (V)	WF (m/min)	Spark v (Hz)	DE/spark (μJ)	NSR	OSR	ASR	SSR
1	40	114	40	31	7	3450	1732.99	0.58	0.04	0.13	0.25
2	40	107	30	35	4	39050	667.74	0.34	0.05	0.32	0.29
3	10	106	46	50	3	950	29.55	0.21	0.67	0.02	0.09
4	40	112	33	40	3	25550	848.58	0.56	0.05	0.17	0.22
5	10	105	47	49	3	850	33.38	0.13	0.70	0.09	0.08
6	10	110	40	48	3	950	10.56	0.16	0.66	0.03	0.15
7	40	113	32	30	4	1495	935.02	0.49	0.01	0.14	0.36
8	40	115	30	30	5	3150	1002.09	0.44	0.03	0.26	0.27
9	40	108	31	32	5	30150	778.22	0.53	0.16	0.07	0.24
10	10	108	38	50	4	450	15.32	0.24	0.54	0.09	0.12
11	10	106	43	48	7	800	50.08	0.21	0.58	0.03	0.18
12	40	109	38	31	6	26150	1227.46	0.45	0.04	0.17	0.34
13	40	115	35	35	3	13350	501.21	0.31	0.16	0.28	0.25
14	10	105	40	35	3	40150	29.11	0.37	0.23	0.20	0.20

### 6.11 EFFECT OF ABNORMAL PULSES ON MICROSTRUCTURE

The effect of discharge characteristics on surface integrity is discussed in this section. SEM images of machined surfaces with 36 % short circuit sparks (Exp. No. 7) and 20 % sort circuit sparks (Exp. No. 14) are considered for comparison. The 16 % reduction in short circuit sparks have resulted in surface morphology improvement as seen in Fig. 6.19. Higher short circuit sparks have led to numerous undesirable surface features like micro globules, micro pits, and porosity. These surface features can reduce the load bearing capacity of machined components especially at high temperatures. Reduction in abnormal spark ratio has led to significant smoothing of machined surface with no visible micro

features. Higher short circuit sparks have also led to significantly higher wire wear as evident from Fig. 6.20. At higher proportion of short circuit sparks, zinc coating is severely damaged or removed with a number of debris impinged to the wire surface. Zinc coating removal can expose the unprotected inner brass core to thermal shocks leaving the wire electrode susceptible to breakage. If the proportion of short sparks are increased further, wire breakages are observed. The machining condition is more stable in the second case with only marginal visible wire wear.

**Table 6.4** Performance comparison of predictive models

S. No.	Exp. CS (mm/min)	Exp. Ra (μm)	ANN CS (mm/min)	ANN Ra (μm)	CS % dev	Ra % dev	Failure condition – Exp.	Failure condition - Model
1	1.28	3.21	1.35	3.38	0.06	0.05	NM	NM
2	1.41	2.42	1.35	2.51	0.04	0.04	WB	WB
3	0.01	0.68	0.01	0.58	0.10	0.14	SA	SA
4	1.72	2.36	1.82	2.41	0.06	0.02	NM	NM
5	0.08	0.77	0.10	0.62	0.29	0.20	SA	SA
6	0.21	0.71	0.20	0.69	0.07	0.03	SA	SA
7	1.87	2.59	2.02	2.51	0.08	0.03	WB	WB
8	2.01	2.65	1.92	2.71	0.05	0.02	NM	NM
9	1.35	2.29	1.39	2.49	0.03	0.09	NM	NM
10	0.06	0.75	0.05	0.69	0.14	0.08	SA	SA
11	0.21	0.61	0.21	0.50	0.02	0.17	SA	SA
12	1.59	2.47	1.62	2.39	0.02	0.03	WB	WB
13	1.48	1.99	1.52	2.17	0.03	0.09	WB	WB
14	0.32	0.81	0.33	0.78	0.05	0.04	NM	NM

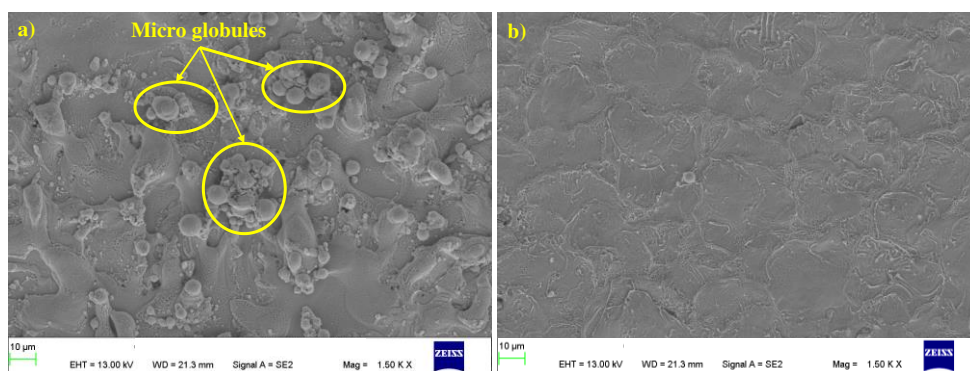


**Fig. 6.19** Microstructural comparison of machined surfaces when short spark ratio is reduced by 16 %

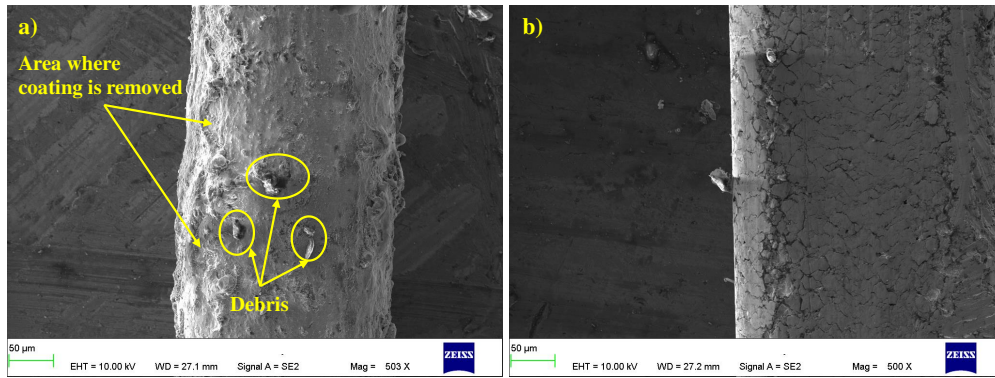


**Fig. 6.20** Microstructural comparison of worn wire surfaces when short spark ratio is reduced by 16 %

## 6.12SUMMARY

The chapter dealt with the setting up of a condition monitoring system for wire EDM process. A pulse classification system, based on ignition delay time is developed. Various discharge characteristics are extracted from the filtered voltage and current signals. The effect of discharge characteristics on process failures like wire breakage and spark absence are investigated. The study also analysed the variations in pulse cycle leading to failures. A neural network prediction model is developed to predict the process responses accurately based on input parameters and discharge characteristics. Finally, a failure detection algorithm is developed to forecast the events of machining failures based on abnormal pulse proportions, discharge energy, and spark frequency. The effect of short circuit sparks on surface integrity and wire wear are studied by comparing SEM images.

## CHAPTER 7

### FAILURE DETECTION AND PROCESS CONTROL

#### 7.1 INTRODUCTION

The chapter deals with the development of failure detection and process control algorithm based on pulse train analysis. Initially, a heuristic rule-based failure detection and process control method is proposed. The process failure and severity are predicted based on extracted signal features like pulse proportions, pulse frequency and discharge energy. Then based on the severity of instability, the control algorithm recommends retuning of parameter settings to regain the process stability. Further, instead of heuristic method, a neural network classifier-based failure prediction model is proposed. In this model, severity is assessed based on remaining useful life (RUL) prediction. Through process control, machining interruptions through wire breakage and spark absence is avoided, and surface integrity of machined components are improved.

#### 7.2 EXPERIMENTAL DETAILS

Inconel 718 plate of thickness 10 mm is chosen as the work material. Wire electrode is hard zinc coated brass wire of 0.25 mm diameter. Deionized water of conductivity 20  $\mu\text{S}/\text{cm}$  is selected as dielectric fluid. Profile machined is a straight cut of 50 mm length. The process parameters varied to develop the algorithm and train the machine learning models are given in Table 7.1. The parameter ranges and levels are selected based on pilot experiments, wire EDM manual, and literature survey. Input current and wire feed rate is selected at two levels due to machine specification restrictions and lesser impact on process failure respectively. A few parameter combinations are purposely selected to cause machining failure to analyse its cause and effect. A few other parameters given in Table 7.2 are kept constant due to machine limitations and relatively lower effect on the process failures. The condition monitoring system consisting of

Tektronix made current probe (TCP 303), amplifier (TCP A300), differential probe (P 5200A) and acquisition system (MDO 34 200) is set up as shown in Fig. 7.1. Pulse classification, feature extraction and modelling are performed using Matlab 2019a software. Filtering of raw waveform is performed by SignalAnalyzer toolbox. Neural network toolbox is used to develop classification and prediction models.

**Table 7.1** Process parameters and levels

Process parameters	Symbol	Level 1	Level 2	Level 3
Pulse on Time ( $\mu\text{s}$ )	$T_{\text{ON}}$	115	110	105
Pulse off Time ( $\mu\text{s}$ )	$T_{\text{OFF}}$	50	40	30
Servo voltage (V)	SV	50	40	30
Wire feed rate (m/min)	WF	9	3	
Input Current (A)	$I_{\text{P}}$	40	10	

**Table 7.2** Parameters maintained constant

Parameter	Value
Wire electrode diameter	250 $\mu\text{m}$
Open circuit voltage	12 V
Dielectric fluid pressure	$1.9 \times 10^5$ N
Axial wire tension	10 N

### 7.3 SIGNAL PROCESSING AND PULSE CLASSIFICATION

Low pass filter is applied to the raw signals to avoid the high frequency noisy data. The health indicators are extracted from the filtered data. Based on the results from the previous chapter, features extracted from the pulse data are abnormal pulse proportion, discharge energy, and discharge frequency. A pulse classification algorithm, the details of which are discussed in the previous chapter, categorises the pulses into normal spark pulse, arc sparks, open circuit sparks, and short circuit sparks. Pulse classification is performed based on ignition delay time. Normal pulses are the ideal pulses where a discharge happens following an ignition delay time for ionization and dielectric breakage. Discharge pulses associated with zero ignition delay time are regarded as spark discharges

and the ones with negligible ignition delay time are called arc pulses. Both of these are considered as abnormal pulses since they lead to wire breakage failure and surface damages. The open circuit pulses are associated with a long ignition delay time, or absence of discharge pulses. Such pulses affect the productivity and efficiency of machining process. Pulse proportions are computed as the ratio of number of individual pulses to the total number of pulses.

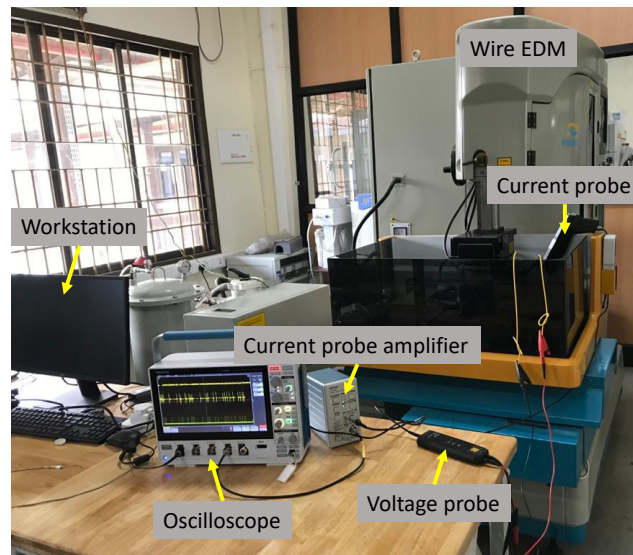


**Fig. 7.1** Wire EDM condition monitoring setup

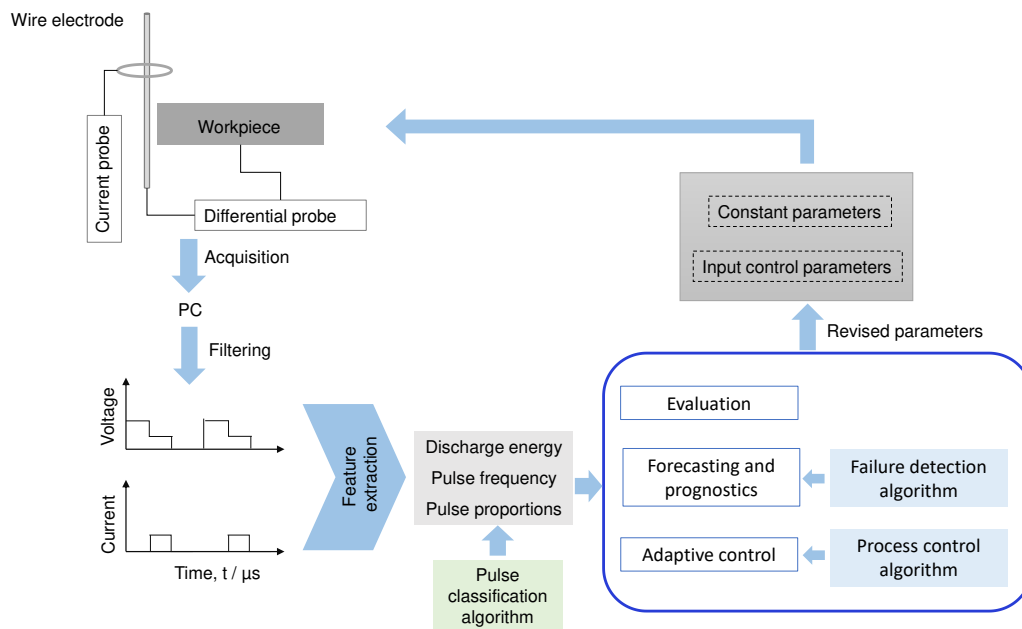


**Fig. 7.2** Process control strategy

The proposed algorithms detect the potential failure situations based on the extracted discharge features and pulse proportions. Also, a failure severity assessment is performed, based on which the control algorithm revises the process parameters by adjusting pulse off time, servo voltage and pulse on time. The overall process control strategy is given in Fig. 7.2.

#### **7.4 RULE BASED MODEL FOR FAILURE DETECTION**

Two types of machining failures are considered in this study, wire breakage and spark absence. To identify the potential failures during the process, detailed pulse train analysis is performed. The pulse train analysis revealed different types of discharge pulses as shown in Fig. 7.3. The variations in wire EDM pulse cycles leading to wire breakage and spark absence are also studied. A wire breakage event is preceded by a series of short circuit sparks, which increases the average discharge energy of sparks and spark frequency of pulse cycle. A typical pulse cycle leading to wire breakage is given in Fig. 7.4. Debris accumulation and spark gap bridging are regarded as the main reasons for wire breakage. Spark absence, on the other hand, is indicated by long open circuit regions. The situation is less critical than wire breakage since it does not cause breakages or surface damages. But spark absence severely effects process efficiency and productivity due to process interruptions and shall be avoided. Extremely low discharge frequency, and low discharge energy per sparks are the characteristics before spark absence. The pulse cycle leading to spark absence is given in Fig. 7.5.

The steps involved in rule-based failure detection and process control system is given below

- **Step 1 – Failure prediction:** The failure prediction is based on abnormal spark ratio and spark frequency, based on the discharge characteristics observed before machining failures. The pulse cycle leading to wire breakage is observed to be dominated by short circuit and arc sparks. Also, the spark frequencies in such cases are high due to ignition delay free discharges. Thus, if the ratio of arc and short pulses combined are high, with pulse cycle

exhibiting high pulse frequency, then wire breakage is predicted. On the other hand, spark absence is indicated by a higher than normal ( $< 20\%$ ) open circuit voltages, combined with very low spark frequency and spark discharge energy. Table 7.3 and Table 7.4 shows a few conditions of wire breakage and spark absence respectively.

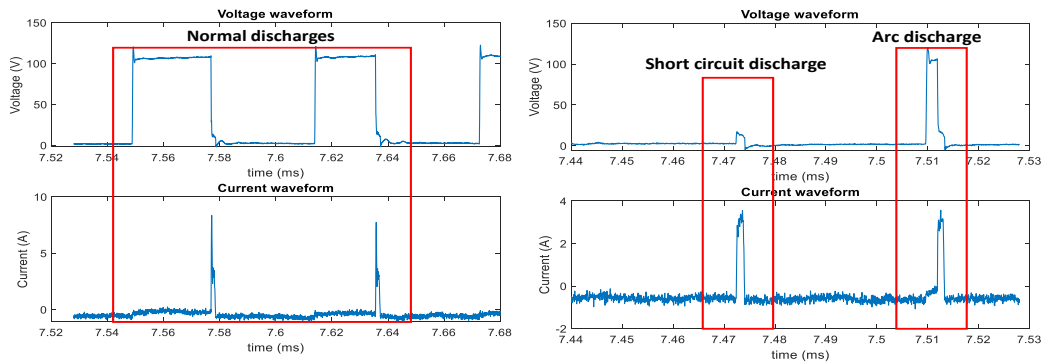


**Fig. 7.3** Types of discharge pulses observed from the pulse chain

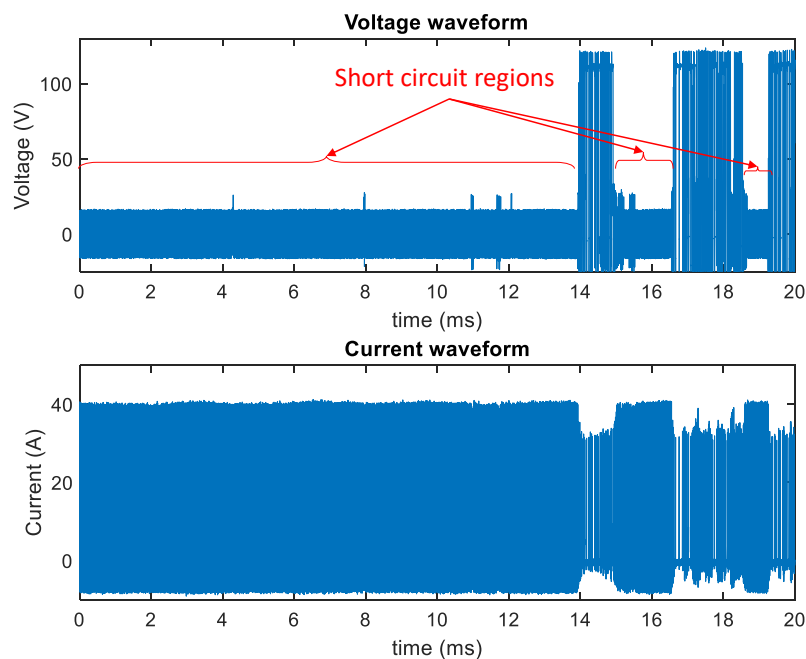


**Fig. 7.4** The pulse cycle behaviour leading to wire breakage failure

- **Step 2 – Assessment of failure severity:** The severity of predicted wire breakage failure is judged based on the discharge energy per spark. The parameter is selected since discharge energy of individual sparks is directly related to the extent of wire wear. A higher intensity spark is expected to cause a deeper crater on the wire surface, thus causing faster wire degradation,

eventually leading to wire rupture. The algorithm categorises the discharge energies into three, for potential wire break machining conditions, based on which the wire break severity is classified as high, medium, and low critical cases.

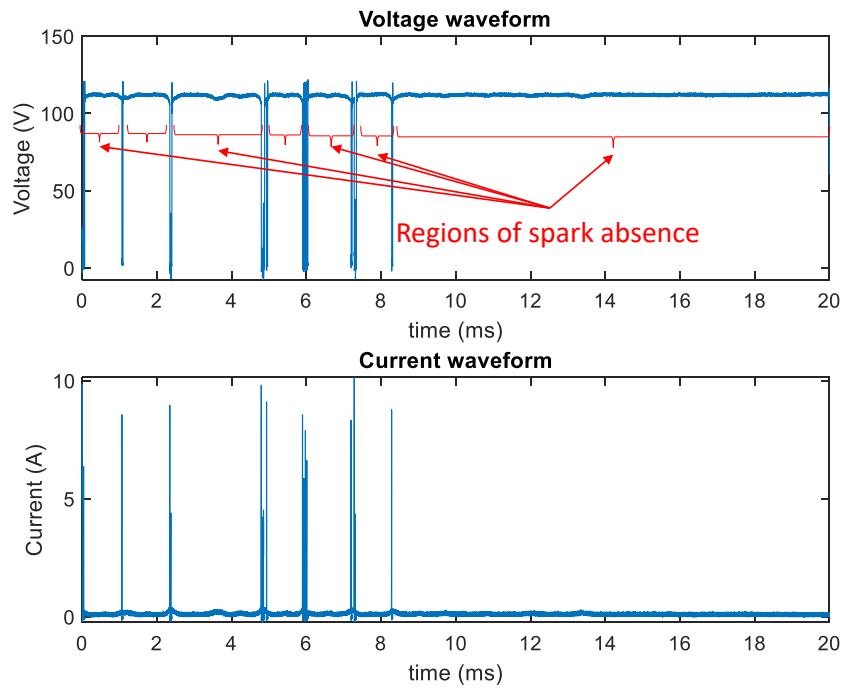


**Fig. 7.5** The pulse cycle behaviour leading to spark absence failure

- **Step 3 – Process control:** From the mechanism of material removal and process failures, a process control methodology is devised. Since the root cause of wire breakage is debris accumulation and spark gap bridging, measures are taken to improve the flushability of accumulated debris. For this, pulse off time and servo voltage was increased based on severity. To regulate the high severity condition, discharge energy is also controlled by reducing pulse on time, in addition to the other parameters. To avoid spark absence, the algorithm adjusts discharge energy and spark gap.

Threshold values of all the rules are fixed based on the experimental observations. The overall failure prediction and process control methodology is given as a flowchart in Fig. 7.6.

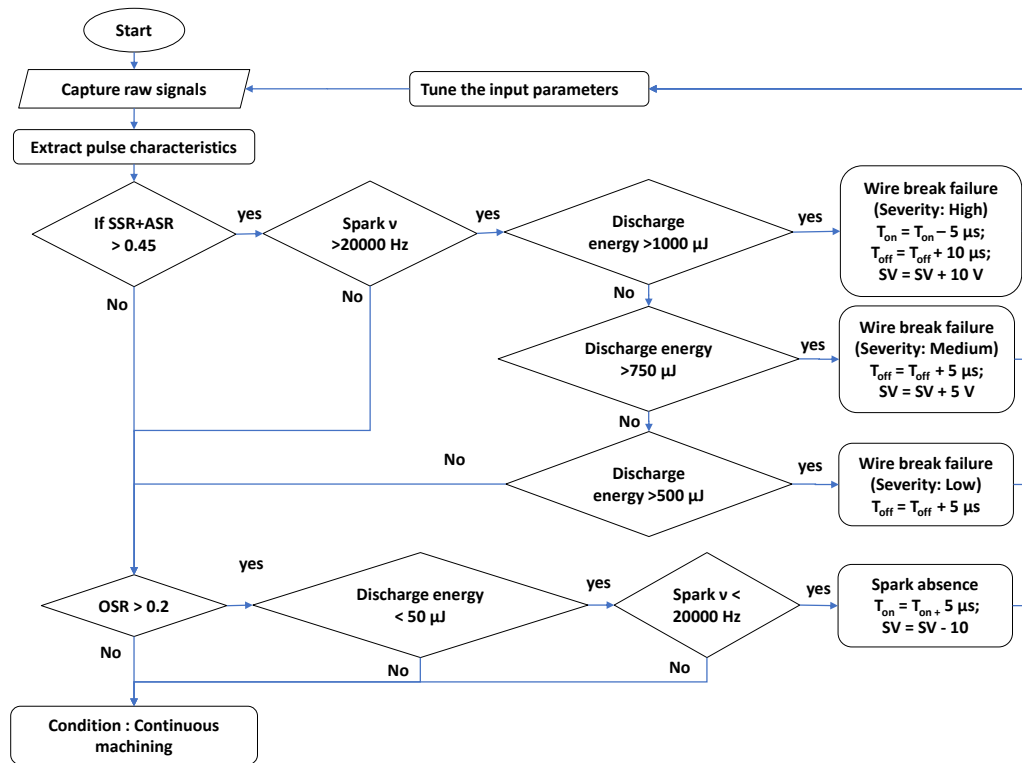


**Fig. 7.6** Flowchart of failure detection and control method

**Table 7.3** Extracted discharge characteristics leading to wire break failure

S. No	Input parameters				1	Extracted signal features			Observed failure
	Pulse on time (μs)	Pulse off time (μs)	Servo voltage (V)	Input current (A)		SSR + ASR	Spark v (Hz)	Discharge energy (μJ)	
1	105	30	30	40	0.84	75000	613.68	Wire breakage	
2	110	30	30	40	0.43	26500	1044.30		
3	110	30	50	40	0.44	45000	1066.32		
4	110	40	50	40	0.53	29000	986.55		
5	110	50	50	40	0.54	20500	1002.03		
6	115	30	30	40	0.59	22500	1476.84		
7	115	40	30	40	0.75	25500	1484.71		

ASR- Arc spark ratio, SSR- Short spark ratio

**Table 7.4** Extracted discharge characteristics leading to spark absence failure

S. No	Input parameters				1	Extracted signal features			Observed failure
	Pulse on time ( $\mu\text{s}$ )	Pulse off time ( $\mu\text{s}$ )	Servo voltage (V)	Input current (A)		Open spark ratio	Spark v (Hz)	Discharge energy ( $\mu\text{J}$ )	
1	105	40	50	10	0.58	12000	47.62	Spark absence	
2	105	50	30	10	0.31	13500	32.06		
3	105	50	50	10	0.44	19500	42.60		
4	110	50	50	10	0.45	14500	42.55		
5	115	50	50	10	0.48	15500	65.58		

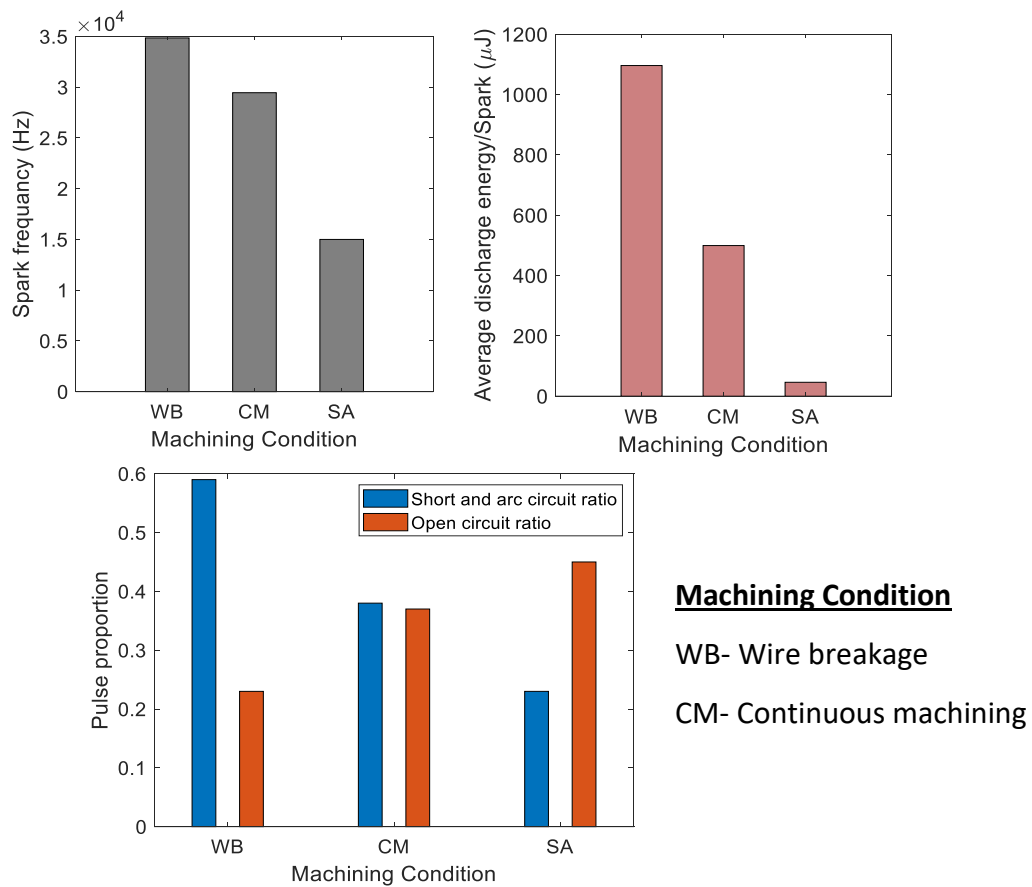


**Fig. 7.7** Average values of pulse characteristics at different machining conditions

The comparison of discharge characteristics extracted from pulse cycles before various machining outcomes are given in Fig. 7.7. Discharge energy of discharge sparks are observed to be higher than ideal before wire breakages. This is due to the higher intensity short circuit sparks which dominate the pulse cycle during unstable machining conditions leading to wire breakage. On the contrary, average

discharge energy is observed to be lower than ideal before spark absence failure. Spark frequency was also found to increase before wire breakage due to spark gap bridging. The pulse cycle leading to spark absence, however, is observed to have lesser than ideal spark frequency. Regarding abnormal spark proportions, the short circuit and arc sparks are higher before wire breakage and lower before spark absence. Similarly, open circuit sparks are higher leading to spark absence and lower for wire breakage.

### ***Effects of process control***

To demonstrate the effects of process control, discharge characteristic comparison of six cases of machining failures are listed in Table 7.5. With the initial parameter settings, first four cases have led to wire breakage, and the last two resulted in spark absence. The failure situations are rightly predicted, based on the process control algorithm. Then the severity is assessed, based on which the parameter settings are retuned for each case to restore the machining stability. The recommended parameter settings by the process control algorithm are successful in overcoming the machining failures and it ensured a continuous uninterrupted machining.

For the cases where wire breakage is predicted, high discharge energy, spark frequency, and proportion of abnormal sparks are brought back to normal levels by the process control algorithm. The control algorithm reduces the debris production by bringing down the pulse on time. Also, it reduces the debris accumulation by increasing the pulse off time and inter electrode distance. The parameters and the degree of parameter revision are based on the severity assessment. By revising the parameters, the debris accumulation is avoided, the effectiveness of flushing is restored, and thus process stability is established. For the case of spark absence, process regulation involves increasing the pulse on time and reducing the spark gap. By doing so, time for ionization and dielectric breakage is increased. Simultaneously, by reducing the spark gap, dielectric barrier is reduced. Thus, the revised situation promotes a stable and continuous operation by avoiding open circuit sparks. A comparison of pulse waveform

before and after process control is given in Fig. 7.8 for the case of wire breakage. It can be seen that the long chain of short circuit sparks is replaced by continuous normal spark discharges. Similarly, Fig. 7.9 shows the controlled pulse cycle for spark absence case. Open circuit pulses are replaced by normal sparks.

**Table 7.5** Comparison of machining outcomes before and after process control

S. No	Condition	Input parameters				Extracted signal features				MO	R <sub>a</sub> (μm)
		T <sub>ON</sub> (μs)	T <sub>OFF</sub> (μs)	SV (V)	I <sub>P</sub> (A)	ASR + SSR	OSR	SF (Hz)	DE (μJ)		
1	Initial	113	30	35	40	0.97	0	84600	1569	WB	3.47
	Controlled	108	40	55	40	0.08	0.08	9650	433	CM	2.37
2	Initial	115	32	33	40	0.92	0.01	61200	1705	WB	3.31
	Controlled	110	42	43	40	0.10	0.24	7600	503	CM	2.43
3	Initial	110	33	31	40	0.79	0.01	21350	990	WB	3.12
	Controlled	110	38	36	40	0.18	0.18	7700	87	CM	2.29
4	Initial	112	30	30	40	0.83	0	62500	559	WB	3.37
	Controlled	112	35	30	40	0.23	0.21	7450	102	CM	1.96
5	Initial	105	50	48	10	0.17	0.5	300	59	SA	-
	Controlled	110	50	38	10	0.24	0.01	3215	24	CM	0.96
6	Initial	107	45	50	10	0.36	0.64	550	49	SA	-
	Controlled	112	45	40	10	0.26	0	3015	27	CM	0.83

WB – Wire breakage, CM- Continuous machining, ASR- Arc spark ratio, SSR- Short spark ratio, OSR- Open spark ratio, SF – Spark frequency, DE – Discharge energy, MO – Machining outcome

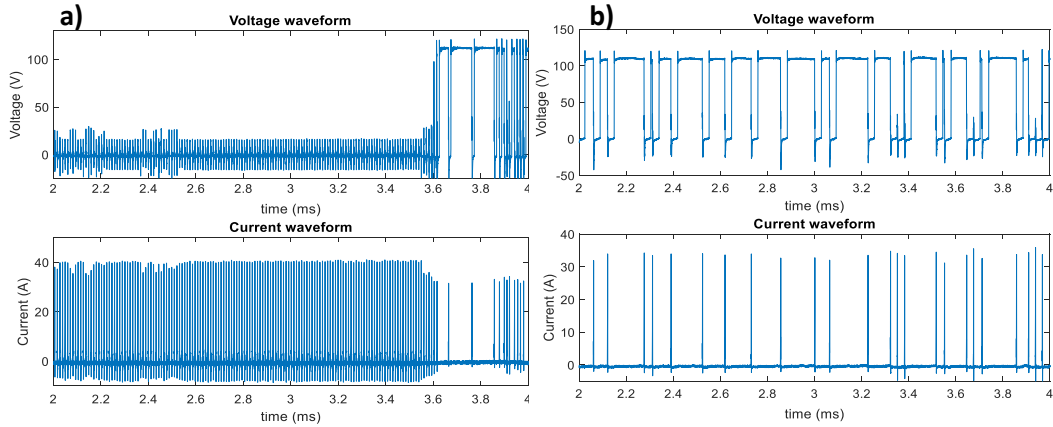


**Fig. 7.8** Discharge pulse waveform (a) leading to wire breakage (b) after parameter tuning based on the control algorithm

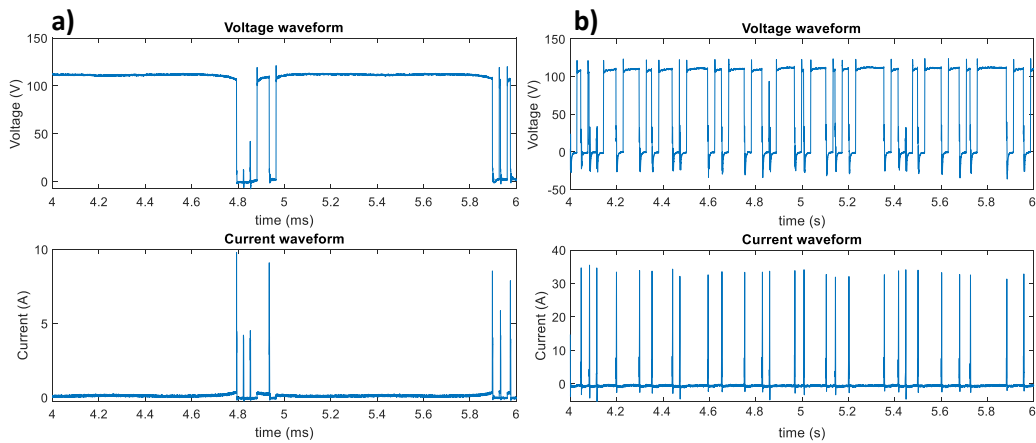


**Fig. 7.9** Discharge pulse waveform (a) leading to spark absence (b) after parameter tuning based on the control algorithm

Restoration of machining stability by the proposed algorithm, is also analysed from wire wear point of view. Fig. 7.10 shows the comparison of wire wear by analysing the SEM images of worn wires before and after process control. Severely worn wire surface is observed when machined with original parameter settings corresponding to Exp. No. 1 of Table 7.5. The zinc coating is completely degraded in patches, with several debris particles impinged on the wire surface as seen in Fig. 7.10 (a). This indicates debris stagnation and a short circuit dominated pulse train. If the machining conditions are not regulated, the wire degradation will worsen further, leading to wire rupture. Wire tip image of

ruptured wire electrode is shown in Fig. 7.10 (b). Debris impingement is still visible in this case. Wire electrode surface obtained after revising the process parameters is showed in Fig. 7.10 (c). A substantial reduction in wire wear is observed compared to the original settings. The wire electrode is only marginally eroded with zinc coating still intact. The coating protects the wire from thermal shocks by ‘heat sink effect’ thus preventing sudden rupture. Thus, the machining stability is found to be restored by the proposed algorithm, thus preventing the wire break failure.

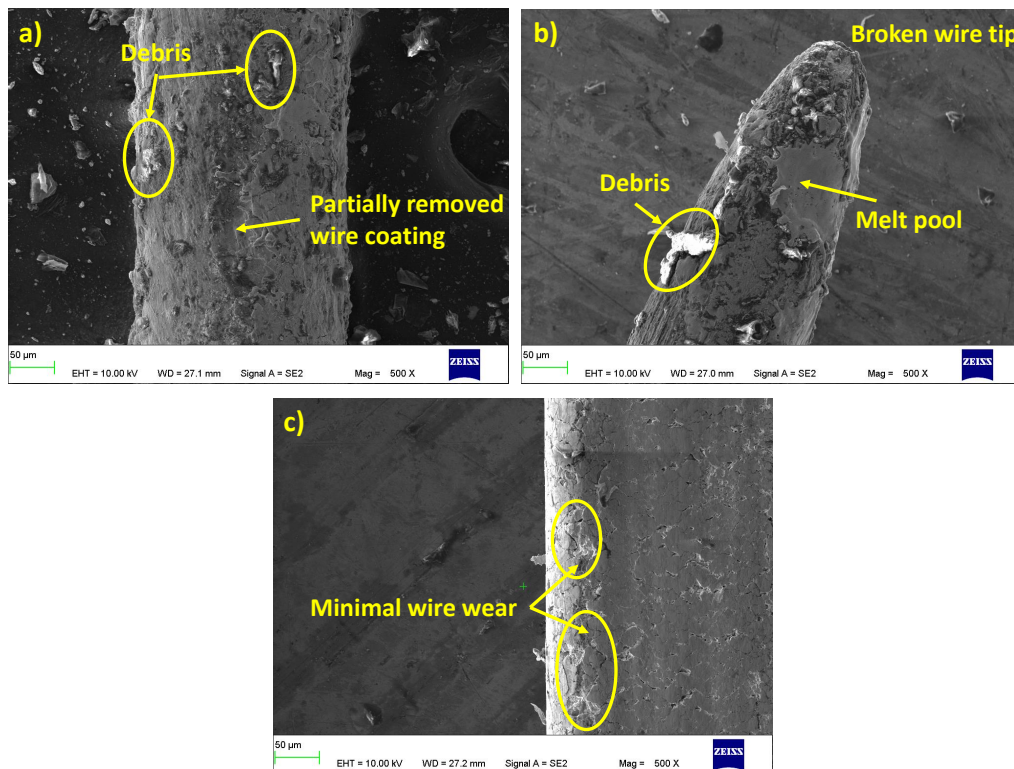


**Fig. 7.10** (a) Worn wire surface leading to wire breakage (b) broken wire tip  
(b) worn wire after process control

Apart from ensuring a continuous machining, the control algorithm is also observed to improve the surface morphology and surface finish of the machined surfaces. Firstly, SEM images of the machined surfaces are compared to perform microstructural analysis as shown in Fig. 7.11. The machined surface under unstable conditions corresponding to original parameter settings of Exp. No. 1 is compared against the controlled settings in this regard. Machined surface under

original settings is observed to have numerous micro features like micro globules, voids and porosity (Fig. 7.11 (a)). Such surfaces are unrecommended for several applications, especially in aerospace components due to its susceptibility to fatigue failure. The improved process conditions resulted in a smoother surface with no visible micro features (Fig. 7.11 (b)).

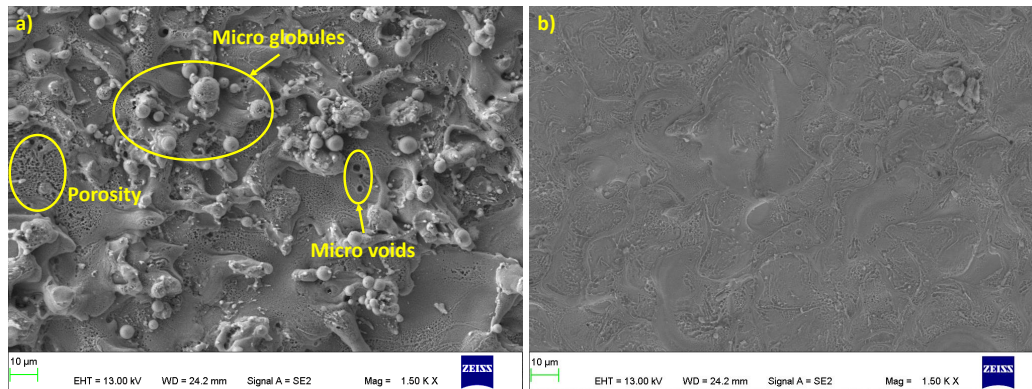


**Fig. 7.11** SEM image of machined surface (a) under original settings (b) after process control

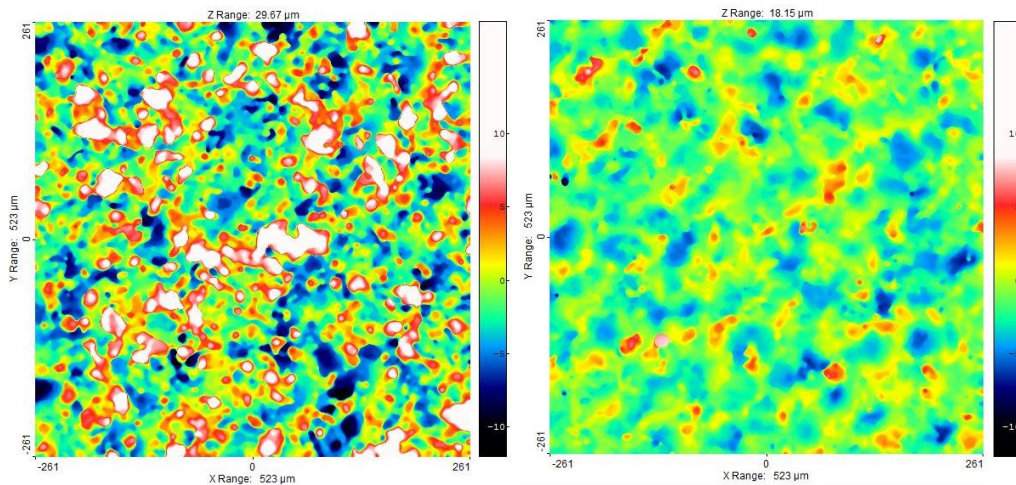


**Fig. 7.12** Non-contact 3D profilometer image of machined surface (a) under original settings (b) after process control

Secondly, non-contact 3D profilometer images are compared to understand morphological improvements. A coarse surface is observed with high peaks and deep valleys under original settings (Fig. 7.12 (a)). This is due to larger craters

and surface damages caused by short circuit sparks. However, after process control, the machined surface is much smoother with shallow peaks and valleys (Fig. 7.12 (b)). Reduction of abnormal sparks and an improvement in flushing conditions resulted in better machined surface. A bar chart showing the effect of discharge energy on surface roughness, as given in Fig. 7.13, supports the idea that, reduction in surface roughness can be achieved by restoring the process stability.

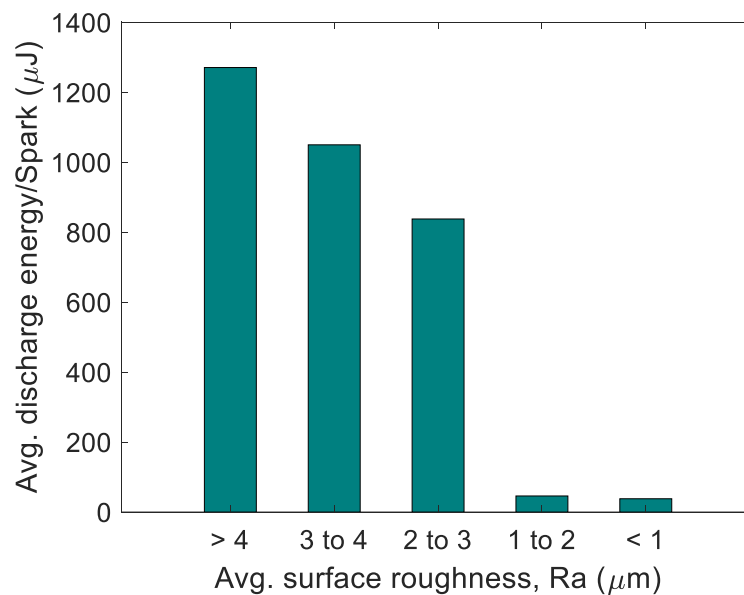


**Fig. 7.13** Effect of discharge energy on the surface roughness

## 7.5 MACHINE LEARNING APPROACH TOWARDS FAILURE PREDICTION AND PROCESS CONTROL

This section deals with the development of machine learning models for failure prediction and severity assessment during wire EDM process. Training dataset for the supervised machine learning models are from the 108 experiments conducted according to full factorial design. The input parameters and levels are given in Table 7.1. The proposed system works in three layers. Firstly, a neural network classifier predicts the mode of failure – wire breakage or spark absence. Secondly, for each failure cases, a second neural network model assesses the failure severity. A parameter called remaining useful life (RUL) is introduced as

an indicator of machining instability. Finally, process control is achieved through a thresholding approach.

### 7.5.1 Artificial neural network classification

Artificial neural network (ANN) is a supervised machine learning tool which tries to bio-mimic the human neurons to learn and process information. The technique is capable of accurately modelling complex real-world phenomena. In the present case, the model classifies the process conditions into three machining outcomes based on extracted discharge characteristics and abnormal pulse proportions. The multiple class labels are normal machining, spark absence and wire breakage. The inputs to the model are spark frequency, discharge energy, short spark ratio, and open spark ratio. ANN classifier parameters and details are given in Table 7.6. Also, different ANN structures are tested for performance and among them, 4-10-10-10-3 is chosen based on maximum accuracy. The ANN structure is given in Fig. 7.14.

**Table 7.6** Parameters of neural network multiclass classifier

<b>Parameter</b>	<b>Properties</b>
Number of inputs	4
Input layer neurons	Spark frequency, discharge energy, short circuit ratio, open circuit ratio
Number of classes	3
Output layer neurons	Probability of normal machining, wire breakage, and spark absence
Number of hidden layers	3
Number of neurons in each hidden layer	10
Cross validation	5-fold cross validation

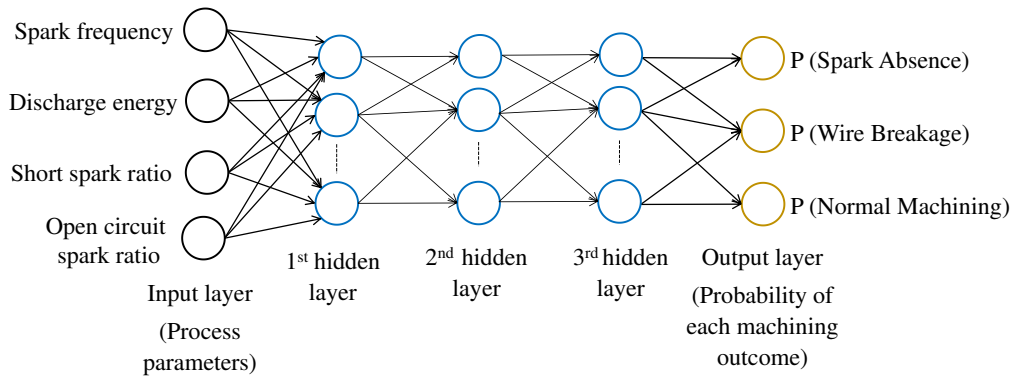


**Fig. 7.14** ANN classifier structure

1	79		
2	1	15	
3	1		12
	1	2	3
	Predicted Class		

**Fig. 7.15** Confusion matrix showing classifier performance

### 7.5.2 Performance of ANN classifier

Neural network classification is the first stage in this process control approach. The classifier is trained to predict whether the machining outcome is normal machining, wire breakage or spark absence. ANN classifier is trained by a dataset of size 108 x 4. Being a supervised model, true class labels for all training cases are also fed during the training phase. The neural network model adjusts its weights and biases to minimize the error between the model prediction and experimental results. Performance of ANN classifier is represented through a confusion matrix in Fig. 7.15. The model is observed to be 98.1 % accurate in

classifying the machining outcomes. A 5-fold cross validation is performed on the dataset.

In case the machining outcome predicted is wire breakage or spark absence, then the next stage is initiated, which is to assess the severity of the situation.

### 7.5.3 Assessment of failure severity

A parameter called remaining useful life (RUL) is used to assess the criticality of predicted failure. RUL is the machining time left before the predicted failure occurs. The representation of RUL parameter in a ‘machining condition vs. time’ graph is represented in Fig. 7.16. A lesser RUL value is considered more critical, since it indicates sudden failure. Such a situation demands an immediate intervention to restore the machining stability to overcome the potential failure. A higher value of RUL indicates initial stages of an instability, which can accumulate over the time and result in a failure. For every failure condition among the 108 experiments, RUL value is also noted. These details are used to train a neural network regression model to predict RUL value. The performance of ANN model is given in Fig. 7.17. A correlation coefficient of 0.988 is obtained for the developed model. Based on the type of failure and predicted values of RUL, a process control algorithm recommends parameter adjustments to restore the machining stability.

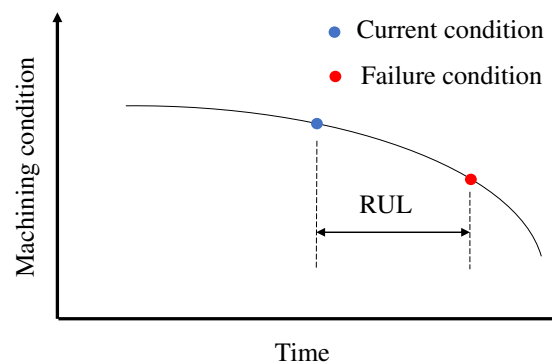


**Fig. 7.16** Remaining useful life (RUL) based on failure condition

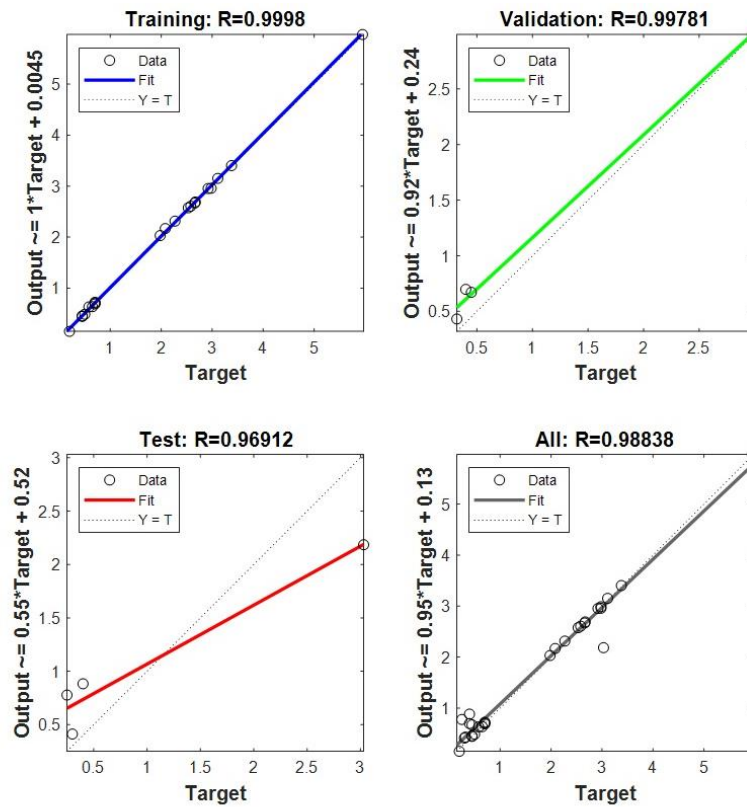
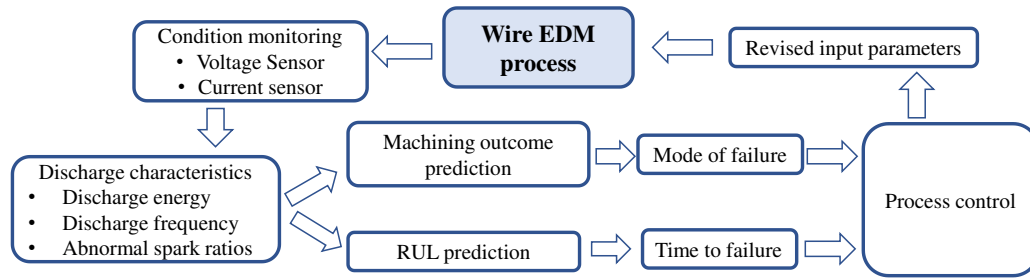


Fig. 7.17 ANN regression plot

#### 7.5.4 Process control algorithm

Process control algorithm determines the level of parameter corrections based on RUL predictions. Two types of wire breakage mechanisms are documented in the literature. Failure mode is Type I when the wire breaks immediately on application of voltage across the electrodes. The reason for Type I failure is reported to be the physical contact between the electrodes. Type II failure is gradual, where the unstable conditions build up over the time to reach a critical point where wire breaks. Spark gap bridging by debris accumulation and increased short circuit sparks are reported to be the reasons for type II failure. Such failures can be forecasted in advance by monitoring the discharge characteristic features. Also, the control algorithm can intervene to restore the instability build-up by re-tuning the process parameters. The proposed process control algorithm facilitates gap flushing which can overcome the debris accumulation. However, the retuning of parameters is not done equally for every

failure prediction. The proposed algorithm tunes the process parameters according to the predicted RUL values. Lower RUL value indicates severe instability and demands greater levels of parameter retuning. On the contrary, higher RUL value indicates initial stages of instability which requires only slight modifications to the parameter settings. Unlike in the previous case, here process control to prevent spark absence is also performed based on the predicted severity in different levels. Overall approach for process control is given in Fig. 7.18.



**Fig. 7.18** Approach for wire EDM process control

In the case of a wire breakage prediction, the algorithm adjusts pulse on time, pulse off time and servo voltage. The severity of predicted failure is categorised into three – high, medium and low, based on RUL value. For high severity, all the three parameters are adjusted. Pulse on time is lowered, whereas servo voltage and pulse off time is increased. For medium severity, pulse off time and servo voltage is increased, but pulse on time is unchanged. For low severity, only the pulse off time is adjusted. In case of spark absence prediction, the algorithm adjusts pulse on time and servo voltage. Here, the severity is categorised into two: High and low. At high severity (low RUL), pulse on time is increased and servo voltage is reduced. For low severity, only the servo voltage is increased. Fig. 7.19 shows the flowchart for proposed process control.

It has to be noted that the proposed process control algorithm gives a set of guidelines/procedure for wire EDM process control during the machining of Inconel 718. The results obtained so far are very promising and this can later evolve to be a generic process control procedure for all material combinations. As a future work, multiple workpiece materials can be considered to fine tune the control algorithm, to build its capability further.

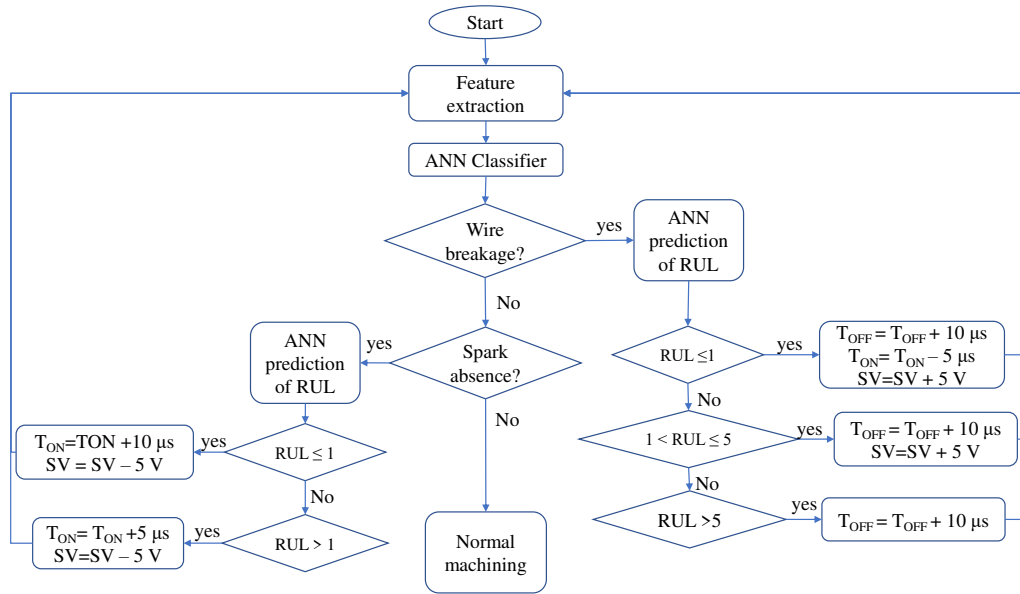


**Fig. 7.19** Flowchart of process control

### 7.5.5 Case studies

To evaluate the real-world performance of machine learning based process control system for wire EDM, 20 additional tests are conducted. The parameter combinations are selected randomly for these confirmation tests. The extracted discharge parameters, and abnormal spark ratio are also shown in Table 7.7. With these extracted features and abnormal spark ratios as input, the ANN classifier predicts the machining outcome. In case the predicted outcome is wire breakage or spark absence, a second ANN model predicts the RUL for the given machining conditions. The accuracy of predicted class and RUL for each of the confirmation tests are compared with actual experimental results in Table 7.7. It can be observed that the class prediction was accurate in every instance. The RUL prediction was also observed to be close to the experimental value. To demonstrate the effect of process control on pulse cycles, Exp No. 1 and Exp. No. 7 from confirmation tests are considered. The following section discusses these effects.

**Table 7.7** Machining outcome and RUL predictions during confirmation tests

S. No	Extracted features				Predicted		Observed	
	DE ( $\mu$ J)	SSR	OSR	SF (Hz)	EVENT	RUL (min)	EVENT	RUL (min)
1	1568.8	0.94	0.00	84600	WB	2.23	WB	3.2
2	221.4	0.33	0.00	22800	NM	-	NM	-
3	4030.2	0.54	0.26	1950	WB	10.18	WB	9.57
4	3168.9	0.41	0.28	4500	WB	1.47	WB	1.21
5	3252.9	0.15	0.19	7800	WB	0.00	WB	0.55
6	435.3	0.84	0.04	8050	NM	-	NM	-
7	58.58	0.17	0.50	300	SA	3.05	SA	2.91
8	3299.0	0.30	0.01	17000	WB	0.00	WB	0.3
9	207.7	0.03	0.24	7600	NM	-	NM	-
10	4007.0	0.43	0.40	1500	WB	8.16	WB	9.53
11	456.1	0.64	0.09	7450	NM	-	NM	-
12	227.0	0.79	0.00	68450	WB	2.26	WB	2.42
13	14.5	0.62	0.24	1050	SA	9.70	SA	8.29
14	2527.7	0.83	0.05	7500	WB	10.83	WB	11.51
15	459.8	0.62	0.18	6800	NM	-	NM	-
16	14.8	0.54	0.19	6200	SA	6.32	SA	7.86
17	479.6	0.66	0.07	11150	NM	-	NM	-
18	2611.9	0.94	0.03	8350	WB	10.98	WB	12.37
19	15.4	0.58	0.28	1800	SA	9.43	SA	8.57
20	16.1	0.75	0.00	200	SA	12.87	SA	12.24

DE- Discharge Energy/spark, SSR- Short Circuit Ratio, OSR- Open Circuit Ratio, SF- Spark Frequency, NM- Normal Machining, WB- Wire Breakage, SA- Spark Absence, RUL- Remaining Useful Life

### ***Case I: Process control to prevent wire breakage***

Exp. No. 1 from Table 7.7, ( $T_{ON} = 113 \mu s$ ,  $T_{OFF} = 30 \mu s$ ,  $SV = 35 V$ ,  $I_p = 40 A$ ,  $WF = 3 m/min$ ) is considered to represent the wire break case. The extracted discharge characteristics showed very high pulse frequency and discharge energy per spark. Experimentally, the said settings resulted in wire breakage when left unattended. To prevent this situation, the proposed process control algorithm is applied.

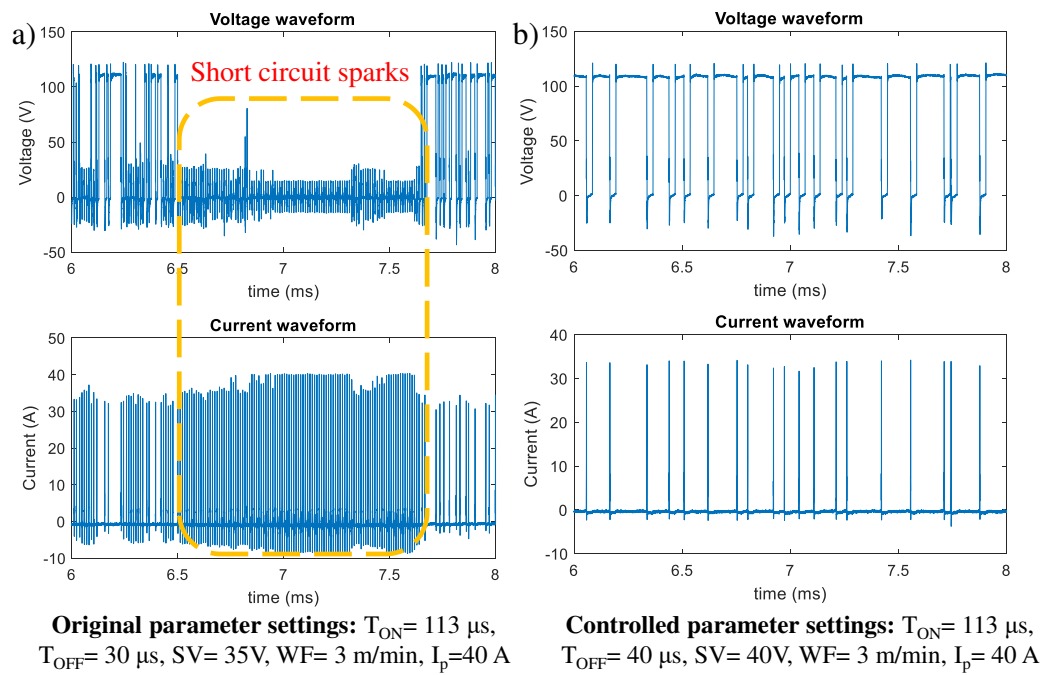


**Fig. 7.20** (a) Original settings (Conf test: Exp. No. 1) (b) Controlled settings

Initially, the classifier model rightly classified the wire breakage possibility. Then, the discharge parameters are sent to the second neural network model, which predicted the RUL value. The RUL was verified to be identical to the actual time for failure. The RUL is categorised as medium severity by the process control algorithm. Based on this assessment, a parameter revision is recommended (Pulse off time  $+10\ \mu\text{s}$ ,  $SV+5\ \text{V}$ ). When machined with the controlled settings ( $T_{ON} = 113\ \mu\text{s}$ ,  $T_{OFF} = 40\ \mu\text{s}$ ,  $SV = 40\ \text{V}$ ,  $I_p = 40\ \text{A}$ ,  $WF = 3\ \text{m/min}$ ) a continuous machining is observed. Through process control, a substantial reduction in discharge energy and spark frequency is observed. To further evaluate the process stability improvement, pulse cycle is compared with the original pulse cycle as given in Fig. 7.20. The controlled settings are able to reduce the series of short circuits which are observed in original settings. The improvement in process stability is evident, since a short circuit dominant pulse cycle is changed to a normal spark dominant pulse cycle after the machining condition regulation. This is due to an improvement in spark gap condition by overcoming debris accumulation through better flushing conditions.

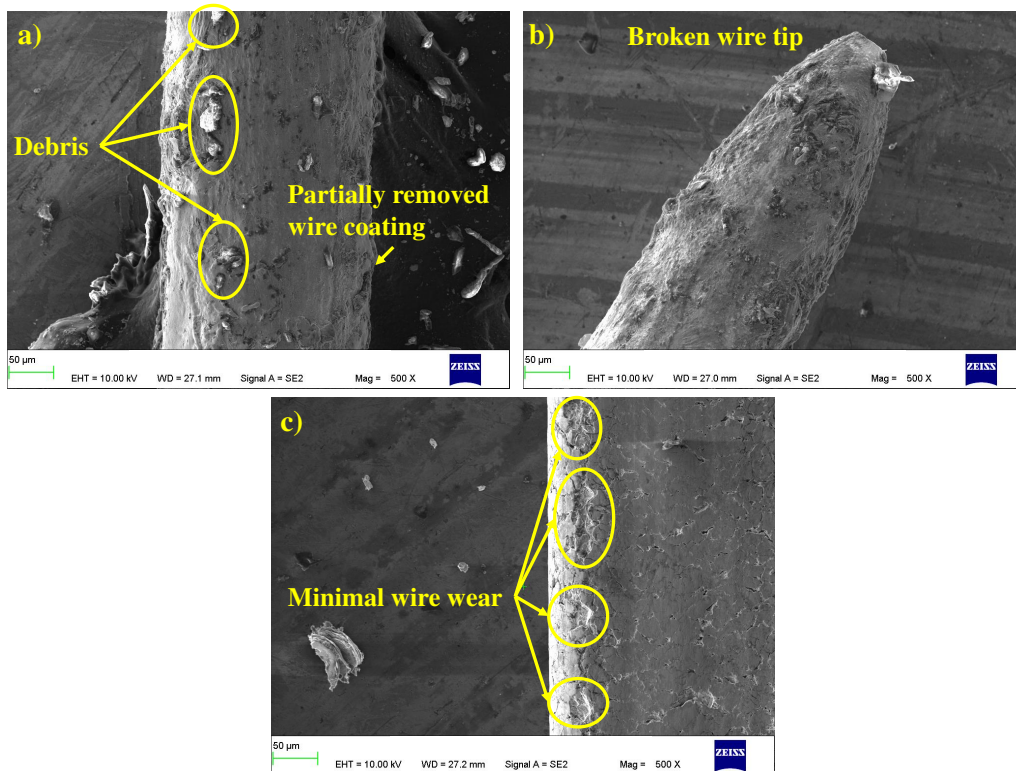


**Fig. 7.21** (a) Severely degraded wire surface under original settings (b) Broken wire tip (c) Minimal wear after process control

The improvement in process stability through process control, in case of wire breakage prediction, is also analysed considering the improvements to wire wear. As shown in Fig. 7.21, SEM images of worn wire surfaces are compared in this regard. For the case considered (Exp. No. 1), using the original settings, worn wire showed considerable degradation as seen in Fig. 7.21 (a). The surface coating is observed to be removed at several areas, exposing the brass inner core. The instability builds up till a point where the wire will break at a later stage. Fig. 7.21 (b) shows the SEM image of broken wire tip. The process control is successful in restoring the process stability, which is indicated by a significantly less wire wear as shown in Fig. 7.21 (c).

The overall improvement to the machining continuity and surface integrity due to process control is reported in Table 7.8. A total machining length of 100 mm was considered to test the effect of process control. With original settings, machining interruptions are reported before a machined length of 20 mm.

However, through process control, uninterrupted continuous machining is reported for the entire profile length of 100 mm. An improvement in surface finish is also reported in each failure case. The effect is more pronounced in cases of wire breakage due to the reduction of short circuit discharge percentage during parameter regulation. The surface roughness comparison of the machined surfaces before and after process control for all the failure cases are shown in Fig. 7.22. The improvement in surface morphology is shown separately in Fig. 7.23. Here the SEM images of machined surfaces shows significant improvement in surface quality. An improved surface finish is reported in each case after process control.

**Table 7.8** Effects of process control

S. No	Extracted features				Under original settings			After process control			
	DE ( $\mu$ J)	SSR	OSR	SF (Hz)	MO	RUL (min)	R <sub>a</sub> ( $\mu$ m)	ML (mm)	MO	R <sub>a</sub> ( $\mu$ m)	ML (mm)
1	227.0	0.79	0.00	68450	WB	2.26	2.76	3.80	NM	1.24	100
2	2527.7	0.83	0.05	7500	WB	10.83	1.62	20.36	NM	1.51	100
3	2611.9	0.94	0.03	8350	WB	10.98	1.97	20.64	NM	1.37	100
4	1568.8	0.94	0.00	84600	WB	2.23	3.21	2.89	NM	1.78	100
5	16.1	0.75	0.00	200	SA	12.87	1.35	1.03	NM	1.24	100
6	14.5	0.62	0.24	1050	SA	9.70	1.27	0.97	NM	1.43	100
7	3168.9	0.41	0.28	4500	WB	1.47	3.08	3.53	NM	1.21	100
8	3299.0	0.30	0.01	17000	WB	0.00	3.54	0.00	NM	1.43	100
9	3252.9	0.15	0.19	7800	WB	0.00	3.22	0.00	NM	1.12	100
10	4030.2	0.54	0.26	1950	WB	10.18	2.03	16.40	NM	1.05	100
11	4007.0	0.43	0.40	1500	WB	8.16	2.62	14.77	NM	1.53	100
12	14.8	0.54	0.19	6200	SA	6.32	1.35	0.38	NM	1.32	100
13	58.58	0.17	0.50	300	SA	3.05	0.98	0.19	NM	0.99	100
14	15.4	0.58	0.28	1800	SA	9.43	1.51	1.04	NM	1.57	100

DE- Discharge Energy/spark, SSR- Short Circuit Ratio, OSR- Open Circuit Ratio, SF- Spark Frequency, MO – Machining Outcome, NM- Normal Machining, WB- Wire Breakage, SA- Spark Absence, RUL- Remaining Useful Life, ML – Machined Length

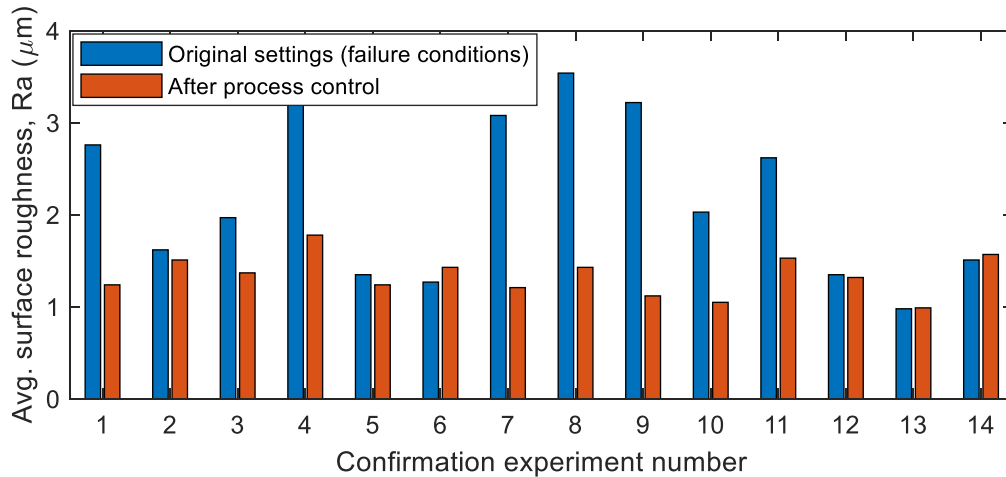


**Fig. 7.22** Effect of process control on surface roughness of machined components

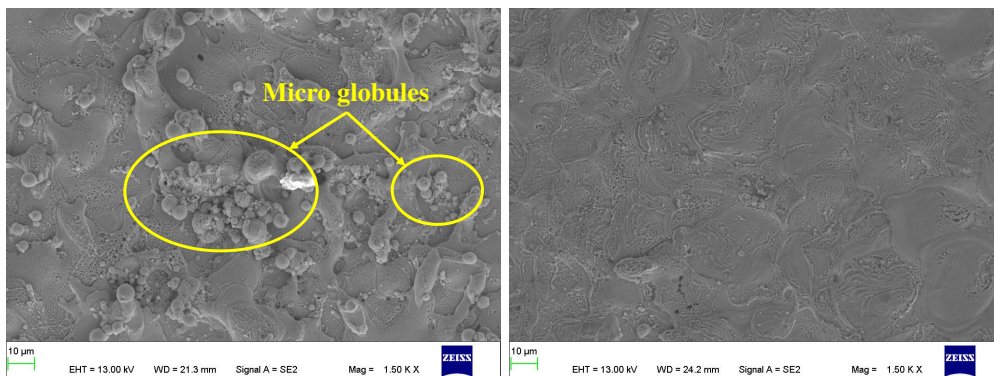


**Fig. 7.23** SEM images of machined surface (a) under original settings (b) after process control

***Case II: Process control to prevent spark absence***

To demonstrate the effects of process control in spark absence situation Exp. No. 7 ( $T_{ON} = 105 \mu s$ ,  $T_{OFF} = 50 \mu s$ ,  $SV = 38 V$ ,  $I_p = 10 A$ ,  $WF = 3 m/min$ ) is considered. Pulse train analysis of this condition showed less discharge energy and negligible pulse frequency, along with higher proportion of open circuit pulses. Based on these, ANN classifier predicted spark absence failure. Then the RUL value is predicted by the second neural network model. The predicted failure mode and RUL value is verified to be correct experimentally. Based on the RUL value, the recommendation settings ( $T_{ON} = 110 \mu s$ ,  $T_{OFF} = 50 \mu s$ ,  $SV = 43 V$ ,  $I_p = 10 A$ ,  $WF = 3 m/min$ ) are applied, which prevents the spark absence failure. The discharge characteristics improved to result in higher

discharge energy and spark frequency. Pulse cycle comparison showed that the open circuit sparks are replaced by normal spark discharges as shown in Fig. 7.24.

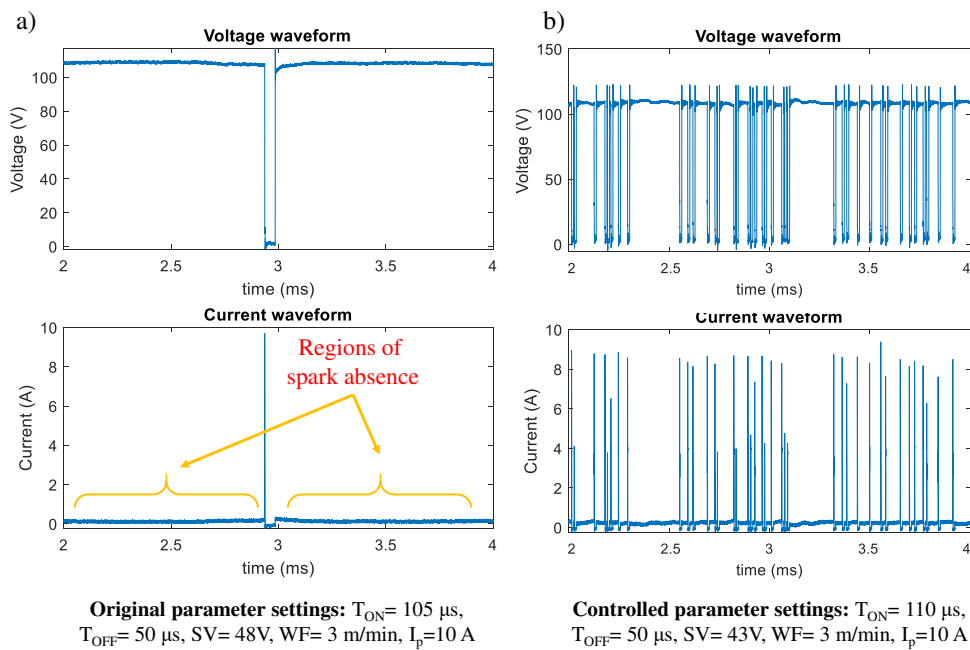


**Fig. 7.24** (a) Original settings (Conf test: Exp. No. 5) (b) Controlled settings

## 7.6 COMPARISON WITH EXISTING MODELS

The section compares the capabilities of the proposed system with the existing wire EDM monitoring systems. One distinguishing feature of the proposed model is that it considered multiple failure modes of wire EDM process. Most of the failure detection and alert systems proposed thus far have only address the wire breakage failure (Kwon and Yan, 2006; Cabanes et al., 2008). Several strategies have been implemented by researchers in the past for failure identification. Instantaneous energy based (Kwon and Yan, 2006), peak current and ignition delay time based (Cabanes et al., 2008) and unstable discharge ratio based (Conde et al., 2018) systems some of the notable wire break detection systems. However, a process control strategy to restore the machining stability to avoid the predicted failures are not proposed with these systems. Process control models which are not based on pulse classification may have limited capability to address the implications due to abnormal harmful discharges (Mendes et al., 2014; Zhidong et al., 2014; Bufardi et al., 2015).

Fuzzy logic based wire EDM condition monitoring systems may be inaccurate in failure identification and control since such models are expert knowledge dependent and they cannot be trained based on experimental data (Yan and Liao, 1996; Bufardi et al., 2015; Liao and Woo, 2000). A neural network model is reported to be better suited to handle such stochastic phenomena like wire EDM failure event, which led to its implementation in the proposed system.

The proposed model implements a pulse classification based failure prediction system, which is integrated with a process control system based on failure severity. The parameter remaining useful life (RUL) is chosen as an indicator of severity of predicted failure. Even though RUL is already used in tool condition monitoring research, its capability is not yet utilised in the context of process control. Finally, apart from ensuring a failure-free operation, the proposed algorithm is reported to result in improved surface integrity for the machined parts, which most of the existing algorithms have failed to report. Table 7.9 compares the capabilities of the existing models with the model proposed in this study. The mode of operation (online, offline or hybrid), machine learning algorithm used, pulse classification, failure alert facility, modes of failure considered, availability of process control algorithm and general capabilities are compared in this table. Only the models proposed since 2005 is shown in this comparative analysis.

## **7.7 SUMMARY**

The chapter discusses wire EDM process control system, which is developed based on the pulse train analysis. Firstly, a rule-based algorithm is developed to assess failure severity based on average discharge energy of pulse cycles. Short circuit dominant pulse cycle will have highest discharge energy and is regarded as most critical. This system performs severity-based variable process control for wire break situations. Such a system is suitable in case of lesser training data. If the amount of training data is more, then neural network-based systems can perform better in process control. The proposed neural network-based process

control system works in three stages. Failure detection is performed by ANN classification. The trained classifier model predicts the mode of failure.

**Table 7.9** Comparison of existing wire EDM monitoring models

S. No	Author, year	Mode	Algorithm / Method	Pulse classification	Alert/ alarm	Failure modes	Process control	Capability
1	Kwon and Yan, 2006	Online		✓	✓	Wire breakage	–	Suggests stable working region based on instantaneous energy
2	Cabanes et al., 2008	Online	Heuristic rule based	–	✓	Wire breakage	–	Triggers multiple alarms based on risk of wire breakage
3	Kumar and Choudhury, 2011	Offline	Regression	–	–	Wire breakage	–	Offline prediction of wire breakage
4	Kumar et al., 2013	Offline	Regression	–	–	Wire breakage	–	Offline prediction of wire breakage
5	Mendes et al., 2014	Offline	N.A.	–	–	N.A.	–	Performance evaluation based on cutting rate, time and energy consumption
6	Zhidong et al., 2014	Online	Rule based	–	–	N.A.	✓	Proposes spark gap regulation based on current pulse probability
7	Kwon et al., 2015	Online	Rule based	✓	–	Wire breakage	✓	Reduces unstable discharge ratio and discharge energy to improve cutting speed and $R_a$
8	Bufardi et al., 2015	Hybrid	Fuzzy logic	–	–	N.A.	✓	Prevention of surface damages
9	Caggiano et al., 2018	Online	Threshold based	✓	–	N.A.	–	Proposed a methodology for feature extraction from wire EDM pulse signals
10	Osswald et al., 2018	Online	Threshold based	✓	–	N.A.	–	Pulse classification algorithm based on ignition delay for high speed WEDM
11	Conde et al., 2018	Online	N.A.	✓	–	N.A.	–	Found relation between abnormal spark ratio, wire lag and geometric error
12	Bergs et al., 2018	Online	N.A.	✓	✓	Wire breakage	–	Proposed a basis for early detection of wire breakage
13	<b>Proposed model</b>	Hybrid	Threshold based, Neural network	✓	✓	Wire breakage, Spark absence	✓	Prediction of mode of failure (wire breakage or spark absence), evaluation of failure severity, and process control through parameter regulation Prevents process failure and improves machining performance

In second stage, a neural network model predicts the remaining useful life (RUL) at the time of assessment. The RUL based variable process control is applied to both modes of failures in this case. Finally, a process control algorithm revises the process parameters like pulse on time, pulse off time, and servo voltage to restore the process stability. The effectiveness of process control is evaluated by pulse cycle comparison, surface integrity analysis, and wire wear study. Confirmation tests are conducted to evaluate the system performance in real world machining situation. Process control ensured failure free continuous machining in every case. Pulse train originally dominant by abnormal pulses is brought back to a stable cycle with normal discharges. Also, process control is observed to reduce wire wear substantially. Surface integrity analysis showed significant reduction in average surface roughness values after process control. Micro structural studies revealed a smoother surface with no visible surface damages after process control.

## CHAPTER 8

### CONCLUSIONS AND FUTURE SCOPE

#### 8.1 CONCLUSIONS

Wire EDM process has immense potential over the conventional machining techniques to cut intricate and complex shapes in 'difficult to cut' materials. However, the process is often regarded as less efficient and reliable due to unexpected failures and process interruptions. Even after several attempts to optimize the settings, the failures are reported to happen due to the stochastic process mechanism and involvement of several uncontrollable factors. To make the process sustainable, efficient and future proof, there need to be a system which can predict the events of process failures, and control the process parameters to overcome those machining interruptions. In this regard, the current research work aims to develop a condition monitoring and process control system for wire EDM process.

Following are the salient conclusions drawn from this research study:

- Microstructural analysis of wire surface revealed distinct characteristics leading to wire breakage, like extensive degradation of wire coating, presence of melt pool, and presence of impinged debris.
- At higher instabilities, the surface integrity is found to degrade significantly which is evident from an increase in surface roughness from 1.55  $\mu\text{m}$  to 2.97  $\mu\text{m}$  at conditions C2 and C6 respectively. Similarly, flatness error increased from 0.6  $\mu\text{m}$  to 2.95  $\mu\text{m}$ , circularity error increased from 0.9  $\mu\text{m}$  to 2.9  $\mu\text{m}$ , and cylindricity error increased from 1.9  $\mu\text{m}$  to 3.8  $\mu\text{m}$  at conditions C2 and C6 respectively.

- An offline artificial neural network (ANN) classifier is developed to predict the mode of machining failure with 90.1 % classification accuracy. The classifier performed with 95 % accuracy during confirmation tests.
- Using 31-central composite design (CCD) experimental runs as training data, an ANFIS model based decision support system is developed to alert the operators on potential wire breakages. The system rightly predicted all occurrences of wire breakages during 9 confirmation test runs.
- Using a sensor based condition monitoring system, discharge characteristics like spark energy, spark frequency, and abnormal spark ratios are found to have significant effect on cutting speed and surface roughness. An ANN model is developed with closeness coefficient of 0.984 to predict the responses based on in-process data.
- A pulse classification algorithm is designed based on the ignition delay time to classify the discharge pulses into normal, arc, open and short circuit discharges. Higher proportion of short circuit and open circuit pulses are observed before wire breakage and spark absence failures respectively.
- During the analysis of process failures, the wire breakages are observed to be preceded by a short circuit predominant discharge cycle, having an average spark discharge energy greater than 500  $\mu\text{J}$ , and a sparking frequency greater than 10000 Hz. On the other hand, discharge cycle leading to spark absence failures are observed to have a higher proportion of open circuit discharges, with an average spark discharge energy less than 50  $\mu\text{J}$ , and a sparking frequency less than 10000 Hz.
- A threshold based online failure prediction and process control system is developed based on the extracted discharge features like discharge energy, pulse frequency, short circuit spark ratio, and open circuit spark ratio. The system not only succeeded in forecasting and preventing the process failures, but also improved the average surface roughness by 31 %.

- Finally, a neural network based process control system is developed to predict mode of failure with 98.1 % classification accuracy. The system considers ‘remaining useful life (RUL)’ as an indicator of failure severity. A trained ANN regression model predicts the RUL with a closeness coefficient of 0.988.
- Based on mode and severity of predicted failure, the process control system prevents the occurrences of machining failures and improves the average surface roughness by 38 %.

## **8.2 SCOPE OF FUTURE WORK**

The existing study gives more emphasis on the failure prediction and its eradication. A follow-up study can be conducted to extend the proposed monitoring system to predict and control the surface integrity in real time. Such a system can double up as an online inspection system for the machined components. Effectiveness of such a model during the machining of industrially significant profiles like fir tree slots can be explored. Also, further analysis can be conducted on the dependency of material properties on the discharge characteristics. For e.g., in order to make the predictive model effective against multiple materials, the model shall be retrained with a sufficiently large dataset generated by considering several materials which are commonly machined by wire EDM. Also, the process control algorithm can be further developed to perform parameter tuning as a function of RUL or any suitable indicator of failure severity, instead of discrete incremental steps. Since the problem of arcing is common to every electric discharge machining process, the proposed monitoring system can be further extended to other varieties of EDMs.

## APPENDIX I

**Table 1** Details of 108 experiments

S. No	T <sub>ON</sub> (μs)	T <sub>OFF</sub> (μs)	SV (V)	I <sub>P</sub> (A)	WF (m/min)	DE /spark (μJ)	SSR	OSR	SF	MO	RUL (min)
1	105	30	30	40	3	1614	0.83	0.05	75000	WB	2.66
2	105	30	50	40	3	508	0.35	0.29	31000	NM	-
3	105	40	30	40	3	544	0.38	0.15	12000	NM	-
4	105	40	50	40	3	560	0.40	0.48	26000	NM	-
5	105	50	30	40	3	549	0.42	0.30	28500	NM	-
6	105	50	50	40	3	583	0.36	0.57	14000	NM	-
7	110	30	30	40	3	1044	0.38	0.32	56500	WB	0.32
8	110	30	50	40	3	1066	0.41	0.28	45000	WB	2.08
9	110	40	30	40	3	1034	0.31	0.40	22500	NM	-
10	110	40	50	40	3	987	0.52	0.29	69000	WB	3.11
11	110	50	30	40	3	1124	0.38	0.13	16000	NM	-
12	110	50	50	40	3	1002	0.51	0.32	50500	WB	5.95
13	115	30	30	40	3	1477	0.54	0.26	82500	WB	0.58
14	115	30	50	40	3	1596	0.11	0.29	9000	NM	-
15	115	40	30	40	3	1485	0.53	0.10	65500	WB	2.67
16	115	40	50	40	3	1646	0.17	0.24	11500	NM	-
17	115	50	30	40	3	1618	0.17	0.32	11500	NM	-
18	115	50	50	40	3	1659	0.20	0.10	5000	NM	-
19	105	30	30	10	3	157	0.23	0.11	25000	NM	-
20	105	30	50	10	3	77	0.33	0.31	24500	NM	-
21	105	40	30	10	3	135	0.24	0.31	34000	NM	-
22	105	40	50	10	3	48	0.04	0.58	12000	SA	0.70
23	105	50	30	10	3	32	0.00	0.31	13500	SA	0.70
24	105	50	50	10	3	43	0.31	0.44	19500	SA	0.30
25	110	30	30	10	3	141	0.38	0.23	6500	NM	-
26	110	30	50	10	3	145	0.34	0.30	39500	NM	-
27	110	40	30	10	3	239	0.39	0.16	13500	NM	-
28	110	40	50	10	3	123	0.37	0.25	37500	NM	-
29	110	50	30	10	3	253	0.36	0.38	21000	NM	-
30	110	50	50	10	3	43	0.45	0.45	14500	SA	0.50
31	115	30	30	10	3	135	0.14	0.11	27000	NM	-
32	115	30	50	10	3	161	0.16	0.33	32000	NM	-
33	115	40	30	10	3	122	0.28	0.05	57500	NM	-
34	115	40	50	10	3	139	0.41	0.31	19500	NM	-
35	115	50	30	10	3	241	0.24	0.38	22500	NM	-
36	115	50	50	10	9	66	0.13	0.48	15500	SA	0.45
37	105	30	30	40	9	1382	0.79	0.00	68450	WB	2.98
38	105	30	50	40	9	483	0.26	0.02	25150	NM	-
39	105	40	30	40	9	477	0.33	0.00	23400	NM	-
40	105	40	50	40	9	528	0.24	0.01	24000	NM	-
41	105	50	30	40	9	503	0.33	0.00	22800	NM	-

42	105	50	50	40	9	553	0.10	0.09	11500	NM	-
43	110	30	30	40	9	958	0.53	0.01	77000	WB	2.27
44	110	30	50	40	9	1031	0.15	0.19	7800	NM	-
45	110	40	30	40	9	981	0.62	0.03	55250	WB	2.98
46	110	40	50	40	9	1044	0.16	0.12	8950	NM	-
47	110	50	30	40	9	1059	0.24	0.01	12100	NM	-
48	110	50	50	40	9	1062	0.18	0.20	7550	NM	-
49	115	30	30	40	9	1627	0.51	0.00	48600	WB	1.98
50	115	30	50	40	9	1693	0.11	0.11	9150	NM	-
51	115	40	30	40	9	1643	0.42	0.01	55200	WB	2.53
52	115	40	50	40	9	1642	0.21	0.12	9400	NM	-
53	115	50	30	40	9	1631	0.26	0.00	12750	NM	-
54	115	50	50	40	9	1640	0.16	0.17	7550	NM	-
55	105	30	30	10	9	123	0.18	0.00	29950	NM	-
56	105	30	50	10	9	228	0.25	0.01	37900	NM	-
57	105	40	30	10	9	339	0.31	0.00	20750	NM	-
58	105	40	50	10	9	351	0.24	0.07	19650	NM	-
59	105	50	30	10	9	245	0.30	0.01	23950	NM	-
60	105	50	50	10	9	37	0.32	0.04	17650	SA	0.45
61	110	30	30	10	9	135	0.33	0.00	20550	NM	-
62	110	30	50	10	9	248	0.26	0.26	6600	NM	-
63	110	40	30	10	9	140	0.31	0.00	15900	NM	-
64	110	40	50	10	9	249	0.28	0.06	12400	NM	-
65	110	50	30	10	9	136	0.40	0.01	14700	NM	-
66	110	50	50	10	9	152	0.25	0.21	6550	NM	-
67	115	30	30	10	9	144	0.23	0.02	15450	NM	-
68	115	30	50	10	9	253	0.21	0.12	9400	NM	-
69	115	40	30	10	9	138	0.32	0.02	16300	NM	-
70	115	40	50	10	9	50	0.27	0.19	8400	NM	-
71	115	50	30	10	9	149	0.21	0.02	12600	NM	-
72	115	50	50	10	9	55	0.29	0.16	7950	NM	-
73	105	30	40	40	3	515	0.23	0.00	27950	NM	-
74	105	40	40	40	3	567	0.21	0.00	23000	NM	-
75	105	50	40	40	3	523	0.21	0.03	17400	NM	-
76	110	30	40	40	3	1650	0.57	0.00	46100	WB	2.92
77	110	40	40	40	3	1087	0.22	0.03	10950	NM	-
78	110	50	40	40	3	1104	0.16	0.03	10600	NM	-
79	115	30	40	40	3	1600	0.15	0.04	12800	NM	-
80	115	40	40	40	3	1654	0.41	0.03	50650	WB	3.03
81	115	50	40	40	3	1586	0.24	0.03	11500	NM	-
82	105	30	40	10	3	134	0.34	0.00	21900	NM	-
83	105	40	40	10	3	228	0.26	0.01	38500	NM	-
84	105	50	40	10	3	151	0.17	0.04	20400	NM	-
85	110	30	40	10	3	55	0.10	0.51	16200	SA	0.65
86	110	40	40	10	3	35	0.27	0.29	15150	SA	0.40
87	110	50	40	10	3	43	0.22	0.50	11800	SA	0.25
88	115	30	40	10	3	134	0.31	0.06	15850	NM	-
89	115	40	40	10	3	138	0.35	0.09	13200	NM	-
90	115	50	40	10	3	51	0.19	0.42	8400	SA	0.20

91	105	30	40	40	9	1542	0.31	0.00	39250	WB	3.38
92	105	40	40	40	9	554	0.21	0.00	28400	NM	-
93	105	50	40	40	9	541	0.14	0.01	16850	NM	-
94	110	30	40	40	9	512	0.39	0.00	27750	NM	-
95	110	40	40	40	9	1134	0.17	0.06	10250	NM	-
96	110	50	40	40	9	1101	0.21	0.02	11200	NM	-
97	115	30	40	40	9	1625	0.41	0.03	40900	WB	2.58
98	115	40	40	40	9	1554	0.19	0.05	11000	NM	-
99	115	50	40	40	9	1594	0.18	0.04	10050	NM	-
100	105	30	40	10	9	131	0.30	0.00	13350	NM	-
101	105	40	40	10	9	235	0.30	0.00	34000	NM	-
102	105	50	40	10	9	135	0.22	0.07	15750	NM	-
103	110	30	40	10	9	237	0.23	0.00	20750	NM	-
104	110	40	40	10	9	258	0.20	0.14	9900	NM	-
105	110	50	40	10	9	30	0.14	0.29	13400	SA	0.45
106	115	30	40	10	9	239	0.36	0.03	21100	NM	-
107	115	40	40	10	9	33	0.16	0.39	14350	SA	0.70
108	115	50	40	10	9	41	0.16	0.42	11750	SA	0.40

---

DE- Discharge Energy/spark, SSR- Short Circuit Ratio, OSR- Open Circuit Ratio, SF- Spark Frequency, NM- Normal Machining, WB- Wire Breakage, SA- Spark Absence,  
RUL- Remaining Useful Life

---

## REFERENCES

1. Ahmed, N., Pervez Mughal, M., Shoaib, W., Farhan Raza, S., & M Alahmari, A. (2020). WEDM of Copper for the Fabrication of Large Surface-Area Micro-Channels A Prerequisite for the High Heat-Transfer Rate. *Micromachines*, 11(2), 173
2. Alduroobi, A. A., Ubaid, A. M., Tawfiq, M. A., & Elias, R. R. (2020). Wire EDM process optimization for machining AISI 1045 steel by use of Taguchi method, artificial neural network and analysis of variances. *International Journal of System Assurance Engineering and Management*, 1-25.
3. Al-Habaibeh, A., Cai, R., Jackson, M. R., & Parkin, R. M. (2004). Modern developments in sensor technology and their applications in condition monitoring of manufacturing processes. In *Proceedings of the VIIth International Conference on Monitoring and automatic supervision in manufacturing* (pp. 47-58).
4. Alhadef, L. L., Curtis, D. T., Marshall, M. B., & Slatter, T. (2018). The application of wire electrical discharge machining (WEDM) in the prototyping of miniature brass gears. *Procedia CIRP*, 77, 642-645.
5. Ali, M. Y., & Mohammad, A. S. (2008). Experimental study of conventional wire electrical discharge machining for microfabrication. *Materials and Manufacturing Processes*, 23(7), 641-645.
6. Antar, M. T., Soo, S. L., Aspinwall, D. K., Sage, C., Cuttell, M., Perez, R., & Winn, A. J. (2012). Fatigue response of Udimet 720 following minimum damage wire electrical discharge machining. *Materials & Design*, 42, 295-300.
7. Anurag, S. (2018). Wire-EDM: a potential manufacturing process for gamma titanium aluminides in future aero engines. *The International Journal of Advanced Manufacturing Technology*, 94(1), 351-356.
8. Arunachalam, C., Aulia, M., Bozkurt, B., & Eubank, P. T. (2001). Wire vibration, bowing, and breakage in wire electrical discharge machining. *Journal of Applied Physics*, 89(8), 4255-4262.

9. Azhiri, R. B., Teimouri, R., Baboly, M. G., & Leseman, Z. (2014). Application of Taguchi, ANFIS and grey relational analysis for studying, modeling and optimization of wire EDM process while using gaseous media. *The International Journal of Advanced Manufacturing Technology*, 71(1-4), 279-295.
10. Babu Rao, T., & Gopala Krishna, A. (2013). Simultaneous optimization of multiple performance characteristics in WEDM for machining ZC63/SiCp MMC. *Advances in Manufacturing*, 1(3), 265–275.
11. Beltrami, I., Bertholds, A., & Dauw, D. (1996). A simplified post process for wire cut EDM. *Journal of materials processing technology*, 58(4), 385-389.
12. Bergs, T., Tombul, U., Herrig, T., Olivier, M., Klink, A., & Klocke, F. (2018). Analysis of characteristic process parameters to identify unstable process conditions during Wire EDM. *Procedia Manufacturing*, 18, 138-145.
13. Bogue, R. (2013). 3D printing: the dawn of a new era in manufacturing?. *Assembly Automation*, 2013;33:307–11
14. Bufardi, A., Akten, O., Arif, M., Xirouchakis, P., & Perez, R. (2017). Towards zero-defect manufacturing with a combined online-offline fuzzy-nets approach in wire electrical discharge machining. *WSEAS Transactions on Environment and Development*, 13, 401-409.
15. Cabanes, I., Portillo, E., Marcos, M., & Sánchez, J. A. (2008). On-line prevention of wire breakage in wire electro-discharge machining. *Robotics and Computer-Integrated Manufacturing*, 24(2), 287-298.
16. Caggiano, A., Teti, R., Perez, R., & Xirouchakis, P. (2015). Wire EDM monitoring for zero-defect manufacturing based on advanced sensor signal processing. *Procedia CIRP*, 33, 315-320.
17. Caiazzo, F., Cuccaro, L., Fierro, I., Petrone, G., & Alfieri, V. (2015). Electrical discharge machining of René 108 DS nickel superalloy for aerospace turbine blades. *Procedia CIRP*, 33, 382-387.
18. Camposeco-Negrete, C. (2019). Prediction and optimization of machining time and surface roughness of AISI O1 tool steel in wire-cut EDM using

- robust design and desirability approach. *International Journal of Advanced Manufacturing Technology*, 103(5–8), 2411–2422.
19. Camposeco-Negrete, C. (2019). Prediction and optimization of machining time and surface roughness of AISI O1 tool steel in wire-cut EDM using robust design and desirability approach. *International Journal of Advanced Manufacturing Technology*, 103(5–8), 2411–2422.
  20. Çaydaş, U., Hasçalık, A., & Ekici, S. (2009). An adaptive neuro-fuzzy inference system (ANFIS) model for wire-EDM. *Expert Systems with Applications*, 36(3), 6135-6139.
  21. Chaudhari, R., Vora, J. J., Prabu, S. S. M., Palani, I. A., Patel, V. K., & Parikh, D. M. (2019). Pareto optimization of WEDM process parameters for machining a NiTi shape memory alloy using a combined approach of RSM and heat transfer search algorithm. *Advances in Manufacturing*.
  22. Chaudhary, T., Siddiquee, A. N., Chanda, A. K., Abidi, M. H., & Al-Ahmari, A. (2020). Multi-response optimization for Nimonic alloy miniature gear fabrication using wire electrical discharge machining. *Advances in Mechanical Engineering*, 12(10), 1687814020967580.
  23. Cheng, S., Azarian, M. H., & Pecht, M. G. (2010). Sensor systems for prognostics and health management. *Sensors*, 10(6), 5774-5797.
  24. Conde, A., Sanchez, J. A., Plaza, S., Ostolaza, M., de la Puerta, I., & Li, Z. (2018). Experimental Measurement of Wire-lag Effect and Its Relation with Signal Classification on Wire EDM. *Procedia CIRP*, 68, 132-137.
  25. Das, P. P., & Chakraborty, S. (2020). A grey correlation-based TOPSIS approach for optimization of surface roughness and micro hardness of Nitinol during WEDM operation. *Materials Today: Proceedings*, 28, 568-573.
  26. Das, S. S., & Patowari, P. K. (2018). Fabrication of serpentine micro-channels on glass by ultrasonic machining using developed micro-tool by wire-cut electric discharge machining. *The International Journal of Advanced Manufacturing Technology*, 95(5), 3013-3028.

27. Debnath, T., & Patowari, P. K. (2019). Fabrication of an array of micro-fins using Wire-EDM and its parametric analysis. *Materials and Manufacturing Processes*, 34(5), 580-589.
28. Debnath, T., & Patowari, P. K. (2019). Fabrication of an array of micro-fins using Wire-EDM and its parametric analysis. *Materials and Manufacturing Processes*, 34(5), 580–589. <https://doi.org/10.1080/10426914.2019.1566959>
29. Descoedres, A. (2006). *Characterization of electrical discharge machining plasmas* (No. 3542, THESIS). EPFL.
30. Dou, S. C., Xi, X. C., & Zhao, W. S. (2013). Workpiece height estimation in wire electrical discharge machining by using support vector regression. *Proceedings of the Institution of Mechanical Engineers, Part B: Journal of Engineering Manufacture*, 227(4), 565-577.
31. Ebisu, T., Kawata, A., Okamoto, Y., Okada, A., & Kurihara, H. (2018). Influence of jet flushing on corner shape accuracy in wire EDM. *Procedia CIRP*, 68, 104-108.
32. El-Hofy, H. A. G. (2005). *Advanced machining processes: non-traditional and hybrid machining processes*. McGraw Hill Professional.
33. Fan, Y. S., & Bai, J. C. (2018). Study on volt-ampere characteristics of spark discharge for transistor resistor pulse power of EDM. *International Journal of Advanced Manufacturing Technology*, 96(9–12), 3019–3031.
34. Garg, S. K. R., Manna, A., & Jain, A. (2013). *Multi-objective optimization of machining characteristics during wire electrical discharge machining of Al / ZrO<sub>2</sub> - particulate reinforced metal matrix composite. I*(December), 145–160.
35. Goswami, A., & Kumar, J. (2014). Optimization in wire-cut EDM of Nimonic-80A using Taguchi's approach and utility concept. *Engineering Science and Technology, an International Journal*, 17(4), 236–246.
36. Gupta, K., & Jain, N. K. (2014). Comparative study of wire-EDM and hobbing for manufacturing high-quality miniature gears. *Materials and Manufacturing Processes*, 29(11-12), 1470-1476.

37. Habib, S., & Okada, A. (2016). Study on the movement of wire electrode during fine wire electrical discharge machining process. *Journal of Materials Processing Technology*, 227, 147-152.
38. Ho, K. H., & Newman, S. T. (2003). State of the art electrical discharge machining (EDM). *International Journal of Machine Tools and Manufacture*, 43(13), 1287–1300.
39. Holmberg, J., Berglund, J., Wretland, A., & Beno, T. (2019). Evaluation of surface integrity after high energy machining with EDM, laser beam machining and abrasive water jet machining of alloy 718. *The International Journal of Advanced Manufacturing Technology*, 100(5), 1575-1591.
40. Hsieh, S. F., Chen, S. L., Lin, H. C., Lin, M. H., & Chiou, S. Y. (2009). The machining characteristics and shape recovery ability of Ti–Ni–X (X= Zr, Cr) ternary shape memory alloys using the wire electro-discharge machining. *International Journal of Machine Tools and Manufacture*, 49(6), 509-514.
41. Huang, D. C., Lin, C. F., Chen, C. Y., & Sze, J. R. (2018, May). The Internet technology for defect detection system with deep learning method in smart factory. In *2018 4th International Conference on Information Management (ICIM)* (pp. 98-102). IEEE.
42. Huang, G., Xia, W., Qin, L., & Zhao, W. (2018). Online workpiece height estimation for reciprocated traveling wire EDM based on support vector machine. *Procedia CIRP*, 68, 126-131.
43. Huang, J. T., & Liao, Y. S. (2000). A wire-EDM maintenance and fault-diagnosis expert system integrated with an artificial neural network. *International Journal of Production Research*, 38(5), 1071-1082.
44. Jain, V. K. (2009). *Advanced machining processes*. Allied publishers
45. Janak, L., & Hadas, Z. (2015). Machine Tool Health and Usage Monitoring System: An Initial Analyses. *MM Science Journal*, 4, 794-798.
46. Janardhan, V., & Samuel, G. L. (2010). Pulse train data analysis to investigate the effect of machining parameters on the performance of wire electro discharge turning (WEDT) process. *International Journal of Machine Tools and Manufacture*, 50(9), 775-788.

47. Karidkar, S. S., Dabade, U. A., Ginting, B., & Sembiring, R. W. (2018). Evaluation of surface integrity of WEDM processed inconel 718 for jet engine application Evaluation of surface integrity of WEDM processed inconel 718 for jet engine application. *IOP Conf. Series: Materials Science and Engineering*.
48. Kawata, A., Okada, A., Okamoto, Y., & Kurihara, H. (2017). Influence of nozzle jet flushing on wire breakage in 1st-cut wire EDM from start hole. In *Key Engineering Materials* (Vol. 749, pp. 130-135). Trans Tech Publications Ltd.
49. Klocke, F., Schwade, M., & Klink, A. (2012). Development of a process evaluation system for wire-EDM applications using an intelligent process monitoring tool. In *Key Engineering Materials* (Vol. 504, pp. 1159-1164). Trans Tech Publications Ltd.
50. Klocke, F., Welling, D., Dieckmann, J., Veselovac, D., & Perez, R. (2012). Developments in Wire-EDM for the manufacturing of fir tree slots in turbine discs made of Inconel 718. In *Key Engineering Materials* (Vol. 504, pp. 1177-1182). Trans Tech Publications Ltd.
51. Klocke, F., Welling, D., Klink, A., & Perez, R. (2014). Quality assessment through in-process monitoring of wire-EDM for fir tree slot production. *Procedia CIRP*, 24, 97-102.
52. Klocke, F., Welling, D., Klink, A., Veselovac, D., Nöthe, T., & Perez, R. (2014). Evaluation of advanced wire-EDM capabilities for the manufacture of fir tree slots in Inconel 718. *Procedia CIRP*, 14, 430-435.
53. Kumar, A., Kumar, V., & Kumar, J. (2013). Parametric effect on wire breakage frequency and surface topography in WEDM of pure titanium. *Journal of Mechanical Engineering and technology*, 1(2), 51-56.
54. Kumar, A., Soota, T., & Kumar, J. (2018). Optimisation of wire-cut EDM process parameter by Grey-based response surface methodology. *Journal of Industrial Engineering International*, 8, 1–9. <https://doi.org/10.1007/s40092-018-0264-8>

55. Kumar, R., & Choudhury, S. K. (2011). Prevention of wire breakage in wire EDM. *International Journal of Machining and Machinability of Materials*, 9(1-2), 86-102.
56. Kumar, S., Dhanabalan, S., & Narayanan, C. S. (2019). Application of ANFIS and GRA for multi-objective optimization of optimal wire-EDM parameters while machining Ti-6Al-4V alloy. *SN Applied Sciences*, 1(4), 1-12.
57. Kwon, S., & Yang, M. Y. (2006). The benefits of using instantaneous energy to monitor the transient state of the wire EDM process. *The International Journal of Advanced Manufacturing Technology*, 27(9-10), 930-938.
58. Kwon, S., Lee, S., & Yang, M. (2015). Experimental investigation of the real-time micro-control of the WEDM process. *The International Journal of Advanced Manufacturing Technology*, 79(9), 1483-1492.
59. Lee, J., Kao, H. A., & Yang, S. (2014). Service innovation and smart analytics for industry 4.0 and big data environment. *Procedia Cirp*, 16, 3-8.
60. Li, L., Wei, X. T., Guo, Y. B., Li, W., & Liu, J. F. (2014). Surface integrity of Inconel 718 by wire-EDM at different energy modes. *Journal of Materials Engineering and Performance*, 23(8), 3051-3057. <https://doi.org/10.1007/s11665-014-1048-y>
61. Liao, Y. S., & Woo, J. C. (1997). The effects of machining settings on the behavior of pulse trains in the WEDM process. *Journal of Materials Processing Technology*, 71(3), 433-439.
62. Liao, Y. S., & Woo, J. C. (2000). Design of a fuzzy controller for the adaptive control of WEDM process. *International Journal of Machine Tools and Manufacture*, 40(15), 2293-2307.
63. Liao, Y. S., Chang, T. Y., & Chuang, T. J. (2008). An on-line monitoring system for a micro electrical discharge machining (micro-EDM) process. *Journal of Micromechanics and Microengineering*, 18(3), 035009.
64. Liao, Y. S., Chu, Y. Y., & Yan, M. T. (1997). Study of wire breaking process and monitoring of WEDM. *International Journal of Machine Tools and Manufacture*, 37(4), 555-567.

65. Liao, Y. S., Chuang, T. J., & Yu, Y. P. (2013). On-line workpiece height estimation and its application in servo feed control of WEDM process. *Procedia CIRP*, 6, 226-231.
66. Lin, C. T., Chung, I. F., & Huang, S. Y. (2001). Improvement of machining accuracy by fuzzy logic at corner parts for wire-EDM. *Fuzzy sets and systems*, 122(3), 499-511.
67. Luo, Y. F. (1999). Rupture failure and mechanical strength of the electrode wire used in wire EDM. *Journal of Materials Processing Technology*, 94(2-3), 208-215.
68. Maher, I., Sarhan, A. A., Marashi, H., Barzani, M. M., & Hamdi, M. (2016). White layer thickness prediction in wire-EDM using CuZn-coated wire electrode–ANFIS modelling. *Transactions of the IMF*, 94(4), 204-210.
69. Majumder, H., & Maity, K. P. (2018). Predictive analysis on responses in WEDM of titanium grade 6 using general regression neural network (GRNN) and multiple regression analysis (MRA). *Silicon*, 10(4), 1763-1776.
70. Mandal, A., Dixit, A. R., Chattopadhyaya, S., Paramanik, A., Hloch, S., & Królczyk, G. (2017). Improvement of surface integrity of Nimonic C 263 super alloy produced by WEDM through various post-processing techniques. *International Journal of Advanced Manufacturing Technology*, 93(1–4), 433–443. <https://doi.org/10.1007/s00170-017-9993-x>
71. Mandal, A., Dixit, A. R., Das, A. K., & Mandal, N. (2016). Modeling and Optimization of Machining Nimonic C-263 Superalloy using Multicut Strategy in WEDM. *Materials and Manufacturing Processes*, 31(7), 860–868. <https://doi.org/10.1080/10426914.2015.1048462>
72. Mandal, S., Pramanick, A., Chakraborty, S., & Dey, P. P. (2018, June). ANFIS based model to forecast the Wire-EDM parameters for machining an Ultra High Temperature Ceramic composite. In *IOP Conference Series: Materials Science and Engineering* (Vol. 377, No. 1, p. 012088). IOP Publishing.
73. Manoj, I. V., & Narendranath, S. (2020). Variation and artificial neural network prediction of profile areas during slant type taper profiling of triangle

- at different machining parameters on Hastelloy X by wire electric discharge machining. *Proceedings of the Institution of Mechanical Engineers, Part E: Journal of Process Mechanical Engineering*, 234(6), 673-683.
74. Markopoulos, A. P., Manolakos, D. E., & Vaxevanidis, N. M. (2008). Artificial neural network models for the prediction of surface roughness in electrical discharge machining. *Journal of intelligent Manufacturing*, 19(3), 283-292.
75. Mendes, L. A., Amorim, F. L., & Weingaertner, W. L. (2015). Automated system for the measurement of spark current and electric voltage in wire EDM performance. *Journal of the Brazilian Society of Mechanical Sciences and Engineering*, 37(1), 123-131.
76. Menezes, B. C., Kelly, J. D., & Leal, A. G. (2019). Identification and Design of Industry 4.0 Opportunities in Manufacturing: Examples from Mature Industries to Laboratory Level Systems. *IFAC-PapersOnLine*, 52(13), 2494-2500.
77. Miner, M. J., Phelan, P. E., Odom, B. A., & Ortiz, C. A. (2013). Experimental measurements of critical heat flux in expanding microchannel arrays. *Journal of heat transfer*, 135(10).
78. Mohapatra, K. D., Sahoo, S. K., & Bhaumik, M. (2016). Thermal Modeling and Structural Analysis in Wire EDM Process for a 3D Model. In *Applied Mechanics and Materials* (Vol. 852, pp. 279-289). Trans Tech Publications Ltd.
79. Mwangi, J. W., Bui, V. D., Thüsing, K., Hahn, S., Wagner, M. F. X., & Schubert, A. (2020). Characterization of the arcing phenomenon in micro-EDM and its effect on key mechanical properties of medical-grade Nitinol. *Journal of Materials Processing Technology*, 275, 116334.
80. Nain, S. S., Sihag, P., & Luthra, S. (2018). Performance evaluation of fuzzy-logic and BP-ANN methods for WEDM of aeronautics super alloy. *MethodsX*, 5, 890-908.

81. Nain, S. S., Sihag, P., & Luthra, S. (2018). Performance evaluation of fuzzy-logic and BP-ANN methods for WEDM of aeronautics super alloy. *MethodsX*, 5, 890-908.
82. Ong, P., Lee, W. K., & Lau, R. J. H. (2019). Tool condition monitoring in CNC end milling using wavelet neural network based on machine vision. *The International Journal of Advanced Manufacturing Technology*, 104(1), 1369-1379.
83. Ong, S. K., Yuan, M. L., & Nee, A. Y. C. (2008). Augmented reality applications in manufacturing: a survey. *International journal of production research*, 46(10), 2707-2742.
84. Oßwald, K., Lochmahr, I., Schulze, H. P., & Kröning, O. (2018). Automated analysis of pulse types in high speed wire EDM. *Procedia CIRP*, 68, 796-801.
85. Pan, H., Liu, Z., Li, C., Zhang, Y., & Qiu, M. (2017). Enhanced debris expelling in high-speed wire electrical discharge machining. *The International Journal of Advanced Manufacturing Technology*, 93(5), 2913-2920.
86. Pandey, A. B., & Brahmankar, P. K. (2016). A method to predict possibility of arcing in EDM of TiB<sub>2</sub> reinforced ferrous matrix composite. *The International Journal of Advanced Manufacturing Technology*, 86(9), 2837-2849.
87. Parida, A. K., & Maity, K. (2018). Comparison the machinability of Inconel 718, Inconel 625 and Monel 400 in hot turning operation. *Engineering Science and Technology, an International Journal*, 21(3), 364-370.
88. Park, H. S., & Tran, N. H. (2014). Development of a smart machining system using self-optimizing control. *The International Journal of Advanced Manufacturing Technology*, 74(9-12), 1365-1380.
89. Phate, M. R., & Toney, S. B. (2019). Modeling and prediction of WEDM performance parameters for Al/SiCp MMC using dimensional analysis and artificial neural network. *Engineering Science and Technology, an International Journal*, 22(2), 468-476.

90. Pramanik, A., & Basak, A. K. (2018). Sustainability in wire electrical discharge machining of titanium alloy: understanding wire rupture. *Journal of Cleaner Production*, 198, 472-479.
91. Prasad, A. V. S. R., Ramji, K., & Datta, G. L. (2014). An Experimental Study of Wire EDM on Ti-6Al-4V Alloy. *Procedia Materials Science*, 5, 2567–2576. <https://doi.org/10.1016/j.mspro.2014.07.517>
92. Prohaszka, J., Mamalis, A. G., & Vaxevanidis, N. M. (1997). The effect of electrode material on machinability in wire electro-discharge machining. *Journal of Materials Processing Technology*, 69(1–3), 233–237.
93. Rajeswari, R., & Shunmugam, M. S. (2019). Investigations into process mechanics of rough and finish die sinking EDM using pulse train analysis. *The International Journal of Advanced Manufacturing Technology*, 100(5), 1945-1964.
94. Rajurkar, K. P., & Wang, W. M. (1993). Thermal modeling and on-line monitoring of wire-EDM. *Journal of Materials Processing Technology*, 38(1-2), 417-430.
95. Rajurkar, K. P., Wang, W. M., & Lindsay, R. P. (1991). On-line monitor and control for wire breakage in WEDM. *CIRP annals*, 40(1), 219-222.
96. Rajurkar, K. P., Wang, W. M., & McGeough, J. A. (1994). WEDM identification and adaptive control for variable-height components. *CIRP annals*, 43(1), 199-202.
97. Ramakrishnan, R., & Karunamoorthy, L. (2008). Modeling and multi-response optimization of Inconel 718 on machining of CNC WEDM process. *Journal of materials processing technology*, 207(1-3), 343-349.
98. Ramamurthy, A., Sivaramakrishnan, R., Muthuramalingam, T., & Venugopal, S. (2015). Performance Analysis of Wire Electrodes on Machining Ti-6Al-4V Alloy using Electrical Discharge Machining Process. *Machining Science and Technology*, 19(4), 577–592.
99. Rao, T. B. (2016). Optimizing machining parameters of wire-EDM process to cut Al7075/SiCp composites using an integrated statistical approach. *Advances in Manufacturing*, 4(3), 202–216.

100. Reed, R. C. (2008). *The superalloys: fundamentals and applications*. Cambridge university press.
101. Sanchez, J. A., Rodil, J. L., Herrero, A., De Lacalle, L. L., & Lamikiz, A. (2007). On the influence of cutting speed limitation on the accuracy of wire-EDM corner-cutting. *Journal of Materials Processing Technology*, 182(1-3), 574-579.
102. Sarkar, S., Sekh, M., Mitra, S., & Bhattacharyya, B. (2011). A novel method of determination of wire lag for enhanced profile accuracy in WEDM. *Precision Engineering*, 35(2), 339-347.
103. Shakeri, S., Ghassemi, A., Hassani, M., & Hajian, A. (2016). Investigation of material removal rate and surface roughness in wire electrical discharge machining process for cementation alloy steel using artificial neural network. *the International Journal of Advanced Manufacturing Technology*, 82(1-4), 549-557.
104. Sharma, P., Chakradhar, D., & Narendranath, S. (2015). Evaluation of WEDM performance characteristics of Inconel 706 for turbine disk application. *Materials and Design*, 88, 558–566.
105. Shunmugam, M. S., Kumar, S. S., & Kaul, I. K. (2000, October). Fuzzy logic modeling of wire-cut EDM process. In *Intelligent Systems in Design and Manufacturing III* (Vol. 4192, pp. 417-425). International Society for Optics and Photonics.
106. Soepangkat, B. O. P., Norcahyo, R., Rupajati, P., Effendi, M. K., & Agustin, H. C. K. (2019). Multi-objective optimization in wire-EDM process using grey relational analysis method (GRA) and backpropagation neural network–genetic algorithm (BPNN–GA) methods. *Multidiscipline Modeling in Materials and Structures*.
107. Sommer, C., & Sommer, S. (2017). *Complete EDM handbook*. Advance Publishing Incorporated. 2nd edition (January 1, 2017) ISBN-13 : 978-1575373034
108. Soo, S. L., Antar, M. T., Aspinwall, D. K., Sage, C., Cuttell, M., Perez, R., & Winn, A. J. (2013). The effect of wire electrical discharge machining on

- the fatigue life of Ti-6Al-2Sn-4Zr-6Mo aerospace alloy. *Procedia CIRP*, 6, 215-219.
109. Thakur, D. G., Ramamoorthy, B., & Vijayaraghavan, L. (2009). Study on the machinability characteristics of superalloy Inconel 718 during high speed turning. *Materials & Design*, 30(5), 1718-1725.
  110. Thellaputta, G. R., Chandra, P. S., & Rao, C. S. P. (2017). Machinability of nickel based superalloys: a review. *Materials Today: Proceedings*, 4(2), 3712-3721.
  111. Tondy, H. R., & Tigga, A. M. (2019). An empirical evaluation and optimization of performance parameters of wire electrical discharge machining in cutting of Inconel 718. *Measurement: Journal of the International Measurement Confederation*, 140, 185–196.
  112. Tosun, N., & Cogun, C. (2003). An investigation on wire wear in WEDM. *Journal of materials processing technology*, 134(3), 273-278.
  113. Tosun, N., & Pihtili, H. (2003). The effect of cutting parameters on wire crater sizes in wire EDM. *The International Journal of advanced manufacturing technology*, 21(10-11), 857-865.
  114. Ubale, S. B., Deshmukh, S. D., & Ghosh, S. (2018). Artificial Neural Network based Modelling of Wire Electrical Discharge Machining on Tungsten-Copper Composite. *Materials Today: Proceedings*, 5(2), 5655–5663. <https://doi.org/10.1016/j.matpr.2017.12.159>
  115. Velterop, L. (2003). Influence of wire electrical discharge machining on the fatigue properties of high strength stainless steel.
  116. Wang, J., & Ravani, B. (2003). Computer aided contouring operation for traveling wire electric discharge machining (EDM). *Computer-Aided Design*, 35(10), 925-934.
  117. Wang, J., Ma, Y., Zhang, L., Gao, R. X., & Wu, D. (2018). Deep learning for smart manufacturing: Methods and applications. *Journal of Manufacturing Systems*, 48, 144-156.

118. Wang, J., Sanchez, J. A., Ayesta, I., & Iturrioz, J. A. (2018). Unsupervised machine learning for advanced tolerance monitoring of wire electrical discharge machining of disc turbine fir-tree slots. *Sensors*, 18(10), 3359.
119. Wang, J., Sanchez, J. A., Iturrioz, J. A., & Ayesta, I. (2019). Geometrical defect detection in the wire electrical discharge machining of fir-tree slots using deep learning techniques. *Applied Sciences*, 9(1), 90.
120. Welling, D. (2014). Results of surface integrity and fatigue study of wire-EDM compared to broaching and grinding for demanding jet engine components made of Inconel 718. *Procedia CIRP*, 13, 339-344.
121. Xia, M., Li, T., Xu, L., Liu, L., & De Silva, C. W. (2017). Fault diagnosis for rotating machinery using multiple sensors and convolutional neural networks. *IEEE/ASME Transactions on Mechatronics*, 23(1), 101-110.
122. Xia, W., Li, Z., Zhang, Y., & Zhao, W. (2020). Breakout detection for fast EDM drilling by classification of machining state graphs. *The International Journal of Advanced Manufacturing Technology*, 106(5), 1645-1656.
123. Yan, J., Meng, Y., Lu, L., & Guo, C. (2017, July). Big-data-driven based intelligent prognostics scheme in industry 4.0 environment. In *2017 Prognostics and System Health Management Conference (PHM-Harbin)* (pp. 1-5). IEEE.
124. Yan, M. T., & Hsieh, P. H. (2015). An on-line monitoring system for wire electrical discharge turning process. *Proceedings of the Institution of Mechanical Engineers, Part B: Journal of Engineering Manufacture*, 229(11), 1945-1954.
125. Yan, M. T., & Huang, P. H. (2004). Accuracy improvement of wire-EDM by real-time wire tension control. *International Journal of Machine Tools and Manufacture*, 44(7-8), 807-814.
126. Yan, M. T., & Lai, Y. P. (2007). Surface quality improvement of wire-EDM using a fine-finish power supply. *International journal of machine tools and manufacture*, 47(11), 1686-1694.

127. Yan, M. T., & Liao, Y. S. (1996). A self-learning fuzzy controller for wire rupture prevention in WEDM. *The International Journal of Advanced Manufacturing Technology*, 11(4), 267-275.
128. Yan, M. T., & Liao, Y. S. (1998). Adaptive control of the WEDM process using the fuzzy control strategy. *Journal of Manufacturing Systems*, 17(4), 263-274.
129. Yan, M. T., Li, H. P., & Liang, J. F. (1999). The application of fuzzy control strategy in servo feed control of wire electrical discharge machining. *The International Journal of Advanced Manufacturing Technology*, 11(15), 780-784.
130. Yan, M. T., Liao, Y., & Chang, C. C. (2001). On-line estimation of workpiece height by using neural networks and hierarchical adaptive control of WEDM. *The International Journal of Advanced Manufacturing Technology*, 18(12), 884-891.
131. Zhang, X., Liu, Y., Wu, X., & Niu, Z. (2019). Intelligent pulse analysis of high-speed electrical discharge machining using different RNNs. *Journal of Intelligent Manufacturing*, 1-15.
132. Zhang, Z., Ming, W., Zhang, G., Huang, Y., Wen, X., & Huang, H. (2015). A new method for on-line monitoring discharge pulse in WEDM-MS process. *The International Journal of Advanced Manufacturing Technology*, 81(5), 1403-1418.
133. Zheng, P., Sang, Z., Zhong, R. Y., Liu, Y., Liu, C., Mubarak, K., ... & Xu, X. (2018). Smart manufacturing systems for Industry 4.0: Conceptual framework, scenarios, and future perspectives. *Frontiers of Mechanical Engineering*, 13(2), 137-150.
134. Zhidong, L., Haoran, C., Huijun, P., Mingbo, Q., & Zongjun, T. (2015). Automatic control of WEDM servo for silicon processing using current pulse probability detection. *The International Journal of Advanced Manufacturing Technology*, 76(1-4), 367-374.
135. Zhong, M., Sun, H., Liu, W., Zhu, X., & He, J. (2005). Boundary liquation and interface cracking characterization in laser deposition of Inconel 738

- on directionally solidified Ni-based superalloy. *Scripta materialia*, 53(2), 159-164.
136. Zhu, K., Li, G., & Zhang, Y. (2019). Big data oriented smart tool condition monitoring system. *IEEE Transactions on Industrial Informatics*, 16(6), 4007-4016.